CHARACTERIZATION OF PROMOTED SUPPORTED PLATINUM CATALYST

Mushtaq Ahmad

Thesis Submitted for the Degree of

Doctor of Philosophy

University of Edinburgh

1990

To My Parents....

Rehana, Amina and Haris too.....

DECLARATION

I certify that, unless otherwise stated, all the work described in this thesis was performed by myself at the laboratories of the University of Edinburgh.

Mushtaq Ahmad

ACKNOWLEDGEMENTS

I would like to thank my supervisors, Gordon McDougall and Frank Leach for their help and guidance throughout my stay in Edinburgh. I am particularly indebted to Dr. McDougall for his advice, encouragement, critical comments and his close involvement with my work. I wish also to acknowledge the invaluable assistance and friendship of Ronald Brown in both practical and helpful discussions throughout the course of my work. Thanks are due to John Broom for the construction of the glass vacuum line and from time-to-time repairs. A special commendation goes to Ann Dolan who helped with most of the proof reading. Thanks are also due to my valued colleagues and friends, Hilary, Phillip and Ian.

I would like to thank National Physical and Standards Laboratories of Pakistan Council of Scientific and Industrial Research for selecting me for this course. For provision of finances I am thankful to the Ministry of Science and Technology, Government of Pakistan.

Thanks to Mrs. Lynn Marouf for typing the manuscript.

Finally, I would like to thank my wife Rehana for her encouragement and patience in spite of the Scottish weather.

ABSTRACT

Characterisation of 'as-received' and alkali doped EUROPT-1 has been studied by gravimetric adsorption measurements, temperature programmed reduction and temperature programmed desorption (TPD) of H_2 and CO. The presence of alkali changes the chemisorptive characteristics of CO and H_2 on catalyst's surface. The total surface area and metal dispersion of EUROPT-1 decreases concomitantly with alkali.

Hydrogenolysis activity of alkali doped EUROPT-1 catalysts were studied using a conventional static reactor. The overall rate of reaction decreases with increasing alkali, and there is considerable influence on the selectivity of the catalysts towards isomerisation.

Diffuse reflectance infrared fourier transform spectroscopy (DRIFTS) has been applied to the study of adsorption and thermal desorption of CO, adsorption of ethylene, benzene, ethane and n-butane on the alkali doped catalysts. The CO stretching vibrational frequencies are shown to decrease with increasing alkali concentration. This can be interpreted in terms of a substantial charge donation from potassium through the platinum and into the $2\pi^*$ CO orbital. The adsorption of ethylene gives rise to peaks identified as π adsorbed ethylene and ethylidyne. With the π species increasing in prominence with increasing alkali, benzene adsorption showed substantial physisorption onto the SiO_2 support.

CONTENTS

CHAPTER 2 (Cont'd) Page No.

CHAPTER 3 (Cont'd) Page No.

CHAPTER 4 (Cont'd) Page No.

CHAPTER 5 (Cont'd) Page No.

CHAPTER 5 (Cont'd) Page No.

CHAPTER 6 (Cont'd) Page No.

CHAPTER 1

INTRODUCTION

At present a large number of industrial and technical chemicals are manufactured using processes involving heterogeneous catalysis. Due to increasing costs of fuel, energy and raw materials, a great deal of work is being devoted to the improvement of heterogeneous catalysis. Alkali promotion provides a route for possible improvement in the performance of the catalysts[1].

Promoters are defined as substances which may increase the activity of the catalysts per unit surface area. This effect was first emphasised by Badische Anilin and Soda Fabrik[2]. Later on, Taylor and Pease[3], in a review article, suggested a definition of promoter action as that in which a mixture of two or more substances is capable of producing a greater catalytic activity than can be accounted for on the supposition that each substance in the mixture acts independently and in proportion to the amount present. This definition is still in use with certain limitations.

The economic importance of alkali promotion is very well illustrated by reactions such as synthesis of ammonia and hydrogenation of carbon monoxide. The early attempts to combine nitrogen and hydrogen without involving a catalyst were unsuccessful because of the little knowledge

of the thermodynamics of the system. In the first decade of this century Haber, Bosch and Mittasch showed that the reaction of nitrogen and hydrogen was exothermic so high pressure and low temperature will favour the formation of highest equilibrium product. It was soon realised that a catalyst can bring the system to equilibrium at the lowest possible temperature. Between the years 1905-1910, an extensive investigation of such a catalyst began in Germany, by Haber and his associates[4]. A catalyst made from iron ore, showing some satisfactory stability, was analysed. This contained some alumina and potassium oxide. This discovery opened the door to industrial scale production of ammonia[5]. The present day catalyst, a fused iron oxide catalyst (magnetite) promoted by K_2O, has been the standard catalyst for ammonia synthesis for more than sixty years[6-8]. This catalyst contains about 1% (wt.) K_2O as electronic promoter and 3-6% (wt.) Al_2O_3, MgO + CaO as structural promoters. It is assumed that the main function of alumina is to preserve a large surface area and to prevent the iron crystallites from sintering. The role of potassium oxide used as promoter is still not clear[9-10]. In the synthesis of ammonia over an iron catalyst, alkali promotion increases the rate of synthesis while the total iron area available decreases. This suggests that the promotion is chemical in nature[11-12]. It has been postulated that alkali metal alters the electronic state of the surface iron atoms[11-12]. It is

understood that when nitrogen adsorbs onto the iron surface, the molecules tend to draw electrons from the iron. Potassium is a strong electron donor, donating its valence electrons to the iron surface. This results in a more pronounced "Π-back-bonding" of the metallic 'd' electrons into the nitrogen Π_g orbital due to the lowering of the local work function. In this way K_2O addition may promote dissociative adsorption of N_2, the rate determining step of the reaction.

In Fischer-Tropsch synthesis reactions, the hydrogenation of CO on metals leading to the formation of methane has a long history. The reaction

$$nCO + (2n + 2)\ H_2 \longrightarrow C_nH_{2n+2} + nH_2O$$

was discovered in 1923. Potassium promoted iron is used commercially to catalyse the Fischer-Tropsch reaction[13-14]. In spite of the extensive application of this catalyst, the question concerning the mechanism of this important catalytic reaction remains unanswered.

Methane is produced exclusively over nickel catalysts[14-15]. Hence the catalytic methanation reaction over transition metal surfaces has been of great interest. Practical nickel catalysts for CO hydrogenation include alkali promoters as K_2O or K_2CO_3[16-19]. It is reported that at atmospheric pressure, potassium increases the average molecular weight of the hydrocarbons produced over the Ni catalyst[20]. This may be due to increase in the chain growth process[17].

The synthesis of higher molecular weight hydrocarbons by reaction of CO and H_2 over a metal catalyst has achieved prime industrial importance. Metals which are active in the Fischer Tropsch reaction include iron, cobalt, nickel and ruthenium. All these metals other than ruthenium require a support or/and promoter. Ruthenium is used in its pure state to produce high molecular weight solid paraffin[9]. Iron which is used for the production of olefins and alcohols is usually promoted by oxides of potassium or sodium. Cobalt or nickel catalysts yielding mainly straight chain hydrocarbons of intermediate molecular weight, are often supported on Kieselguher and with small quantities of alkali promoters.

The development of sophisticated surface techniques including ultra high vacuum (UHV) systems has provided better conditions for studying well characterised low surface area materials such as metal single crystals of the size of about 1 cm^2. On the other hand the high surface area oxide supported and promoted metals, catalyse the reactions of practical interest at atmospheric conditions. The differences in the nature of the two catalysts has created interest to see if any correlation between the two systems exists. Good correlation would provide a wealth of information and results of the studies on model catalyst systems could be used to understand the complex real or practical catalyst systems.

Recently experimental systems have been designed to

provide the facility of a high pressure reactor linked with the UHV surface analysis chamber[20-21]. In such experimental systems it was possible to study the surface of the catalyst after reaction, without removing the catalyst samples.

The model catalysts can help to understand how surface structure and chemical additives can control the surface chemistry in heterogeneous catalysis. This can be easily achieved by studying the surface structure of a single crystal, the position of additives or surface modifiers and the interaction of reacting gases with the single crystal model catalysts.

The surface chemical reaction at low pressure can establish a relationship between structure, composition and reactivity. During the reaction the chemisorbed species can be observed and characterised in detail under UHV by various techniques such as low energy electron diffraction (LEED), Auger electron spectroscopy (AES), ultra violet photo-electron spectroscopy (UPS), and high resolution electron energy loss spectroscopy (HREELS). Studying the same reaction at high pressure, the reaction kinetics are determined. Hence the product distribution obtained can be compared with those of the practical catalyst systems.

Ertl and associates[22] first studied adsorption of N_2 on a well defined iron single crystal. Initially N_2 adsorption was studied on a Fe(100) single crystal and

then on other crystal faces such as Fe(110) and Fe(111)[22]. It was observed that the initial sticking coefficient for dissociative adsorption of N_2 at 430 K was greater on a potassium doped Fe(111) single crystal compared with the clean Fe(111) single crystal by more than two orders of magnitude[22]. This effect is important in heterogeneous catalysis, as the availability of atomic nitrogen determines the overall rate of ammonia synthesis[22]. Based on the studies of different crystal faces, the authors further observed a greater effect on Fe(110) planes, suggesting differences in activities of various crystal facets of the supported catalyst. The decrease in work function by 2.35 eV at a concentration of 4×10^{19} K atoms m^{-2} suggested a complete ionization of potassium atoms as a result of charge transfer.

Similarly CO hydrogenation reaction over potassium promoted Ni(100) single crystals has been extensively studied[20-21]. The reactions were carried out in a high pressure reactor combined with UHV and a surface analysis chamber. The Auger electron spectroscopy (AES) was used to monitor the distribution of potassium. It was observed that a one-tenth monolayer of potassium decreased the rate of methane formation by a factor of two. On the other hand the rate of formation of higher hydrocarbons increased compared with a clean Ni(100) single crystal. The essential reaction intermediate, which proved to be surface carbide, increased as a result of a marked

decrease in the activation energy in the presence of potassium for CO dissociation. The preferential formation of higher hydrocarbons was explained by the higher probability of reaction involving C-C bond formation; i.e. increase in the availability of reactants for chain growth. These two reactions, i.e. ammonia synthesis and the CO methanation reaction (Fischer-Tropsch), are the most widely studied potassium promoted heterogeneous catalysis reactions. It is suggested that in both reactions potassium acts as an electron donor, enhancing the charge transfer to the adsorbate. These effects are explained by the assumption that alkali adatoms on transition metal surfaces exist in a partially ionic state, donating a large fraction of their valence electrons to the metal surfaces, causing a lowering of the work function[24-27]. The additional electron density on the transition metals plays an important role in altering the chemisorptive properties of reacting molecules such as N_2 and CO.

The results of these reactions over model catalysts Ni(110) and Fe(111) single crystals corresponded very well with the more practical high surface area supported promoted metal catalysts[17-19,28-29]. This suggests that the promotional effect can be achieved even without the support material. Hence the model catalysts can be used to study the fine details of the experiments involving supported promoted metal catalysts[30]. However, it is

important to note that the studies of surface reactivity on single crystals in UHV conditions are far from the normal operating conditions of practical catalysts.

The importance of investigations of CO adsorption/ desorption studies is quite evident from the point of view of Fischer-Tropsch synthesis reactions. In particular the use of infrared spectroscopy as a tool to study the structure of adsorbed CO species has led to the important conclusions which influence the understanding of the catalytic activity. Following the earlier reviews of Eischen and Pliskin[31], several detailed surveys have appeared in the literature[33]. Recently the adsorption of carbon monoxide on Pt(111) single crystals has been studied by many researchers. The vibrational spectra suggest that CO adsorbs molecularly on the platinum surface in the linear and the bridged configurations with CO stretching vibrations at 2100 and 1870 cm^{-1} respectively[32-35]. At low coverages CO is adsorbed linearly, while with increasing coverages, the bridged position becomes partially filled. As the coverage increases the frequency for the linearly bonded CO shifts by 30-40 cm^{-1} to higher frequencies. The shift has been attributed to the increased dipole-dipole interaction as a function of CO coverages[31,32,43].

The adsorption of carbon monoxide on the Pt(111) single crystal surface in the presence of potassium was investigated in an ultra high vacuum system with the base

pressure of ~ 10^{-10} torr. AES and LEED techniques were used to monitor the surface structure and composition. The vibrational frequencies were determined by HREELS. The vibrational data provided information about the adsorption sites and relative site concentrations of CO when coadsorbed with potassium. Changes in the heat of adsorption of the coadsorbed systems were determined by thermal desorption spectroscopy. Potassium adsorption on a Pt(111) single crystal exhibits a larger work function change of 4.7 eV[42].

Most of the adsorption studies have been carried out with CO and alkali metals on noble and transition metal surfaces such as Fe, Ni, Cu, Ru, Rh, W, Ir and Pt[41]. The temperature of the adsorption peak shifts appreciably to higher temperature. The maximum CO coverages decrease markedly as observed for Ni(100) and Pt(111) single crystals[41-43]. The TDS data suggests that the presence of K induces a new CO state with higher adsorption energy[41-43].

Reflection absorption infrared spectra from Pt(111)[32] show significant shift of the CO stretching frequencies as a function of coverage. For CO adsorption on a Pt(111) single crystal, it has been extensively reported that a band first appears at 2065 cm^{-1} and moves to 2100 cm^{-1} at saturation coverages.

A recent HREELS study[43] shows that CO adsorbs molecularly on the platinum surface in linear (2100 cm^{-1})

and bridged (1870 cm^{-1}) configurations. Significant changes in the TDS and HREELS can be seen when potassium is coadsorbed with CO on a Pt(111) single crystal. As the potassium coverage increases the desorption peaks broaden, the peak maxima shift to higher temperature and the CO coverage decreases markedly. It is also observed that at first, the CO coverage increases slightly and then decreases at high potassium coverages. This effect is explained by the competing effect of an increase in CO binding energy in the presence of potassium and also by the direct site blocking due to potassium[43]. At low potassium coverage there is tighter CO packing which compensates for the decrease in CO coverage due to site blocking of exposed platinum surface.

Potassium has a marked effect on the vibration frequencies. Both linear and bridged bands shift to lower frequencies compared with the potassium free Pt(111)[43]. The coadsorption study by Crowell and associates[43] shows a decrease of linear and bridged band frequencies by 65 and 100 cm^{-1} at a K-coverage of $\theta \sim 0.1$. The changes in the peak intensities are also significant. At the highest K coverage of $\theta \sim 0.6$, the spectrum is dominated by only one peak at 1400 cm^{-1}. This large shift is very important. The absence of the linear band indicates that CO at such K-coverages may adsorb on bridge sites only. These effects have been explained in terms of three important factors: (i) there may be a long range interaction between

K and CO; (ii) potassium pushes CO from linear (on top) sites into bridge sites; (iii) potassium transfers its valence electrons through the platinum, d-orbitals into the antibonding 2Π orbitals of CO. The latter effect is thought to be responsible for the drastic changes in the CO stretch frequencies decreasing down to 1565 cm^{-1} in the presence of K[43].

Although the interaction of alkali metal atoms with transition metal surfaces has been extensively studied in the past, little is known about the effect of potassium on the adsorption and reaction of ethylene on a Pt(111) single crystal or supported platinum catalysts.

Ethylene adsorbed on Pt(111) at 100 K, is di-σ bonded[45-47] and no Π bonded or physisorbed ethylene was observed[48]. At room temperature di-σ bonded ethylene undergoes dehydrogenation forming a new more stable species assigned as ethylidyne identified using LEED[3], HREELS[46] and SIMS[49] techniques.

Recent studies of adsorption and desorption of ethylene on Pt(111) single crystals[50-51] have shown that potassium coadsorption can result in a considerable alteration of the Pt(111) surface chemistry. Potassium alters the bonding from di-σ to Π. This effect has been explained in the terms of charge transfer from potassium to the platinum as described earlier.

Although promoted platinum catalysts are not normally used in heterogeneous catalysis, the drastic alterations

in the chemisorptive properties of simple reactive molecules on potassium doped Pt(111) single crystals suggested an investigation of the potassium promotional effect on a supported platinum catalyst, EUROPT-1. The use of this catalyst provided an excellent opportunity to study the promotional effect of potassium on a catalyst which had been fully characterised by several independent laboratories.

EUROPT-1 is a model catalyst prepared by Johnson-Mathey Plc, by an ion exchange method. The support material used is Sorbosil AQU30 silica gel. The use of a standard catalyst can help avoid many complications arising from variation of characteristics, such as the particle size distribution and the shapes of the crystallites. EUROPT-1 has been characterised in detail by many European laboratories[44]. Although supported catalysts usually have a large distribution of particle size, EUROPT-1 proved to have a relatively narrow size distribution, with 75% of the platinum particles less than 20 Å in diameter. This interesting property and the availability of the data of other charactertistics of EUROPT-1 make it a useful reference catalyst.

This thesis is concerned in particular with the study of the effect of alkali doping on EUROPT-1. Various techniques have been applied to characterise and study the catalytic activity of these alkali doped systems.

1. Gravimetric technique (Cahn electro-balance) using N_2

physisorption for surface area measurements (BET), and the effect of potassium doping on O_2 chemisorption.

2. Temperature programmed reduction and temperature programmed desorption (H_2 and CO) to estimate metal dispersions.
3. Diffuse reflectance fourier transform infrared spectroscopy (DRIFTS) of CO adsorption and desorption.
4. n-Butane hydrogenolysis to measure the activities and selectivities of the catalysts using a conventional static reactor and by DRIFTS.
5. The characteristics of adsorption of ethylene, benzene, ethane and butane, on the catalysts were also studied by DRIFTS.

A detailed account of these techniques is given in the relevant chapters.

REFERENCES

1. W.D. Mross, *Catal.Rev.Sci.Eng.*, 25 (1983) 591.
2. Badische Anilin Und Soda Fabrik, B.P. 19249/10, B.P. 27963/13.
3. Pease and H.S. Taylor, *J.Phys.Chem.* 24 (1920) 241.
4. F. Haber and G. Van Dordt, *Z.Anorg.Chem.* 43 (1904) 111.
5. I.R. Shannon, A specialist periodical report "Catalysis" 2 (1977) 28.
6. A. Mittasch, *Adv.Catal.* 2 (1950) 81.
7. C. Bokhoven, C. Heerden, R. Westrik and P. Zwietering in: *Catalysis*, Vol. 3, ed. P.H. Emmett (Reinhold, New York, 1956).
8. A. Nelson, *Adv.Catal.* 5 (1953) 1.
9. G.C. Bond, *Catalysis by Metals* (Academic Press, London and New York, 1962).
10. J.M. Thomas and W.J. Thomas, *Introduction to the Principles of Heterogeneous Catalysis* (Academic Press, 1967).
11. M.E. Dry and G.J. Oosthuizen, *J.Catal.* 11 (1968).
12. H. Kolbel, Inter. Congr.Catalysis, Paris, 2 (1960) 2075.
13. M.E. Dry, *Ind.Eng.Chem.Prod.Res.Develop.*, 15 (1976) 282.
14. R.W. Joyner, *Vacuum*, 38 (1988), 309.
15. G.A. Somorjai, *Catal.Rev.Sci.Eng.* 23 (1981) 189.

16. C.P. Huang and J.T. Richardson, *J.Catal.* 51 (1978) 1.

17. P.H. Emmett in: *Catalysis*, Vol. 4 (Reinhold, New York, 1956), pp. 46-47, 330-334.

18. G.A. Mills and F.W. Steffgen, *Catalysis Rev.* 8 (1973) 159.

19. P. Schoubye, *J.Catal.* 14 (1969) 238.

20. C.T. Campbell and D.W. Goodman, *Surf. Sci.* 123 (1982) 413.

21. G.A. Somorjai, *Catal.Rev.-Sci.Eng.* 23 (1981) 189-202.

22. G. Ertl, M. Grunze and M. Weiss, *J.Vacuum.Sci. Technol.* 13 (1976) 314.

23. R.L. Gerlach and T.N. Rhodin, *Surf.Sci.* 19 (1970) 403.

24. M. Kiskinova, L. Surneu and G. Bliznakov, *Surf.Sci.* 104 (1981) 240.

25. R.L. Gerlach and T.N. Rhodin, *Surf.Sci.* 17 (1969) 584.

26. M. Kiskinova, *Surf.Sci.* 111 (1981) 584.

27. S. Anderson and U. Jostell, *Surf.Sci.* 46 (1974) 625.

28. D.W. Goodman, R.D. Kelley, T.E. Madey and J.T. Yates, *J.Catal.*, 63 (1980), 226.

29. R.D. Kelley and D.W. Goodman in: *The Chemical Physics of Solid Surfaces and Heterogeneous Catalysis*, Vol. 4, Eds. D.A. King and D.P. Woodruff (Elsevier, Amsterdam) 1982.

30. D.W. Goodman, *Ann.Rev.Phys.Chem.* (1986) 455.

31. R.P. Eischin, W.A., Pliskin and S.A. Francis, *J.Chem. Phys.* 22 (1954) 786.

32. A. Crossley and D.A. King, *Surf.Sci.* 95 (1980) 131.

33. N. Sheppard and T.T. Nguyen in: *Advances in Infrared and Raman Spectroscopy*, Vol. 5, eds. R.J.H. Clark and R.E. Hester, Heyden (London 1978).

34. J.E. Katz, P.W. Davies, J.E. Crowell and G.A. Somorjai, *Rev.Sci.Instr.* 53 (1982) 785.

35. P.R. Norton, J.W. Goodale and E.B. Selkirk, *Surf.Sci.* 83 (1979) 189.

36. A. Ozaki and K.I. Aika in: *A treatise on Nitrogen Fixation*, Eds. R.W.F. Hardy, F. Bottomley and R.L. Burns, (Wiley, 1979), p. 169.

37. M.E. Dry, T. Shingles, L.J. Boshoff and G. Oosthuizen, *J.Catal.* 15 (1969) 190.

38. R.W. Gurney, *Phys.Rev.* 47 (1935) 479.

39. N.D. Lang and A.R. Williams, *Phys.Rev.Lett.* 37 (1976) 212.

40. J.P. Muscat and D.M. Newns, *Surf.Sci.* 74 (1978) 355.

41. H.P. Bonzel, *Surf.Sci.Rept.* 8 (1987) 43.

42. M. Kiskinova, G. Pirug and H.P. Bonzel, *Surf.Sci.* 133 (1983) 321.

43. J.E. Crowell, E.L. Garfunkel and G.A. Somorjai, *Surf.Sci.* 121 (1982) 303.

44. G.C. Bond and P.B. Wells, *Appl.Catal.* 18 (1985) 221.

45. J.E. Demuth, *Surf.Sci.* 80 (1979) 867.

46. H. Steninger, H. Ibach and S. Lehwald, *Surf.Sci.* 117 (1982) 685.

47. H. Ibach, H. Hopster and B. Sexton, *Appl.Surf.Sci.* 1 (1977) 1.

48. M. Salmeron and G.A. Somorjai, *J.Phys.Chem.* 86 (1982) 685.

49. J.R. Creighton and J.M. White, *Surf.Sci.* 129 (1983) 327.

50. R.G. Windham, M.E. Bartram and B.E. Koel, *J.Phys. Chem.* 92 (1988) 2860.

51. X.L. Zhou, X.Y. Zhu and J.M. White, *Surf.Sci.* 193 (1988) 387.

CHAPTER 2

INITIAL CHARACTERISATION OF 'AS-RECEIVED' AND 'ALKALI DOPED' EUROPT-1 CATALYST

This chapter describes the preparation of the potassium doped EUROPT-1 catalysts and the techniques used for their initial characterisation. These techniques were all carried out on a Cahn electrobalance and included N_2 physisorption and oxygen chemisorption.

2.1 PREPARATION OF THE ALKALI DOPED EUROPT-1 CATALYSTS

The alkali doped catalysts were prepared by soaking EUROPT-1; surface area 185±5 m^2 per gram, in a KOH/K_2CO_3 solution containing a known amount of KOH or K_2CO_3 (wt)%. The resulting slurry was then dried using a rotary evaporator. The variations in the alkali concentrations were achieved by making appropriate dilutions of alkali solution. After drying, the catalyst samples were calcined overnight at 400 K. The finished material had alkali concentrations of (% weight) 0.25%, 0.5% and 1.0% on EUROPT-1. The concentrations are all nominal, being based on the concentration of alkali solution used.

Attempts to measure the concentration of potassium in the EUROPT-1 by atomic absorption spectroscopy were unsuccessful due to incomplete digestion of the EUROPT-1 by hydrofluoric acid or aqua regia.

2.2 CHARACTERISATION

The initial characterisation of the 'as-received' and alkali doped EUROPT-1 samples was carried out, determining the total surface area (B.E.T.) and oxygen chemisorption. Nitrogen physisorption isotherms were recorded at 77 K to determine the B.E.T. surface area, where oxygen chemisorption studies were carried out at room temperature.

The use of the microbalance for adsorption studies has been described by several authors[1-4]. It allows the direct measurements of small weight changes and may be used to great advantage in adsorption studies.

2.3 APPARATUS

2.3.1 The Balance

In this study a Cahn RG electrobalance with a maximum sensitivity of 1×10^{-7} g was used. The balance is illustrated in figure 2:1, and operates on the null-balance principle. When the sample weight changes, the beam tends to deflect momentarily; the attached flag moves correspondingly changing the amount of light falling on the phototube, resulting in the change of phototube current. The current is then amplified by a two stage servo amplifier and applied to a coil attached to the beam. The coil is situated in a magnetic field, which acts like a D.C. motor exerting a force to restore the

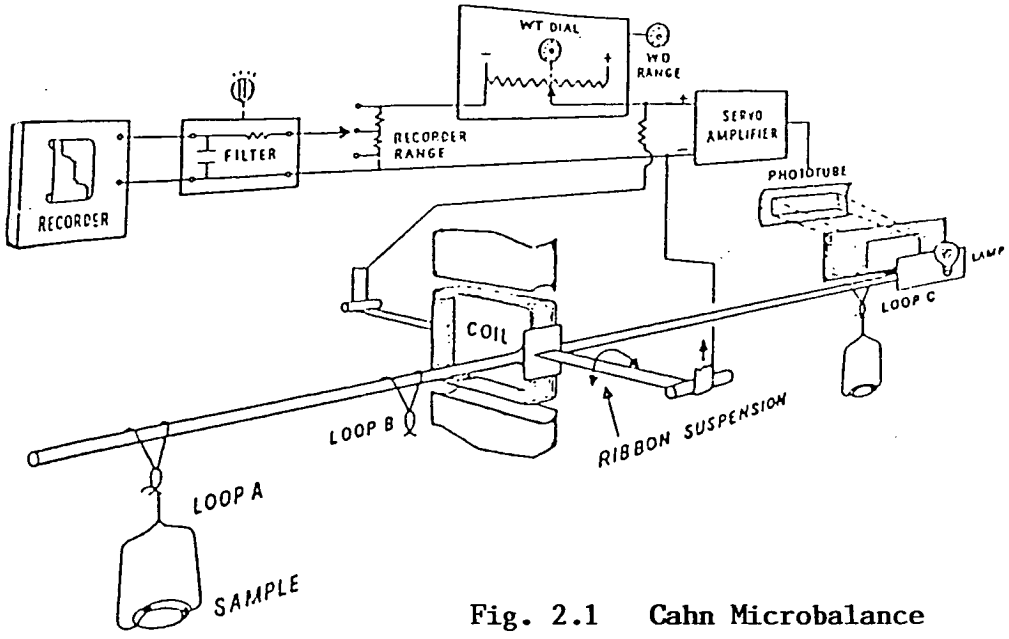

Fig. 2.1 Cahn Microbalance

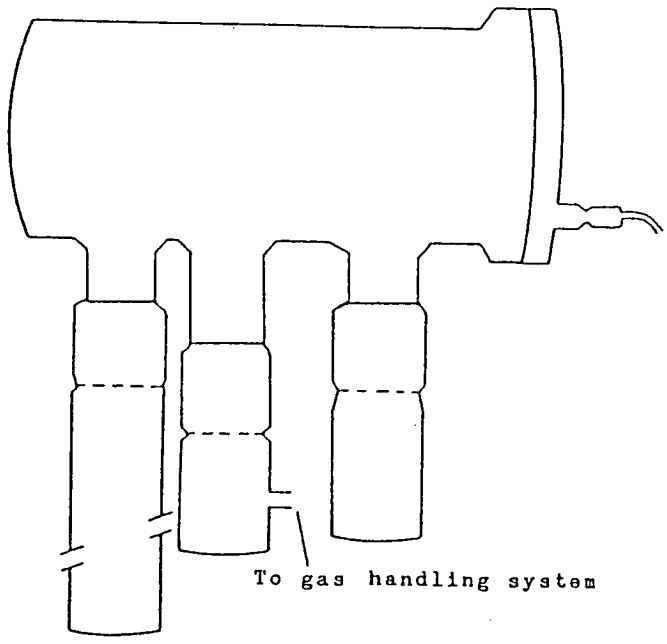

Fig. 2.2 The Vacuum Bottle in which the Balance is placed

beam to its original position.

The restoring current and the voltage developed across the coil are directly proportional to any change in sample weight. A known, accurately calibrated voltage across the coil must be subtracted using a potentiometer to get an accurate display on a recorder. The mass dial on the potentiometer is calibrated in milligrams corresponding to the amount of voltage being subtracted, followed by application of excess coil voltage to a servoscribe potentiometric chart recorder. The voltage attentuation can be used to display various weight ranges on the recorder.

The catalyst sample was placed in a specially designed silica bucket with a nichrome wire handle. The sample bucket was suspended from a loop A by a nichrome hangdown wire. The maximum load which could be suspended was 1 g. A counter weight consisting of small metal or wire pieces placed in a similar silica bucket was suspended from loop 'C' by a hangdown wire.

The electrobalance (figure 2:1) was housed in a large vacuum bottle (2:2). The electrical connecting cable was accommodated on a metal cap which was clamped in position with strong removable springs. A vacuum seal was achieved by viton 'O' ring and high vacuum silicone grease. The hangdown wires of the sample and counter weight passed through ground glass joints into an attached cylindrical adsorption vessel. The balance chamber was connected to

the vacuum system through a third joint.

2.3.2 The Vacuum Line

The apparatus used consisted of a gas handling line and an adsorption section. The gas handling apparatus which was constructed of pyrex glass, is shown in figure 2:3. Greaseless taps (high vacuum Springham) were used throughout the vacuum line. A McLeod gauge was used to measure the vacuum in the line. All other gas measurements were made with a mercury manometer. The gases to be studied were introduced into the main apparatus, from the gas cylinder through the taps and needle valves, after purification. The gas handling apparatus was connected to the adsorption chamber through pyrex tubing.

The adsorption section consisted of the vacuum bottle housing the balance and the hangdown tubes attached to it. To facilitate easy removal, the hangdown tube, containing the sample bucket and its wires, was in two sections. The lower section, which was subjected to higher temperatures during sample outgassing and reduction, was constructed of silica. The upper pyrex section had a graded seal at its lower end and was joined to the lower section by a ground silica joint lubricated with Apiezon 'T' grease.

A vacuum of 1×10^{-6} torr was achieved in the gas handling line and adsorption apparatus by the use of two rotary oil pumps (Edward) supplying roughing vacuum to two

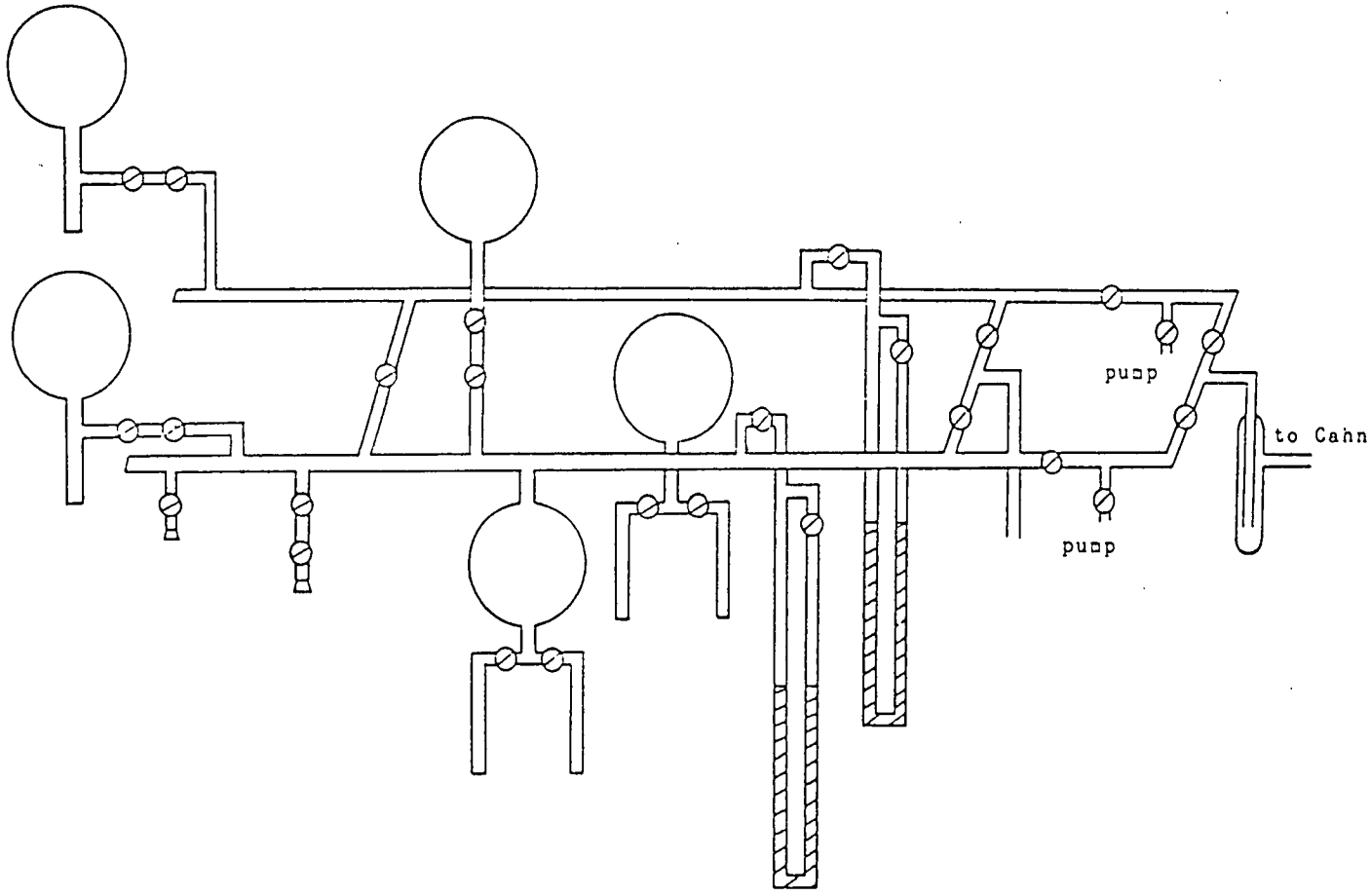

Fig. 2.3 Gas Handling Apparatus for Adsorption Studies

glass, three stage mercury diffusion pumps.

A close fitting tubular furnace was used to heat the sample. A linear temperature programmer (Stanton Redcroft) incorporating a Eurotherm unit was used to control the heating rate and temperature of the furnace. Another thermocouple connected to a digital thermometer was used to measure the accurate temperature of the sample, down a silica pocket in the adsorption vessel to a position level with the sample.

2.4 PROCEDURE

The balance was calibrated according to the manufacturer's instructions[5] using accurately standardised calibration weights. A sample weight of 0.05 g was used, counter balanced by a suitable substitution weight. The accurate determination of the sample weight could be made by summation of the mass dial value, the recorder deflection and the substitution weight.

The adsorption section of the apparatus was evacuated. It was necessary to introduce gases and degassing slowly in order to avoid disturbance of the balance system and "spurting" of the sample.

Utilising the gravimetric arrangement it was possible to carry out adsorption isotherms by admitting successive doses of adsorbate to the adsorption section and recording the equilibrium weight and the equilibrium pressure.

2.4.1 Catalyst Pretreatment

Prior to the adsorption of gases, the samples were reduced in static hydrogen (400 torr) for two hours and heated in a programmed way at the rate of 20 K per minute to 673 K. The sample was then degassed at this temperature and finally cooled down to room temperature. The reducing hydrogen was purified by passage through a 4A molecular sieve trap immersed in a liquid nitrogen bath.

2.4.2 Nitrogen Adsorption

Nitrogen physisorption isotherms were recorded at 77 K. Weight uptake of nitrogen per g of catalyst was recorded against each pressure of nitrogen up to a maximum of 250 torr. The weight uptake was then converted to the volumes of nitrogen physisorbed per g of catalyst and each pressure of nitrogen was converted to P/P°, where P is the pressure of the adsorbing nitrogen and P° is the saturated vapour pressure of the adsorbing nitrogen.

2.4.3 Oxygen Chemisorption

Chemisorption of oxygen studies were carried out at room temperature. The adsorbing oxygen gas was passed through a dry ice/methanol slush bath, and admitted to the sample. The weight uptake per g of catalyst was recorded against each pressure of oxygen. The weight uptake was then converted to the number of μmoles of oxygen chemisorbed per g of catalyst.

2.5 TREATMENT OF RESULTS

Surface Area Measurements

A measured volume of the gas was admitted to the sample and after equilibrium had been established the residual pressure was measured and the amount of gas remaining in the gas phase was calculated. The difference in these two quantities corresponds to the volume of adsorbate adsorbed. The results are plotted according to the B.E.T. equation[6].

$$\frac{P}{V(P_o-P)} = \frac{1}{V_m C(T)} + \frac{[C(T)-1]P}{V_m C(T) P_o} \qquad 2.1$$

where P = Equilibrium adsorbate gas pressure at the isotherm temperature.

V = Volume of gas adsorbed at pressure P.

P_o = Saturated vapour pressure of the adsorbate at isotherm temperature.

V_m = Volume of gas corresponding to monolayer coverage of the surface.

$$C(T) \alpha \exp (\Delta H_{ads} - \Delta H_{liq})/RT$$

A plot of $P/V(P_o-P)$ versus the relative pressure P/P_o should give a straight line of slope $S = C(T)-1/V_m\ C(T)$ and intercept $I = 1/V_m\ C(T)$ such that $V_m = \frac{1}{S+I}$. The surface area of the catalyst can be calculated from V_m provided that the cross-sectional area of the adsorbate molecule is known.

The area of the catalyst sample A (m^2) is given by

$$A = \frac{V_m \times N_A \times A_m}{22.4 \times 10^{-3}} \qquad 2.2$$

where N_A = Avogadro's constant.

V_m = Volume of gas corresponding to monolayer coverage.

A_m = Molecular cross sectional area of the adsorbate. The molecular cross sectional area of nitrogen was taken as 16.2 $\AA^2$.

So that the area of 1 g of sample (specific surface area) is given by $A/X(m^2\ g^{-1})$ if the weight of the sample used is X g.

2.6 RESULTS

2.6.1 B.E.T. Specific Surface Area

The specific surface area of each sample was evaluated from the nitrogen adsorption isotherm by using the conventional B.E.T. method. The B.E.T. equation was applied in the relative pressure range of 0.03-0.3. The isotherms are shown in figure 2:4. The specific surface areas of the samples are summarised in table 2:1.

The estimated specific surface area of the 'as-received' sample is in excellent agreement with the previously reported value in the literature[7]. As listed in table 2:1 and illustrated in figure 2:4 the specific surface area decreased with increasing alkali concentration. The effects of the alkali on the total

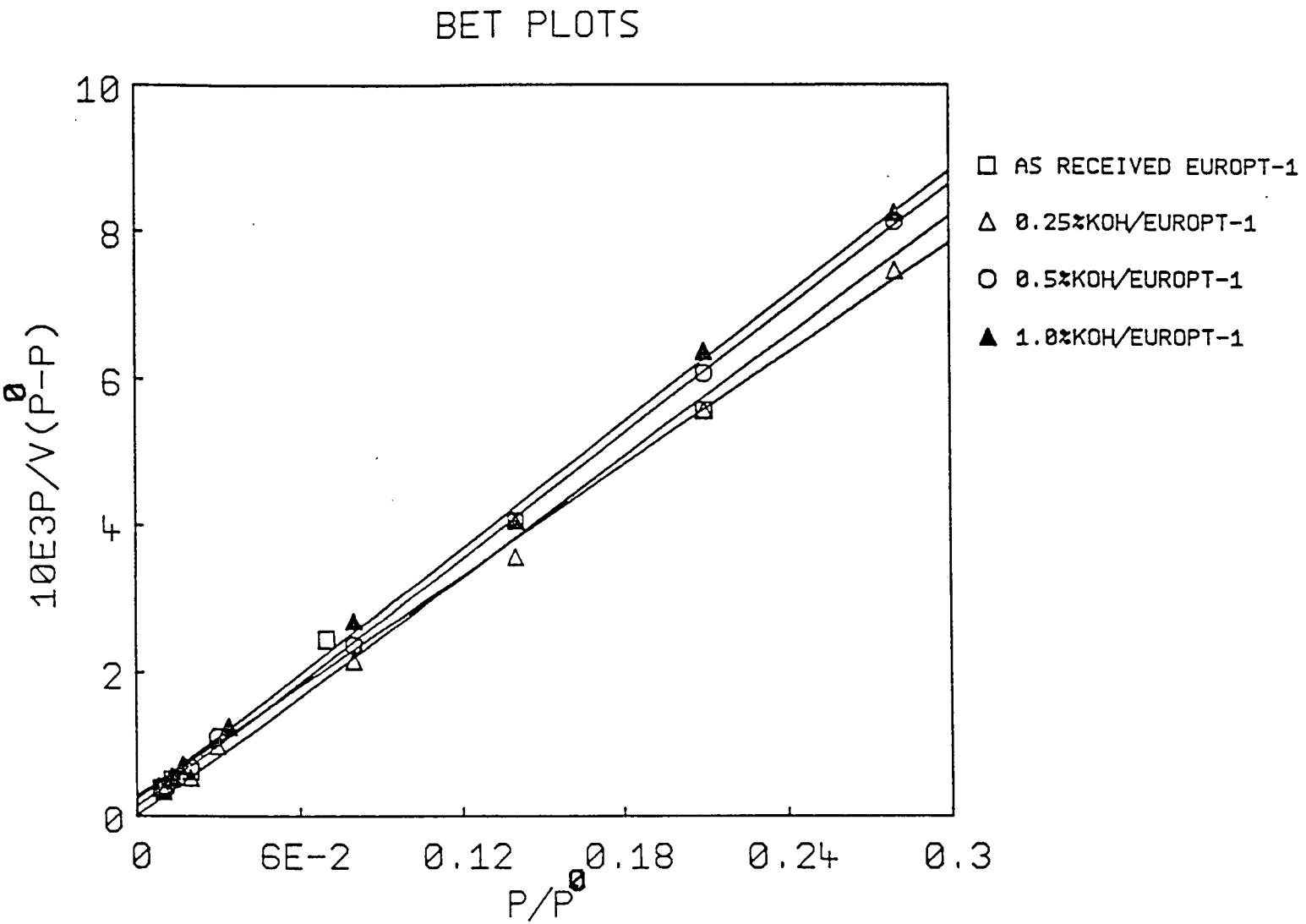

Fig. 2.4 BET Plots

TABLE 2.1

TOTAL SURFACE AREAS BY ADSORPTION OF NITROGEN

AT 77 K AND OXYGEN CHEMISORPTION AT ROOM TEMPERATURE

Catalyst	Surface Area $m^2\ g^{-1}$	% Surface Area	Oxygen Uptake μ moles g^{-1}	% Oxygen Uptake
As-received EUROPT-1	186	100	86	100
0.25 % KOH (wt)/EUROPT-1	170	92	72	83
0.50% KOH (wt)/EUROPT-1	148	81	62	72
1.0% KOH (wt)/EUROPT-1	132	71	38	44

surface area were similar to those reported earlier by others[8-11]. The alkali effects are dealt with in detail in the forthcoming chapters.

2.6.2 Oxygen Chemisorption

The adsorption isotherms of oxygen at room temperature are shown in figure 2:5. The isotherms extending to an equilibrium pressure of 13.33 K Pa or higher, give values for the total extent of chemisorption, obtained by extrapolating the low gradient region to zero pressure, of 86 micromol oxygen per gram catalyst ('As-received' EUROPT-1). Again we find an excellent agreement with the previously reported mean value of 85.7 μ mol g^{-1}, in the literature[12].

Figure 2:5 shows that with increasing alkali concentration, the extent of oxygen chemisorption decreases. The reduction of oxygen uptake goes beyond that expected for the loss in surface area. When there is ~ 30% loss in the total surface area, oxygen uptake is reduced by 55.8%, listed in table 2:1. This reduction is explained by an alkali effect, as some of the available sites may be blocked by alkali, making the metal no more accessible to the adsorbing gases, as has been reported for other gases such as hydrogen, and carbon monoxide in alkali doped supported catalysts[8-11]. The trends in the decrease of the amount of oxygen chemisorbed are listed in table 2:1. Further details of the alkali effects are

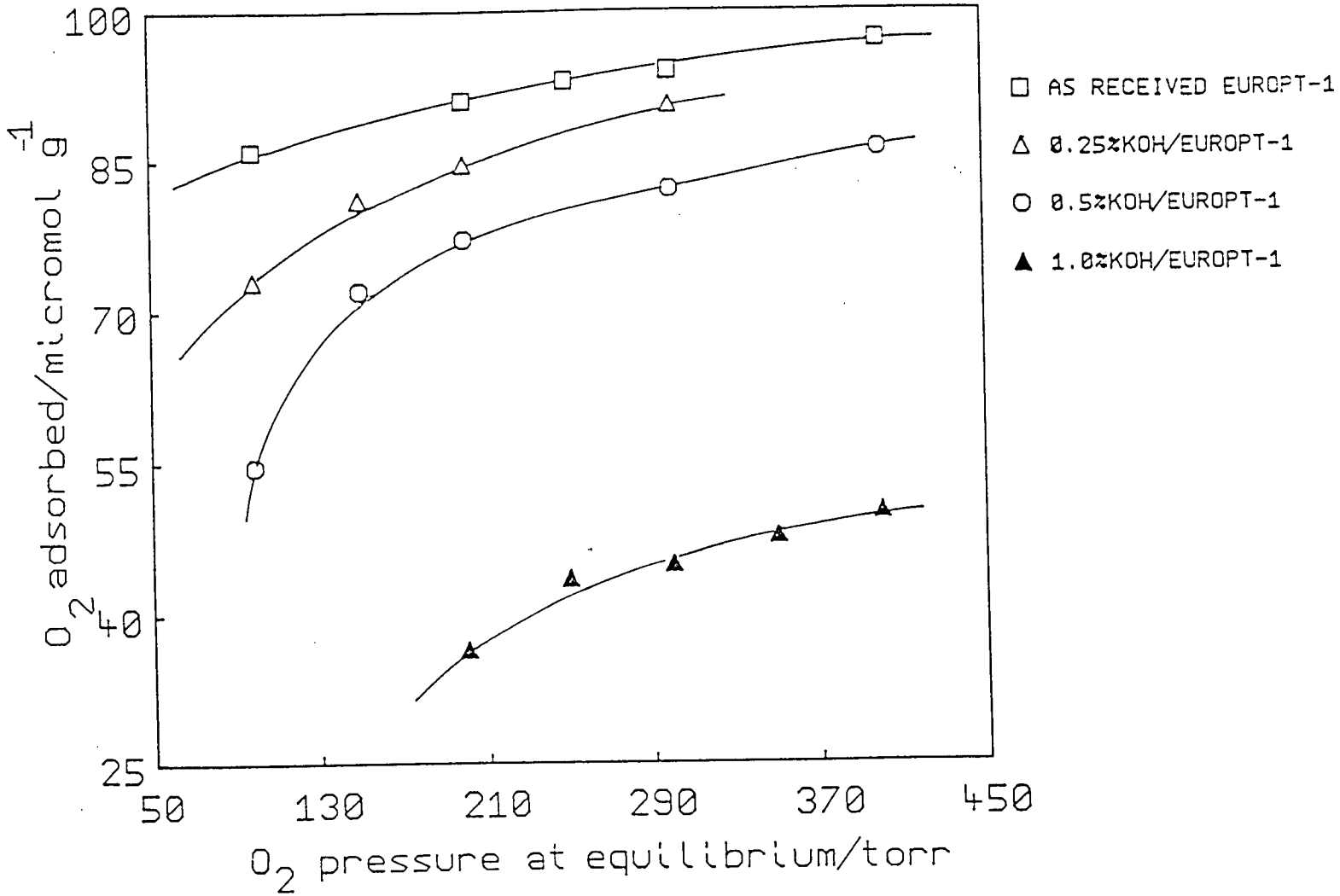

Fig. 2.5 Isotherm for the Adsorption of O_2 at Room Temperature

discussed in the rest of the thesis in appropriate sections.

REFERENCES

1. R.B. Anderson in: *Experimental Methods in Catalytic Research*, Vol. 1, Eds. R.B. Anderson and R.J. Dawson (Academic Press, New York, 1976).
2. G. Lohrengel and M. Baerns, *Appl.Catal.* 1 (1981) 37.
3. G.C. Bond, *Catalysis by Metals* (Academic Press, London and New York, 1962).
4. J.R. Anderson, *Structure of Metallic Catalysts* (Academic Press, New York, 1975).
5. Instruction Manual "Cahn Electrobalance", R.G. Cahn Instrument Company, California, U.S.A.
6. P.H. Emmett in: *Catalysis*, Vol. 1, ed. P.H. Emmett (Reinhold, New York, 1954).
7. G.C. Bond and P.B. Wells, *Appl.Catal.* 18 (1985) 225.
8. M.E. Dry and C.L. Ferreira, *J.Catal.* 7 (1967) 352.
9. F.E. Shephard, *J.Catal.* 14 (1969) 148.
10. A. Cimino, M. Boudart and H.S. Taylor, *J.Phys.Chem.* 58 (1954) 796.
11. M.E. Dry, T. Shingles, L.J. Boshoff, and G.J. Oosthuizen, *J.Catal.* 15 (1969) 190.
12. P.B. Wells, *Appl.Catal.* 18 (1985) 259.

CHAPTER 3

TEMPERATURE PROGRAMMED REDUCTION AND TEMPERATURE PROGRAMMED DESORPTION OF H_2 AND CO

3.1 INTRODUCTION

3.1.1 Temperature Programmed Reduction

Temperature programmed reduction (TPR) has gained increasing importance for the characterisation of catalysts since the first application by Robertson *et al.*[1] The TPR technique has been applied successfully to the study of support materials[2-3], pretreatment procedures[4-5], and action of promoters on the reducibility of the catalyst surfaces. A comprehensive review on the basic concepts of the TPR techniques, including many experimental profiles, has been given by Hurst *et al.*[6].

Temperature programmed reduction is a recently developed technique used to chemically characterise supported metal catalysts[6,7]. During TPR a hydrogen containing gas mixture continuously perfuses the catalyst bed, while the temperature of the bed is raised linearly with time. By measuring the consumption of hydrogen as a function of temperature, a TPR profile is obtained. Such profiles are used to determine the chemical constitution and environments of the catalytic components. The area under the resulting reduction peak is proportional to the amount of hydrogen consumed in the process. The practical applications of TPR have increased dramatically because of

its ease in providing quick assessment of the differences between catalysts prepared under different conditions.

This technique has been used to characterise catalysts at different stages of a preparation sequence. The sample can be bulk[8-9], supported monometallic[9-12], or supported bimetallic materials[13-14]. One of the first studies in which TPR was used as a characterisation technique was performed by Robertson *et al.*[1] on the reduction of Cu-Ni/SiO_2 catalysts, and affirmed the complete reduction of the metals, and was able to identify alloying. Later studies of Wagstaff and Prins[4] confirmed the power of TPR in the characterisation of bimetallic Pt-Ru/Al_2O_3 and Pt-Ir/Al_2O_3 catalysts[4].

Vis *et al.*[15] showed that the temperature programmed technique is a very useful way of characterising supported noble metal catalysts. The authors suggested that by using TPR the state of a reduced or oxidised catalyst could be successfully studied.

Bond *et al.*[16] studied a Pt/SiO_2 catalyst (EUROPT-1) by TPR. EUROPT-1 has already been well characterised[17-21]. The catalyst in the as-received condition comprised substantially a platinum oxide rather than metallic platinum, not-withstanding the fact that it had been reduced by the manufacturer as part of its preparation. The TPR results showed that hydrogen consumption began at subambient temperature ($\approx$ 200 K). The single peak of the reduction profile was centred at 330 K, hydrogen

consumption being 317-347 μmole per g catalyst and the corresponding H/Pt ratio being 1.96-2.11. There followed immediately a small but clear hydrogen desorption having a broad minimum at 480 ± 20 K which indicated that during the process of reduction some of the hydrogen is chemisorbed and is then desorbed at higher temperatures. There was evidence of further desorption of hydrogen above about 670 ± 20 K and this was attributed to spillover hydrogen.

Sermon *et al.*[22] obtained temperature programmed bulk reduction (TPBR) profiles and results for the reduction of hexachloroplatinum acid supported upon silica in 298-693 K temperature range. The sample had an average platinum particle size of 4.27 nm and yielding 6% (wt.) Pt after reduction. These peaks showed maximum rates of hydrogen consumption at 373, 373-523 and > 523 K. The average quantities of hydrogen consumed in each peak are shown to be 5, 53 and 7% of the consumption predicted for complete reduction. Results indicated that reduction is a two- or three-step process with maximum rate appearing at temperatures affected by ultimate platinum dispersions, the nature and porosity of support and the pretreatments, and starting conditions used.

Huizinga *et al.*[10] studied the reduction and oxidation behaviour of platinum (supported on γ-alumina and TiO_2) catalysts. The reduction peak temperature was found to be dependent on the temperature of the primary oxidation.

The higher the oxidation temperature the lower the TPR peak temperature and the higher the hydrogen consumption. During the oxidation small particles were formed which were more easily reduced. For Pt/Al_2O_3 no decomposition of PtO_2 was observed up to 750 K, while the bulk PtO_2 decomposed around 600 K. This demonstrated that there is substantial interaction between PtO_2 and Al_2O_3. For PtO_2 supported on TiO_2 and SiO_2 this interaction was much weaker and on these supports, PtO_2 decomposed at lower temperatures than on alumina. Reduction of Pt/TiO_2 led to metal assisted reduction of the support. Below 500 K only a small part of the support has been reported to be reduced (reversibly) in the near vicinity of the metal particles. Above 500 K further metal assisted reduction of TiO_2 support took place, probably promoted by increased ion mobility.

3.1.2 Temperature Programmed Desorption

The interaction of gases such as hydrogen, nitrogen and carbon monoxide with metal surfaces have shown that the process of adsorption, surface reactions and desorption can be very complex in nature[20-23]. Even when the catalyst is a single crystal and the experiments are carried out in a well controlled environment using ultra high vacuum conditions, the interpretation of the mechanisms of desorption or adsorption are not clear[6,23]. A reasonably consistent basis for analysis of these

processes has emerged from experiments performed on unsupported metals, under ultra high vacuum conditions. Many insitu techniques such as Auger electron spectroscopy, ultraviolet photoemission spectroscopy, X-ray photoelectron spectroscopy, work function changes, flash desorption, mass spectrometry and thermal desorption spectra have been employed[23].

The technique of flash desorption when applied to porous catalysts, finds its analogue in what is generally called temperature programmed desorption (TPD). Both techniques consist of observing the products desorbing from the surface as a function of temperature. Originally TPD was applied to oxide catalysts to get information on binding and reaction sites.

Frennet *et al.*[20] studied hydrogen desorption from the Pt/SiO_2 catalyst (EUROPT-1) as a function of variation of the initial content of adsorption. Desorption from an initially highly covered surface showed evidence for three adsorbed states of hydrogen over a temperature range of 100-700 K, whereas medium and low initial coverages gave desorptograms which showed only two components. Desorption over the range 293-823 K from a surface having initially a high coverage of adsorbed hydrogen showed two components of desorption, completed at 680 K. Further desorption occurred over the range 680-830 K, and the size of this feature varied with the time of pretreatment of the sample in hydrogen at 673 K (reduction temperature).

When the desorption temperature was extended to 900 K, the desorptogram showed three components desorbed in the region 100-350 K, 300-700 K and 700-900 K. Thus, temperature programmed desorption provided evidence of the existence of four states of adsorbed hydrogen on EUROPT-1. The fourth state, i.e. high temperature peak, was attributed to the spillover hydrogen.

Vong *et al.*[24] reported temperature programmed desorption profiles extending from 273-900 K, obtained for hydrogen preadsorbed at 273 K and 101 KPa for 30 minutes on a 6% Pt/SiO_2 catalyst. Three different maximum rates of chemisorbed hydrogen on platinum were indicated by peaks appearing in the TPD spectra at specific temperatures (T_{max}) at *ca.* 347-397, 573-633 and 693-786 K named as β_1, β_2 and β_3 respectively. The total size of the peaks was too large to be accounted for in terms of desorption of Pt-held hydrogen alone, although this quantity did vary significantly with adsorption pressures. No desorption peak was reported in the TPD of the support alone. It indicated that the β_3 peak was associated with the spillover hydrogen, which migrates back from the silica support to the platinum metal and then desorbs.

Komer *et al.*[25] in 1969 studied hydrogen desorption from Pt/SiO_2 and reported the desorption of hydrogen between 370-570 K, depending on the amount of preadsorbed hydrogen. In an early TPD study of supported metals, Contour *et al.*[26] reported two types of sites for hydrogen

desorption from Ir/Al_2O_3. They reported only one hydrogen desorption peak from unsupported Ir and an additional low temperature peak was present on alumina supported Ir.

Aben *et al.*[27] characterised a supported catalyst (Pt/Al_2O_3) by using hydrogen TPD for their study of benzene hydrogenation. They observed a complex spectrum showing three peaks in the temperature range of 240-670 K, which they related to a heterogeneous surface with at least three adsorption sites. They changed the H/Pt ratio by pretreatment from 670-1070 K, and observed a change in the ratio in which the various sites contributed to the overall change in H/Pt value. The authors pointed out that the amount of hydrogen adsorption is widely used to determine specific metal surface area but this does not account for the surface heterogeneity. They obtained a correlation between hydrogenation activity for benzene at 320 K and the low temperature hydrogen desorption peak. Thus they concluded that a large part of platinum surface area measured by the hydrogen chemisorption fails to contribute to the number of sites essential for benzene hydrogenation.

Study of hydrogen desorption from supported Pt (Al_2O_3, SiO_2 and TiO_2 supports) demonstrated the value of TPD for understanding processes on supported catalysts. Menon *et al.*[28] studied hydrogen desorption following catalyst reduction at various temperatures; higher reduction temperatures shifted the hydrogen desorption peaks to

higher temperatures. However, some hydrogen was retained irreversibly after reduction and they carried out TPD in a 5% H_2/Ar stream to analyse the reuptake of hydrogen. For a Pt/TiO_2 catalyst reduced at 470 K, they observed H_2 desorption at 570 K followed by reuptake to reduction of Pt and TiO_2.

Carbon monoxide desorption has also been studied by TPD from several metals. Komer *et al.*[25] first reported CO desorption from supported platinum. The authors observed a flat broad spectrum from 320-870 K. Carbon monoxide desorption has since been studied by several workers. Foger and Anderson[29] reported a broad CO desorption spectrum from room temperature to 850 K, for CO desorption from Pt/SiO_2 and Pt/Al_2O_3. Way and Falconer[30] likewise reported CO desorption over a broad temperature range for a series of Pt/SiO_2 catalysts of varying dispersions. Herz *et al.*[31] carried out CO desorption from Pt/Al_2O_3 into vacuum and observed desorption from 295-770 K, but most of their CO desorbed between 380-550 K, in contrast to the others' studies.

Foger and Anderson[29] attributed the broad profile to crystallographic inhomogenity of the platinum crystallites. Herz *et al.*[31] however indicated the peaks observed by others broadened by readsorption of CO. Their vacuum conditions significantly decreased the chances of readsorption and decreased the temperature for desorption.

Herz and McCready[32] carried out TPD of CO from 0.1%

(wt.) Pt/Al_2O_3. At a platinum dispersion of 100% (CO/Pt = 0.92) a relatively intense, narrow CO desorption peak was obtained at low temperature (355 K at 0.93 K s^{-1}) followed by a low, broad desorption band extending to 750 K. As the platinum dispersion decreased to 80% (CO/Pt = 0.70) and then 70% (CO/Pt - 0.64) as a result of pretreatment in oxygen and hydrogen, the fraction of CO that desorbed in the low temperature peak decreased and the fraction of CO that desorbed in the broad adsorption band increased. The authors interpreted the low temperature peak as desorption of CO from very small platinum particles supported on transitional Al_2O_3 and the broad desorption peak was interpreted as CO desorption from larger platinum particles.

The interaction of alkali metal atoms with the transition metal surfaces has received considerable attention in the past. Interest in these systems originated from the significant enhancement observed in electron emission upon alkali adsorption[33]. An understanding of the alkali induced phenomenon on transition metal surfaces is also important due to their promoter action in heterogeneous catalysis[34]. In particular, potassium is used in two important catalytic reactions, the hydrogenation of carbon monoxide and synthesis of ammonia. In an attempt to understand the promoter action recent coadsorption experiments have shown that alkali metals change the chemisorptive

characteristics of small reactive molecules (CO, H_2 and N_2) on catalyst surfaces.

Zhou *et al.*[35] studied hydrogen TPD from clean and potassium covered Pt(111) single crystals, and concluded that the saturation coverages of hydrogen adsorption on Pt(111) single crystals decreased with increasing K-coverages, but the desorption energy of H (adsorbed) increased. At higher K coverages (θ K $\geq$ 0.25) no hydrogen was adsorbed. The authors suggested that although K inhibited hydrogen adsorption, it stabilised the adsorbed hydrogen. These results suggested that potassium promotion of catalysts for CO hydrogenation or ammonia synthesis is multifunctional, altering both the hydrogen and carbon monoxide or nitrogen behaviour.

Crowell *et al.*[36] carried out thermal desorption studies for various CO exposures on a Pt(111) single crystal at a constant potassium coverage. They observed a shift of desorption peak temperatures by about 50 K from a clean Pt(111) single crystal. The trend of shifting peaks towards higher temperatures became more apparent as the potassium coverage increased, and at a coverage of θ K = 0.6 no CO adsorption was seen.

Bonzel *et al.*[33] studied CO desorption from clean and K covered Ni(100) single crystal surfaces by thermal desorption spectroscopy (TDS). They reported a shift of desorption temperature by about 90 K to higher temperatures relative to clean Ni(100), and also reported

that the higher the K coverages the lower the CO coverages.

Gochis *et al.*[37] studied CO desorption from Ni/SiO_2 catalysts promoted with Na and K. With increased promotion, CO desorption was observed to be complete at much lower temperatures (775 K on Ni versus 535 K for K/Ni) and the H_2 peak temperature also decreased. In contrast to Gochi's results, Gozalez *et al.*[38] reported CO desorption from K promoted Ru/SiO_2 catalyst. Potassium apparently caused CO to bond more strongly to the surface.

Amenomiya *et al.*[39] studied H_2, N_2, CO and CO_2 desorption from a K_2O promoted iron catalyst. Adsorption was carried out at as low as 77 K in their study. Several states of hydrogen were observed including unactivated H_2 adsorption at low temperature and additional activated adsorption as the temperature was raised. When higher temperatures (570 K) and pressures (98.4 KPa) were used, a new peak was seen at 390 K. The shape of the H_2 peaks in TPD resembled typical isobars observed in doubly promoted iron catalysts. They suggested that the saturated amount of H_2 obtained from TPD could be used to measure the number of metal sites. For CO adsorption at 77 K a large CO peak was reported below 200 K (physical adsorption) and it had a shoulder up to 450 K. A smaller CO peak was reported above 820 K. Adsorption at 195 K gave three peaks between 200 and 450 K and one peak at 920 K.

In the present study the adsorption of carbon monoxide

and hydrogen on the 'as-received' and alkali doped EUROPT-1 catalyst was investigated. It thus helped to know the effectiveness of the promoter and some fine details about the existence of various binding states.

3.2 EXPERIMENTAL

3.2.1 Temperature Programmed Reduction (TPR)

The apparatus used in the temperature programmed reduction experiments (TPR) was similar to that described by Robertson *et al.*[1], and shown schematically in fig. 3.1

The reducing gas, consisting of a mixture of 5% vol. hydrogen in argon, was obtained from the British Oxygen Company (BOC) and was purified by passage through a deoxo unit (Engelhard) and a 4A molecular sieve trap. The gas flowed through one leg of the thermal conductivity detector (from a Perkin Elmer F-33 gas chromatograph), through the sample cell, through a trap immersed in a dry ice/ethanol bath (to condense water formed during reduction) and back to the second leg of the thermal conductivity detector.

A weighed amount of the sample was placed in the quartz reactor (fig. 3.2), heated by a tubular furnace in a programmed way using a Stanton Redcroft universal temperature programmer. The quartz reactor was connected to the apparatus by stainless steel ¼" Swagelok nuts with teflon ferrules (graphite ferrules were used in TPD experiments, as the sample was heated to higher

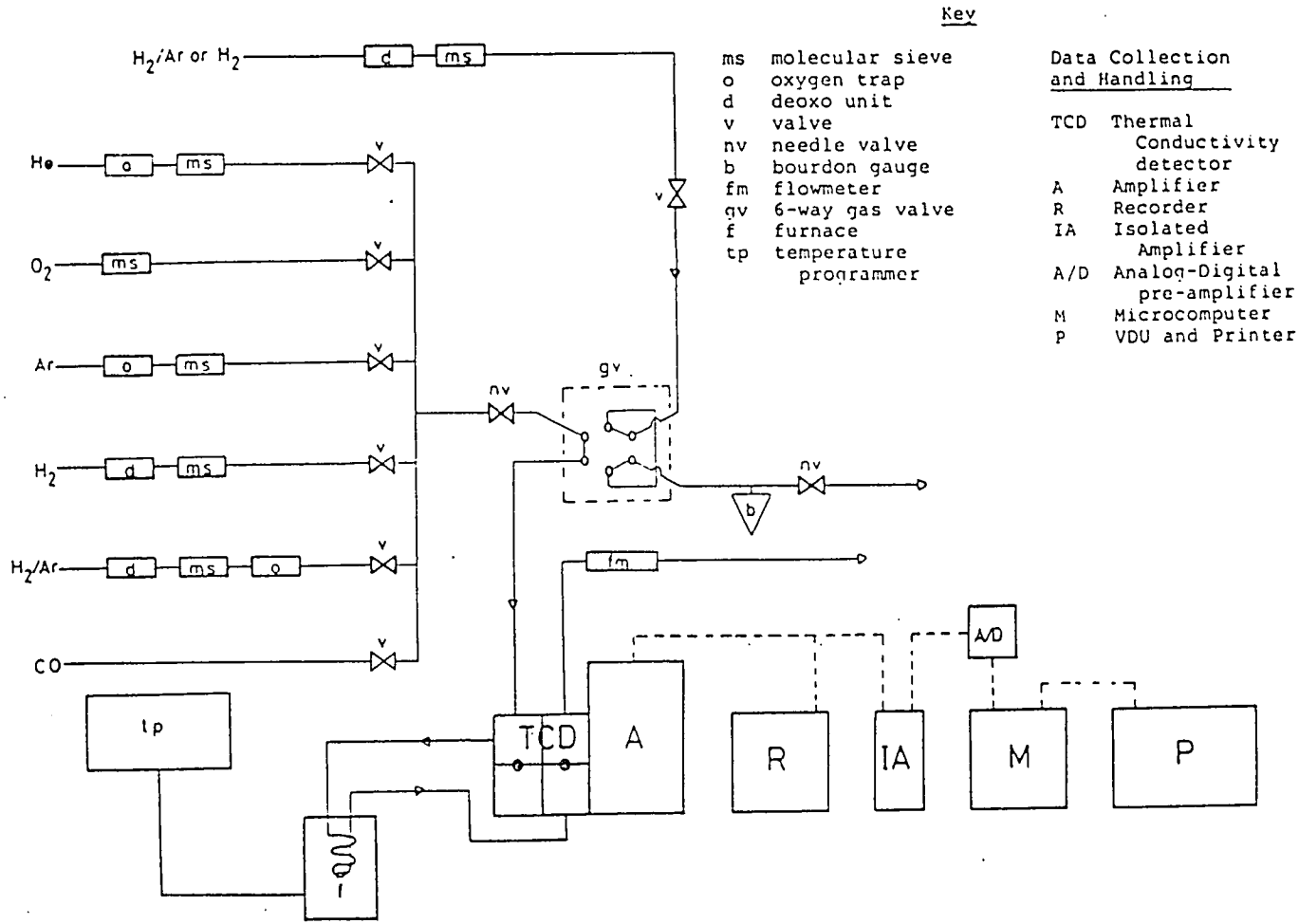

Fig. 3.1 TPR/TPD Apparatus

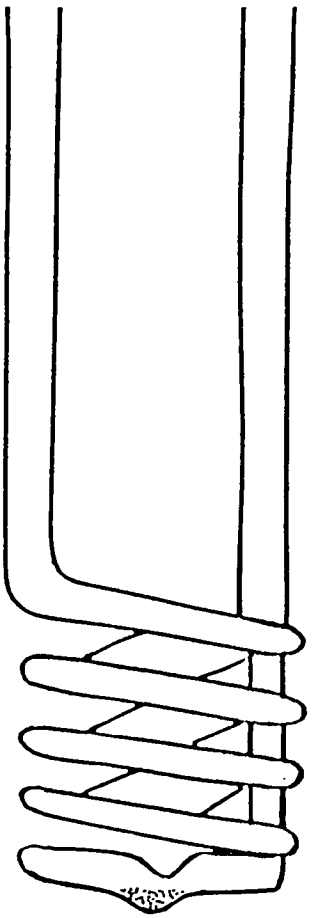

Fig. 3.2 Quartz Reactor

temperatures, typically 900 K). Prior to any measurements the catalysts were subjected to a variety of pretreatments using the gas handling system and furnace. During TPR the 5% H_2/Ar was passed through the system at a flow rate of 10 cm^3 per minute and the reactor was heated at a linear programmed rate of 10 K per minute.

The signal from the thermal conductivity detector was fed to one of the channels of a two channel potentiometric recorder (Kripp and Zonen BD-9). The second channel (temperature channel) received the signal from a Chromel-Alumel thermocouple strapped to the outside of the sample cell directly above the catalyst sample. A second thermocouple, placed in the same position, was connected to a Comark digital thermometer and was used to calibrate the temperature channel of the recorder.

The area under a TPR peak is proportional to the amount of hydrogen consumed in the reduction process. To enable qualitative measurements to be made, the detector was calibrated by determining the area under the reduction profile for a sample of nickel oxide (grade 1, NiO Johnson-Mathey plc). By assuming the oxide to be stoichiometric, and to be fully reduced in the TPR experiments, it was possible to equate the TPR peak areas for a known amount of NiO to the number of moles of hydrogen required to reduce oxide to nickel metal. The change in hydrogen concentration was monitored by an on-line microcomputer. This and its attendant software,

developed by Mr. A. King of this department, allowed the signal from the detector to be digitized, stored on disk, and subsequently to be integrated.

3.2.2 Temperature Programmed Desorption

The apparatus was the same as the one used in TPR experiments. In TPD, the catalysts, following a reduction procedure and cooling to room temperature, are exposed to an adsorbate which is then desorbed as the temperature of the furnace is raised linearly with time into an inert carrier gas. The change in the carrier gas composition is monitored by the thermal conductivity detector. In metal surface area calculations the adsorbate gas is usually hydrogen or carbon monoxide, and the inert carrier gas, argon or helium respectively. By monitoring the amount of adsorbate desorbed, the amount of exposed metal could be determined.

The hydrogen or carbon monoxide adsorbates could be introduced to the catalyst by two methods in this particular apparatus; either by continuous flow over the reduced catalyst for the required amount of time to ensure saturation coverages; or by using the gas sampling valve upstream from the catalyst and injecting pulses of pure hydrogen, carbon monoxide or 5% H_2/Ar.

The latter method could also be used to estimate the metal surface area of the catalyst. The injection of five pulses proved to be adequate in this method, the last

three pulses being of the same area indicating saturation of the adsorption sites. These were used to obtain an average value for the peak area of the pulse and by adding the difference in areas of the first two pulses from this average pulse value the total amount of adsorbed gas could be calculated.

3.3 PROCEDURE

3.3.1 TPR

Samples of 'as-received' and alkali doped EUROPT-1 (0.05 g) were placed in a quartz reactor, lowered into a tubular furnace, cooled to 190 K by liquid nitrogen. Before starting TPR, pure argon was replaced by a 5%H_2/Ar mixture during an isothermal period (at 190 K). At this stage the thermal conductivity detector (TCD) was allowed to stabilise for 30 minutes. TPR was started by heating in a programmed way.

3.3.2 TPD

Samples of 'as-received' and alkali doped EUROPT-1 (0.0125 g) were placed in a quartz reactor, connected to the conventional TPD apparatus. Pure argon gas was allowed to flush the sample for five minutes and was then replaced by pure hydrogen at room temperature. The sample was heated at the rate of 20 K per minute up to 673 K for 90 minutes. At reduction temperature the flow of hydrogen was replaced by flowing argon. The flow of

argon was corrected to 10 cm^3 per minute. The sample was flushed for 30 minutes and cooled down in the furnace to room temperature. Hydrogen or carbon monoxide adsorbates were brought in contact with the reduced sample either by continuous flow or by pulses. Five pulses of 0.8 psi pressure were injected. The uptake of H_2 or CO was displayed and recorded. The integration of the peak areas made it possible to estimate the uptake quantitatively.

The thermal conductivity detector was then stabilised, followed by heating the sample from room temperature to 900 K.

The uncertainties in the temperature measurements, and H/M ratio based on the accuracy of technique used are estimated to be ± 20 K and 2% respectively.

3.4 RESULTS

3.4.1 TPR

Temperature programmed reduction (TPR) experiments on the 'as-received' EUROPT-1 (fig. 3.3) showed that hydrogen consumption began at subambient temperature (≈ 200 K). The T_{max} value for the main reduction peak is 320 K. The amount of hydrogen consumed and the corresponding H/Pt ratios are given in table 3.1. The observed hydrogen uptake must include that which is simultaneously chemisorbed on Pt zero valent particles formed by reduction of the oxide precursor. The slight asymmetry in the main reduction peak was due to a feature at 418 K.

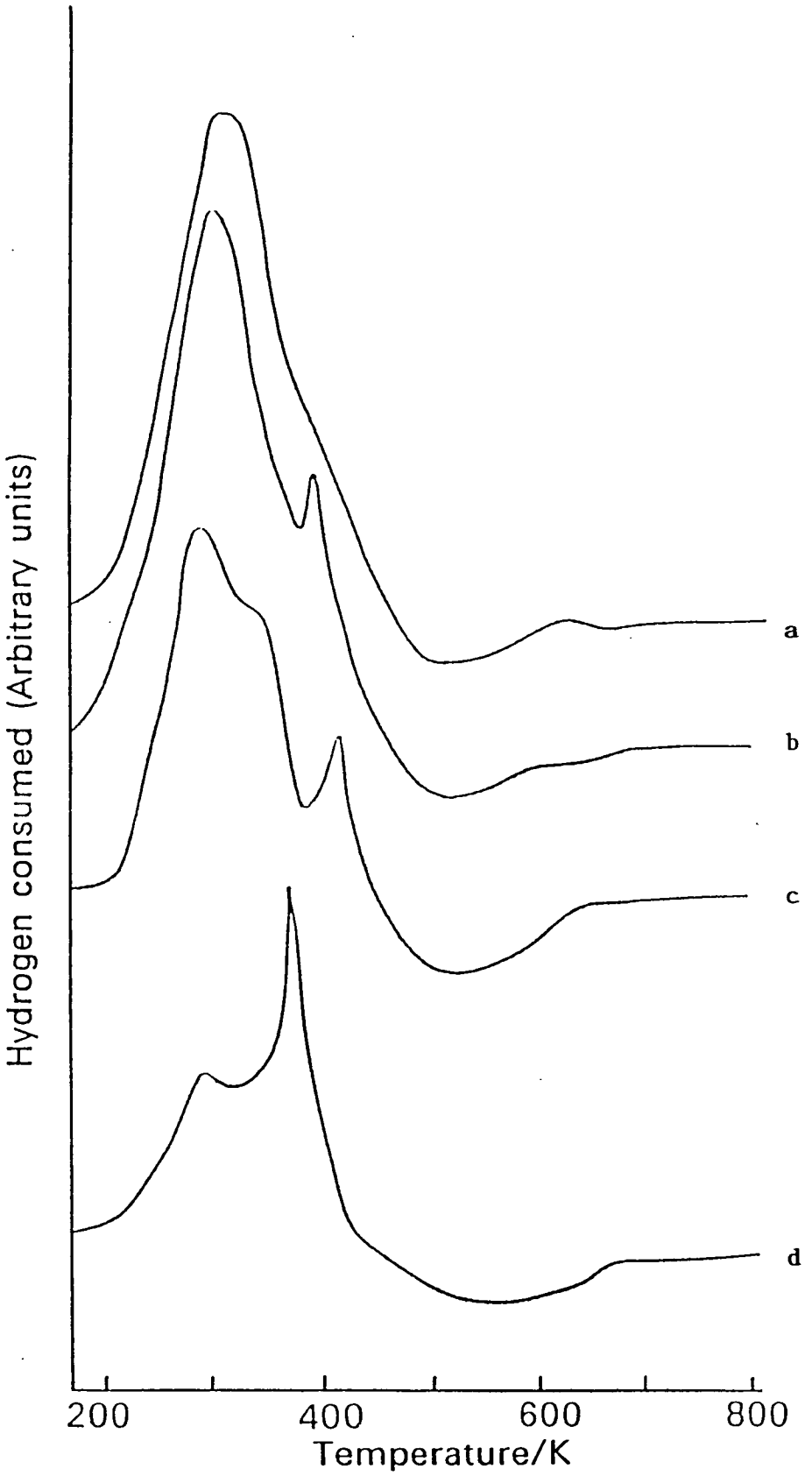

Fig. 3.3 TPR Profiles: (a) as-received EUROPT-1;
(b) 0.25% KOH (wt)/EUROPT-1;
(c) 0.50% KOH (wt)/EUROPT-1;
(d) 1.0% KOH (wt)/EUROPT-1.

TABLE 3.1

TPR MEASUREMENTS ON AS-RECEIVED AND ALKALI DOPED EUROPT-1

Catalyst	T_{max}/K			Hydrogen Uptake H_2 μ moles g^{-1}	H/Pt	Hydrogen Desorption T_{max}/K
As-received EUROPT-1	320	-	-	341	2.10	512
0.25% KOH (wt)/EUROPT-1	308	418	-	300	1.86	520
0.50% KOH (wt)/EUROPT-1	305	365	430	280	1.72	530
1.0% KOH (wt)/EUROPT-1	300	380	-	243	1.50	560

There followed immediately a small but clear hydrogen desorption trough having a broad minimum at 512 K (fig. 3.3a). The area for this desorption feature corresponded to 42-56 μmole per g of catalyst, i.e. H/Pt ratio of 0.24-0.38. There is evidently an overlap between the process of reduction (including hydrogen chemisorption) and hydrogen desorption.

There was evidence of a further small desorption (fig. 3.3a) of hydrogen above about 653 K. Estimation of the amount desorbed in this region was approximately 22 μmol H_2 per g catalyst, and it is probably attributable to spillover hydrogen. Spillover hydrogen has been observed by many workers[40-44]. It has been defined as the migration of hydrogen atoms from a metal which is active in the dissociative adsorption of hydrogen, to the metal support which, by itself, has no or little activity for dissociative hydrogen adsorption[40-44].

The reduction profile of 0.25% KOH (wt.)/EUROPT-1 is shown in figure 3.3b. The reduction started at subambient temperature, similar to that observed for clean EUROPT-1. The reduction profile consisted of two incompletely resolved peaks. The T_{max} of the main peak (low temperature peak) appeared at 308 K. The hydrogen consumption was 300 μmol per g catalyst. The small high temperature peak, which appeared at 418 K, seemed to be consistent with the hint of a shoulder previously observed for clean EUROPT-1 at similar temperature.

The desorption peak has a broad minimum at 520 K, which is slightly higher than that observed for clean EUROPT-1. Again there is some trace of a further small desorption peak which can be attributed to the desorption of spillover hydrogen.

The TPR profile for 0.5% (wt.) KOH/EUROPT-1 is shown in figure 3.3c. The profile indicates existence of three reducible species shown by shoulders or incompletely resolved peaks. The main peak of the profile is centred at 305 K. The consumption of hydrogen and corresponding H/Pt ratios are given in table 1. A small shoulder at 305 K was followed by a distinct small peak at 430 K.

The desorption trough has a broad minimum at 530 K which appears to increase with increasing alkali concentration. The peak area corresponding to hydrogen consumption is listed in table 3.1.

No further desorption was observed at higher temperature.

In figure 3.3 profile 'd' shows the reduction behaviour of 1% KOH (wt.)/EUROPT-1 catalyst. The reduction again started at subambient temperature, similar to all the catalysts previously observed. The reduction profile consisted of two peaks; the first reduction peak with a maximum centred at 300 K followed by a very sharp peak at 380 K. The hydrogen consumption was 243 μmol per g catalyst and corresponding H/Pt ratio was 1.50 (table 3.1).

After reduction, a desorption trough which had a broad minimum at 560 K was again observed. The area under the peak and corresponding H/Pt ratio is given in table 3.1.

At higher temperature no further desorption was observed indicating the absence of spillover hydrogen.

The TPR of the support alone and of 1% KOH (wt.) doped support was carried out. No reduction peak was observed at all, under the same experimental conditions. Hence there was no reduction of support or alkali.

On comparison of the results obtained for the four catalysts the following observations were made.

1. There was a decrease in the amount of reduction with increasing alkali concentration.
2. The small shoulder observed in 'as-received' EUROPT-1 at 418 K becomes more distinct as the lower temperature reduction area decreased with increasing alkali concentrations.
3. As the lower temperature reduction area decreases there is little or no change in T_{max} of $\approx$ 300 K.
4. Spillover desorption is possibly less important in higher percentage alkali doped catalysts.

3.4.2 TPD of Hydrogen : by Flow Method

Temperature programmed desorption (TPD) profiles (273-900 K) obtained for hydrogen preadsorbed at 293 K and 101 K Pa for 30 minutes at the rate of 20 cm^3 per minute on clean and alkali doped EUROPT-1 (figure 3.4) show the

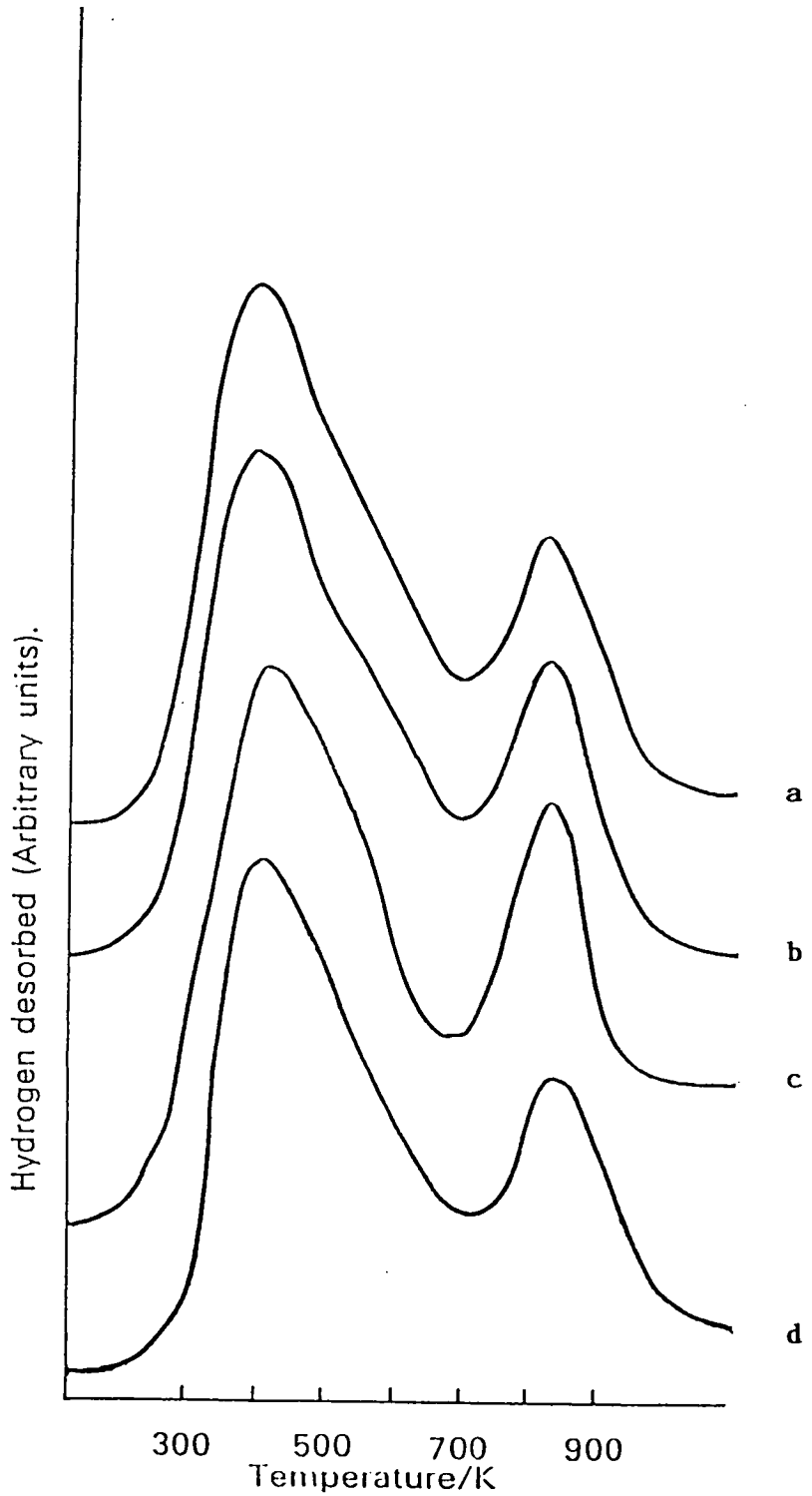

Fig. 3.4 Temperature Programmed Desorption of Hydrogen Preadsorbed at Room Temperature by Flow Method:

(a) as-received EUROPT-1;
(b) 0.25% KOH (wt)/EUROPT-1;
(c) 0.50% KOH (wt)/EUROPT-1;
(d) 1.0% KOH (wt)/EUROPT-1.

TABLE 3.2

TEMPERATURE PROGRAMMED DESORPTION OF HYDROGEN PREADSORBED BY FLOW METHOD AT ROOM TEMPERATURE

Catalyst	Amount of Hydrogen desorbed (μ mol g^{-1})		H/M		T_{max}/K	
	L.T	H.T	L.T	H.T	L.T	H.T
As-received EUROPT-1	140	54	0.84	0.32	400	820
0.25% KOH (WT)/EUROPT-1	139	54	0.79	0.32	400	820
0.5% KOH (wt)/EUROPT-1	128	66	0.77	0.40	440	825
1% KOH (wt)/EUROPT-1	140	54	0.84	0.40	440	830

L.T Low Temperature Peak

H.T High Temperatur Peak

rate of hydrogen desorbed as a function of time and hence temperature. All four experiments were performed under the same experimental conditions.

Two different maximum desorption rates of chemisorbed hydrogen on platinum were indicated by peaks appearing in the TPD spectra at specific temperatures. The quantity of hydrogen desorbed and results so obtained are given in table 3.2

Profile 'A' in figure 3.4 shows the TPD of hydrogen from clean EUROPT-1 catalyst. The desorption began at room temperature (293 K). The profile consisted of two well separated peaks centred at 400 and 820 K. The desorption was complete at 900 K. The estimate of hydrogen desorbed from individual peaks being 140 μmole hydrogen per g and 54 μmole hydrogen per g respectively (table 3.2).

On comparison of the results so obtained for the series of four catalysts the following observations were made.

1. All the four catalysts exhibited similar TPD profiles. However, a small shift towards higher temperature in the desorption maximum is evident.
2. The amount of hydrogen desorbed is too large to give a sensible estimate of metal dispersion.

3.4.3 TPD of Hydrogen : Pulse Chemisorption

The results obtained for desorption of hydrogen

preadsorbed by pulses shown in figure 3.5 a, b, c and d representing catalysts, 'as-received' EUROPT-1, 0.25%, 0.50% and 1.0% KOH (wt.)/EUROPT-1 respectively. The profiles show desorption of hydrogen as a function of temperature over a range of 293-900 K. All four experiments were performed under the same experimental conditions.

The uptakes of hydrogen by the pulse method are given in table 3.3. These agree well with the subsequent amount of hydrogen desorbed in the TPD profiles, for the respective samples.

The 'as-received' EUROPT-1 had the greatest dispersion with the values decreasing with increasing alkali concentrations. The TPD spectra show apart from the decrease in area, a shift towards higher temperatures for the maximum desorption rate, i.e. 390 K for EUROPT-1 for 475 K for the 1% KOH doped EUROPT-1 sample.

3.4.4 TPD of Carbon Monoxide

Profiles of CO desorption from 'as-received' and alkali doped EUROPT-1 are shown in figure 3.6 The CO desorption (TPD) was carried out over a temperature range 298-900 K. The minimum temperature at which the desorption began was 320 K and the maximum temperature of desorption completion was observed to be 900 K. This range of desorption temperatures is significantly higher compared with the previously observed for hydrogen TPD.

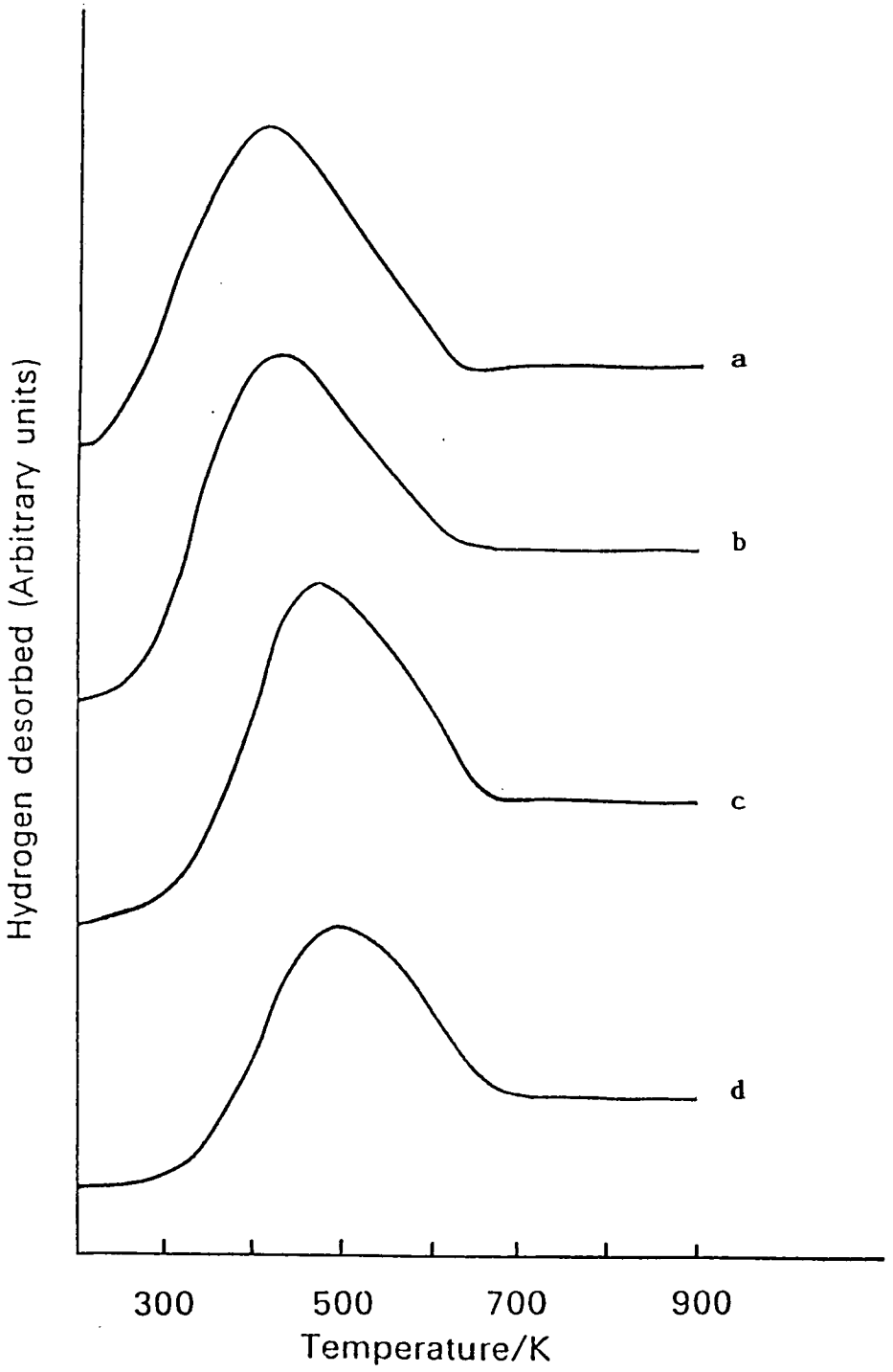

Fig. 3.5 Temperature Programmed Desorption of Hydrogen Preadsorbed at Room Temperature by Pulses:

(a) as-received EUROPT-1;
(b) 0.25% KOH (wt)/EUROPT-1;
(c) 0.50% KOH (wt)/EUROPT-1;
(d) 1.0% KOH (wt)/EUROPT-1.

TABLE 3.3

TEMPERATURE PROGRAMMED DESORPTION OF HYDROGEN PREADSORBED BY PULSES AT ROOM TEMPERATURE

Catalyst	Amount of Hydrogen μ mol g^{-1} Adsorbed	Desorbed	H/M	T_{max}/K
As-received EUROPT-1	112	107	0.60	390
0.25% KOH (wt)/EUROPT-1	92	90	0.54	400
0.50% KOH (wt)/EUROPT-1	73	72	0.44	438
1% KOH (wt)/EUROPT-1	60	58	0.36	475

The CO desorption profiles are broad peaks with shoulders at different temperatures of desorption indicating different unresolved binding states of carbon monoxide.

The CO desorption from 'as-received' EUROPT-1 gave a broad desorption profile with a distinct shoulder at 480 K, indicating a low temperature CO binding state. Following this shoulder there is an immediate rise in the peak height having a maximum at 530 K, indicating that most of the CO is desorbed at this stage. Finally, there is a high temperature shoulder at 700 K, which might be an indication of a third CO binding state.

The amount of CO taken up by the catalyst from pulses, and the amount desorbed during TPD was found to be in fair agreement, given in table 3.4.

The desorption of CO from 0.25% KOH (wt.)/EUROPT-1 is shown in fig. 3.6b. The profile is similar to the 'as-received' sample with a broad spectrum extending across 900 K, with the main peak at 539 K and low and high temperature shoulders at 520 and 700 K respectively.

The spectrum is similar in shape again for 0.5% KOH (wt.)/EUROPT-1 shown in fig. 3.6c, having three components with a continuing shift to higher temperature as a function of alkali. The trend in shift of peak positions is listed in table 3.4.

The TPD profile of CO from 1% KOH (wt.)/EUROPT-1 shown in fig. 3.6 is slightly different. The low temperature

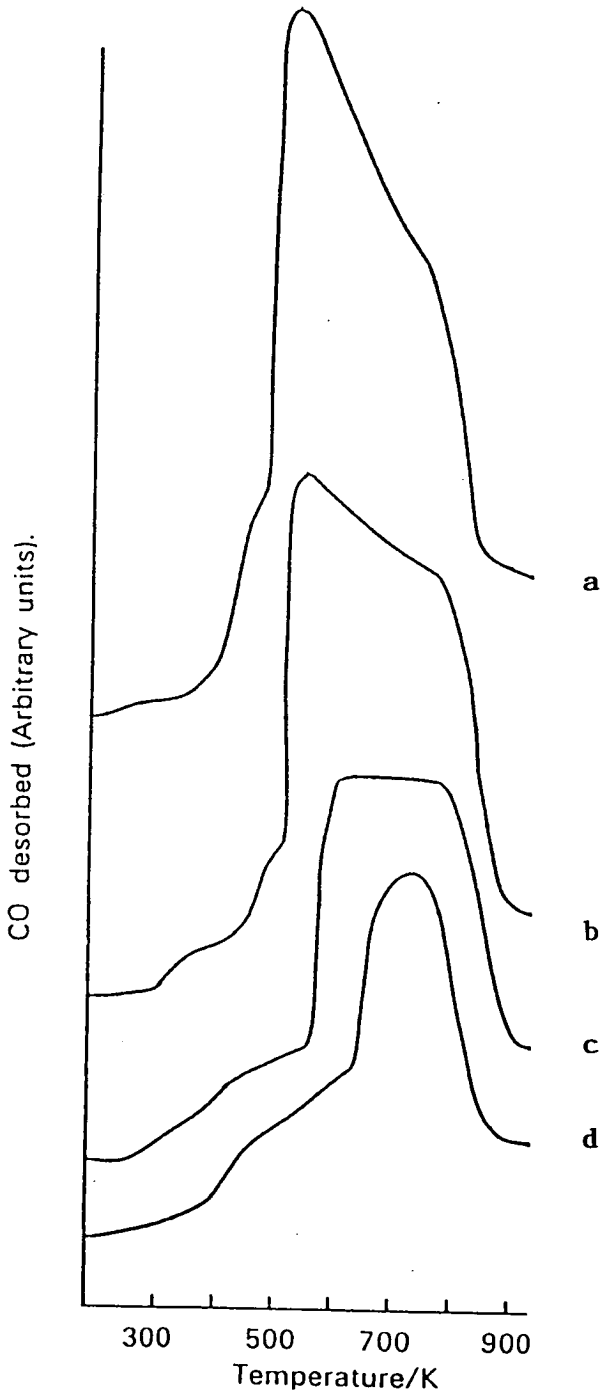

Fig. 3.6 Temperature Programmed Desorption of CO Preadsorbed at Room Temperature by Pulses:

(a) as-received EUROPT-1;
(b) 0.25% KOH (wt)/EUROPT-1;
(c) 0.50% KOH (wt)/EUROPT-1;
(d) 1.0% KOH (wt)/EUROPT-1.

TABLE 3.4

TEMPERATURE PROGRAMMED DESORPTION OF CO PREADSORBED BY PULSES AT ROOM TEMPERATURE

Catalyst	Amount of CO μ mol g^{-1} Adsorbed	Desorbed	CO/M	T_{max}/K		
As-received EUROPT-1	218	214	0.66	450	430	700
0.25% KOH (WT)/EUROPT-1	186	184	0.57	520	439	780
0.50% KOH (wt)/EUROPT-1	148	148	0.46	570	635	820
1.0% KOH (wt)/EUROPT-1	136	128	0.39	630	752	-

shoulder is similar to that previously observed. The shape of the profile indicates that the previous broad desorption profile collapsed into a single sharp high temperature desorption feature.

Accompanying these shifts in desorption maxima and changes in profile shapes there is also a reduction in the area of the desorption profile with increasing alkali.

3.5 DISCUSSION

3.5.1 TPR

The reduction profile of 'as-received' EUROPT-1 is presented in figure 3.3. The reduction peak centred at 320 K is symmetric with indication of a shoulder at about 418 K. The symmetric reduction profile is indicative of the crystallographic homogeneity of the catalyst[16].

Geus *et al.*[19] characterised 'EUROPT-1' by determining the size distribution. The authors also reported some work done by others. Size distribution was determined by high resolution transmission electron microscopy. Joyner[45] studied EUROPT-1 by extended X-ray absorption fine structure (EXAFS). It was reported that the particles consisted of disordered platinum oxide and the size distribution of the visible particles ranged from 0.9 nm to 3.5 nm; 75% of these particle were less than or equal to 2 nm in diameter. It was thus concluded that EUROPT-1 contained an even or homogeneous distribution of platinum particles.

Bond *et al.*[16] in a recent publication characterised EUROPT-1 by the TPR technique and reported a symmetric reduction peak at 330 K. Although this is in very good agreement with present results, where a T_{max} of 320 K was found. In this study it was also found that the reduction peak had a shoulder at 418 K, the origin of which is described later.

The reduction was followed by a small desorption trough (figure 3.3). It suggests that there is an overlap between the process of reduction (including hydrogen chemisorption) and the hydrogen desorption.

Evidence of a further small desorption was shown by the 'as-received' and 0.25% KOH (wt.)/EUROPT-1. This has been attributed to the spillover hydrogen, which is in agreement with the results presented by Bond *et al.*[16].

Hydrogen spillover has been reported by many workers, and various factors have been found to be responsible for the process of spillover. A large number of articles including a detailed review have been published in recent years[40-44].

Kramer *et al.*[40] studied adsorption of atomic hydrogen on alumina and reported definite proof of hydrogen spillover. No spillover was found when preadsorbed hydrogen on pure aluminium or platinum was desorbed. However, TPD hydrogen from alumina supported platinum indicated the desorption of spillover hydrogen in the temperature range similar to the present study. The rate

of hydrogen spillover has been reported to depend on hydrogen pressure, temperature of adsorption and metal dispersion.

Huang *et al.*[46] studied TPR of 4.4% Pt/Al_2O_3. The TPR procedure used was similar to the one used in the present work. The authors observed a long tailed desorption feature in the TPR spectrum at higher temperatures (573-673 K) which they attributed to spillover hydrogen desorbing.

Anderson *et al.*[47] studied the adsorption and TPD of hydrogen with Pt/zeolite and Pt-gold catalysts. In the TPD profiles the high temperature peak (700-750 k) had been assigned to the desorption of hydrogen from the support, this hydrogen consisted of spillover hydrogen.

The phenomenon of spillover seen in the present study is in excellent agreement with the reported results in the literature[16]. Further work towards the study of hydrogen spillover based on the research and postulates of other workers[40-44], concluded that hydrogen adsorption pressure and high metal dispersion would favour hydrogen spillover during TPD.

The reduction profiles of alkali doped EUROPT-1 are presented in figure 3.3. The changed characteristics, shapes and features of the reduction profiles are attributed to the presence of potassium. Potassium doping might affect the uptake of hydrogen during reduction in three ways.

1. Each potassium atom may reduce adsorption of many hydrogen atoms by poisoning or by direct blocking[35].
2. Loss of support structure, i.e. sintering of the support during catalyst preparation may cause encapsulation of the metal, making it no longer accessible to reduction, causing a decrease in the consumption of hydrogen.
3. Changes in crystallographic morphology of the catalyst, i.e. formation of larger crystallites.

Overall, the reduction profiles indicate two or more peaks or shoulders indicating the presence of different reducible species. In other words K-doping has caused inhomogeneity of the catalyst.

It is observed that the area under the reduction peak decreases with increasing alkali concentration and as already stated, a loss of BET area was also observed. This loss in total surface area and area under reduction peak with increasing alkali concentration is similar to that reported for alkali doping of magnetic and Ni/Al_2O_3 catalysts[48,49]. Lowering of metal surface area by potassium doping has been observed in the present study. Zhou *et al.*[35] reported a lowering of hydrogen adsorption on a K covered Pt(111) single crystal. The authors calculated that each K atom blocks 11 hydrogen adsorption sites, and further reported a complete inhibition of hydrogen adsorption at a potassium coverage of θ_K =0.25.

Dry *et al.*[48] studied K_2O promoted reduced magnetite

catalyst. X-ray line broadening studies showed that, those samples containing K_2O had larger crystallites. The authors attributed the loss of surface area to the growth of crystallite size and not due to any other reason such as pore blocking.

The sharp peaks/features seen in TPR of each alkali doped EUROPT-1 catalyst might be related to the originally present shoulder in the reduction profile of 'as-received' EUROPT-1 (fig. 3.3). This became distinct in the alkali doped EUROPT-1 catalysts probably because of the reduction of the overall TPR profile. The experiments on TPR of the support alone or alkali doped support confirm that these sharp features are not associated with the reduction of support or alkali.

It was observed that in each case there followed immediately after the reduction peak a small but clear hydrogen desorption trough having a broad minimum. These desorption minima were found to shift to higher temperature as the alkali concentration increases. This indicated that the stability of adsorbed hydrogen increased with alkali concentration. In the forthcoming section on the TPD studies of clean and alkali doped EUROPT-1 a similar effect is noted. The shifting of the T_{max} in the TPR studies is consistent with the TPD results. This desorption in TPR was unsuitable for estimation of metal dispersion.

Among the series of alkali doped catalyst, spillover

hydrogen desorption was exhibited by 0.25% alkali doped EUROPT-1 only. At higher alkali loading there was little evidence of desorption from spillover hydrogen. However, there may not have been enough hydrogen desorbed to be observed by the instrument. This could be attributed to the loss of metal surface area corresponding to the decreased metal dispersion, hence it could be concluded that low dispersions do not favour hydrogen spillover.

3.5.2 TPD

3.5.2.1 Flow method

The desorption of hydrogen (from 'as-received' and alkali doped EUROPT-1) showed the existence of two states of chemisorbed hydrogen (fig. 3.4). Hydrogen TPD from 'as-received' EUROPT-1 showed a low temperature peak attributed to hydrogen atoms chemisorbed on platinum and a high temperature peak attributable to spillover hydrogen desorption. These results are in fair agreement with the reported literature for hydrogen desorption from Pt black[50], a Pt(111) single crystal[53], from Pt films[52] and silica supported platinum catalysts[24].

Vong *et al.*[24] carried out hydrogen TPD from 6% Pt/Si_2O prereduced at 423 K. The profile is shown in figure 3.7 for comparison with the present work. The authors observed three desorption peaks designated as β_1, β_2 and β_3. The first two peaks (T_{max} 347-397 and 573-633) β_1, β_2 were attributed to the hydrogen held by platinum.

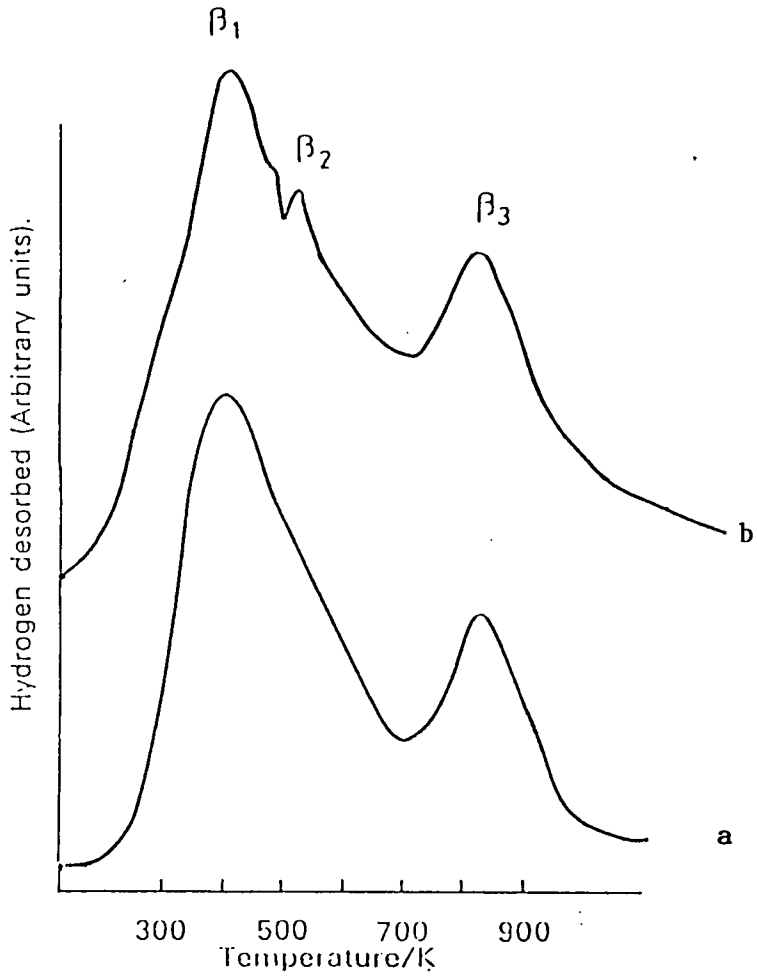

Fig. 3.7 A Comparison of the Hydrogen TPD Spectra:
(a) present study (flow method);
(b) obtained from reference 24.

In the present study, the high temperature peak, attributable to spillover hydrogen, also agrees well with those reported on supported platinum catalysts[18,47,53]. Table 3.2 shows that the total size of the low temperature and high temperature peaks in the present study is too large to be accounted for in terms of desorption of Pt-held hydrogen alone, although this quantity does vary significantly with adsorption temperature. However, no desorption peak was detected in the TPD of Pt-free silica support indicating that the high temperature peak was not dehydroxylation or dehydration of the support surface. It confirms that the high temperature peak is due to the spillover hydrogen. This agrees very well with the β_3 peak observed by Vong *et al.*[24] shown in figure 3.7.

Sermon *et al.*[41] published a detailed review article on hydrogen spillover. The author reported that the flow method of hydrogen adsorption could oversaturate the surface. The over estimated specific surface area becomes too large to be account for by hydrogen adsorbed to the platinum. Hence correct dispersion measurements become difficult.

The process of hydrogen spillover, first detected by Khoobiar[54] has mainly been observed using palladium or platinum. The spillover hydrogen might reside on the surface of support, diffuse into it, and lead to its partial reduction.

The hydrogen spillover complicates the use of hydrogen

in characterising supported metals, but its effect might be minimised by the correct choice of experimental conditions, i.e. adsorption temperature close to ambient and low hydrogen pressure. Some more details will be discussed in the forthcoming section.

The changed interaction of adsorbed molecules on potassium doped supported metal catalysts, and single crystals have been widely studied[33,35-36,48]. The overall conclusions suggest that there is a reduction in the metal surface area and BET area[48,49]. There is also a shift to higher desorption temperature when H_2 or CO is adsorbed on potassium doped Pt catalysts[35,36].

In the flow adsorption TPD study there was essentially no reduction in the desorption peak area from the lowest to highest alkali concentration. A slight shift in the desorption temperature might be of some significance in terms of stability of adsorbed hydrogen. The large amount of hydrogen (spillover) desorption seems to mask any changed characteristics. More or less similar amounts of spillover hydrogen desorption for all the alkali doped and 'as-received' EUROPT-1 irrespective of expected decreasing metal dispersion was observed which made it difficult to determine the correct metal surface area.

Hunt[55], using flash desorption, obtained reasonable agreement between the amount of hydrogen from a Pt/C catalyst, provided only a very short time (2 minutes) was allowed for hydrogen adsorption. However, with the longer

adsorption times at the much higher temperature of 643 K, the quantity of hydrogen desorbed increased 11 fold. Hunt attributed this to hydrogen spillover which they did not however observe with Pt/Al_2O_3 or Pd/Al_2O_3 catalysts.

It was thus decided that for dispersion measurements, the pulse chemisorption method should be used, as it was expected that pulses of hydrogen would saturate the metal surface only, hence minimising the chances of hydrogen spillover.

3.5.2.2 Hydrogen TPD : pulse chemisorption method

The hydrogen TPD results obtained here provide more detailed information on hydrogen chemisorption and desorption from the 'as-received' and potassium doped EUROPT-1 system. The only peak observed in the present study may be assumed to result from hydrogen atoms chemisorbed on the platinum because the extent of chemisorption by pulses to saturation at room temperature is in fair agreement with the amount of hydrogen desorbed. There was little evidence for the desorption of spillover hydrogen at higher temperature, as previously observed in the TPD by flow adsorption method. It suggested that pulses populated the metal surface only[23] and the chances of saturation were controlled to the minimum. Hence the method enables the avoidance of spillover hydrogen and the accurate measurement of the metal dispersion becomes possible.

Frennet *et al.*[20] in their study of characterisation of EUROPT-1 using TPD reported evidence for the existence of four states of adsorbed hydrogen at saturation coverages. For the sake of comparison the desorption profile presented by the authors, shows (fig. 3.8) three components desorbed in the range 100-350 K, 300-700 K and 700-900 K. These components were referred to as features A, (B+C) and D. State "A" was attributed to very weakly adsorbed hydrogen desorbing at 240 ± 25 K. Less strongly adsorbed hydrogen desorbing at 380 ± 25 K was indicated by profile "B". Strongly adsorbed hydrogen underwent desorption at 555 ± 25 K indicated by state "C". State "D" indicated the desorption of spillover hydrogen. The authors suggested that state "A" and "B+C" was the amount of hydrogen chemisorbed to metallic platinum.

In the present work the desorption peak (fig. 3.5) observed, can be attributed to the state B+C. The T_{max}, amount of hydrogen desorbed and the shape of the profile is in fair agreement. Since all the desorption runs commence at room temperature, state "A" was not observed.

In the present study no further desorption of hydrogen beyond 600 K was observed, indicating little evidence of spillover hydrogen. Hence the results of the present study suggest that the pulse chemisorption method could provide a method of populating the platinum surface. Absence of spillover hydrogen also supports this explanation. Based on these experimental conditions it

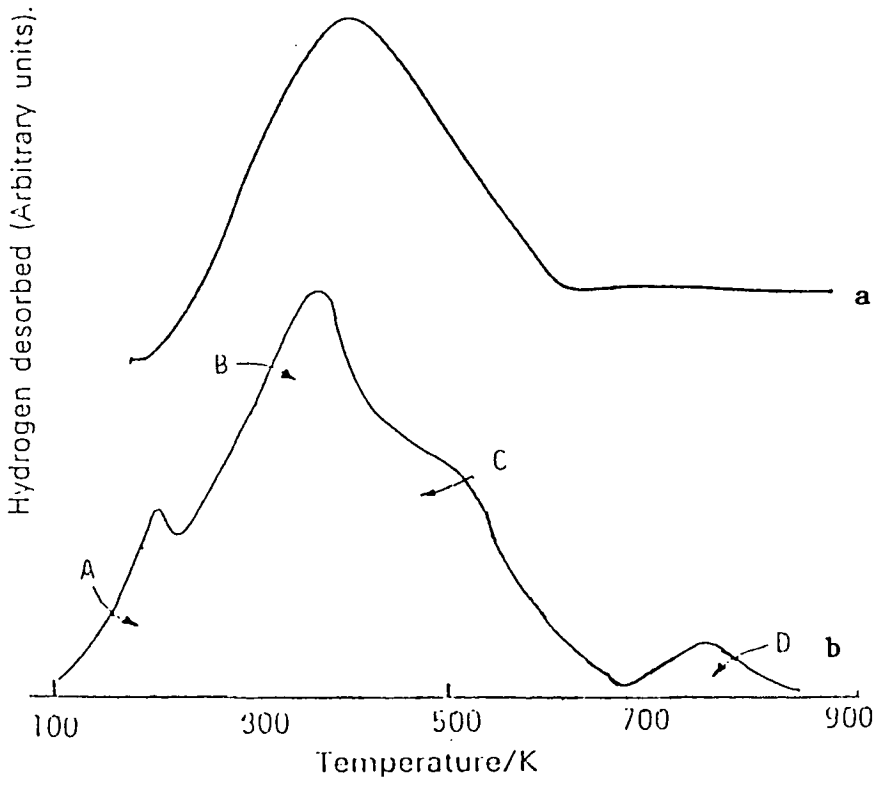

Fig. 3.8 A Comparison of the Hydrogen TPD:
(a) present study (pulse chemisorption method);
(b) obtained from reference 20.

was possible to determine the degree of dispersion of Pt in EUROPT-1 in a straightforward fashion.

Studying TPD of hydrogen over the potassium doped EUROPT-1 system, the observed reduction in the desorption peak and a higher shift of T_{max} with increasing alkali concentration are of great significance. Peak area is reduced by predosed pottasium, showing that potassium is inhibiting hydrogen adsorption. Although it is not yet fully understood how potassium causes this inhibition, some explanation appears in the literature[35,48] as discussed earlier.

Increased thermal stability of adsorbed hydrogen in the presence of alkali has been observed in the present study, indicated by a shift of desorption maxima towards higher temperature with increasing alkali concentration. These results are in good agreement with the TPD of hydrogen from the potassium covered Pt(111) single crystal studied by Zhou *et al.*[35]. The explanation for the thermal stability of adsorbed hydrogen comes from the electronic changes induced by the alkali promoter. It has been reported that hydrogen adsorption on Pt induces a negative work function change. A negative work function may suggest a charge transfer from adsorbed hydrogen to Pt. Electron density on the Pt surface is enriched when potassium is adsorbed. Consequently, electron population or electron density in hydrogen (adsorbed) is higher than on clean platinum. The extra charge strengthens the Pt-H

bonding resulting in higher desorption energy for adsorbed H.

Similar effects have been reported by Ertle *et al.*[51] in studying hydrogen coadsorption with potassium on a Fe(100) single crystal. The authors noted a drop in the sticking coefficient by a factor of two, and an increased desorption temperature for a surface precovered with $1x10^{14}$ K atoms per cm^2. In contrast, Benziger *et al.*[56] reported that potassium enhanced the adsorption of hydrogen on a Fe(100) single crystal, as evidenced by an increased sticking coefficient and desorption energy for hydrogen.

3.5.3 TPD of CO (Pulse Chemisorption)

The desorption profile of CO (from 'as-received' EUROPT-1) showed that desorption started at about 320 K and shifted towards higher temperature with increasing alkali concentration. Comparing CO desorption with hydrogen TPD, it is evident the CO is desorbed at significantly higher temperatures, indicating a stronger bonding of CO. As indicated by the appearance of a shoulder at 450 K, a distinct peak centred at 530 K and another shoulder at 700 K, a total of three different adspecies of carbon monoxide seem to exist on EUROPT-1.

This is similar to that observed previously by Kramer *et al.*[57] for the thermal desorption spectrum of CO from EUROPT-1, an example of which is reproduced in Fig. 3.9

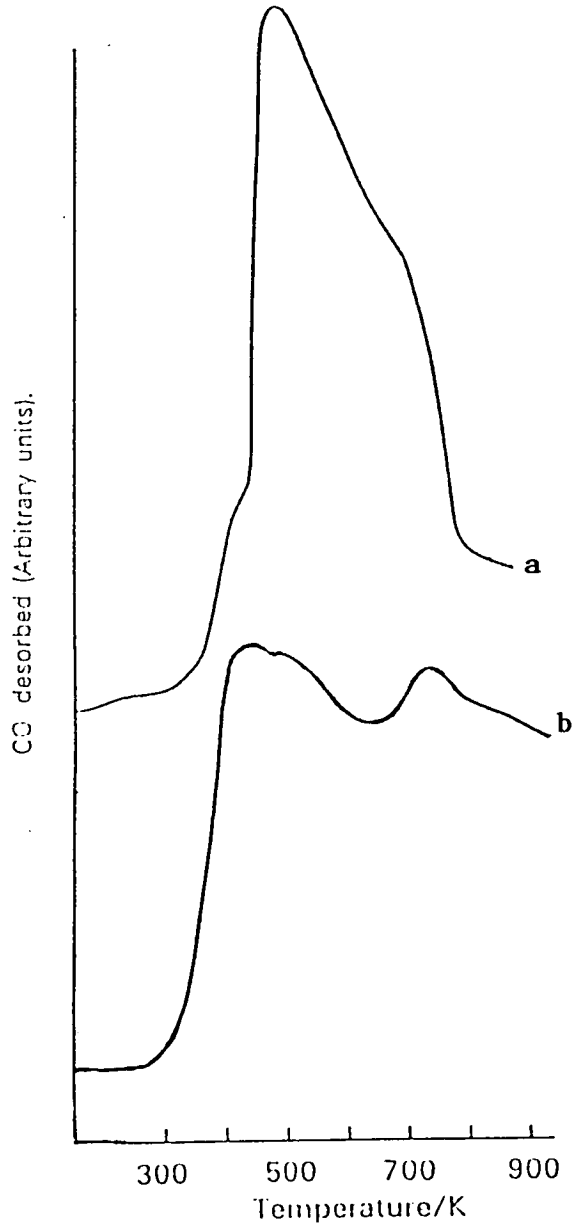

Fig. 3.9 A Comparison of the Hydrogen TPD:
(a) present study;
(b) obtained from reference 57.

for comparison. The desorption profile from room temperature to 800 K showed broad double peak maxima at 403, 533 K and a third desorption peak at 753 K. Thus a total of three different adspecies of CO seem to exist on EUROPT-1. The temperature and relative intensities are expected to be somewhat different depending upon different experimental conditions, such as in Kramer's work CO is desorbed in vacuum. In the extensive literature on the carbon monoxide adsorption on Pt single crystal model catalysts only two carbon monoxide species are reported, with desorption maxima corresponding approximately to the first two peaks in the present work. Of these two species the lower temperature one is ascribed to adsorption on flat, low index planes, and the higher temperature one to adsorption on more open, high index planes, or on steps, edges and corners. Kramer *et al.*[57] used the same interpretation, and it is intended to give the same interpretation for the two species found in the low and high temperature peaks in the present study. The third high temperature peak observed in the present study at 750 K can be assigned to the CO sites existing on metal-support interface which is in agreement to that observed by Kramer *et al*[57]. This state has obviously not been reported in the case of single crystal model catalysts.

Way and Falconer[30] reported CO desorption over a wide temperature range for a series of Pt/SiO_2 catalysts of

varying dispersions. They observed a broad desorption peak attributable to the crystallographic inhomogenity of platinum crystallites.

Herz *et al*[31] reported measurements of the TPD of CO from Pt/Al_2O_3 catalysts. They observed that most of the CO desorbed in a peak between 380 and 550 K. These desorptions were made in vacuum. Substantially higher temperatures have been observed during TPD of CO into a carrier gas and have been widely reported in the literature. The authors used pulses of CO in flowing helium to saturate platinum (at 300 K), very similar to the method of pulse chemisorption used here. The broad profile was attributed to the readsorption of CO.

Komer *et al.*[25] reported CO desorption from silica supported platinum. They observed a flat broad spectrum extending over a range of temperature from 323 to 873 K (this is the same range as noted here and reported by many others[49,54]). They described the unusual behaviour of CO, perhaps related to surface interconversion of the two forms (linear and bridge) of adsorbed CO.

Foger and Anderson[29] reported CO desorption from Pt/Al_2O_3 over the range 300-800 K, in flowing helium. The authors attributed the breadth of the desorption band to the presence in the sample of a distribution of adsorption sites with different CO binding energies. Their explanation is reasonable in view of the complex surface structure of supported metal particles and the possible

influence of the oxide support on small metal particles.

The CO desorption behaviour from alkali doped EUROPT-1 proved to have some interesting features. First, the area of the desorption profile decreased with increasing alkali concentration, initially suggesting that alkali doping is either inhibiting the CO adsorption or reducing the accessible sites for CO adsorption.

In addition to reduction in area, the desorption peak maxima shifted towards higher temperatures as the alkali concentration increased, again suggesting the thermal stability of adsorbed CO being increased upon potassium doping (as previously observed for hydrogen desorption).

In addition to reduction in area, the desorption peak maxima shifted towards higher temperatures as the alkali concentration increased, again suggesting the thermal stability of adsorbed CO being increased upon potassium doping (as previously observed for hydrogen desorption).

The catalysts 0.25% and 0.50% KOH (wt.)/EUROPT-1 exhibited three distinct states of adsorbed CO, similar to that previously observed for clean EUROPT-1. It is interesting that the CO desorption profile of 1% KOH (wt.)/EUROPT-1 is somewhat different from others of the series. There is one clear T_{max} intermediate in temperature between the original high miller index peak and desorption assigned to single metal atom site/metal-support sites. Although the latter is shifted to lower temperature, this still has the appearance of single metal

atom peak.

The effects of potassium doping have already been discussed in the previous sections. Important points relevant to this discussion are as follows.

1. Alkali can cause direct site blocking.
2. Enlargement of crystallite size can occur.
3. It can cause destruction of the support structure or loss of support structure porosity, sintering of the support, encapsulating the metal as no longer accessible, causing reduction in the uptake of CO.

Any of these, or most probably the third one, could be the cause of the disappearance of the third binding state of CO. Sites exhibiting such dependence could be either atoms of lower coordination such as edges and corners or platinum atoms adjacent to support[57]. Thus the higher temperature peaks at 700, 800, 820 K on the 'as-received', 0.25%, 0.50% KOH (wt.)/EUROPT-1 has to be assigned to the sites at Pt/support phase boundry[58,59].

What explanations are there for the shift of CO desorption peak maxima towards higher temperatures as the amount of alkali on EUROPT-1 increases? Significant changes in the CO desorption process from alkali doped EUROPT-1 are evident. Although there has been no work done related to the potassium doped supported platinum catalysts, analogies from the K-doping of model catalysts can be drawn. Thermal desorption results for CO from a Ni(100) single crystal and a K/Ni(100) single crystal[33]

showed that for the clean Ni(100) single crystal, there was a single desorption peak with maximum centred at 723 K. For the alkali doped Ni(100) single crystal two desorption peaks appeared and the desorption temperature (T_{max}) shifted by more than 90 K to higher temperatures relative to the one on the clean Ni(100) single crystal.

The results presented here are similar to those observed previously by Crowell *et al.*[36] from thermal desorption spectra (TDS) of CO adsorbed on a clean and a K-covered Pt(111) single crystal. An example of the single crystal results is reproduced in fig. 3.10 for comparison with the results obtained here.

Figure 3.10a shows plots of TDS of saturation coverages of CO from a Pt(111) single crystal as a function of increasing alkali concentration. From this one can extract figure 3.10b and figure 3.11 which show the change in relative CO coverage and ΔT (shift in desorption temperatures from clean surface) as a function of alkali.

Figure 3.10b shows that as θK varies from $\theta \longrightarrow 1$ (corresponding to 36% atomic density). The adsorbed CO first passes through a small maximum at about $\theta K=0.2$ then drops and is close to zero at $\theta K=1$.

On the supported catalyst integration of the desorption profile gave CO uptake as a function of alkali; these figures are likely to overestimate the effect of alkali since it includes the effect of loss of surface

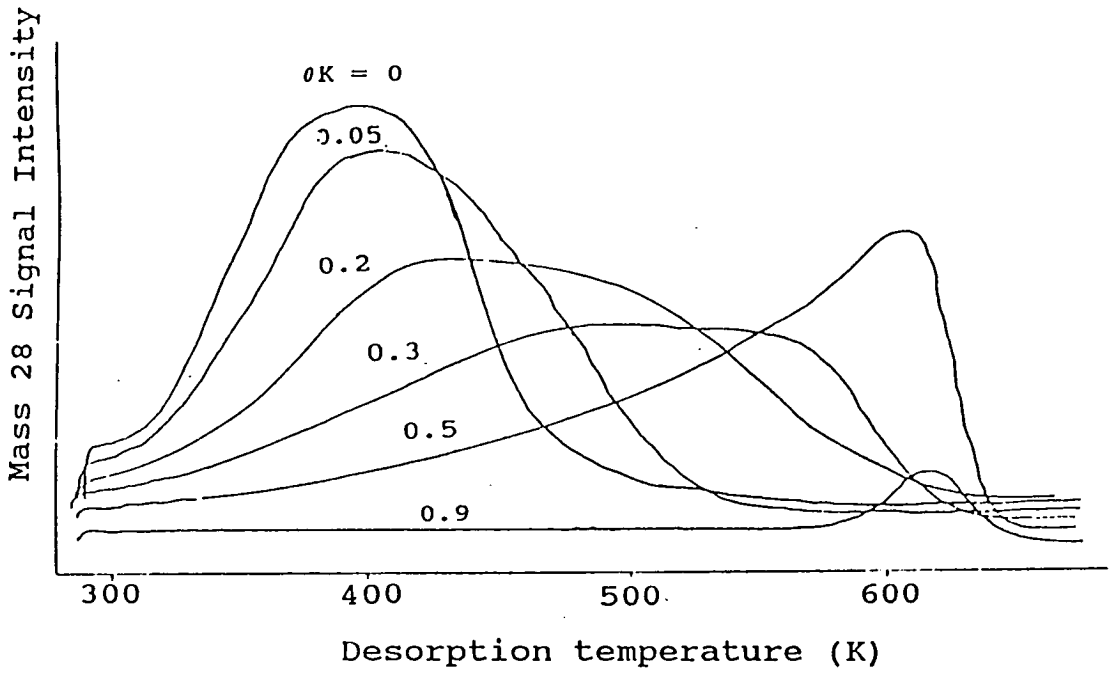

a

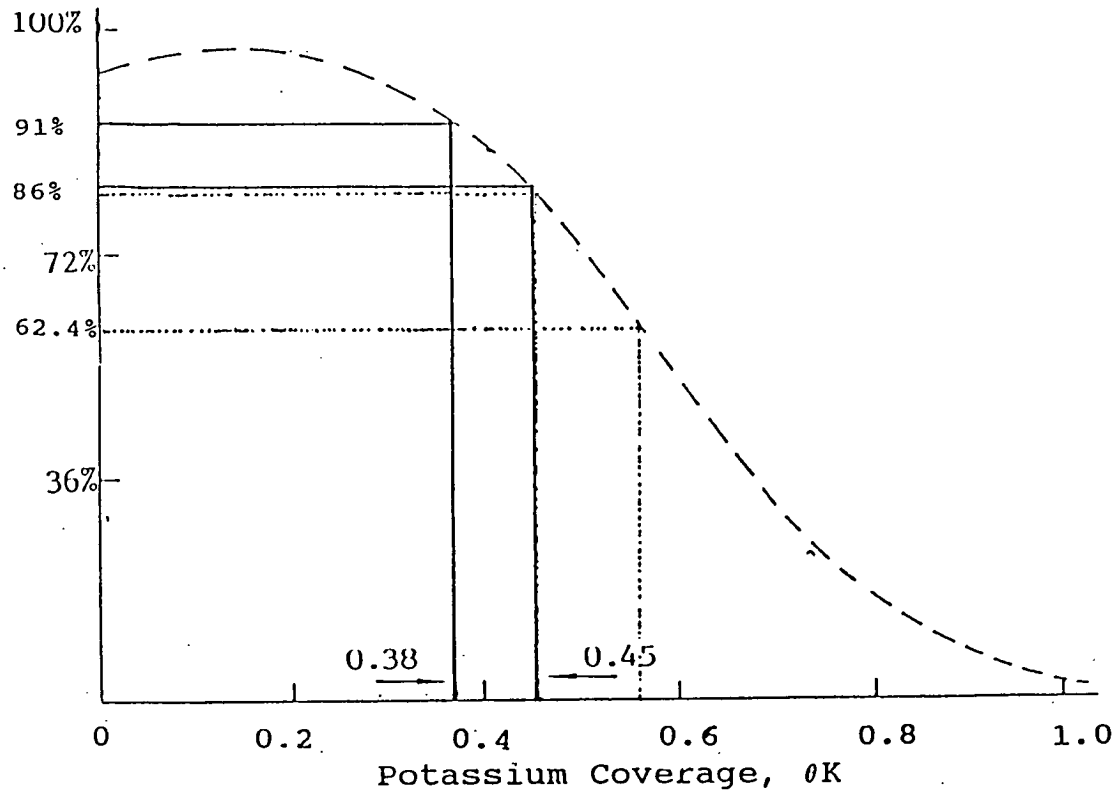

b

Fig. 3.10a Thermal Desorption Spectra with Various Potassium Coverages.

3.10b Total CO Coverage versus Potassium Coverage (these figures are taken from reference 36).
Changes in relative CO coverages expressed as % uptake per unit area and % uptake observed in this work with potassium coverage are shown by solid and dotted lines respectively.

area. The % reduction in CO uptake per unit surface area is likely to give a better estimate of the influence of alkali and the range of surface concentration of alkali estimated by assuming that the reduction in CO uptake as a function of alkali follows identical behaviour on the single crystal and supported catalyst is shown by the solid lines in figure 3.10b. This is expressed in Table 3.5, first of all as % CO uptake relative to EUROPT-1 = 100% and then % CO uptake per unit surface area to compensate for loss in surface area during sample preparation.

Fitting these figures to the single crystal data suggests an effective coverage for the supported catalyst of 0.45-0.6 (θK) based on the % CO uptake indicated by the dotted lines and 0.38-0.45 (θK) for the CO uptake per unit surface area indicated by solid lines.

Figure 3.11 shows similar extracted data for ΔT as a function of alkali (where T_{max} is taken as the band centre since desorption profiles are strongly assymmetric at θK values other than zero and one). Taking a similar measurement from CO desorption profiles from the supported Pt catalyst gives the ΔT values given in table 3.5. Fitting these to the single crystal data gives an approximate effective alkali coverage of θK = 0.13 to 0.33 corresponding roughly to 3.6 to 12% atomic density. These are slightly smaller than the values of θK = 0.38-0.44 corresponding to atomic density 13.7% to 15.8%

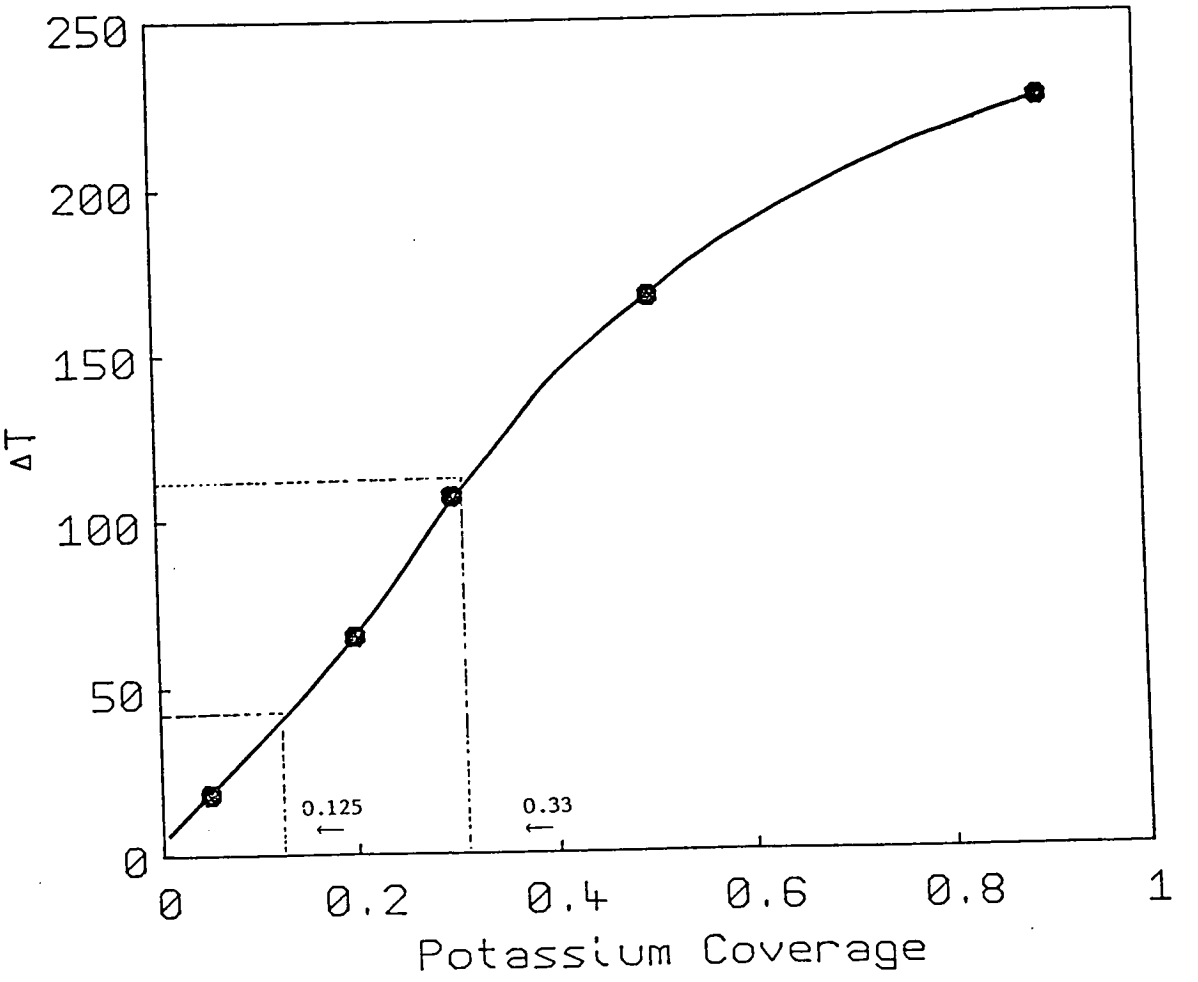

Fig. 3.11 A Plot of ΔT versus Potassium Coverage (extracted from data presented by Crowell et al) ref. 36.

The dotted lines related the shift in desorption temperature observed in this work to potassium coverage.

Table 3.5

Shift in Δt, Reduction in % CO Uptake and % CO Uptake per Unit Area as a Function of Alkali Concentration

Catalyst	CO Uptake μ mole g^{-1}	% Uptake of CO	% CO Uptake Unit Surface Area	Δt* K
As-received EUROPT-1	218	100	100	-
0.25% KOH (wt)/EUROPT-1	186	85.5	91.3	41
0.50% KOH (wt)/EUROPT-1	148	68	83.6	68
1.0% KOH (wt)/EUROPT-1	136	62.4	86.0	109

* Band centre taken as T_{max} of desorption

respectively, estimated from the relative CO desorption areas above.

These values can be compared with the range of surface alkali concentrations that might be expected to arise from the nominal % wt of alkali initially introduced. First, if all the alkali is considered to lie on the Pt metal surface then calculation of the ratio of alkali atoms to surface Pt atoms for the 0.25 ——〉 1% alkali loading by weight catalysts would yield 28-100% atomic density alkali respectively, much higher values than apparently indicated from the experiments above. If instead the alkali is assumed to be partitioned across the available surface area of the catalyst, i.e. metal surface area and support, then the 0.25 and 1.0% by weight loadings give 1.5 and 5.8% atomic density respectively (θK = 0.04 and 0.16). These values lie closer to the experimental estimates than those which assume all alkali to lie on the metal and in particular appear to correlate moderately well with the estimate of the alkali loading based on the temperature shift of the desorption peak. This correlation is perhaps fortuitous due to the fact that alkali is present as atomic K on the single crystal but almost certainly as K^+ (or K_2O) on the supported metal catalyst and that the single crystal study refers in particular to the (111) crystal planes, which is likely to correspond to only around 20% of the available metal area of the supported catalyst, based on the model of ideal metal particles

developed by Hardeveld and Hartog[60].

As already noted, Kramer *et al.*[57] published the CO desorption spectra from the EUROPT-1 catalyst in association with the study of the effect of CO preadsorption on benzene hydrogenation. Their spectrum reproduced in figure 3.9 shows a broad desorption extending from 300 to 800 K with three features, at a similar temperature to those noted here. These desorption peaks were assigned to adsorption on low and high miller index planes, and the third one assigned to the adsorption at the platinum/support phase boundary.

Although there are similarities in temperature range and peak positions between Kramer's and this work, some differences in the band profiles can be accounted for in terms of different experimental conditions. Kramer's work involved desorption into a carrier gas. Kramer attributed intense low temperature desorption to high proportion low miller index sites.

If Kramer's assignment of desorption features to low and high miller index and metal/support phase boundary sites on the basis of comparison with CO desorption from a range of Pt samples is accepted, then it is possible to interpret the CO desorption spectra in terms of changes in morphology of the catalyst. Loss in relative intensity of the CO desorption spectra at "low temperature" would suggest a preferential effect of K on what is assigned to low and high miller index sites, apparently leaving the

phase boundary site desorption peak relatively unchanged.

3.5.4 Conclusion

The present study has shown that the chemisorptive properties of reactive molecules such as H_2 or CO change significantly when EUROPT-1 is doped with alkali. The conclusions drawn are listed below.

1. The decrease in reducible area, with increasing alkali concentration is due to a loss of metal surface area. The additional peaks in the reduction profiles are attributed to the inhomogeneity of the EUROPT-1 upon alkali doping.

   There is little evidence (or undetectable) of hydrogen spillover desorption from alkali doped EUROPT-1 suggests its dependence on metal dispersion.
2. The increase in desorption maxima with increasing alkali concentration may be due to stabilisation of adsorbed molecules. These effects are explained by a charge transfer from potassium adatoms to the platinum substrate. Hence enhanced electron density on the metal surfaces results in the stabilisation of the adsorbed hydrogen.

   The increased back donation from the platinum surface to the coadsorbed CO molecule results in strengthening of Pt-CO bonding.
3. The decrease in desorption peak area (H_2 and CO) may be due to:

i) direct site blocking

ii) loss of metal surface area by growth of crystallite size.

4. The desorption spectra of CO on the EUROPT-1 catalyst are similar to that observed on other supported Pt catalysts. The shift of desorption maxima to higher temperature upon subsequent doping, together with reduction in CO uptake and change in the overall band profile is very similar to that observed on an alkali doped Pt(111) single crystal, and is consistent with the alkali loading of the catalysts.

5. Strongly held CO dominates on the highest alkali loaded catalyst (1% KOH). This can be attributed to the strongly bound CO on Pt planes or original CO species thought to exist at the metal/support interface.

REFERENCES

1. S.D. Robertson, B.D. McNicol and J.H. de Bass, *J.Catal.* 37 (1975) 424.
2. S.J. Gentry and P.T. Welsh, *J.Chem.Soc. Faraday Trans.I* 78 (1982) 1515.
3. P.A. Jacobs, J. Linart, H. Nijs and Uytterhoeven, *J.Chem.Soc. Faraday Trans.I* 73 (1977) 1745.
4. N. Wagstaff and R. Prins, *J.Catal.* 59 (1979) 434.
5. H.B. Isaac and E.E. Peterson, *J.Catal.* 77 (1982) 43.
6. N.W. Hurst, S.J. Gentry, A. Jones and B.D. McNicol, *Catal.Rev.-Sci.Eng.* 24 (1982) 233.
7. A. Jones and B.D. McNicol, Temperature programmed reduction for solid materials characterisation, (Dekker; New York, 1986).
8. R. Brown, M.E. Cooper and D.A. Whan, *Appl.Catal.* 3 (1982) 177.
9. C.H. Yao, M. Sieg and K.H. Plummer, *J.Catal.* 59 (1979) 365.
10. T. Huizinga, J.V. Grondelle and R. Prins, *Appl.Catal.* 10 (1984) 199.
11. J.B. Kipp, J.V. Grondelle, J.H.A. Martin and R. Prins, *Appl.Catal.* 26 (1986) 353.
12. M.F. Johnston and E.D. Keith, *J.Phys.Chem.* 67 (1963) 200.
13. N. Wagstaff and R. Prins, *J.Catal.* 67 (1981) 255.
14. K. Foger and H. Jaeger, *J.Catal.* 67 (1981) 252.

15. J.C. Vis, H.F.J. Van't Blik, T. Huizinga, J.C. Grondelle and R. Prins, *J.Catal.* 95 (1985) 333.

16. G.C. Bond and R. Gelsthorpe, *Appl.Catal.* 35 (1987) 169.

17. G.C. Bond and P.B. Wells, *Appl.Catal.* 18 (1985) 221.

18. G.C. Bond and P.B. Wells, *Appl.Catal.* 18 (1985) 225.

19. J.W. Geus and P.B. Wells, *Appl.Catal.* 18 (1985) 231.

20. A. Frenent, P.B. Wells, *Appl.Catal.* 18 (1985) 243.

21. P.B. Wells, *Appl.Catal.* 18 (1985) 259.

22. N.D. Hoyle, P.H. Newbatt, K. Rollins, P.A. Sermon and A..T. Wurie, *J.Chem.Soc. Faraday Trans.I* 81 (1985) 2605.

23. John L. Falconer and J.A. Schwarz, *Catal.Rev.-Sci.Eng.* 25 (1983) 141.

24. S.W. Vong, Mariana and P.A. Sermon, *J.Chem.Soc. Faraday Trans.I* 83 (1987) 1369.

25. R. Komer, V. Amenomiya and R.J. Cvetanovic, *J.Catal.* 15 (1969) 293.

26. J.P. Contour and G. Pannetier, *J.Catal.* 24 (1972) 434.

27. P.C. Aben, H. Van der Eijk and J. Oelderik, *Proc. 5th Int.Cong.Catal.* 1 (1973) 717.

28. P.G. Menon and G.F. Froment, *Appl.Catal.* 1 (1981) 31.

29. K. Foger and J.R. Anderson, *Appl.Surf.Sci.* 2 (1979) 335.

30. J.D. Way and J.L. Falconer, Proceedings of the second chemical congress of North America, Las Vegas; Nevada, Aug. 1980.

31. R.K. Herz, J.B. Kiela and S.P. Marin, *J.Catal.* 73 (1982) 66.

32. R.K. Herz and D.F. McCready, *J.Catal.* 81 (1983) 358.

33. H.P. Bonzel, *Surf.Sci.Rep.* 8 (1988).

34. M.E. Dry, T. Shingles and L.J. Boshoff, *J.Catal.* 15 (1969) 190.

35. X.L. Zhou and J.M. White, *Surf.Sci.* 185 (1987) 450.

36. J.E. Crowell, E.L. Garfunkel and G.A. Somorjai, *Surf.Sci.* 121 (1982) 303.

37. P.D. Gochis and J.L. Falconer, *Chem.Ind.* 1985 (Dekker), 22 (*Catal.Org.React.*), 135.

38. R.D. Gonzalez and H. Miura, *J.Catal.* 77 (1982) 338.

39. Y. Amenomiya and G. Plazier, *J.Catal.* 28 (1973) 442.

40. R. Kramer and M. Andre, *J.Catal.* 58 (1979) 281.

41. P.A. Sermon and G.C. Bond, *Catal.Rev.* 8 (1973) 211.

42. P.A. Sermon and G.C. Bond, *J.Chem.Soc. Faraday Trans.I* 72 (1976) 745.

43. E. Baumgarten and E. Dericke, *J.Catal.* 95 (1985) 296.

44. D.A. Dowden in: Specialist Periodical Reports, "*Catalysis*", Vol. 3, Eds. C. Kemball and D.A. Dowden (the Chemical Society, London, 1978).

45. R.W. Joyner, *J.Chem.Soc.,Faraday Trans.I* 76 (1980) 357.

46. Y.J. Huang, J. Xue and J.A. Schwarz, *J.Catal.* 111 (1988) 59.

47. J.R. Anderson, K. Foger and R. Breakspere, *J.Catal.* 57 (1979) 458.

48. M.E. Dry and G.J. Oosthuizen, *J.Catal.* 11 (1968) 18.

49. F. Shephard, *J.Catal.* 14 (1969) 148.

50. S. Tsuchiya, Y. Amenomiya and R.J. Cvetanovic, *J.Catal.* 19 (1970) 245.

51. R. Christman and G. Ertl, *Surf.Sci.* 60 (1976) 365.

52. J.J. Stephen, V. Ponec and W.H. Sachtler, *J.Catal.* 37 (1975) 81.

53. Y. Amenomiya, *J.Catal.* 22 (1971) 109.

54. S.J. Khoobiar, *J.Phys.Chem.* 68 (1964) 411.

55. C.E. Hunt, *J.Catal.*, 23 (1971) 93.

56. J. Benziger, R.J. Madix, *Surf.Sci.* 94 (1980) 119.

57. R. Kramer, M. Fischbacher and H.L. Gruber, *Appl.Catal.* 42 (1988) 337.

58. R.W. McCabe and L.D. Schmidt, *Surf.Sci.* 66 (1977) 101.

59. M.R. McLellan, J.L. Gland and F.R. McFeely, *Surf.Sci.* 112 (1981) 63.

60. R. Hardeveld and F. Hartog, *Surf.Sci.* 15 (1969) 189.

CHAPTER 4

HYDROGENOLYSIS OF n-BUTANE OVER AS-RECEIVED AND POTASSIUM DOPED EUROPT-1

4.1 INTRODUCTION

The hydrogenolysis and skeletal isomerisation of saturated hydrocarbons has been extensively studied[1-8]. Group VIII metals are among the most active catalysts for this reaction, but the metals have very different behaviours, platinum for example is one of the least active metals for hydrogenolysis but shows a high activity for alkane isomerisation. Such reactions involve rupture of C-C bonds. There may be several stages in the interaction of saturated hydrocarbons with the metal surfaces. The initial process is the loss of hydrogen atoms, with the formation of radicals which may be held to the surface by multipoint adsorption[9]. The hydrogen deficient species formed from rupture of the C-H bond then undergoes C-C bond scission, and is followed by hydrogenation to complete the reaction.

The catalytic hydrogenolysis of n-butane has been studied on Pt metal[10], Pt black[11], Pt/Al_2O_3[12] and Pt/SiO_2 catalysts[13]. As previously mentioned platinum is less active for the hydrogenolysis reaction, i.e. rupture of C-C bond. The important effect is explained by assuming, as proposed by Anderson[2] and others[14], that on platinum metal 1,2-di- adsorbed species responsible for ethane

hydrogenolysis are less easily formed than 1,3-diadsorbed species which can be formed with higher hydrocarbons.

Bond *et al.*[13] reported n-butane hydrogenolysis on EUROPT-1 and observed formation of CH_4, C_2H_6 and C_3H_8 via rupture of the bonds between the primary and secondary carbons, CI-CII, and the bond between the secondary carbons, CII-CII. After heat treatment of EUROPT-1, the authors observed a falling catalytic activity attributed to the loss of hydrogen chemisorption capacity, which was then assumed to be due to enlargement of the crystallite size due to sintering.

On Pt/Al_2O_3[12] the reaction products showed formation of CH_4, CH_6, C_3H_8 via fragmentation of the C(I)-C(II) and C(II)-C(II) bond respectively. Guczi *et al.*[11] in their study showed that on Pt black, single C-C bond rupture and selective formation of 2-methyl propane occurred. Hence the results suggested that hydrogenolysis and isomerisation activity are independent of the support.

The published literature relating to Pt reveals that (i) the principal emphasis has been on the mechanism of skeletal isomerisation and its dependence on metal particle size[15] and morphology[16], also on the relative rate of rupture of the various C-C bonds in the molecule[17-18], (ii) the reaction of alkanes has been effected on Pt black[11], Pt film or platinum particles in zeolite[18], while traditional Pt/SiO_2 catalysts have rarely been used[11-12], (iii) the reaction of n-butane, the

simplest alkane able to show skeletal isomerisation as well as selectivity in hydrogenolysis is frequently cited and used as a structure-sensitive test reaction[19-20].

There is little evidence of the use of alkali-doped platinum catalysts in the hydrogenolysis reaction of saturated hydrocarbons. However, some other parameters that change the catalyst's morphology in a possibly similar manner to alkali doping, have been widely reported[13].

As already mentioned, Bond *et al.*[13] observed a falling activity with increasing particle size upon heat treatment of EUROPT-1 catalyst. Somerjai *et al.*[20] reported a similar conclusion, that activity decreases when the average metal particle size is increased. The authors explained that the concentration of active corners, kinks and microfacets responsible for C-C bond breaking decrease markedly with increasing crystallite size.

Sinfelt *et al.*[21] studied ethane hydrogenolysis over a series of silica supported metal catalysts of varying dispersions. The authors assumed a correlation between catalytic activity and metal dispersion.

Work by Dry *et al.*[22] and Shephard[23] on potassium doped (K_2O) Fe_2O_3 and Ni/Al_2O_3 respectively showed that the alkali dopant caused a decrease in total surface and metal area and an increase of crystallite size. From his propane hydrogenolysis studies, Shephard concluded that the alkali metal reduced the degree of dissociation on the

catalyst surface.

A structure sensitive reaction is usually defined as one whose rate (turnover number) varies with particle size[23-25]. High activity in hydrogenolysis requires easy formation of multiple bonds. A further study has been performed on the influence of the particle size of supported platinum on forming these multiple bonds. It was thus established that the smallest particles are the most active in hydrogenolysis[26].

Anderson and Avery[26] were among the first to show that platinum is notably active for isomerisation. The authors proposed a bond shift mechanism which is based on a 1,3-diadsorbed intermediate, later termed by Foger and Anderson[27] as the iso-unit mode. Bond *et al.*[13] observed isomerisation during hydrogenolysis of n-butane on EUROPT-1. Isomerisation of n-butane has also been reported on Pt black[11] and Pt/Al_2O_3[12] catalysts. It was found to be more favoured on samples of low catalytic activity. F. Gault[28] suggested that small particles active in hydrogenolysis may also cause some isomerisation by an iso-unit mode, as shown in the scheme below.

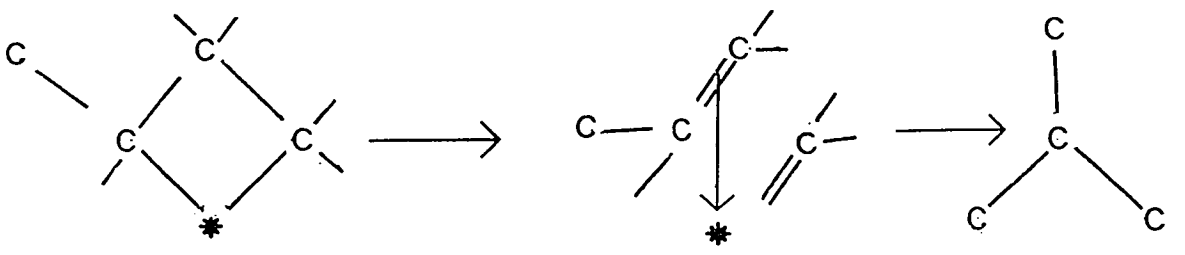

F. Gault[28] observed a complete change of mechanism and selectivity with changing the particle size in hydrogenolysis of n-butane on a Pt/Al_2O_3 catalyst. The author concluded that two types of sites existing on smaller and larger crystallites are responsible for normal hydrogenolysis activity and for bond shift or isomerisation respectively.

Bearing in mind the importance of alkali additives in heterogenous catalysis and understanding the changed morphology of the EUROPT-1 catalyst upon alkali doping, it was thus intended to use the structure-sensitivity of butane hydrogenolysis to gain a further insight into the morphological changes induced by the potassium doping of EUROPT-1.

4.2 MECHANISM OF HYDROGENOLYSIS

The reaction of n-butane with excess of hydrogen gives a mixture of methane, ethane, propane and some isobutane. The methane:propane ratio is sometimes unity[17,29,30]. This mechanism is occasionally discussed qualitatively in terms of selectivity for central and terminal bond fission[11], but more usually in terms of the mechanism presented by Bond *et al.* as follows.

$$C_4H_{10} + H_2 \longrightarrow CH_4 + C_3H_8 \qquad \text{I}$$

$$C_4H_{10} + H_2 \longrightarrow 2C_2H_6 \qquad \text{II}$$

When the methane:propane ratio exceeds unity then a third reaction is also involved.

$$C_4H_{10} + 3H_2 \longrightarrow 4CH_4 \qquad \text{III}$$

and there can be a further possible reaction

$$C_4H_{10} + 2H_2 \longrightarrow C_2H_6 + 2CH_4 \qquad \text{IV}$$

which is a combination of equations II and III, and for skeletal isomerisation yet another equation is needed.

An important consideration in the mechanism of hydrogenolysis of hydrocarbons is the structure of the chemisorbed species that undergoes scission of the carbon-carbon bond. In the hydrogenolysis of n-butane over EUROPT-1, the main reaction was stepwise hydrogenolysis.

A mechanism by Kempling and Anderson[31] has been presented by Bond *et al.*[13] for the hydrogenolysis of n-butane, the reaction network is as follows.

$$C_4 \underset{}{\overset{k_4}{\rightleftarrows}} C_4^* \xrightarrow{k^4} \begin{cases} \xrightarrow{1-F} C_3^* + C_1^* \\ \xrightarrow{F} 2C_2^* \end{cases}$$

$$C_3 \overset{k_3}{\underset{k_3'}{\rightleftarrows}} C_3^* \xrightarrow{k_3^*} C_2^* + C_1^*$$

$$C_2 \overset{k_3}{\underset{k_2'}{\rightleftarrows}} C_2^* \xrightarrow{k_2^*} 2C_1^*$$

$$C_1 \overset{k_1}{\underset{k_1'}{\rightleftarrows}} C_1^*$$

C_i represents a linear alkane containing i carbon atoms in the gas phase and C_1^* its adsorbed form. It has

been suggested[13] that there is only one type of site on which n-butane can adsorb and the probability of central and terminal bond breaking are represented by the parameter F, the value of which is characteristic of the geometric or the electronic structure of the sites[13].

4.3 EXPERIMENTAL

4.3.1 Apparatus

All the experiments were carried out in a static glass reactor (fig. 4.1) of approximately 177 cm^3 volume, attached to a conventional gas handling line. Samples were drawn periodically from the reaction vessel and injected into a gas chromatograph for analysis of the products.

4.3.2 The Vacuum Lines, Reactor and Sampling System

A schematic drawing of the vacuum line is shown in fig. 4.2. Conventional ground glass stopcocks lubricated with Apiezon L vacuum grease were used.

The vacuum line was equipped with two pumping systems, each comprised of an Edwards ED50 rotary pump and an electrically heated mercury diffusion pump made of glass. One of the pumping systems was used to evacuate exclusively the reactor volume, while the rest of the line was evacuated by means of the second pumping system. The ultimate vacuum attainable with these systems was of *ca* 10^{-6} torr. The residual pressure in the line was measured

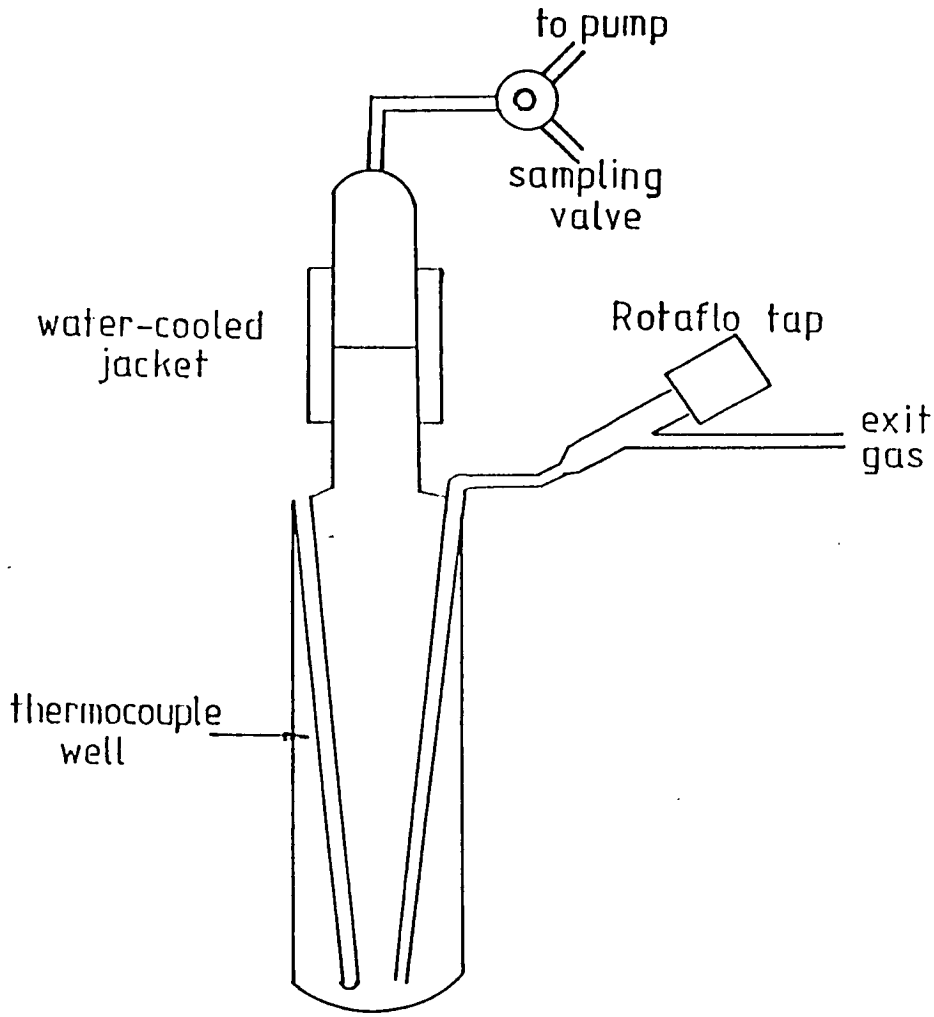

Fig. 4.1 Static Glass Reaction Vessel

by means of a McLeod gauge and was frequently checked to ensure that after pretreatment and before the start of an experiment, the catalyst was in contact only with the best possible vacuum. Liquid nitrogen traps were inserted between each pumping system and the vacuum lines in order to prevent contamination with mercury vapour.

Hydrogen used in preparing the reaction mixture was purified by diffusion through an electrically heated Pd-thimble (TH in fig. 4.2). During purification, hydrogen flowed from a bulb containing the "impure" gas , through the Pd-thimble and through a cold trap immersed in liquid nitrogen, into a storage bulb permanently attached to the line. The n-butane reactant was introduced through the glass joint from a gas lecture bottle according to the procedure described in a subsequent section. After purification gaseous reactants were stored in bulbs permanently attached to the lines.

The reaction mixture was prepared by placing a known pressure of each reactant into a mixing bulb (M). The pressures were monitored by means of a Bourdon type gauge (Leybold model 16044 or similar), previously calibrated against a mercury manometer (HG).

The hydrogen used in catalyst reduction was fed from a cylinder and was purified by passage through a 'deoxo' unit (Englehard) to remove oxygen, then through a 4A molecular sieve cooled in liquid nitrogen to complete the removal of water. After purification, hydrogen flowed

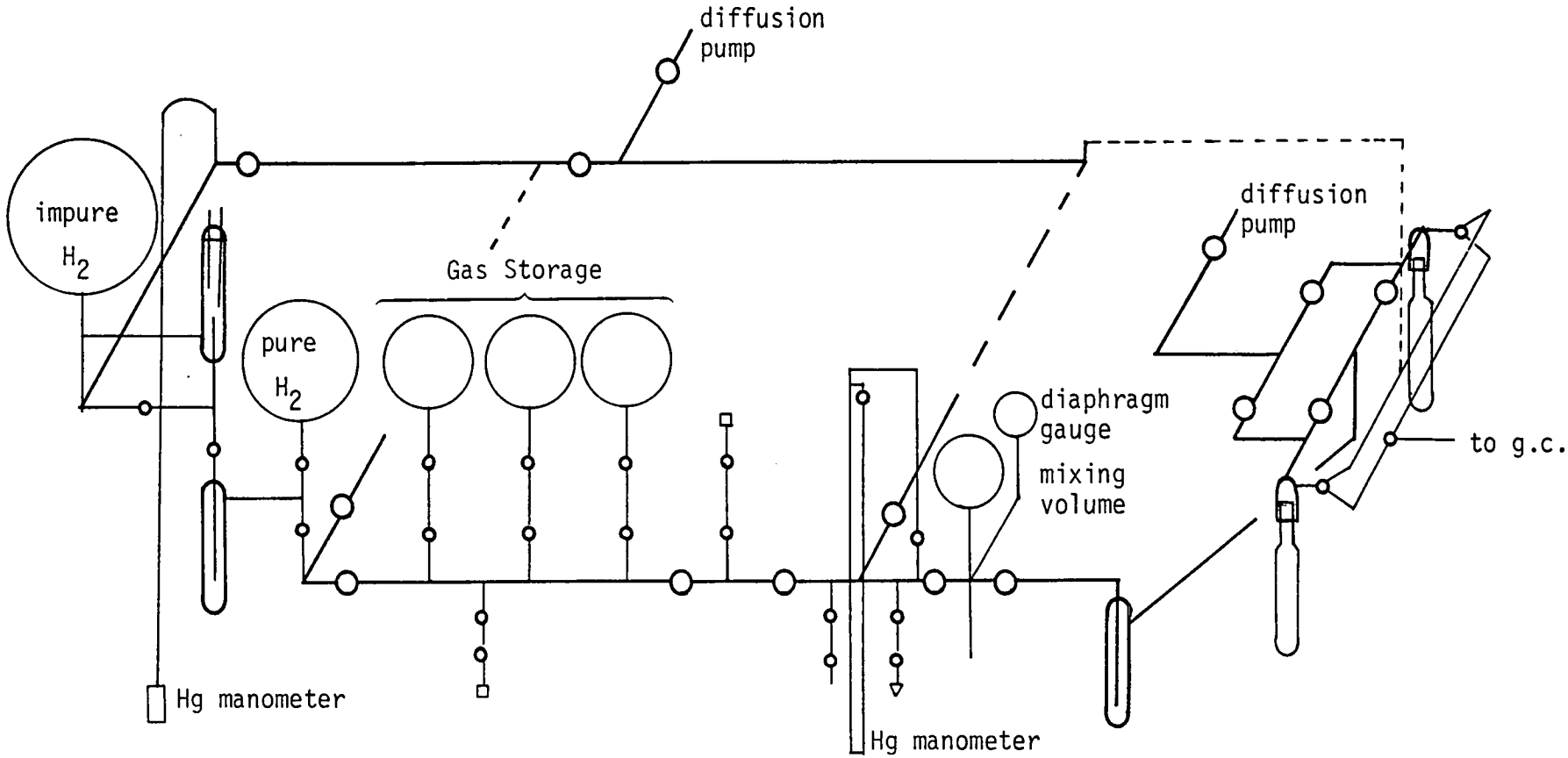

Fig. 4.2 Conventional Glass Gas Handling Line

into the line via one of the ground glass joints, through the reactor and out via the venting tube.

The reactor was heated using an externally placed close fitting tubular furnace consisting of a silica tube around which a resistance wire was wound. A Chromel-Alumel thermocouple was strapped to the outside of the reaction vessel and was connected to a "Eurotherm", proportional temperature controller (model PID-SCR or similar). The temperature inside the reactor was monitored by means of a Chromel-Alumel thermocouple inserted into the thermocouple well and connected to a 'Comark' digital thermometer (model 3000). In all experiments the temperature was held constant to within ±1K.

Figure 4.3 shows a schematic drawing of the sampling system used in the line. The glass part of the sampling system was built using capillary tubing so that only about 1% of the reaction mixture was drawn for each sample, with three-way tap S_1 in the position shown in figure 4.3. By turning S_1 60° anticlockwise the sampling system was isolated from the reactor. The sample contained in the sampling loop L (0.2 cm^3) was then injected into the gas chromatograph by means of the three-way sampling valve S_3. After the injection, Valve S_3 was returned to the sampling position and tap S_1 was turned further 60° anticlockwise to evacuate the sampling system in preparation for the next sample.

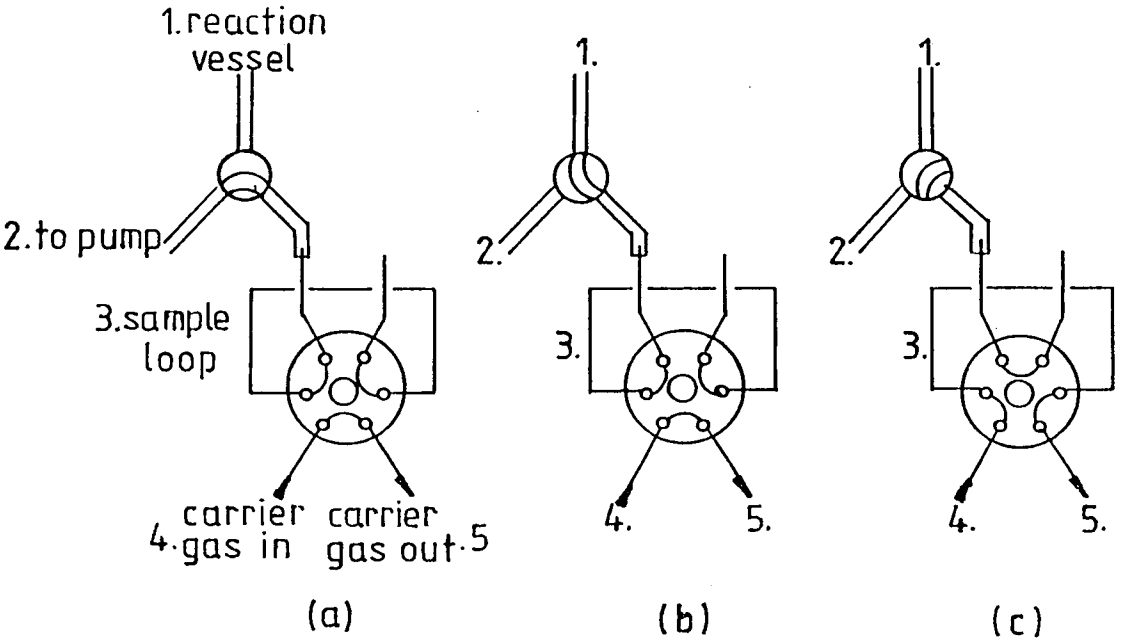

Fig. 4.3 Operational Gas Sampling Carl Valve

(a) Evacuation of Sample Loop;
(b) Expansion of Reactants into Sample Loop;
(c) Sampling to Gas Chromatograph.

4.3.3 Gas Chromatography

Analysis of the reaction mixture was performed with a Perkin-Elmer model F-33 gas chromatograph equipped with a flame ionization detector. A 4m, 1/8" (3.18 mm) external diameter column containing 15% OV101 on chromosorb W was installed in the gas chromatograph and was operated at room temperature with nitrogen at 8 p.s.i.g. as the carrier gas. Under these conditions, all alkanes from methane to 2-methyl propane were separated completely in about 10 minutes.

4.4 PROCEDURE

4.4.1 Volume Calibration

The volumes in the vacuum lines relevant to the preparation of reaction mixture were the volume Vm of the mixing bulb M, the total volume VE of the portion of line comprising the mixing bulb, the reactor and any piping between these two parts of the system (e.g. trap CT_2 in figure 4.2) and the volume VR of the reactor. These volumes were calibrated by attaching a bulb of known volume containing a known pressure of helium and expanding the helium into evacuated parts of the system. Knowing the volume of standard bulb, the initial pressure of helium and the pressure after expansion, the volume of any selected parts of the system could be determined using Boyle's law ($P_1V_1 = P_2V_2$).

4.4.2 Catalyst Pretreatment

The reaction vessel containing the desired amount of catalyst was attached to the line and evacuated for about 30 minutes, using pumping system 1. Hydrogen was admitted into the gas handling part of the apparatus and the increase in pressure was measured using the mercury manometer 'HG'. When the pressure was near to 1 atmosphere, the reaction vessel was isolated from pumping system 1 and opened to the gas handling line. Hydrogen flowed into the reactor and when the pressure in the system was 1 atmosphere the 'Rotaflo' tap in the venting tube 'V' was opened to allow hydrogen to flow continuously over the catalyst. The catalyst was reduced for 2 hours at 673 K, and following the reduction, the flow of hydrogen was stopped by closing the appropriate taps in the hydrogen inlet. The tap in the venting tube was then closed and the reactor was isolated from the gas handling line and evacuated at the reduction temperature using pumping system 1 for about 30 minutes. While the reaction mixture was prepared in the gas handling line, the reactor was cooled to the reaction temperature, i.e. 523 K, and kept under vacuum until the start of the experiment.

4.4.3 Purification of Hydrocarbons

n-Butane from a lecture bottle was expanded into one of the storage bulbs available in the vacuum line. A glass tube was attached to one of the inlets to the line

and was evacuated. n-Butane from the storage bulb was condensed into the glass tube at liquid nitrogen temperature. A portion of n-butane was removed by evacuation and another portion was expanded back into the storage bulb by momentarily removing the liquid nitrogen bath from around the glass tube. The remaining n-butane, probably containing condensible impurities was discarded. The purified n-butane was stored in the storage bulb for subsequent preparation of the reaction mixture. The purity of the gas was checked by gas chromatography.

4.4.4 Preparation of the Reaction Mixture

The storage tube containing the n-butane was attached to the gas-handling line. The n-butane was degassed by repeated freeze-pump-thaw cycles to remove any air that could have leaked into the storage tube. The desired pressure of n-butane (10 Torr) was expanded into the evacuated mixture bulb 'M' which was then isolated from the rest of the system. A liquid nitrogen bath was placed around the cold finger located at the bottom of the mixing bulb (fig. 4.2) in order to condense the n-butane. The desired pressure of purified hydrogen was then allowed into the mixing bulb. The bulb was again isolated from the rest of the system and the liquid nitrogen bath was removed from around the cold finger.

The reaction mixture was left standing for about one hour before the start of an experiment so that good

homogenisation of the gas could be achieved. After this period the reaction mixture was then expanded into the reactor.

4.4.5 Performing the Experiments

Samples were drawn for injection into the gas chromatograph every 10-15 minutes. The first sample was generally drawn 2 minutes after the start of the experiments.

In performing experiments the main interest was in obtaining data relating to the initial rates of reaction, initial product distribution and isomerisation product. For this purpose it was generally sufficient to analyse 9-10 samples for each experiment performed so that the duration of the experiment was between 90 to 120 minutes. The amount of catalyst used in each experiment was 0.075 gm.

4.4.6 Treatment of Data

Reaction of n-butane with hydrogen

From the chromatographic peak areas A_i, the fraction S_2 of the reactant converted to substance i was calculated using expression 4.1

$$X_i = \frac{\frac{C_i}{C_R} \cdot \frac{A_i}{f_i}}{\sum_i \frac{Ci}{C_R} \cdot \frac{C_i}{f_i}} \qquad (4.1)$$

where C_i and C_R are the numbers of carbon atoms in the substance i and in the reactant, R, respectively, and f_i is a sensitivity factor which converts the peak areas A_i into a number proportional to the numbers of molecules of substance i in the reactor.

If we define n_i as the number of molecules of substance i in the reactor per molecule of reactant initially present in the system, n_i values may be calculated from X_i fractions using expression 4.2.

$$n_i = \frac{C_R}{C_i} X_i \qquad (4.2)$$

Expression 4.2 is actually an approximation, since no account was taken of the fact that the number of molecules of reactant decreases with time, not only because they are converted into products, but also because samples are periodically withdrawn for chromatographic analysis. Expression 4.2 also does not take into account that some reactant molecules may be converted into species that remain adsorbed on the catalyst surface and do not appear in the gas phase. When these approximations are accepted, the rate of formation of substance i, R_i may be calculated in terms of the number of molecules of i produced per unit time, from expression 4.3 below

$$R_i = \frac{d_{ni}}{dt} N_R \qquad (4.3)$$

where N_R is the number of molecules of reactant initially present in the reaction vessel.

The peak areas obtained from the flame-ionisation detector are approximately proportional to the molecular weight of hydrocarbon injected into the gas chromatograph. If the f_i factor for methane is defined as 1, f_i values for other hydrocarbons may be approximately calculated from expression 4.4

$$f_i = \frac{W_i}{16} \qquad (4.4)$$

where W_i is the molecular weight of substance i.

Sensitivity factors were also determined experimentally for a number of hydrocarbons by constructing calibration curves of chromatographic peak areas against hydrocarbon pressure in the sampling loop. Straight lines were obtained for a wide range of pressures, and the slopes of these lines are proportional to the f_i factors. Table 4.1 summarises f_i values for a number of substances determined both experimentally and from the expression 4.4.

Initial rates of conversion, V_o were determined by plotting reactant concentrations, calculated from expression 4.1, against time and taking the initial slopes of the curves obtained as in fig. 4.4-4.7.

Methods were used to estimate the surface metal atoms per gram of the catalyst, n_s, as described in section 3.5. Turnover numbers ν, defined as the number of reactant

TABLE 4.1

Relative Sensitivity data for Hydrogen Flame Detector

n-Alkanes	Relative Sensitivity
Methane	0.97
Ethane	0.97
Propane	0.98
Butane	1.09

molecules converted per unit time per surface metal atom, were then calculated from expression 4.5,

$$\nu = \frac{r_o \cdot N_R}{m \cdot n_s} \qquad (4.5)$$

m is the mass of the catalyst used in the experiments.

Initial product distributions (fig. 4.8-4.11) were obtained by plotting the product concentration calculated from expression 2 against conversion. The initial slopes of these curves represent the selectivity s_i for product i, defined as the number of molecules of reactant destroyed. From these parameters it was then possible to calculate 'M_B'

$$M_B = [(S'_4 + \sum_i S_i)/(1-S'_4)]-1 \qquad (4.6)$$

where M_B indicated the depth of hydrogenolysis. A value of M_B of unity indicates a stepwise hydrogenolysis with the cleavage of only one C-C bond for each molecule of reactant destroyed, e.g. the hydrogenolysis of an n-butane molecule to form two molecules of ethane or one of methane and one of propane.

4.5 RESULTS

The total surface area, and the metal dispersions of the 'as-received' and alkali doped EUROPT-1 samples, as discussed in Chapters 2 and 3 respectively, are shown in tables 2.1 and 3.3 respectively. The total surface area (BET) varied from 186 $m^2\ g^{-1}$ to 132 $m^2\ g^{-1}$ catalyst, and

metal dispersion from 66 to 33%.

The rate measurements for the hydrogenolysis of n-butane given in Tables 4.2 and 4.3 were made at conversion levels of between 1 to 20% at 523 K as shown in the plots of $\%C_4$ versus time for the four catalysts, (Figures 4.4-4.7). An initial experiment with 'as-received' EUROPT-1 was carried out at 473 K and this allowed an activation energy of 104 kJ mol^{-1} to be estimated for n-butane hydrogenolysis over the catalyst.

Also included in Tables 4.2 and 4.3 are the turnover numbers (TON) of 'as-received' and alkali doped EUROPT-1 samples. The purpose of determining turnover number is to account for differences in catalytic activity arising solely from differences in metal surface area.

The decrease in the conversion of n-butane with increasing alkali concentration is demonstrated in Figures 4.4-4.7. Although the 0.5% and 1.0% KOH (wt)/EUROPT-1 catalysts showed only a small conversion of n-butane, the rate of reaction of these on the 0.25% alkali doped and 'as-received' EUROPT-1 were readily obtained. The gradual decrease of the rates with time may be caused by a change in the order of reaction, or poisoning due to the formation of carbonaceous materials. Plots of log $\%C_4$ versus time for the faster reactions were made and these proved to be more linear. The rates calculated however were similar to those obtained initially from the conversion versus time plots. Thus the latter were used

n-Butane Hydrogenolysis over EUROPT-1 Doped with KOH at 523 K

Catalyst	Rate of Reaction $S^{-}g^{-1}$	Turnover Number S^{-1} Site^{-1}	Initial Products S_1	S_2	S_3	S_4	M_B
Clean EUROPT-1	1.22×10^{16}	9.8×10^{-5}	0.54	0.76	0.51	0.10	1.0
	2.4×10^{14}*	1.79×10^{-6}	0.28	0.54	0.27	0.49	1.0
0.25% KOH/EUROPT-1	5.76×10^{15}	5.3×10^{-5}	0.48	0.62	0.49	0.22	1.0
0.5% KOH/EUROPT-1	1.31×10^{15}	1.51×10^{-5}	0.37	0.60	0.40	0.29	1.0
1.0% KOH/EUROPT-1	2.25×10^{14}	2.86×10^{-6}	0.25	0.53	0.26	0.47	1.0

* Reaction carried out at 473 K

Table 4.3

n-Butane Hydrogenolysis over EUROPT-1 Doped with K_2CO_3 at 523 K

Catalyst	Rate of Reaction $S^{-}g^{-1}$	Turnover Number S^{-1} Site^{-1}	Initial Products S_1	S_2	S_3	S_4	M_b
As-received EUROPT-1	1.22×10^{16}	9.8×10^{-5}	0.54	0.76	0.51	0.10	1.0
0.25% K_2CO_3/EUROPT-1	9.93×10^{15}	1.84×10^{-4}	0.51	0.64	0.48	0.18	1.0
0.5% K_2CO_3/EUROPT-1	7.24×10^{15}	9.32×10^{-5}	0.38	0.55	0.37	0.44	1.0
1.0% K_2CO_3/EUROPT-1	2.33×10^{15}	3.63×10^{-5}	0.22	0.48	0.22	0.52	1.0

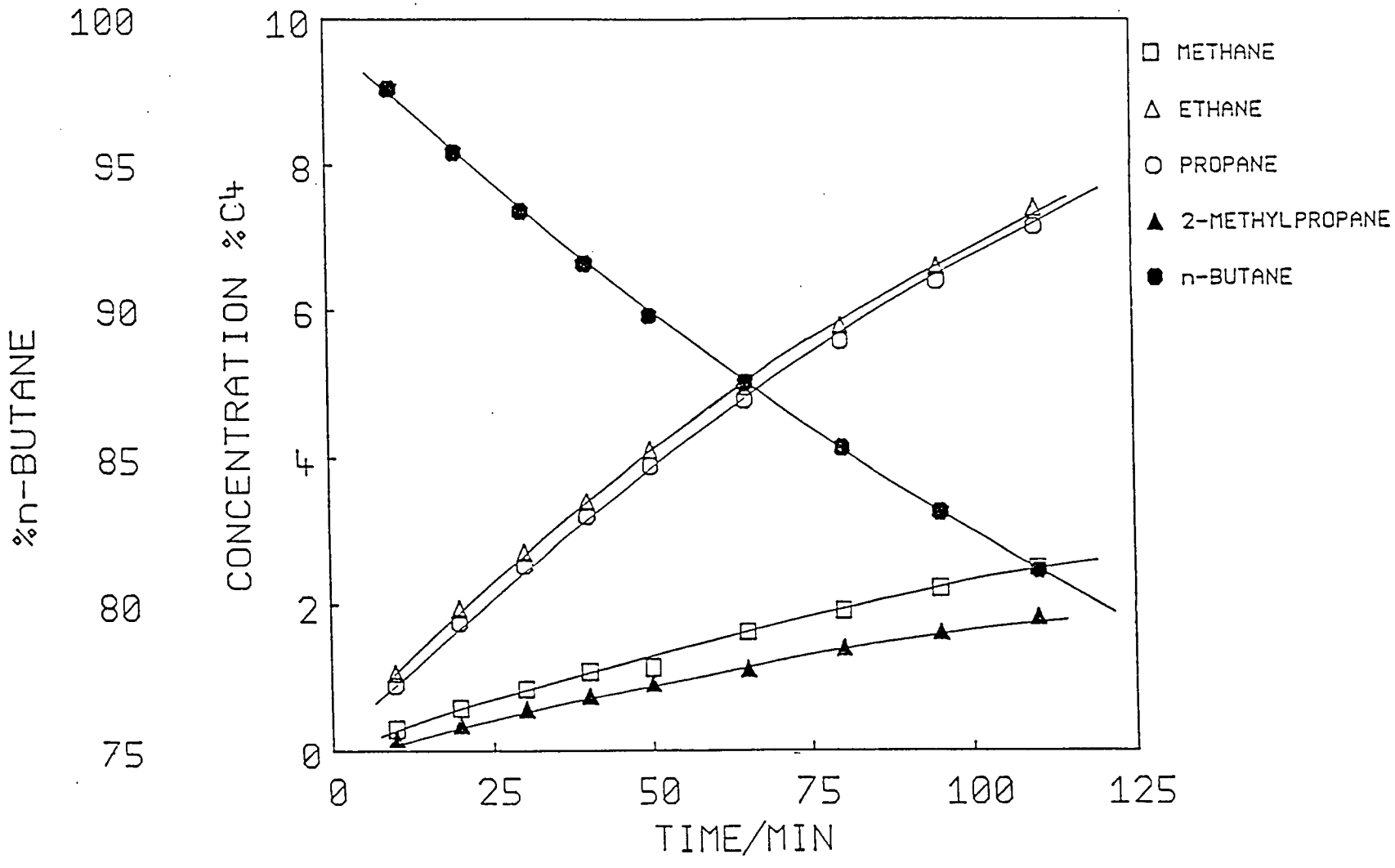

Fig. 4.4 Reaction Profiles for n-butane Hydrogenolysis over as-received EUROPT?1 at 523K.

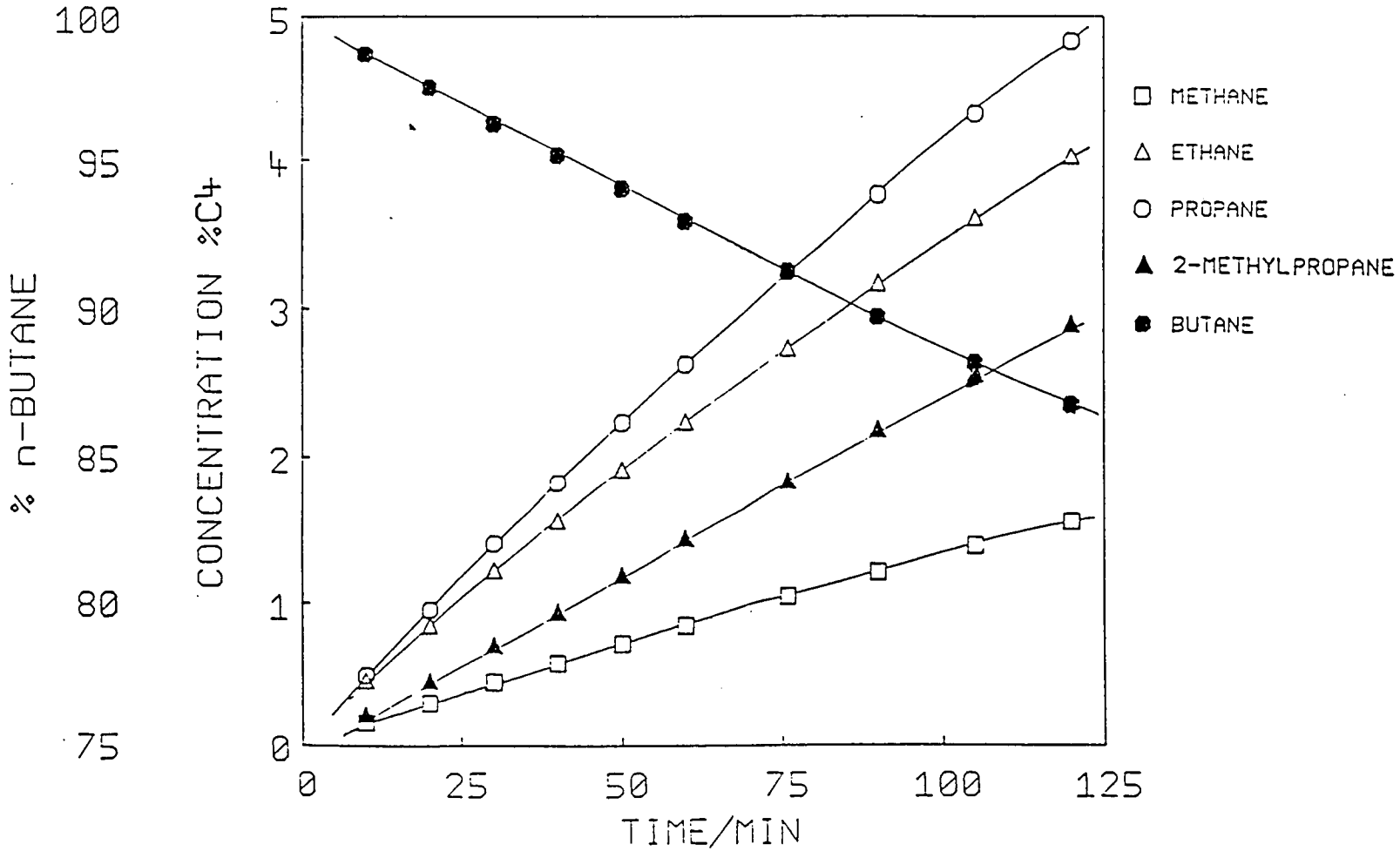

Fig. 4.5 Reaction Profiles for n-butane Hydrogenolysis over 0.25% KOH (wt)/EUROPT-1 at 523K.

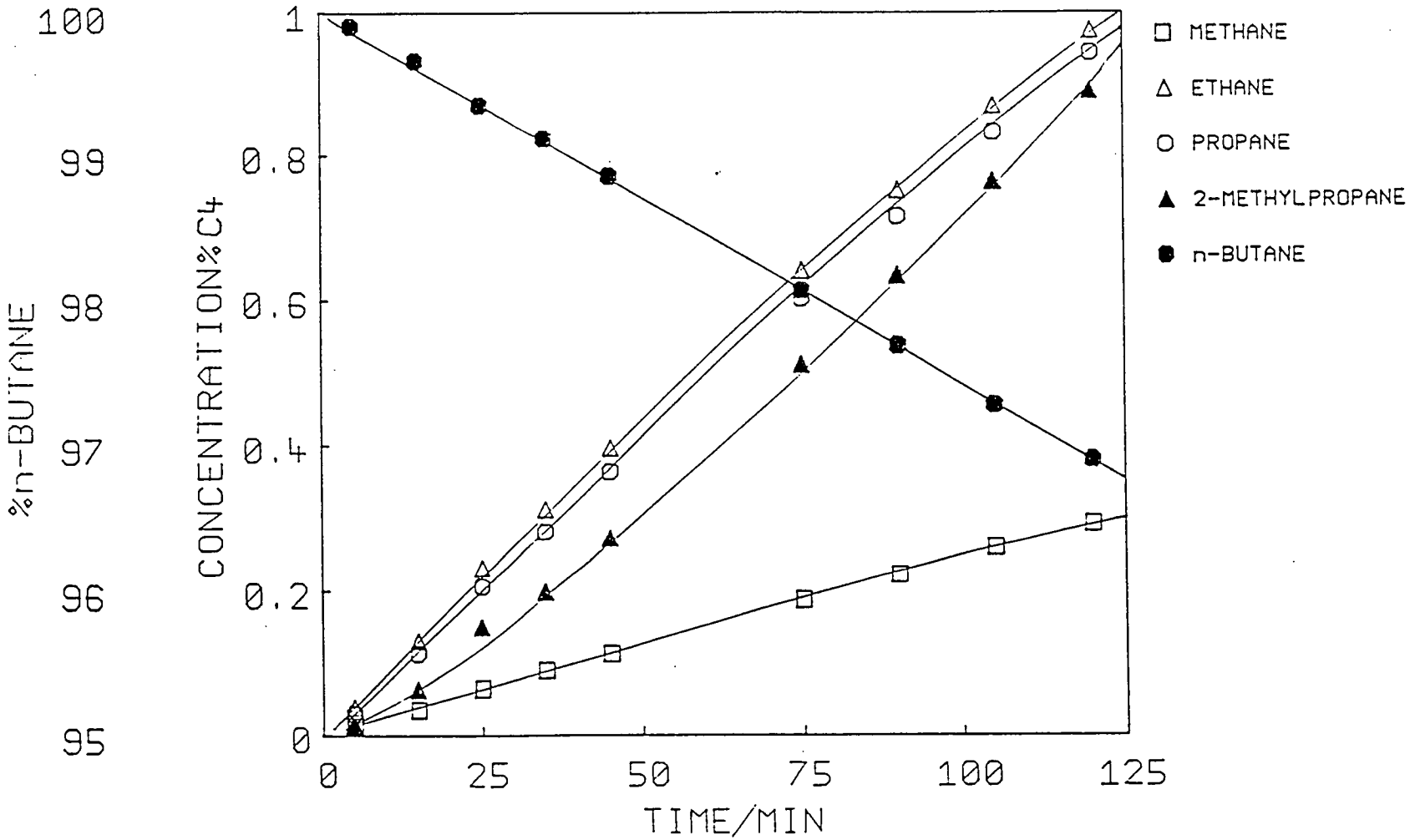

Fig. 4.6 Reaction Profiles for n-butane Hydrogenolysis over 0.5% KOH (wt)/EUROPT?1 at 523K.

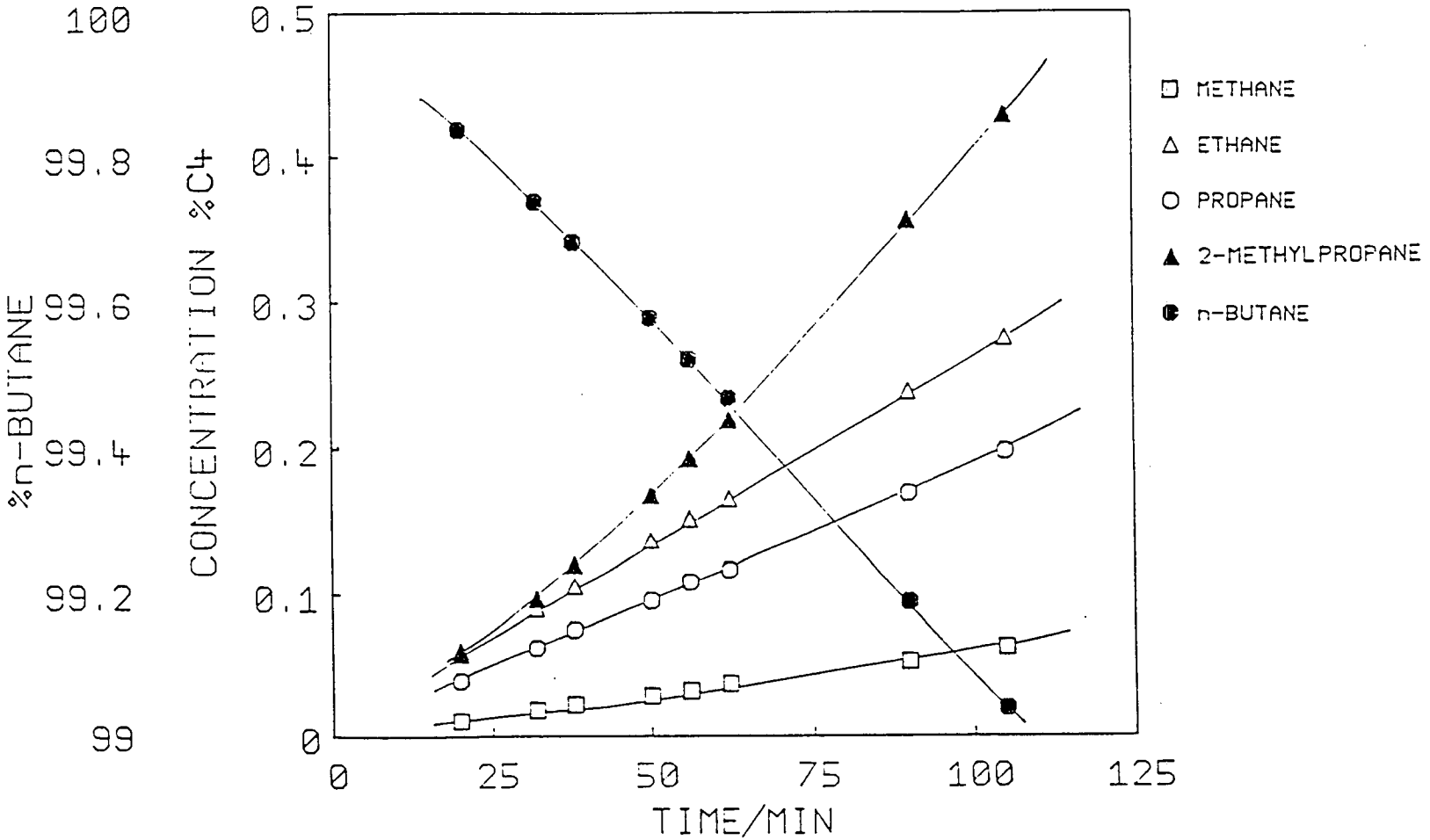

Fig. 4.7 Reaction Profiles for n-butane Hydrogenolysis over 1.0% KOH (wt)/EUROPT-1 at 523K.

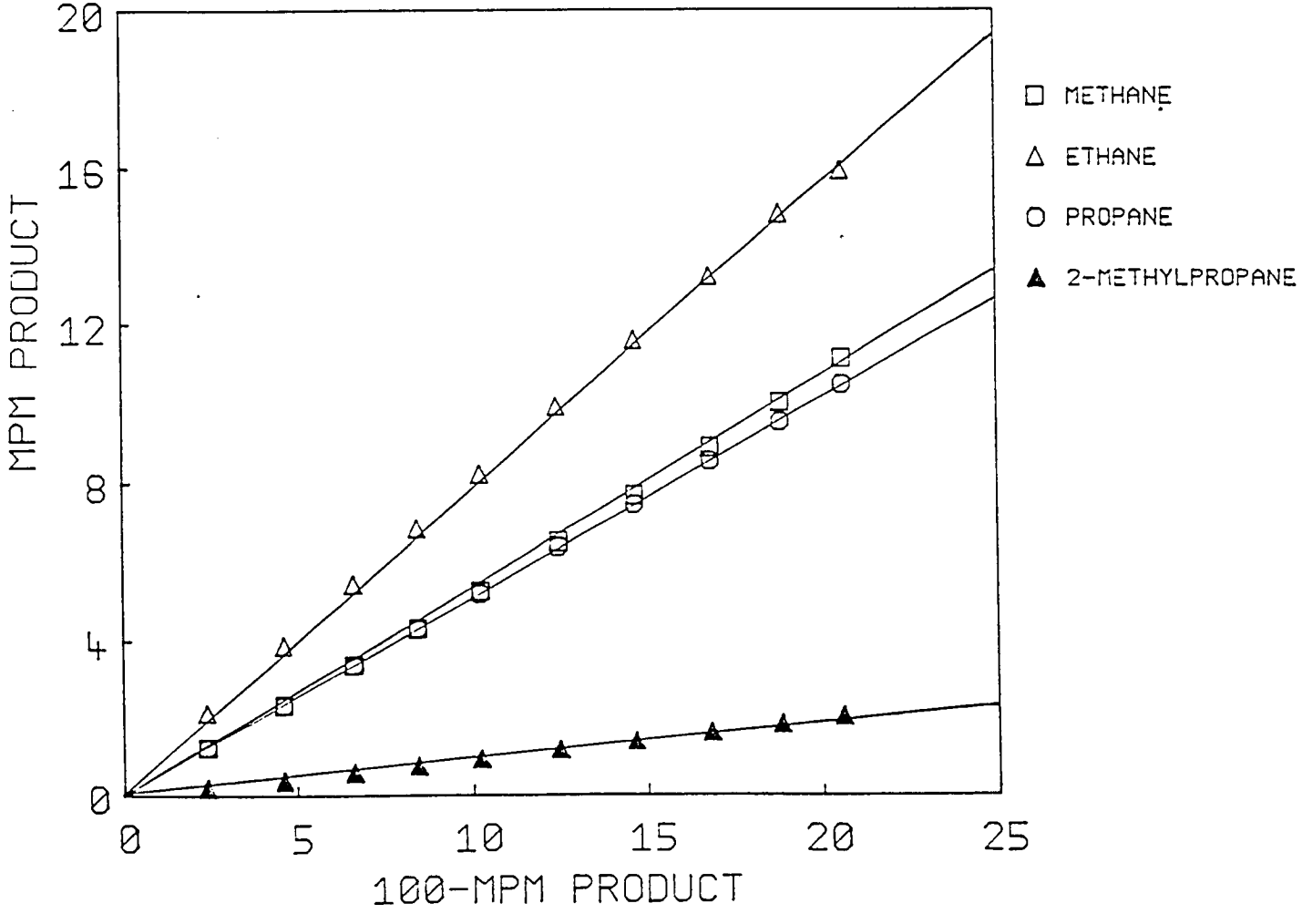

Fig. 4.8 Initial Product Distribution for n-butane Hydrogenolysis over as-received EUROPT-1 at 523K.

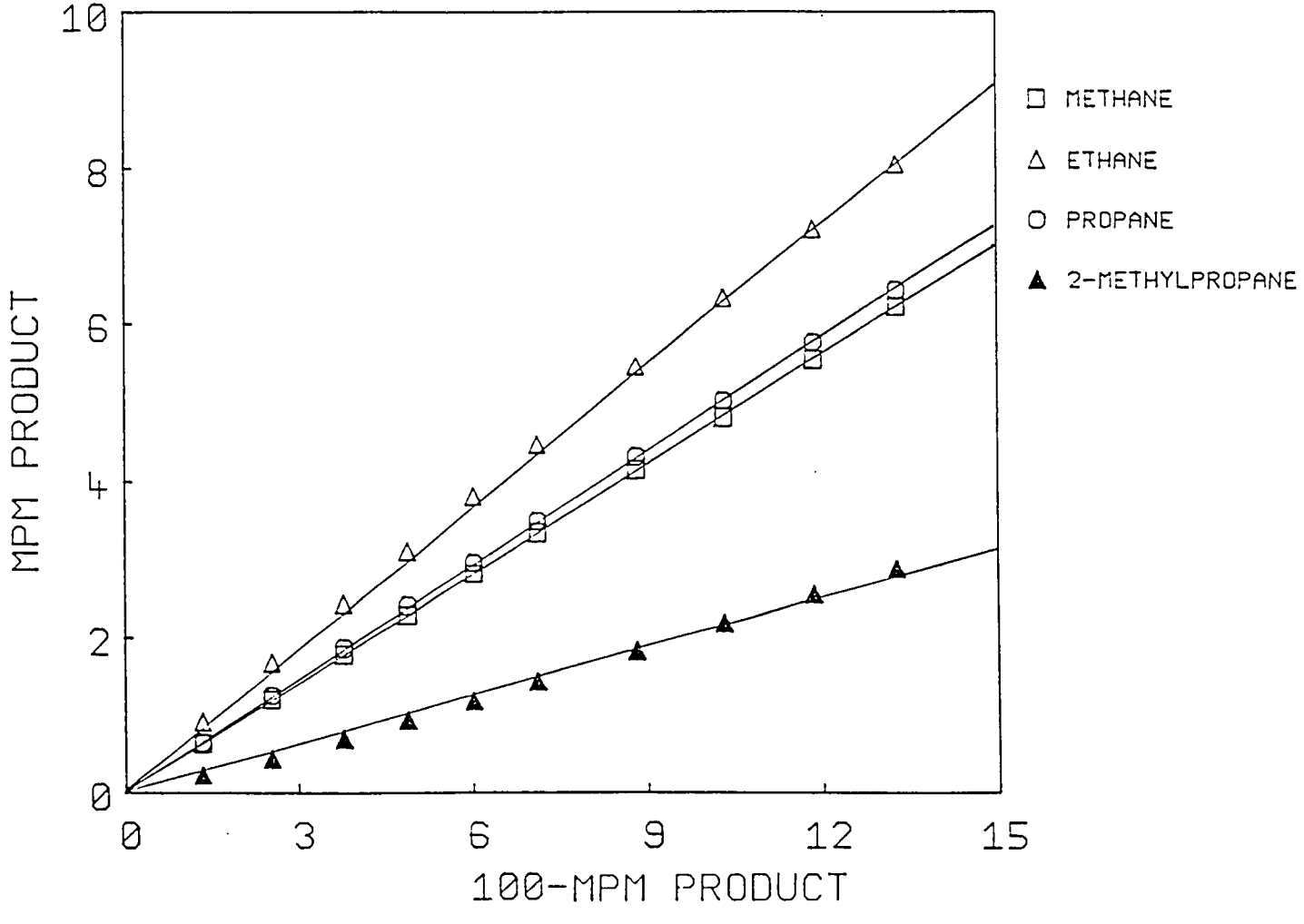

Fig. 4.9 Initial Product Distribution for n-butane Hydrogenolysis over 0.25% KOH (wt)/EUROPT-1 at 523K.

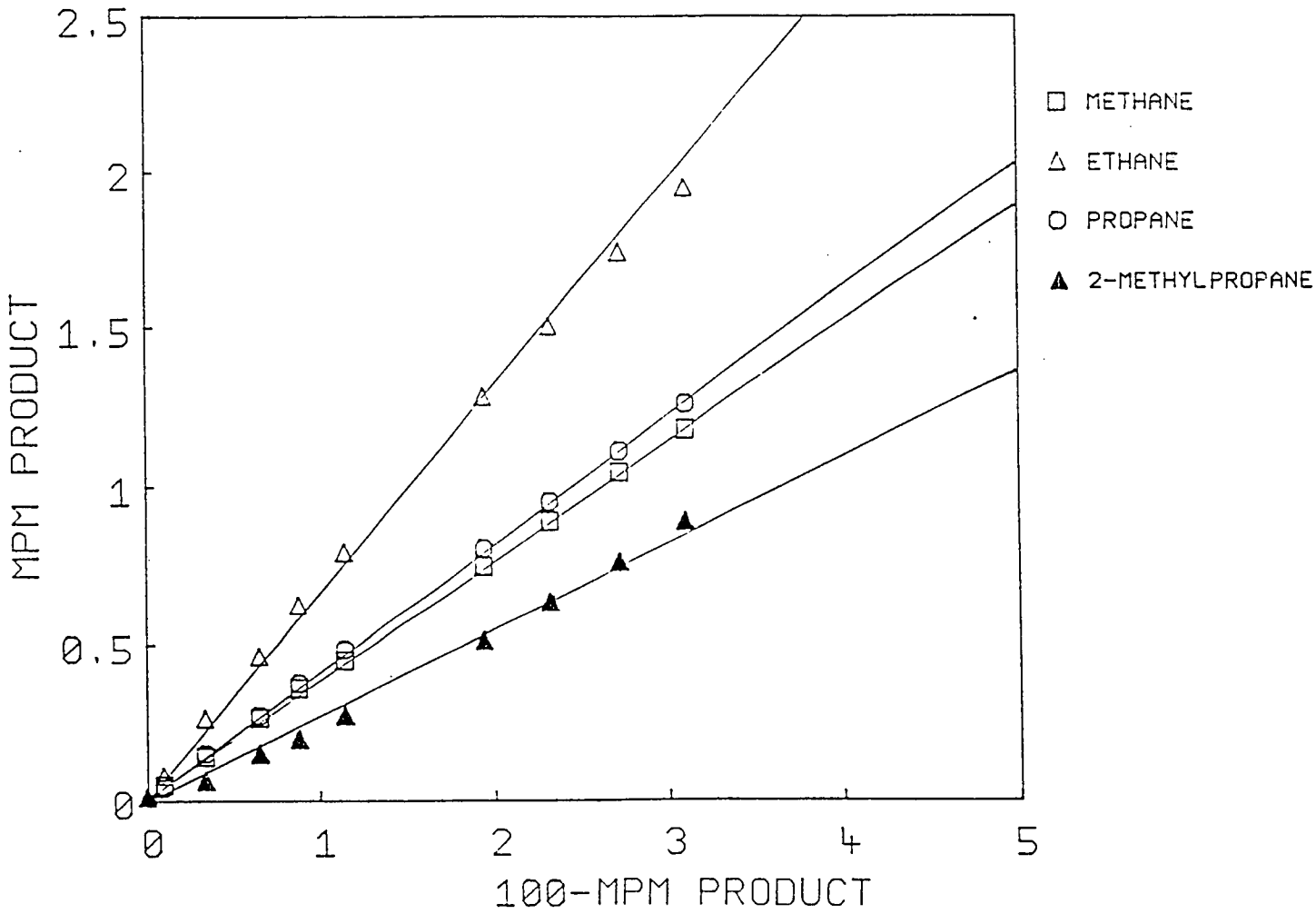

Fig. 4.10 Initial Product Distribution for n-butane Hydrogenolysis over 0.50% KOH (wt)/EUROPT-1 at 523K.

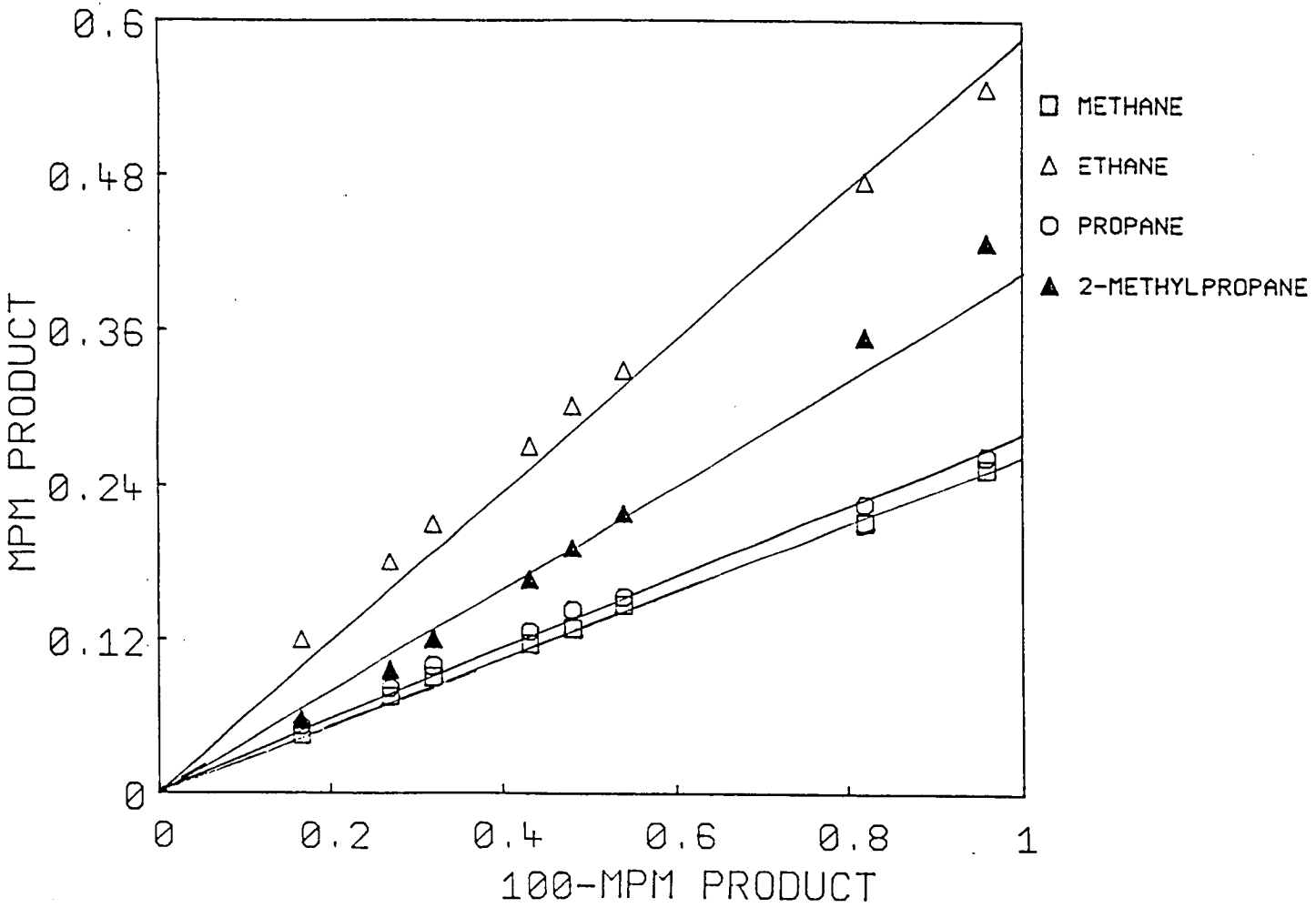

Fig. 4.11 Initial Product Distribution for n-butane Hydrogenolysis over 1.0% KOH (wt)/EUROPT-1 at 523K.

for comparison with the higher alkali doped catalysts.

Similar results were obtained with EUROPT-1 doped with the same concentration of K_2CO_3 as shown in Table 4.3.

It is evident that the rate for each alkali doped EUROPT-1 catalyst decreases compared with the 'as-received' EUROPT-1. In reaction over 'as-received' catalysts, about 20% of n-butane is consumed, which decreases to less than 1% over the same period of time at the highest concentration of alkali (KOH). The decrease in turnover number corresponds directly with increasing amount of alkali. Since turnover number normalizes for loss of surface area/surface sites then this points towards a progressive reduction in rate with increasing alkali over and above any reduction due to sintering or site blocking.

The initial product distributions in Tables 4.2 and 4.3 and Figures 4.8-4.11 show significant variation in selectivities with alkali concentration. In all cases C_2H_6 is the dominant product showing preference for the central bond cleavage which was not altered by the alkali concentration. A gradual decrease in the selectivities for CH_4 and hence for C_3H_8 with increasing alkali concentrations was observed. The ratio of CH_4:C_3H_8 remained unity throughout whereas a significant increase in the selectivities towards the formation of 2-methylpropane (S'_4) with increasing alkali concentration was observed.

The values of M_B listed in Tables 4.2 and 4.3 indicate the depth of hydrogenolysis or the number of C-C bonds ruptured, hence the value of unity suggested the cleavage of one C-C bond and the overall reaction was stepwise hydrogenolysis.

4.6 DISCUSSION

On inspecting the rates of hydrogenolysis of n-butane (Tables 4.2 and 4.3), it became clear that doping the catalyst with alkali leads to a decrease in overall rate with increasing alkali concentration. There is some evidence in the literature that metal surface area and the crystallite size can affect the properties of metals in chemisorption and catalysis[32]. Thus, it is of interest to consider the activities in relation to other properties of the metal such as the surface area and the particle size. The observed loss of catalytic activity with the loss of hydrogen chemisorption capacity (upon alkali doping in the present case) can be correlated with the results reported by Martin *et al.*[33] who found a similar loss of activity upon heat treatment which also caused a loss of metal surface area. Also Bond *et al.*[13] noted similar effects on catalytic activity of EUROPT-1 upon various heat treatments. The authors attributed this loss of activity to the loss of hydrogen chemisorption capacity, primarily ascribed to the growth in particle size.

The initial product distribution at the reaction

temperature (523K) shows that the dominant product of hydrogenolysis was C_2H_6, suggesting preferential central bond rupture. It has been shown[27] that CII-CII bond cleavage occurs more readily on well-dispersed catalysts, thus the results here are not unexpected. The initial product distribution observed in the present study is close to that found by Bond *et al.*[13], at a similar reaction temperature. Based on this evidence it is suggested that the hydrogenolysis mechanism is basically a C_2 unit mode, as defined by Foger and Anderson[27].

The activation energy of 104 kJ $mole^{-1}$ observed in the present study is in fair agreement with the reported values in the literature[11-13,20]. Bond *et al.*[13] reported an activation energy of 114 kJ $mole^{-1}$ for n-butane hydrogenolysis over the EUROPT-1 catalyst. Similar values have been reported by Guczi[11] and Leclerq *et al.*[12] over Pt black and Pt/Al_2O_3 catalysts respectively.

The product distributions indicated that the stepwise hydrogenolysis as defined in Section 4.1 was accompanied by some isomerisation. It suggests that isomerisation took place even on the very small crystallites of EUROPT-1. According to Gault[28] isomerisation takes place on the edge atoms of the crystallites, and not on the regular low index planes. This will be discussed later.

EUROPT-1 behaves in a similar way to Pt black catalyst regarding the hydrogenolysis of n-butane[11]. The activation energy and product distributions are similar.

The selectivity of C_2H_6 is reported to approach a non-zero limiting value due to the direct formation of ethane at low catalytic activities, where hydrocarbon isomerisation becomes more favoured. However, a slightly different mechanism has been reported on Pt/Al_2O_3 catalyst regarding the bond cleavage. Leclercq *et al.*[12] observed n-butane reaction over Pt/Al_2O_3 giving CH_4, C_3H_8 C_2H_6 via fragmentation of CI-CII bond.

Higher activities of the highly dispersed catalysts have been attributed to the smaller crystallites[27,28,34-35]. Carter *et al.*[34] found that the catalytic activity decreased at a greater rate than metal surface area and attributed this effect to higher specific activities of smaller particles.

In addition to metal surface area, reactant composition can also influence rates. For increased hydrogen pressure (i.e. H:HC mixture) as reported by Guczi *et al.*[11], the active sites are thought to be successively covered by randomly deposited carbon residue or hydrogen atoms. In this way not only is the possibility of dissociative adsorption decreased as indicated by the hydrogenolysis activity, but also the reduction of the number of active sites resulting in the lower probability of adsorbed hydrocarbon molecules finding an unoccupied adjacent Pt atom to allow further bond breaking.

A direct comparison of the present result with the literature is difficult as there is little evidence of

alkane hydrogenolysis over potassium doped supported Pt catalysts. There is evidence[23] that a K_2O doped Ni/Al_2O_3 catalyst, used for propane hydrogenolysis, had a significantly changed morphology. The authors reported a loss of metal surface area, B.E.T. area, growth of particle size and decreased hydrogenolysis activity.

The role of potassium in Fischer-Tropsch (F-T) synthesis has been widely studied[36-38]. Boudart[38] determined the role of potassium in the F-T synthesis reaction over iron catalysts. The author emphasised that introduction of potassium into the catalyst markedly decreased the ability to rupture the C-C bond. The role of potassium was thought to preserve at the surface, the CH_2 radical which finally yields higher molecular weight saturated hydrocarbons.

The product distribution in Tables 4.2 and 4.3 shows some isomerisation on 'as-received' EUROPT-1. From the literature it is understood that among the group VIII metals, only Pt shows a high isomerisation selectivity[11,12]. Anderson and Avery[26] reported selective isomerisation on Pt metal. The authors proposed a bond shift mechanism based on 1,3-diadsorbed species.

Isomerisation observed in the present study can be understood with reference to the reported literature. Guczi *et al.*[11] observed isomerisation during hydrogenolysis of n-butane over platinum black catalysts. The authors reported that isomerisation was more favoured

at low catalytic activity. Leclercq *et al.*[12] observed isomerisation of n-butane on a Pt/Al_2O_3 catalyst in a similar way to EUROPT-1. Thus it is assumed that only Pt metal is responsible for isomerisation activity.

Some isomerisation is observed on EUROPT-1 which is a highly dispersed catalyst. This is also highly active in hydrogenolysis following the C_2 unit mode mechanism based on 1,2-diadsorbed species, but the isomerisation observed suggests that a portion of the reaction follows an iso-unit or 1,3-diadsorbed mode.

The product distributions (Table 4.2 and 4.3) show an increasing 2-methylpropane selectivity with increasing alkali concentration. This is attributed to the alkali effect. It has been mentioned earlier that alkali doping may cause significant change in the catalyst morphology (Chapter 3) with formation of larger crystallites, as reported by Dry *et al.*[22]. Hence it is assumed that larger crystallites are responsible for the increased isomerisation selectivity. Due to large ensembles the availability of sites for fragmented hydrocarbons are decreased and methyl shift becomes more favoured, based on 1,3-diadsorbed species, recombining to give 2-methylpropane.

Using the data in table 4.2 a further insight into the effect of alkali doping on the selectivities is shown in figure 4.12. This shows that methane/propane selectivity drops in a parallel fashion consistent with $M_B = 1$ on all

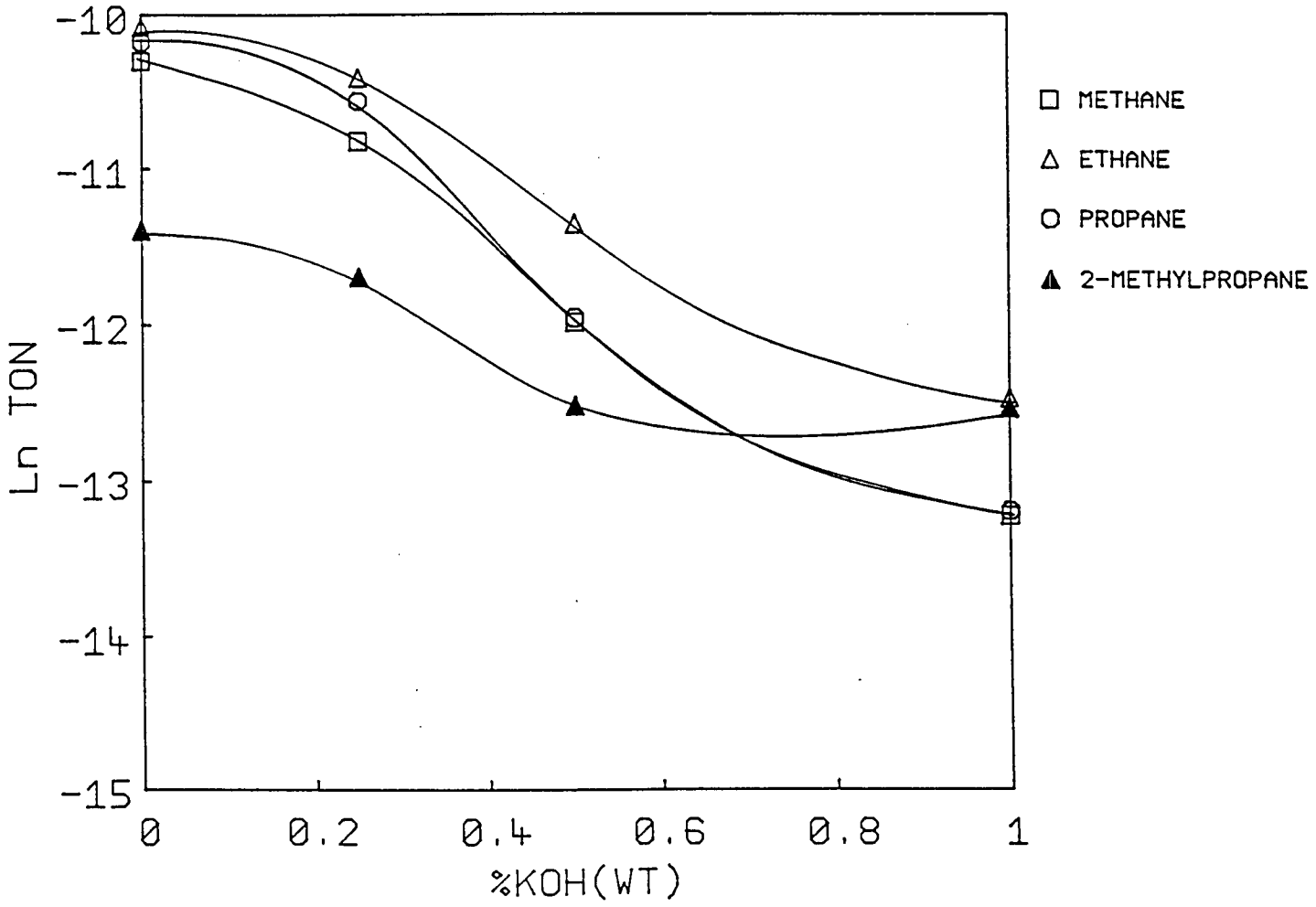

Fig. 4.12 Change in Selectivities (TON) as a Function of Alkali Concentration

catalysts. Ethane shows a similar rate of decreasing T.O.N. within given experimental accuracy. This suggests general suppression of hydrogenolysis activity via C_I-C_{II} and C_{II}-C_{II} unit mode. The absolute value of hdyroisomerisation activity also falls.

This conclusion can be supported by the findings of Gault[28]. The author reported that isomerisation took place on the edge atoms of the crystallites. The author suggested that two types of sites existed on catalysts of small and large particles. The first arising on very small platinum particles responsible for normal hydrogenolysis activity and the second on larger crystallites, responsible for bond shift or isomerisation.

In the present study, it is noted that the turnover numbers (T.O.N.) decreases with increasing alkali concentration (Tables 4.2 and 4.3). If this decrease was due solely to site blocking or loss of chemisorption capacity, the T.O.F. should be the same. The fact that they are not suggests that the potassium must be having some other effect other than purely site blocking.

It is also observed that KOH caused more deactivation as compared with K_2CO_3, inspite of having the same metal surface areas. This suggests some other factors are also involved such as the neutralisation of acid centres of the support.

4.7 CONCLUSION

1. The decrease of overall rate of reaction can partly be attributed to the loss of metal surface area, mainly caused by direct site blocking by the potassium or alternatively by growth of crystallite size. The decreasing T.O.N. with increasing alkali concentration, however, leads to the idea that some factors other than site blocking are also involved. The catalytic behaviour of platinum in some way has been changed by the alkali.
2. The unity value of M_B suggests hydrogenolysis reaction via only one C-C bond rupture.
3. The initial product distribution showed ethane as dominant product of hydrogenolysis suggesting a $C_{(II)}$ unit mode of bond rupture. Some isomerisation on the 'as-received' catalyst suggests that bond shift mechanisms (1,3-diadsorbed species) also exists along with the $C_{(II)}$ unit mode.
4. Increased selectivity towards isomerisation in the case of alkali doped samples indicates that the alkali may in some way favour the formation of 1,3-diadsorbed intermediates. This type of species may well be favoured by the larger ensemble sites available on larger crystallites and so perhaps again points towards sintering of the metal as the main action of the alkali on the hydrogenolysis activity.
5. The observed increase in isomerisation selectivity may

be attributed to the less marked suppression of the isomerisation reaction than the general hydrogenolysis reaction.

6. Although the two alkalis, KOH and K_2CO_3, had the same effect on metal dispersion, and presumably particle size (of EUROPT-1), the catalytic deactivation was found to be more for the KOH doped EUROPT-1 catalysts. This might be due to some other effect of alkali such as the extent of neutralisation of acid centres on the support.

REFERENCES

1. J.H. Sinfelt, *Adv.Catal.* 23 (1973) 91.
2. J.R. Anderson, *Adv.Catal.* 23 (1973) 1.
3. R. Maurel and G. Leclercq, *Bull.Soc.Chim.Fr.* (1971) 1234.
4. H. Matsumoto, X. Saito and Y. Yoneda, *J.Catal.* 19 (1970) 101.
5. C.J. Machiels and R.B. Anderson, *J.Catal.* 58 (1979) 253.
6. G. Leclercq, L. Leclercq and R. Maurel, *J.Catal.* 44 (1976) 68.
7. G. Leclercq, L. Leclercq and R. Maurel, *J.Catal.* 50 (1977) 87.
8. M. Boudart, *Adv.Catal.* 20 (1969) 153.
9. G.C. Bond, Catalysis by Metals (Academic Press, London and New York, 1962).
10. C. Kemball, *J.Chem.Soc.Faraday I* 68 (1973).
11. L. Guczi, K. Matusek, A. Sarkany and P. Tetenyi, *Bull.Soc. Chim.Belg.* 88 (1979) 497.
12. G. Leclercq, L. Leclercq and R. Maurel, *Bull.Soc.Chim.Belg.* 88 (1979), 599.
13. G.C. Bond and X.U. Yide, *J.Chem.Soc.Faraday Trans.I* 80 (1984) 969.
14. G. Leclercq, S. Pietrzyk, and M. Peyroui, *J.Catal.* 99 (1986) 1..
15. A.F. Dauscher, F. Grain, F. Luck and G. Maire, in:

Metal-Support and Metal-additive Effects in Catalysis, Eds. B. Imelik, C. Naccache, G. Couduriev, H. Raliand, P. Meriaudeau, P. Gallezot, G.A. Martin and J.C. Vedrine (Elsevier, Amsterdam, 1982), p. 247.

16. J.M. Dominguez and M.J. Yacamen, *J.Catal.* 64 (1980) 223.
17. G. Xiexian, Y. Zhenkai and Y. Yashu, in: Symposium on Heterogenous Catalysis Related to Energy Problems (Dalian Institute of Chemical Physics, Dalian, China, 1982).
18. Tran Manh Tri, J. Massardier, P. Gallezot and B. Imelik, in: Proc. 7th Intern. Congress Catal., 1981.
19. Tiek Chen Wong, L.F. Brown, G.L. Haller and C. Kemball, *J.Chem.Soc., Faraday Trans.I* (1981) 519.
20. G.A. Somorjai, in: The Chemical Physics of Solid Surfaces and Heterogenous Catalysis, Eds. D.A. King and D.P. Woodruff, Vol. 4, (Elsevier, 1982).
21. J.H. Sinfelt, W.F. Taylor and D.J.C. Yates, *J.Phys.Chem.* 69 (1965) 95.
22. M.E. Dry and L.C. Ferreira, *J.Catal.* 7 (1967) 352.
23. F.E. Shephard, *J.Catal.* 14 (1969) 148.
24. M. Boudart and G. Djega-Mariadasou, Kinetics of Heterogenous Catalytic Reactions (Princeton University Press, N.J., 1984).
25. R.A. Dalla Betta and M. Boudart, in: Proc. 5th Intern. Congress on Catalysis, Palm Beach, 1972.
26. J.R. Anderson and N.R. Avery, *J.Catal.* 5 (1966) 446.

27. K. Foger and J.R. Anderson, *J.Catal.* 59 (1979) 325.

28. F. Gault, *Adv.Catal.* 30 (1981) 1.

29. R.S. Dowie, D.A. Whan and C. Kemball, *J.Chem.Soc. Faraday Trans.I* (1972) 2150.

30. D. Garden, C. Kemball and D.A. Whan, *J.Chem.Soc. Faraday Trans. I* (1986) 3113.

31. C.J. Kempling and R.B. Anderson, *Ind.Eng.Chem.Process Des.Dev.* 11 (1972) 146.

32. J.H. Sinfelt and D.J.C. Yates, *J.Catal.* 8 (1967) 82.

33. G.A. Martin, *React.Kinet.Catal.Lett.* 16 (1981) 329.

34. J.L. Carter, J.A. Cusumano and J.H. Sinfelt, *J.Phys.Chem.* 70 (1966) 2257.

35. P.A. Burke and E.I. Ko, *J.Catal.* 116 (1989) 230.

36. H.E. Dry, T. Shingles, L.J. Boshoff and G.J. Oosth Uizen, *J.Catal.* 15 (1969) 190.

37. C.T. Campbell and D.W. Goodman, *Surf.Sci.* 123 (1982) 413.

38. M. Boudart, *J.Phys.Chem.* 58 (1954) 796.

CHAPTER 5

A DRIFTS STUDY OF ADSORPTION AND THERMAL DESORPTION OF CO

5.1 INTRODUCTION

Early infrared spectroscopic studies of carbon monoxide adsorption on supported platinum catalysts were carried out by Eischen *et al.*[1-2]. Since then a great deal of literature regarding the infrared spectra of carbon monoxide adsorbed on metals and supported metal catalysts has been accumulated[3-12]. The carbon-oxygen stretching frequency for chemisorbed CO has been observed between 2020 and 2100 cm^{-1} arising from CO linearly bonded to Pt and a much weaker band in the 1800-1900 cm^{-1} region.

Eischen and Pliskin[2] were the first to report an infrared spectrum of CO adsorption on supported and unsupported platinum. The band corresponding to the stretching vibration ν(CO) of the species Pt-CO was observed at around 2060 cm^{-1}. The frequency increased with increasing coverage of the metallic surface. Using ^{12}CO and ^{13}CO molecules, these authors concluded that this shift of frequency as a function of coverage was due to dipole-dipole coupling interactions.

Sheppard and Nguyen[3] published a detailed review on the vibrational spectra of chemisorbed CO on the surface of metal catalysts in general. The authors reported a range of frequencies showing an intense peak at 2090-2050 cm^{-1}, and a second weaker broad peak between 1860-1800

cm^{-1}. These peaks were attributed to linear and bridged bonded CO respectively.

The infrared study of CO adsorption on EUROPT-1 at room temperature, to saturation carried out by McDougall[4] indicates the expected linear and bridged bands at 2079 and 1847 cm^{-1} respectively. The spectrum also shows the existence of a third peak at 1703 cm^{-1}. This peak has been assigned to the carbon-oxygen stretching vibration of carbon monoxide chemisorbed at a multi-centre site such as the B_3, B_4 and B_5 sites of (111), (100) and (110) surfaces, using the notation developed for multi-centre sites by Hardeveld *et al.*[13]. Such a low frequency peak has not been noted previously for carbon monoxide adsorbed on platinum surfaces.

Bartok *et al.*[5] performed an infrared study of CO adsorption on a 5% Pt/SiO_2 catalyst. During the stepwise adsorption, the pressure of CO was increased from 10^{-4} torr to 20 torr. The authors observed only one band in the 2000-2100 cm^{-1} region of the spectrum. At an extended coverage of 100 torr, a small shoulder at 2105 cm^{-1} was observed. However this band was reported to disappear by evacuation at 293 K. The authors did not observe any peak in the region 1800-2000 cm^{-1}, indicating absence of bridge bonded CO.

In recent years it has been possible to measure vibrational spectra of carbon monoxide adsorbed on platinum single crystals, either by reflection-absorption

infrared spectroscopy (RAIRS)[6,11], or by electron energy loss spectroscopy (EELS)[9-10]. This enabled researchers to determine the vibrational spectra of carbon monoxide on particular crystal faces of platinum.

The first 'RAIRS' study of CO adsorption on a Pt(111) single crystal at 295 K was carried out by Horn and Pritchard[11]. The low coverage CO adsorption gave a band at 2065 cm^{-1} with a half width of *ca.* 20 cm^{-1}. This band was attributed to isolated adsorbed CO molecules. With increasing coverages this band shifted to higher wave numbers, i.e. 2082 cm^{-1} and was finally at 2089 cm^{-1}, with a half width of 15 cm^{-1}. The 'EELS' results by Ibach and associates[9] for CO adsorption on a Pt(111) single crystal at 320 K, showed a band at 2075 cm^{-1} shifting to higher frequency (2100 cm^{-1}) with increasing coverages. Crossley and King[12] observed a band shift (linear) by 35 cm^{-1} going from low to increasing coverage of CO on Pt(100). This shift was suggested to be due to dipole-dipole coupling, as concluded by others[2-3,9-11].

The technique of thermal desorption infrared spectroscopy, to study the CO-metal interaction, has been developed by Miura and Gonzalez[15]. There are a number of examples of such techniques used[16-18]. Recently Haaland[17] applied thermal desorption infrared technique to supported platinum. The thermal desorption infrared spectra can be obtained by either of two methods. In the first method, the adsorbate is admitted to the sample at a certain

temperature, the sample is then subjected to continuous purging or evacuation, and the temperature is raised steadily as spectra are taken at intervals. In the second method, the adsorbate is admitted at some elevated temperature, the sample is subjected to purging or evacuation at constant temperature, and spectra are taken at intervals. The advantage of the second method is that a constant temperature provides a constant spectral background and hence produces more precise results. In the present study, the CO desorption measurements were performed in flowing helium by heating the sample manually from room temperature to 923 K in 100 K steps with the spectrum recorded during the constant temperature phase of heating programme.

Although there is no example of infrared study of CO adsorption or desorption from alkali doped supported metal catalysts, some work has been done using a potassium covered platinum single crystal. The vibrational properties of CO adsorption on Pt(111) + K system was studies by Crowell *et al.*[19], using the EELS technique. On an unpromoted surface, the CO stretch frequencies were at 1800-2120 cm^{-1}, in agreement with the earlier studies on a clean Pt(111) single crystal. The coadsorption of CO with submonolayer amounts of potassium on the Pt(111) crystal surface showed a continuous decrease in the CO stretching vibrational frequencies with increasing potassium coverage. A decrease in CO vibrational frequencies to as

low as 1400 cm^{-1} was observed, which is the lowest CO stretch frequency observed for CO on metal surfaces to date.

Thermal desorption spectra for various CO exposures on Pt(111) at various potassium coverages were also reported by Crowell *et al.*[19]. Pronounced effects of potassium on the CO desorption were observed. The CO desorption peak maxima shift considerably to higher temperatures. Similar effects of potassium can be seen when CO desorbs from a potassium covered Ni(100)[20,21].

These alkali effects are explained by a simultaneous charge transfer from the potassium adatoms to the platinum surface, and a resulting increase in back donation from the platinum into the coadsorbed CO molecules. This is in accordance with the model of enhanced back donation of electrons from the platinum into the $2\pi^*$ anti-bonding orbital of CO[22].

Investigation of the chemisorptive properties of carbon monoxide on the EUROPT-1 and alkali doped EUROPT-1 catalysts were carried out in the present study. Diffuse reflectance infrared fourier transform spectroscopy (DRIFTS) was used to determine the vibrational frequencies. Thermal desorption infrared spectroscopy (TPD/DRIFTS) was used to determine the interaction, and changes in the interaction of CO when coadsorbed with potassium.

5.2 A DIFFUSE REFLECTANCE INFRARED STUDY : BASIC THEORY AND INSTRUMENTATION FOR FOURIER TRANSFORM INFRARED SPECTROMETRY

The advantages of interferometry over dispersive spectroscopy have been generally recognised since the introduction of mid-infrared transform spectroscopy. In early days of fourier transform spectroscopy, it was used for far-infrared spectroscopic measurements[23]. The success of far-infrared spectroscopy created interest among chemists to investigate the mid-infrared region. In the beginning far-infrared spectroscopy had its use in astronomical studies only.

Felgett[24] was first to use fourier transform to calculate a spectrum from an interferogram in 1949, and realised that the use of a Michelson interferometer could help in reducing the time taken for the measurement of a spectrum of a weak source. The reduction in measurement time which results from measuring all of the radiation during all of the measurement is usually known as Felgett's advantage.

The other major advantage of the use of Michelson interferometer, is a greater throughput of radiation, first pointed out by Jacquinot[25]. This increased the spectral signal to noise ratio resulting from the increased signal at the detector was called Jacquinot advantage.

The two advantages give increased sensitivity and

become very important when experiments involve measurements of low light levels. Studying absorption on supported metal catalysts by infrared spectroscopy, the poor transmittance of the adsorbant often causes difficulties. The FTIR interferometer appeared as an invaluable research instrument[23]. Nowadays FTIR provides a choice of accessories and applications. For powdered samples, a convenient accessory is the diffuse reflectance cell (DRIFTS), where no or little sample preparation is required and the facility of a controlled environmental chamber is available.

The basic principles of theory, instrumentation and advantages of FTIR spectroscopy are outlined below. More detailed information may be found in the references[23,26-29].

5.3 BASIC THEORY AND INSTRUMENTATION

The present day instrument for fourier transform spectroscopy is actually based on the simple Michelson's interferometer. A schematic diagram of this instrument is shown in figure 5.1. Michelson's interferometer consists of two mutually perpendicular plane mirrors. One of these mirrors is a fixed mirror, whereas the other one moves along the axis. A beam splitter is situated in between the two mirrors, bisecting the angle between the planes of the mirrors. In the Digilab FTS40 instrument used in this study, the beam splitter is a thin germanium film on a KBr

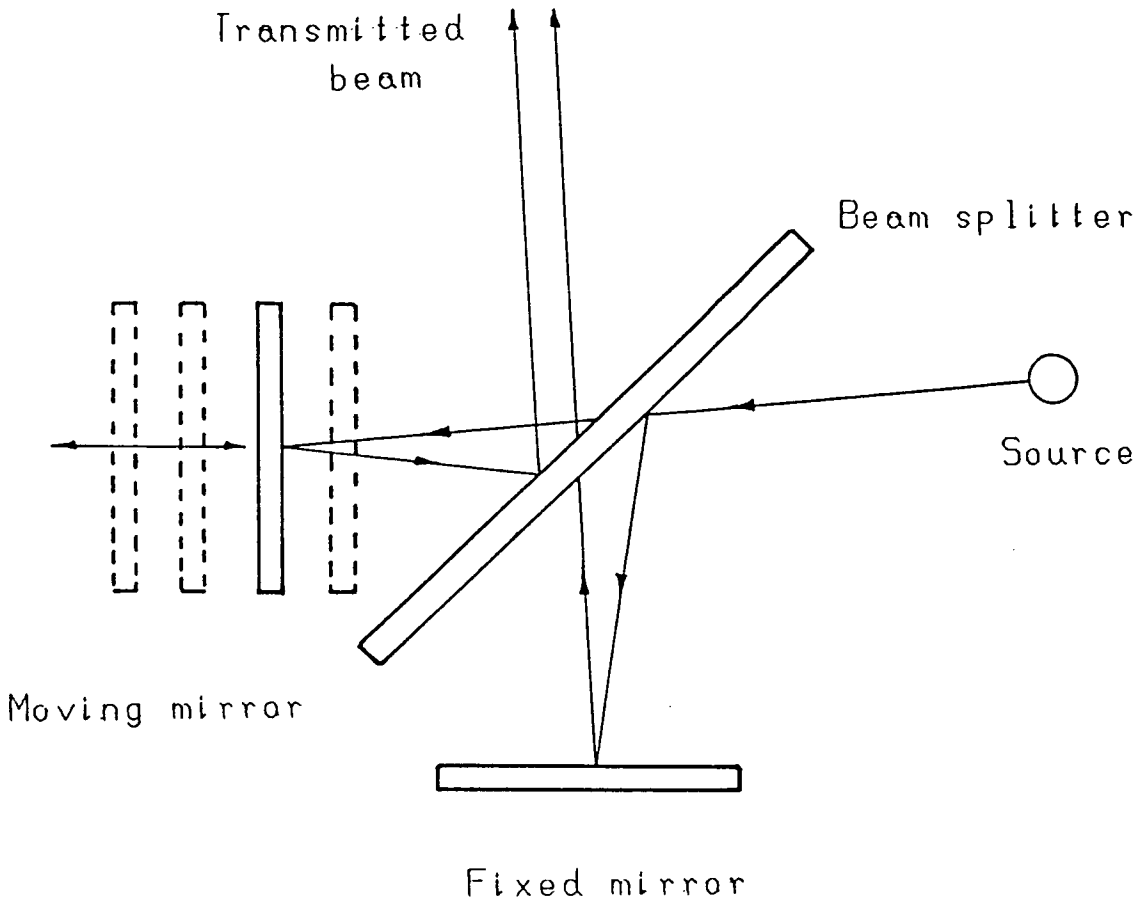

Fig. 5.1 A Schematic Diagram of the Michelson Interferometer

substrate. Radiation from a polychromatic source hits the beam splitter and is partially reflected to the fixed mirror and partially transmitted to the moveable mirror (in the ideal case, it is divided equally into two components). The reflected beams recombine at the beam splitter where each beam is again split into two components. Half of the original intensity is therefore returned towards the direction of the source. The other half emerges from the interferometer at 90° to the original input beam. These two resulting beams are often referred to as the reflected and transmitted beams respectively. It is the transmitted beam which is passed on through the sample and then detected in most FTIR instruments. Due to the motion of the moving mirror, the transmitted beam emerges as an interferogram, which is the sum of individual interferograms due to each wavenumber present in the original frequency distribution of the source. The path difference between the two beams travelling to the fixed and moveable mirrors is called retardation and usually denoted by the symbol "δ". The interferogram arises since as the path difference is changed, the radiation reflected from the moving mirror interferes with that reflected from the fixed mirror. When the fixed and moveable mirrors are equidistant from the beam splitter, i.e. zero retardation, the beams interfere constructively. On the other hand the displacement of the moveable mirror causes a destructive

interference. Whether the result is constructive or destructive, interference depends on δ and the frequency of the radiation. When the retardation is zero, the radiation at all wavelengths is in phase. This makes an intense 'centre burst' in the interferogram. The intensity of the interferogram as a function of the retardation $I(\delta)$ is given by

$$I(\delta) = \int_{o}^{+\alpha} \beta(\bar{\nu}) \cos 2\pi\bar{\nu}(\delta-\epsilon).d\bar{\nu} \qquad (5.1)$$

Where $\beta(\bar{\nu})$ gives the intensity of the source at a frequency $\bar{\nu}$ (cm^{-1}) as modified by the instrumental characteristics, sample and the wavelength response of the detectors. The function $\beta(\bar{\nu})$ is the desired frequency spectrum and it is related to the interferogram $I(\delta)$ by the equation

$$\beta(\bar{\nu}) = \int_{\alpha}^{\alpha} I(\delta) \cos 2\pi\bar{\nu}\delta.d\delta \qquad (5.2)$$

This frequency spectrum may be calculated by fourier transformation of the interferogram. On the Digilab-FTS40 such calculations are performed by a dedicated data system, a Motorolla 6800 based microprocessor architecture with 1M byte memory, 32 bit processing and a high speed arithmetic processor using the Cooley-turkey fast fourier transform alogrithm[26,27,28]. A typical interferogram and the corresponding transformed frequency spectrum are shown in figures 5.2 and 5.3. This type of spectrum, figure 5.3, will be referred to as a single beam spectrum in the following discussion.

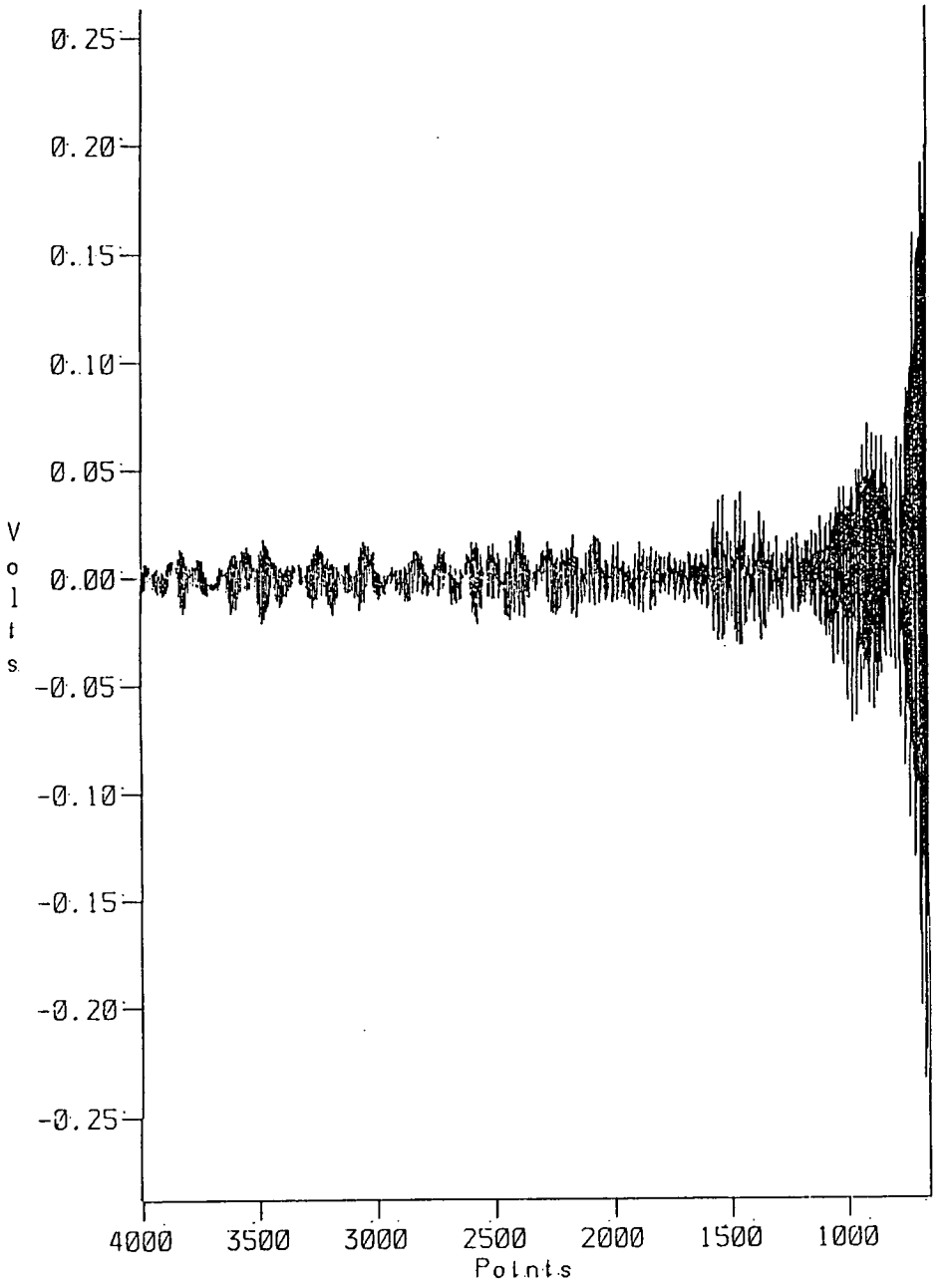

Fig. 5.2 An Example of an Interferogram

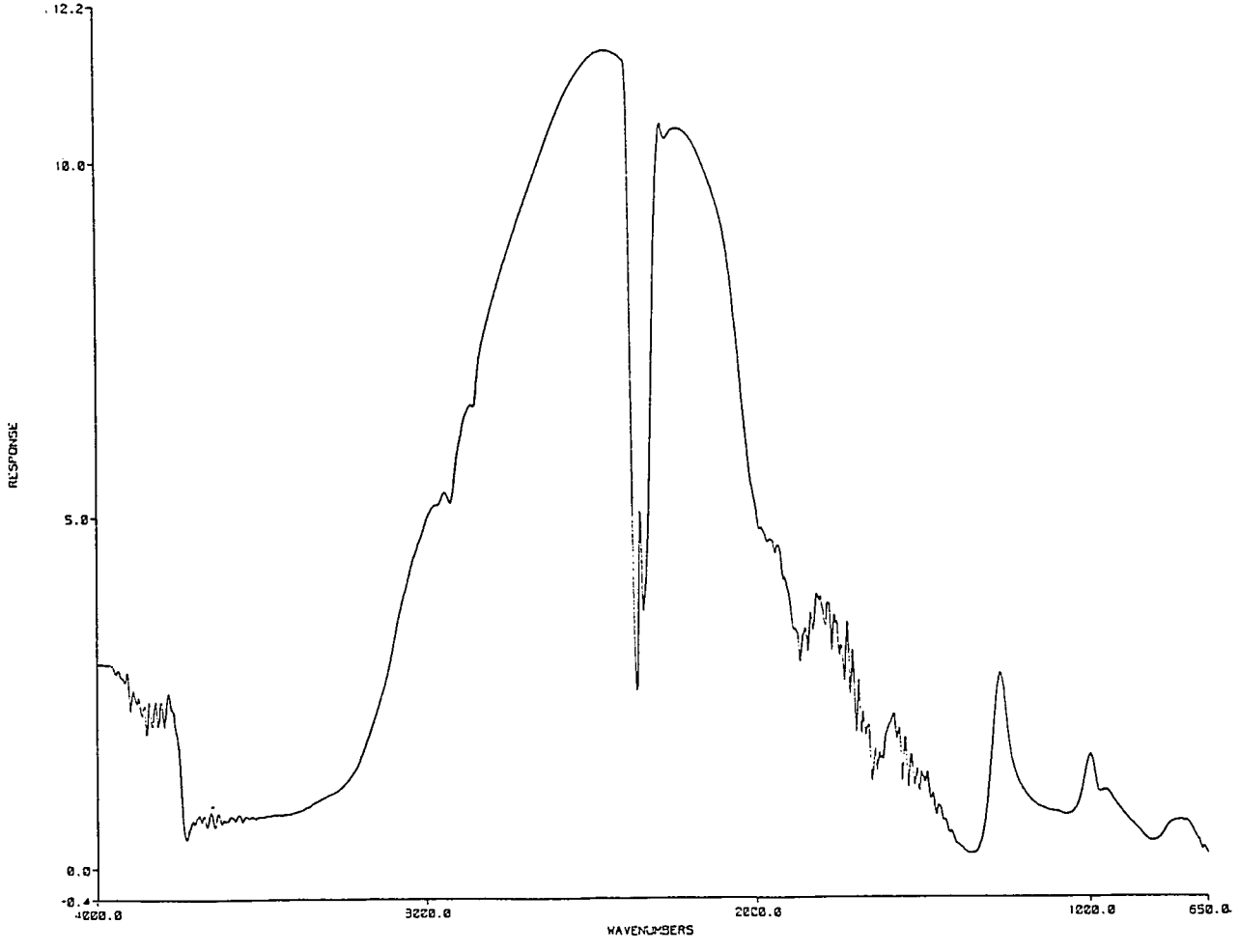

Fig. 5.3 An Example of a Single Beam Spectrum

The use of microcomputers allows a variety of arithmetic operations to be performed on collected data. The most important of these is recording data directly into the memory of the computers and then ratioing one single beam spectrum against the other; for example in adsorption studies, a single beam spectrum (figure 5.3) of a clean catalyst can be ratioed against another single beam spectrum of the adsorbate alone (figure 5.4). The spectrum of the clean catalyst is stored as the "background" (BCK) and that of the adsorbate on the catalyst as the sample (SMP), then a plot of the ratio SMP/BCK gives the adsorbate spectrum with the intensity measured in the % transmittance units (figure 5.4).

Digitised values of the interferogram sampled at precisely equal intervals of retardation are required for the calculation of the spectrum. The accurate sampling of the interferogram is ensured by using sharp interference fringes generated by a second reference interferometer and a He-Ne laser source. This method allows precise measurements of the mirror retardation and gives very accurate characterisation of the frequency in the transformed spectrum. This wavenumber accuracy is one advantage of an interferometer over dispersive instruments and is usually referred to as 'Connes advantage'[23].

Analogue to digital conversion (ADC) is also important in the digitisation of the interferogram. The dynamic

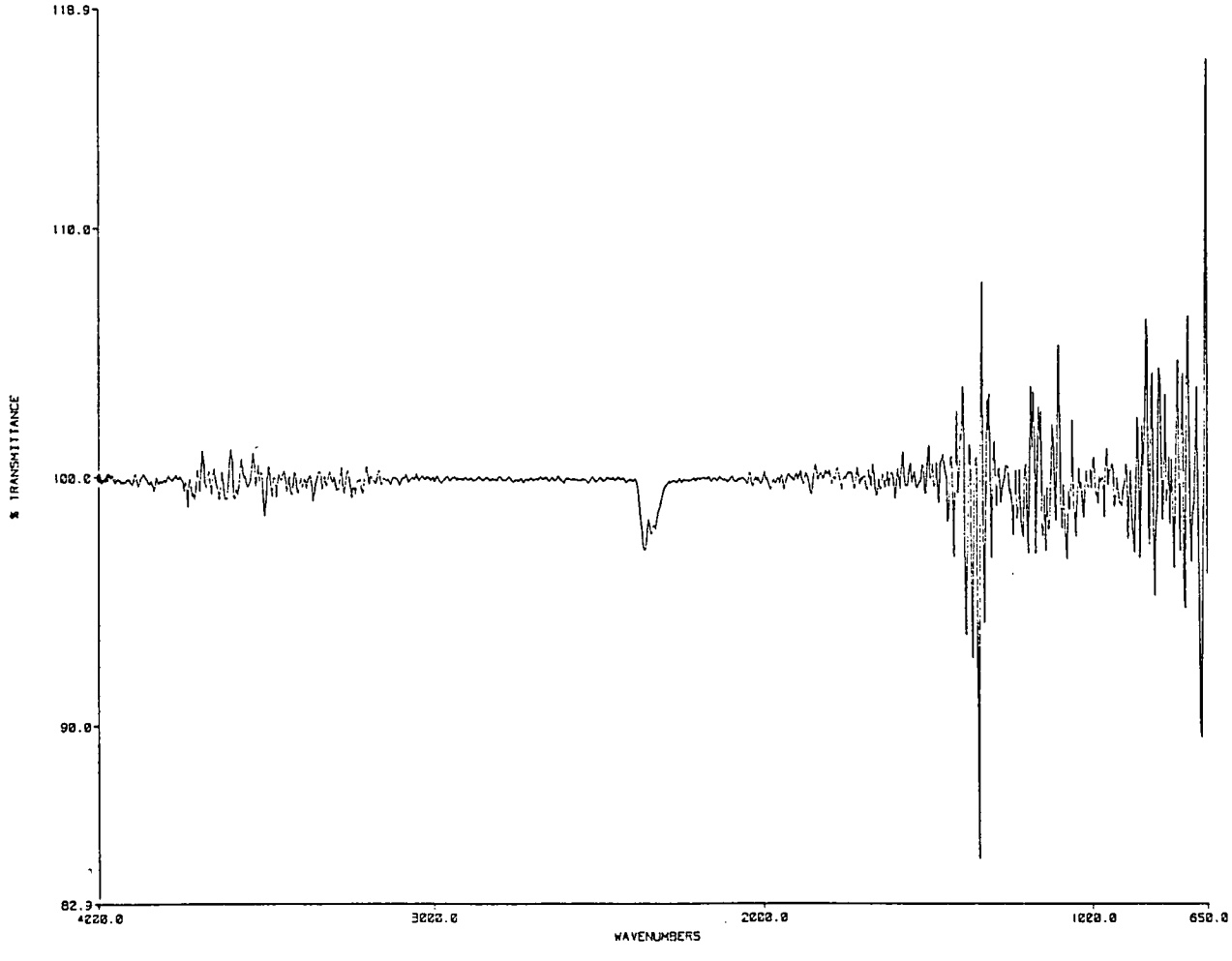

Fig. 5.4 An Example of Ratioed Single Beam Spectra Plotted as % Transmittance

range of the ADC normally limits the signal to noise (S/N) ratio in a single beam, single scan spectrum. The dynamic range must be large enough so that the noise level is greater than the least significant bit of the ADC. If this is not the case then digitisation noise is introduced into the spectrum[23]. The dynamic range of any interferogram can be reduced by scanning the moving mirror faster, and any signal could be sampled accurately provided that the scan speed of the interferometer is increased in order that the signal is reduced. This wide dynamic range is required since the S/N rate at the zero retardation point in the interferogram is normally very large. If the peak to peak noise is digitised by the least significant bit, then the limiting S/N in the interferogram for a 16 bit ADC is 32,765. The S/N ratio in the single beam spectrum from the transformed interferogram is given by

$$\frac{1}{n}(S/N)_I = (S/N)_S \qquad (5.3)$$

Where the I and S subscripts denote the S/N ratio in the interferogram and spectrum respectively. n is the number of spectral elements defined as

$$n = \frac{\bar{\nu}_{max} - \bar{\nu}_{min}}{\Delta\bar{\nu}} \qquad (5.4)$$

where $\bar{\nu}_{max}$ and $\bar{\nu}_{min}$ are the maximum and minimum wavenumbers in the spectrum and $\Delta\bar{\nu}$ is the resolution. For a single scan from 4000-400 cm^{-1} with 4 cm^{-1} resolution,

the limiting S/N ratio in the single beam spectrum is 1092:1, corresponding to a peak to peak noise level of 0.07%. This noise level can easily be improved by increasing the number of scans. A plane polarised single mode He-Ne laser produces an interferogram. The intense, sharp retardation peak of this interferogram in an exactly reproducible point allows the accurate digital co-addition of scans. Many scans may be co-added before introduction of noise. This is because limit of the co-addition process is dependent on the word size of the minicomputer, i.e. effectively the dynamic range of the computer. In the FTS 40, the use of a 16-bit word computer with double precision arithmetic and a high speed arithmetic processor gives an efficient effective dynamic range for the computer of 32 bits. Practically, however, the use of long data collection times often leads to the introduction of noise due to variation in experimental conditions during the acquisition period.

5.4 DETAILS OF THE DIFFUSE REFLECTANCE INFRARED FOURIER TRANSFORM SPECTROSCOPY (DRIFTS) EXPERIMENTS

The requirements of infrared reflectance spectroscopy are often quite different from those of absorption spectroscopy. If the sample under observation has a poor reflectance and scatters incident light very badly so that only a small fraction of radiation reaches the detector,

then such a problem is solved by fourier transform 'DRIFTS' technique. The sample is placed in the cup of the 'DRIFTS' cell block where the incident radiation diffuses into the sample and then is reflected back to the detector. This reflected intensity is measured as % transmittance, absorbance or in the mode of Kubelka-Monk.

In these studies the spectrometer used was the 'Digilab FTS-40', a commercial single beam fourier transform interferometer with its accessory for DRIFTS study, called the 'controlled environmental chamber' (figure 5.5), which allows evacuation, introduction of adsorbates and circulation of cooling water around the heater of the DRIFTS cell block.

5.4.1 Theory of Diffuse Reflectance Spectroscopy

The Kubelka-Munk relationship is the equation most commonly used to describe the reflectance from a scattering medium[30-35]. A comprehensive theory of radiative transfer which governs the radiation field in a medium that adsorbs, emits and scatters radiation has been formulated and elaborated by Chandrasekhar[35-38]. This formulated equation was formally identical to the earlier Kubelka-Munk[30-32] equation, which is as follows:

$$R_\infty = \frac{I}{I_o} \qquad (5.5)$$

According to the K-M theory, the diffuse reflectance component for a 1-3 mm thick layer of a powdered sample at a given wavelength is equal to

$$R_\infty = \frac{I}{I_o} = \frac{1-[K/(K+2S)]^{\frac{1}{2}}}{1+[K/(K+2S)]^{\frac{1}{2}}} \qquad (5.6)$$

I = reflected intensity

I_o = incident intesnity

K = absorption coefficient

S = scattering coefficient

The absorption coefficient is the same as given by the Beer-Lambert law.

By algebric manipulation the equation 5.6 can be written as

$$\frac{(I-R_\infty)^2}{2R_\infty} = \frac{K}{S} \qquad (5.7)$$

The left hand side of the equation is called "remission function" or K-M function and is frequently denoted by $f(R_\infty)$[36-38] and the equation 5.7 can be written in the form

$$f(R_\infty) = \frac{K}{S} = \frac{(I-R_\infty)^2}{2R_\infty} \qquad (5.8)$$

Experimentally one seldom measures the absolute diffuse reflecting power of the sample compared to a suitable standard. In that case K=O in the spectral region of interest, R_∞ standard = I [from equation 5.6], and one determined the ratio

$$\frac{R_\infty \text{ sample}}{R_\infty \text{ standard}} = R_\infty$$

The advantage of plotting spectra in Kubelka-Munk format is that $F(R_\infty)$ is proportional to the molar concentration under constant experimental conditions.

In the present study, spectra are presented in absorbance format. The intensity of the CO band will not be linear due to dipole-dipole interaction on the surface and absorptivity changes as a function of coverage. Hence it is not attempted to quantify the intensities, in terms of the amounts of adsorbed CO.

5.4.2 The Diffuse Reflectance Infrared Accessory

The accessory used in 'DRIFTS' experiments consisted of a controlled environmental chamber, a set of 2 aspheric reflectors and a set of 4 flat reflecting mirrors.

5.4.2.1 Controlled environmental chamber

The controlled environmental chamber of the diffuse reflectance accessory is shown in figure 5.5 and was used for adsorption/desorption studies described in this chapter. The main block of the environmental chamber was made of stainless steel. This standard accessory was connected to the main vacuum system frame and the glass gas handling manifold, described below, through 1/16 inch stainless steel tubing. These 1/16 inch connections enabled the circulation of cooling water around the built-in heater (capable of heating up to 1000 K), introduction of the adsorbates, and evacuation of the

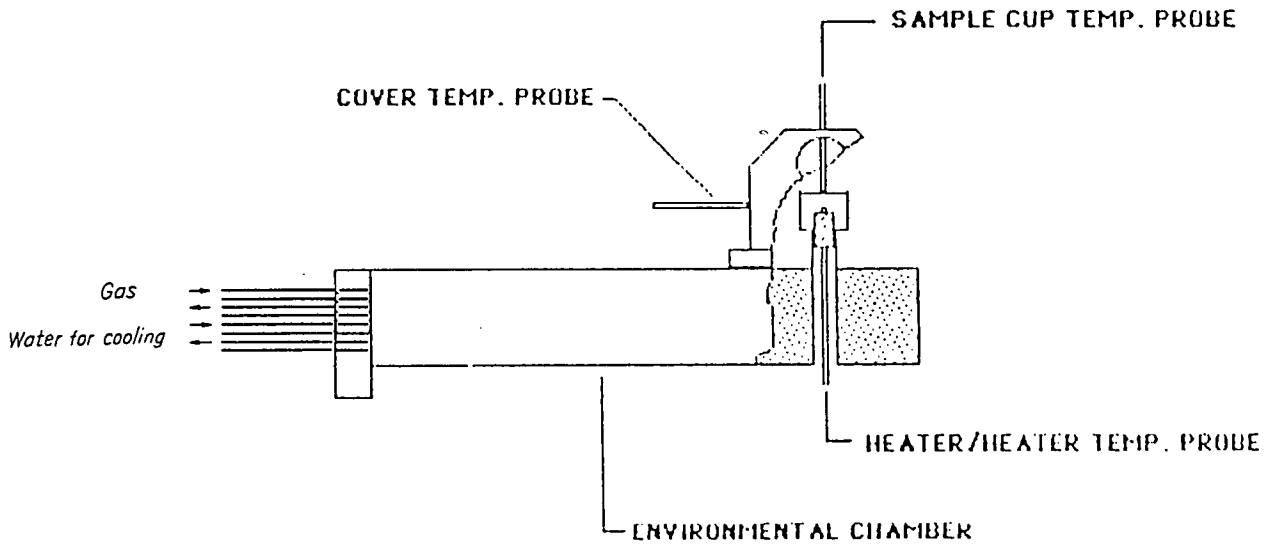

Fig. 5.5 Controlled Environmental Chamber

'DRIFTS' cell.

The sample holder is a machined stainless steel cup of 13 mm diameter and 2 mm deep. It was capable of holding a powdered sample of about 0.05 g. The main block at the base was provided with a groove, holding a rubber 'O' ring. The lid of the sample cell was made of stainless steel, with two KBr windows of about 2.5 mm thickness and 13 mm diameter. This was placed on the main block over the rubber 'O' ring, tightened with the screws and was capable of maintaining vacuum in the cell. Thus it facilitated the evacuation of the cell and introduction of adsorbates. The sample was heated by applying current across the resistance heater. The temperature was measured using two chomel-alumel thermocouples.

5.4.2.2 Mirrors Arrangements

This accessory employed four flat and two aspherical reflectors. The aspheric reflectors are off-axis ellipsoids which focus and collect infrared energy with a 6 x condensation of the beam. Figure 5.6 shows the optical layout of the 'DRIFTS' mirror arrangement accessory, showing the beam path through the attachment. The size of the signal could be increased or reduced by turning the height of the sample by adjusting the screw or by slight adjustment of the four flat mirrors.

5.4.2.3 The Sample and the Sample Preparation

Using the 'DRIFTS' accessory, almost no sample

a

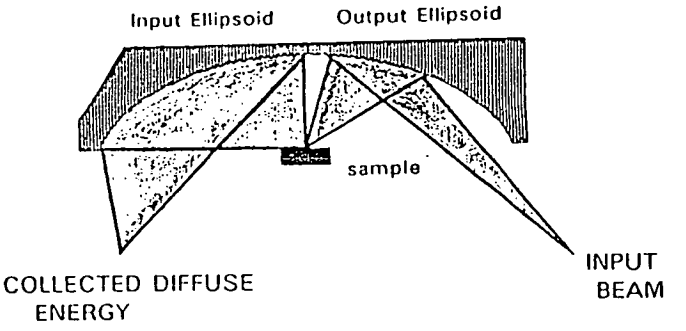

b

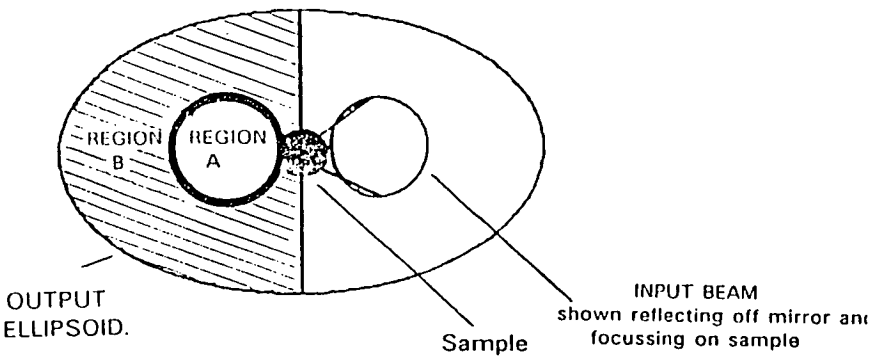

Fig. 5.6 Symmetrical Diffuse Reflectance Accessory (a) Side View; (b) Bottom View

preparation was required. The biggest advantage of the technique being a choice of powdered samples and a convenient alternative to the use of pressed discs of material. The technique also finds a particular use in high temperature, controlled environment studies. In the present study fine powdered samples of the catalyts are used. An Agate mortar was used for this purpose.

5.5 VACUUM SYSTEM

A diagram of the vacuum system used for the diffuse reflectance infrared experiments is shown in figure 5.7. The apparatus consisted of a stainless steel chamber situated above the aluminium table top and a glass gas handling line below as well as a pumping system. Most of the apparatus was contained within a relatively compact dexion/metal frame mounted on wheels. This allowed the apparatus to be easily moved to and from the spectrometer. The 'DRIFTS' cell was connected to the vacuum system with 1/16" stainless steel tubing which proved flexible enough to allow the removal and insertion of the cell from the spectrometer.

The stainless steel vacuum system included a VG-Arga quadrupole mass spectrometer. One leak valve allowed sample gas introduction into the 'DRIFTS' cell, another was used to evacuate the sample cell through the mass spectrometer, to determine any change in the pressure of the system. The third valve allowed the evacuation of the

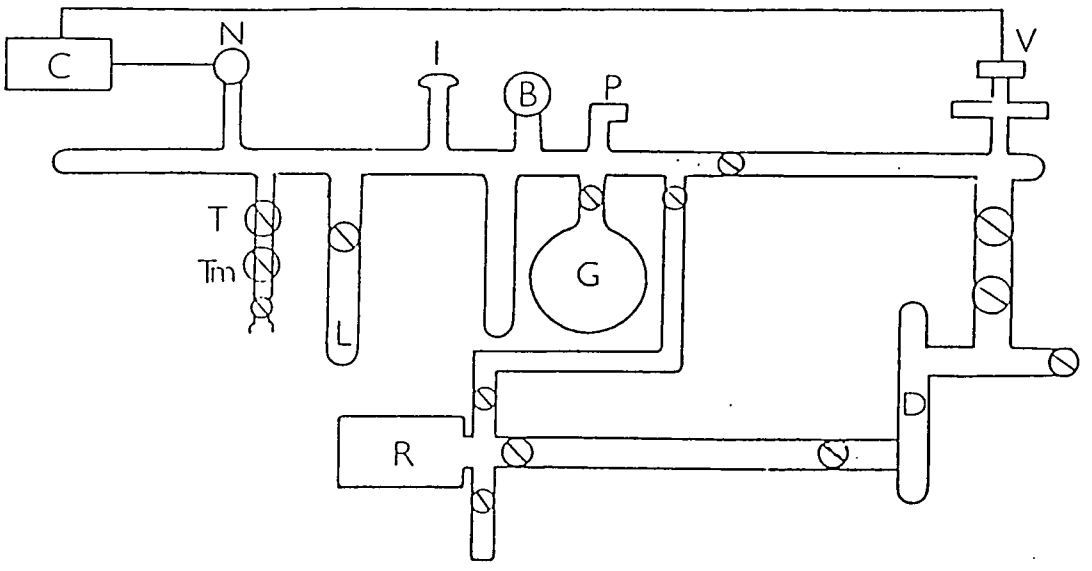

KEY

Q	-	greaseless tap	T	-	cold trap
B	-	dial gauge (bourdon type)	T_m	-	molecular sieve trap
C	-	drift cell	R	-	rotary pump
D	-	oil diffusion pump	G	-	sample gas bulb
V	-	leak valve	N	-	needle valve
I	-	ion gauge	L	-	liquid sample ampule
P	-	Pirani gauge			

Fig. 5.7 A Schematic Diagram of the Vacuum Apparatus used in the DRIFT Experiments

'DRIFTS' cell through the bottom of the controlled environmental chamber.

The pumping system consisted of an oil diffusion pump (EO2) backed by a two-stage rotary oil pump equipped with a foreline molecular sieve trap. The backing pressure at the rear of the diffusion pump was monitored by a pirani gauge (Edwards PR10). The oil diffusion pump was separated from the main chamber by a liquid nitrogen trap which could be further isolated by a large gate valve.

The glass vacuum manifold was constructed with Young's greaseless taps (J. Young Scientific Glassware, Acton, London) and consisted of a number of glass bulbs for storage of gases. Liquid hydrocarbons were introduced from large glass ampoules containing a 'Rotaflo' tap. Gases were introduced from the glass manifold into the 'DRIFTS' cell by means of a metal leak valve (Leisk Engineering Company).

Hydrogen used for reduction was passed through a Deoxo hydrogen purifier (Englehard). The water thus generated was removed by passing the gas over a molecular sieve trap immersed in liquid nitrogen. The pumping system could reduce the pressure from one atmosphere to 10^{-8} torr, within three to four hours. Further improvements were only possible by baking out the apparatus to remove water from the internal surfaces of the vacuum system. The system was periodically baked at 473 K for a period of at least 24 hours. Baking was achieved by wrapping the

stainless steel vacuum chamber with heating jackets and tapes. The pressure during the bakeout could be monitored by the VG-Arga mass spectrometer. After cooling to room temperature an ultimate pressure of 5 x 10^{-9} torr was achieved.

The pressure of the glass manifold was measured by a dial gauge (Leybold-Heraeus), a pirani (Edwards PR10) and an ion gauge (VH9). The base pressure that could be achieved in this section was approximately 10^{-5} torr.

5.6 EXPERIMENTAL DETAILS OF ADSORPTION STUDIES

After enclosing the sample in the 'DRIFTS' cell, the treatment prior to an adsorption experiment first involved evacuation of the cell to around 10^{-6} torr total pressure in the system. The sample was then outgassed for two hours at 500 K, this outgassing normally improved the pressure to 10^{-7} torr. With the sample at room temperature, 400 torr of hydrogen was then introduced into the cell and the sample temperature was increased from room temperature to 700 K in about 30 minutes. This temperature and pressure was maintained for three hours. A flow of hydrogen across the sample was setup. Following the reduction, the hydrogen was evacuated and the sample outgassed at 800 K for a further one hour. Similar reduction procedures have been reported by other workers studying the EUROPT-1 catalyst[4], and other supported platinum catalysts[18,39,40-41]. These conclude that the

procedure used results in complete reduction .

5.6.1 Adsorption of Carbon Monoxide

The adsorption of carbon monoxide was carried out in a stepwise mode from 10^{-3} to 20 torr. The pressure measurements less than 1 torr were made by a pirani gauge, while the higher pressures were monitored on a dial gauge which had previously been calibrated against a mercury manometer. Each dose of CO was expanded over the catalyst at room temperature for five minutes, evacuated, and a 1000 scans at a resolution of 4 cm^{-1} were recorded. This took approximately 25 minutes.

5.6.2 Thermal Desorption of Carbon Monoxide

A few simple modifications to the 'DRIFTS' apparatus allowed some temperature programmed desorption experiments to be carried out *in situ*. As shown by figure 5.8 the use of a thermal conductivity detector as described previously in Chapter 3, also permitted conventional TPD spectra to be recorded.

Prior to desorption, CO was adsorbed from five pulses injected into the stream of helium gas flowing at the rate of 20 cm^3 per minute. The sampling valves and loops used for pulses have been detailed in Chapter 3. The uptake of CO was displayed in the GC recorder of the T.P.D. set-up and monitored by an on-line computer. At the same time for each pulse, 'DRIFT' infrared spectra were recorded.

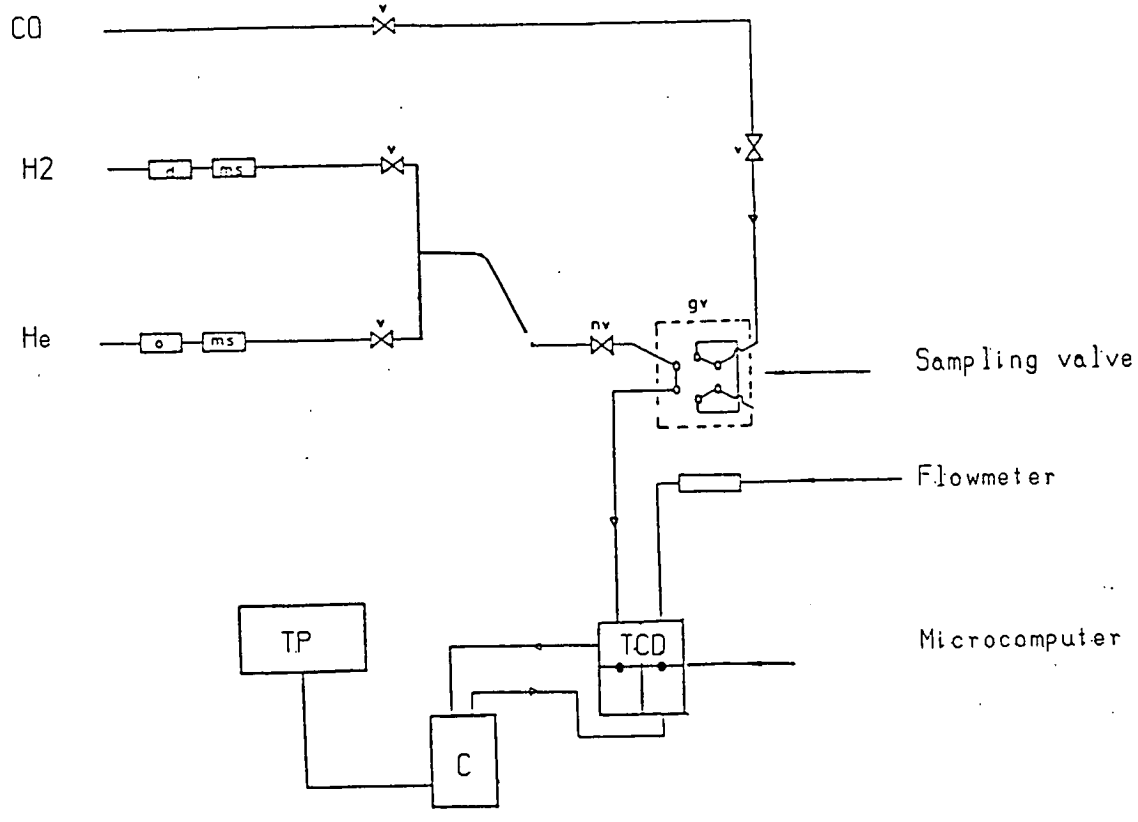

KEY

ms	-	molecular sieve
O	-	oxygen trap
d	-	deoxo unit
V	-	valve
nV	-	needle valve
gV	-	six way gas valve
tp	-	temperature programmer
TCD	-	thermal conductivity detector
C	-	DRIFT cell

Fig. 5.8 TPD/DRIFT Apparatus

All these measurements were made at room temperature.

As temperature programming of the 'DRIFTS' cell was not possible, stepwise temperature desorption was carried out with the temperature being raised from room temperature to 923 K in 100 K intervals with spectra recorded at constant temperature. The rise in temperature between spectra was kept at approximately 20 K/minute. A full desorption profile was monitored by the thermal conductivity cell and displayed on a recorder. Monitoring the desorption on the microcomputer also provided the facility of integrating the area under the desorption peak, to give a quantitative measure of the desorbed carbon monoxide.

5.6.3 Gas Chromatography/DRIFTS : Hydrogenolysis of n-butane

To enable a 'DRIFTS' study of n-butane hydrogenolysis the infrared cell was used as a small static reactor. This allowed spectra of the gas phase to be taken during the reaction, and of the adsorbed reaction residues after evacuation of the system. A flame ionization detector permitted the composition of the reactant gases to be measured. Although the gas sample loop was nominally only 0.13 cm^3, one sample was enough to seriously deplete the amount of gas in the 'DRIFTS' cell volume (5 cm^3). Thus only a measure of the final products after 45 minutes reaction at 523 K was possible.

5.6.4 Temperature calibration

The sample holder of the 'DRIFTS' accessory is located at some distance from the heater of the environmental chamber, and the thermocouple monitored the temperature of the heater and not the sample holder. It was therefore decided to calibrate the sample temperature against heater temperature, in vacuum and in flowing helium. For calibration purposes a nickel-chrome thermocouple was passed through a small hole in the KBr window of the lid of the environmental chamber, containing the sample cup. The hole was then sealed by 'Araldite'. This enabled the cell to hold a vacuum of about 10^{-6} torr as monitored by the VG-Arga mass spectrometer. A 2 ampere power supply unit was used to raise the temperature by varying the voltage. Both temperatures were displayed on individual digital Comark thermometers. A set of temperatures was recorded against voltage in vacuum and in flowing helium. Considerable differences in the temperatures were noted. A detailed account of these temperatures is listed in table 5.2 We observed that the sample temperature varied as a function of pressure in the cell. The temperatures quoted in the present study are heater temperatures unless otherwise stated.

5.6.5 Gases and Gas Handling

Details of the source and purity of the gases used in

Table 5.1

The Source and Purity of the Gaseous Reagents used in the Diffuse Reflectance Infra-red Experiments

Adsorbate Gas/Liquid	Purity	Source
Carbon Monoxide	Research grade	Matheson Gases
Hydrogen	Research grade	Matheson Gases
Hydrogen (Bulk)	165 ft^3 cylinder	B.O.C.
Helium	" " "	B.O.C.
Ethane	99.95%	Matheson Gases
Ethylene	99.95%	" "
Butane	99.95%	" "
Benzene	99.9%	B.D.H

Table 5.2

DRIFT Cell Temperature Calibration

Heater Temperature (K)	Sample Temperature K in Vacuum	Helium
374	348	328
473	393	380
573	453	418
723	523	513
873	623	608
923	648	635

these experiments are given in Table 5.1. With the exception of the bulk hydrogen supply which was deoxygenated and dried as described above, all gases were used without further purification.

Gases prepared in the manifold were introduced into the diffuse reflectance infrared cell by means of the metal leak valve (Fig. 5.7). On reducing the pumping speed to the cell by partially closing valve V, a flow of gas at pressure between 10^{-5} torr and 10^{-1} across the sample, could be achieved. For flowing gases and pulse injection of pressures 0.8 p.s.i.g. were used. Such high pressures were however only necessary during the temperature programmed desorption of carbon monoxide in helium carrier gas flowing at the rate of 20 cm^3 min^{-1}. Higher static pressures, between 1 torr and atmospheric pressure could also be achieved by totally closing valve V.

5.6.6 Treatment of Spectra

Baseline Correction. Baseline correction was carried out using DIGILAB's user software notes 091-0416A programme 'basecorr'. This programme enabled the generation of a baseline array by connecting breakpoints.

Smoothing. Smoothing was performed using command ZAP. Smoothing is equivalent to measuring the spectrum at a lower resolution. The spectrum appears smoother without losing any data points. This procedure eliminates high

frequency noise.

Integration. Integration of peaks was carried out using programme INTERACTIVE CLASS. This programme enabled the marking of peaks on a spectrum from which their intensity, area and centre point could be calculated.

Subtraction. Command SUBTRACT was used to carry out subtraction of spectra. This command produces a plot which is the difference between the sample absorbance spectrum (SAMP) and reference absorbance spectrum (REF). The sample, reference and difference spectra are displayed.

5.7 RESULTS

Figure 5.9 shows a spectrum of CO adsorbed on EUROPT-1 at saturation coverage at room temperature. The spectrum is an expanded plot of the region 2200-1600 cm^{-1} of a complete spectrum from 4000-650 cm^{-1}, recorded at 4 cm^{-1} resolution. The spectrum is the ratio of a single beam spectrum recorded before and after exposure of the EUROPT-1 catalyst to 20 torr of CO for 15 minutes followed by evacuation before recording the second single beam spectrum. The spectrum shows expected linear and bridged bands at 2074 and 1840 cm^{-1} respectively.

The as received EUROPT-1, which has a high dispersion provides typical CO adsorption data for comparison with the alkali doped EUROPT-1 catalysts. The high symmetry of the peak (linear) is indicative of the homogeneity of the

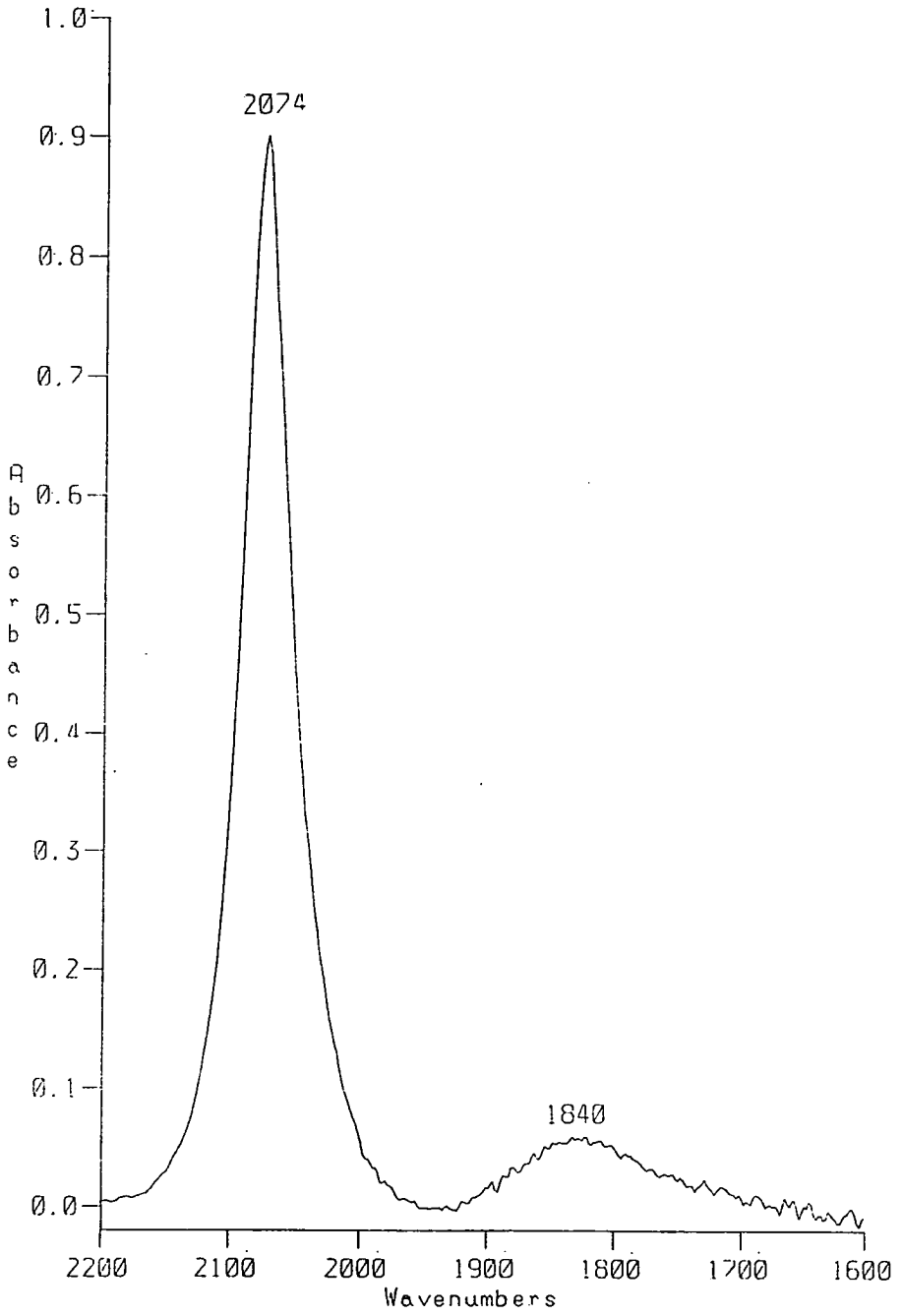

Fig. 5.9 The Spectrum of Carbon Monoxide Adsorbed to Saturation on EUROPT-1

catalyst. A similar symmetric peak due to CO adsorbed on EUROPT-1 has also been noted previously[4].

Figure 5.10 shows a set of spectra of CO adsorbed on 'as-received' and three alkali doped EUROPT-1 catalysts at saturation at room temperature. The spectra show broadening of the linear as well as bridged band, compared with 'as-received' EUROPT-1. The shift in frequencies towards lower wavenumbers is also noted here.

Further spectra of carbon monoxide adsorbed on 'as-received' EUROPT-1 at 298 K are shown in figure 5.11. During the stepwise adsorption, the pressure of CO was increased from 10^{-3} torr to 20 torr. The spectra were recorded after a five minute adsorption period followed by evacuation.

In figure 5.11 the position of the linear band in the initial spectrum recorded for a CO pressure of 10^{-3} torr is 2051 cm^{-1} which is significantly lower than the value expected for saturation pressure (i.e. 2074 cm^{-1}). It was observed that in the initial spectrum (10^{-3} torr CO pressure) only the linear band appeared and with increasing CO pressure the bridged band started appearing. It was also observed that with increasing CO pressure, the linear and bridged peaks shifted towards higher wavenumbers from an initial value of 2051 cm^{-1} and 1800 cm^{-1}f to a final value of 2074 cm^{-1} and 1840 cm^{-1} respectively. It would be worth mentioning here that at a CO pressure of 1 torr the linear band occurred at

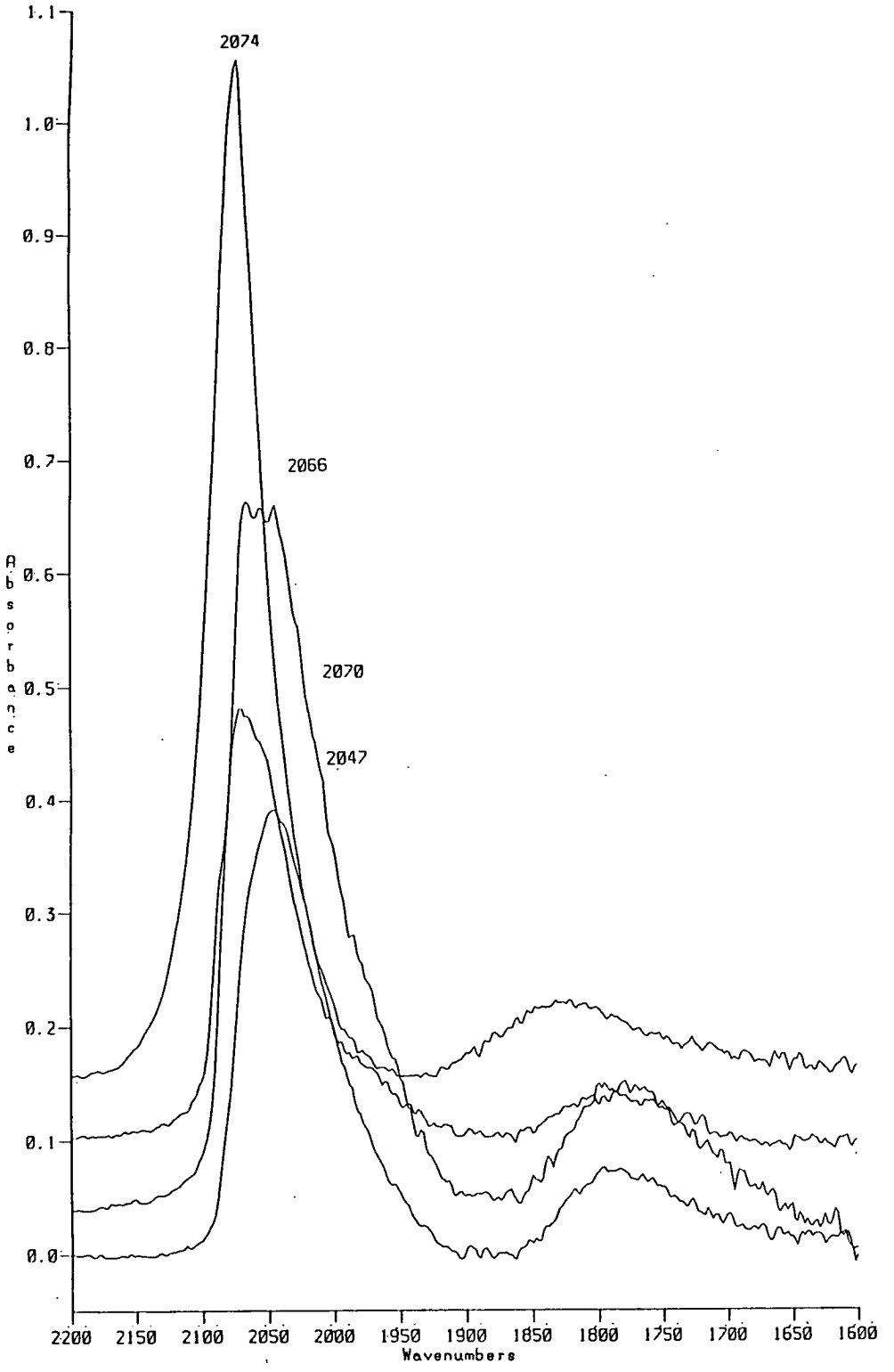

Fig. 5.10 DRIFT spectra of CO Adsorbed to Saturation;
(a) EUROPT-1;
(b) 0.25% KOH (wt)/EUROPT-1;
(c) 0.50% KOH (wt)/EUROPT-1;
(d) 1.0% KOH (wt)/EUROPT-1.

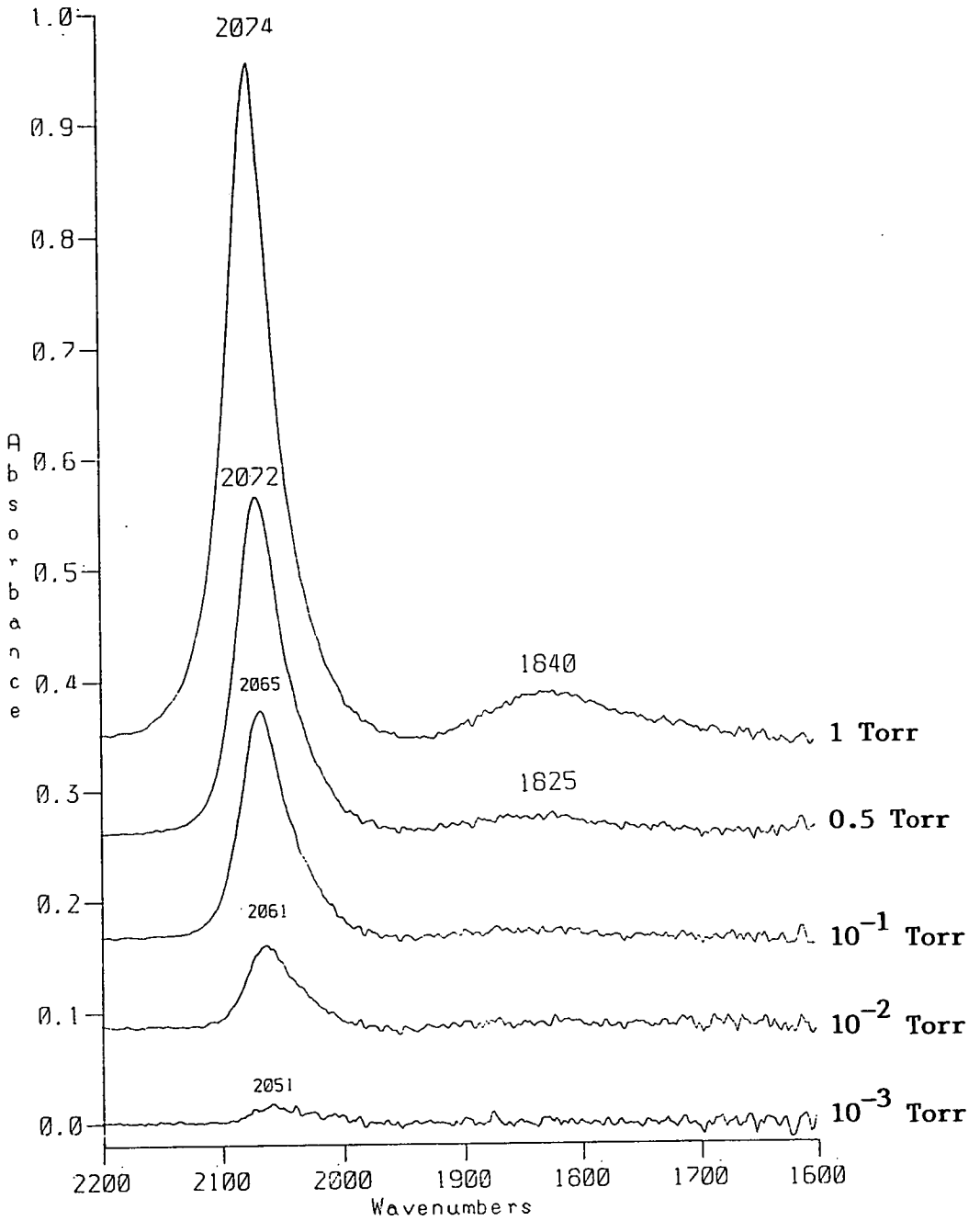

Fig. 5.11 Spectra of EUROPT-1 Exposed to Increasing Pressures of Carbon Monoxide (see Table 5.3).

2074 cm^{-1} and bridged at 1840 cm^{-1}. Increase of pressure from 1 torr to 5 and finally 20 torr did not make any difference. This indicated that saturation was achieved even at 1 torr CO pressure. The peaks due to linearly bonded CO are relatively sharp and symmetrical all the time. The frequency shift over the range of CO pressure for the recorded spectra are listed in table 5.3. The integrated intensity data corresponding to the different CO exposures is also given in table 5.3.

The adsorption of CO on potassium doped EUROPT-1 was investigated. Figures 5.12-5.14 show stacked plots of spectra for CO adsorption on 0.25, 0.5 and 1.0% KOH (wt) doped EUROPT-1 catalysts. At the lowest CO pressure of 10^{-3} torr adsorbed on the three alkali doped catalysts, spectra show some indication of a band near 2000 cm^{-1}. The bridged band did not appear until the third dose of CO (10^{-1} torr). At the highest pressure of CO, the spectra show more pronounced bridged bands as compared with the 'as-received' EUROPT-1 in figure 5.11. As a function of alkali coverages the frequencies shift to lower wavenumbers, noted for all the catalysts (alkali doped). Compared with the 'as-received' EUROPT-1, the frequency of 2074 cm^{-1} shifted down to 2047 cm^{-1} observed for the highest alkali loaded EUROPT-1 (1% KOH wt/EUROPT-1) catalyst. A well behaved frequency shift is observed for all the three potassium doped catalysts as a function of CO pressure, as listed in table 5.3. It was also observed

Table 5.3

Shift of Frequency and Integrated Intensity Area as a Function of CO Coverage
Over as-received and Alkali Doped EUROPT-1

	As-received EUROPT-1					0.25% KOH (wt)/EUROPT-1					0.5% KOH (wt)/EUROPT-1					1% KOH (wt)/EUROPT-1				
CO Pressure Torr	Linear ν cm^{-1}	Band Area	Bridge ν cm^{-1}	Band Area	Ratio of Areas	Linear ν cm^{-1}	Band Area	Bridge ν cm^{-1}	Band Area	Ratio of Areas	Linear ν cm^{-1}	Band Area	Bridge ν cm^{-1}	Band Area	Ratio of Areas	Linear ν cm^{-1}	Band Area	Bridge ν cm^{-1}	Band Area	Ratio of Areas
10^{-3}	2051	1.175	-	0.53	2.21	2029	0.676	-	0.31	2.18	2006	2.08	-	1.408	1.47	2005	1.53	1778	1.22	1.2
10^{-2}	2062	4.76	1820	0.44	10.7	2044	3.351	-	1.45	2.29	2026	5.08	1800	1.563	3.24	2015	5.0	1778	1.78	2.88
10^{-1}	2065	13.02	1820	1.60	8.25	2054	7.23	1758	2.09	3.45	2028	0.43	1758	3.017	3.2	2030	10.49	1778	4.22	2.48
0.5	2072	21.97	1822	1.89	11.5	2061	18.53	1758	4.3	4.2	2061	36.24	1770	9.27	3.9	2038	26.5	1778	7.48	3.7
1-20 torr	2074	51.28	1840	9.3	5.8	2070	27.52	1780	6.3	4.3	2066	55	1790	16.10	3.4	2047	32.9	1800	9.92	3.55

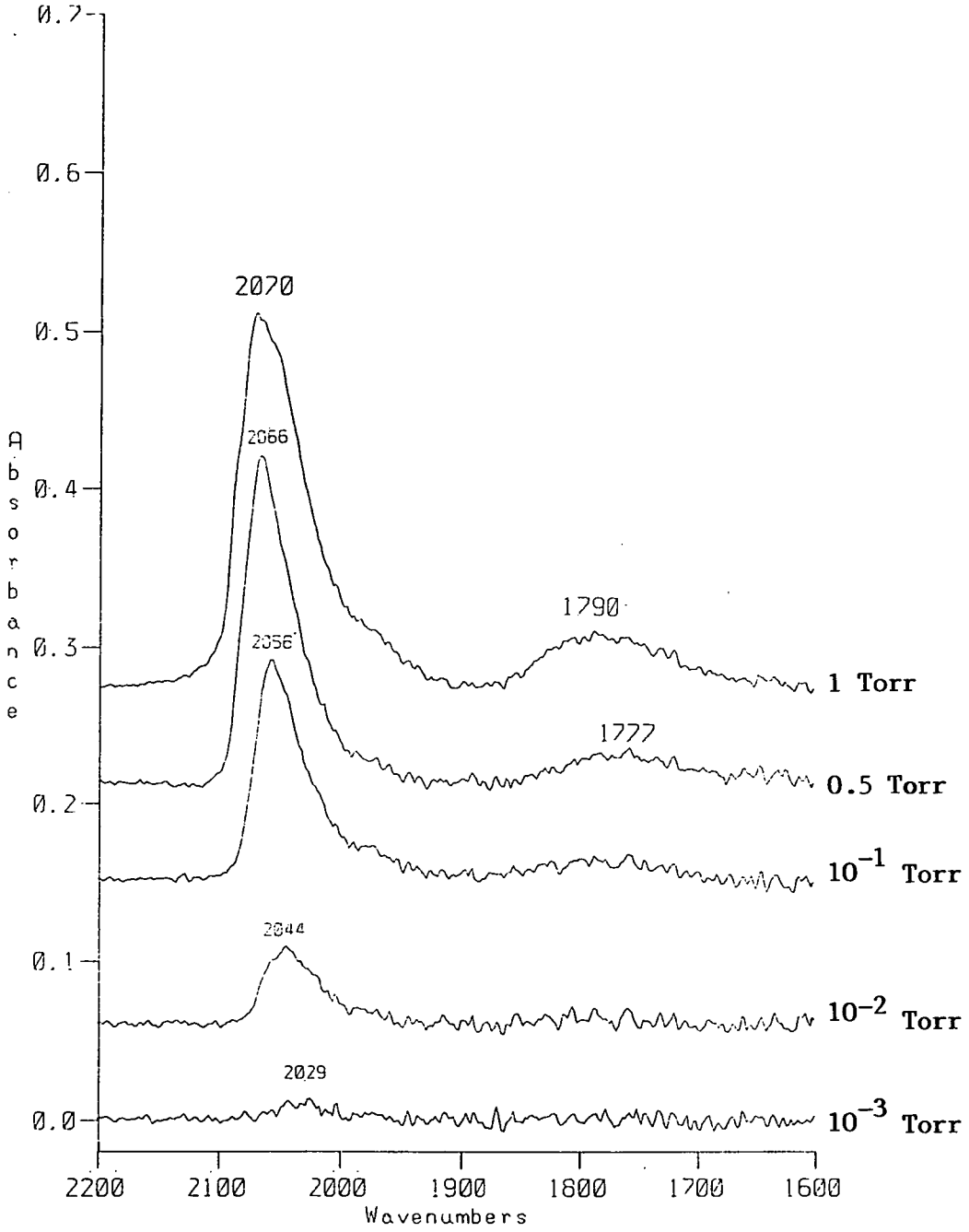

Fig. 5.12 Spectra of 0.25% KOH (wt)/EUROPT-1 Exposed to Increasing Pressure of Carbon Monoxide (see Table 5.3).

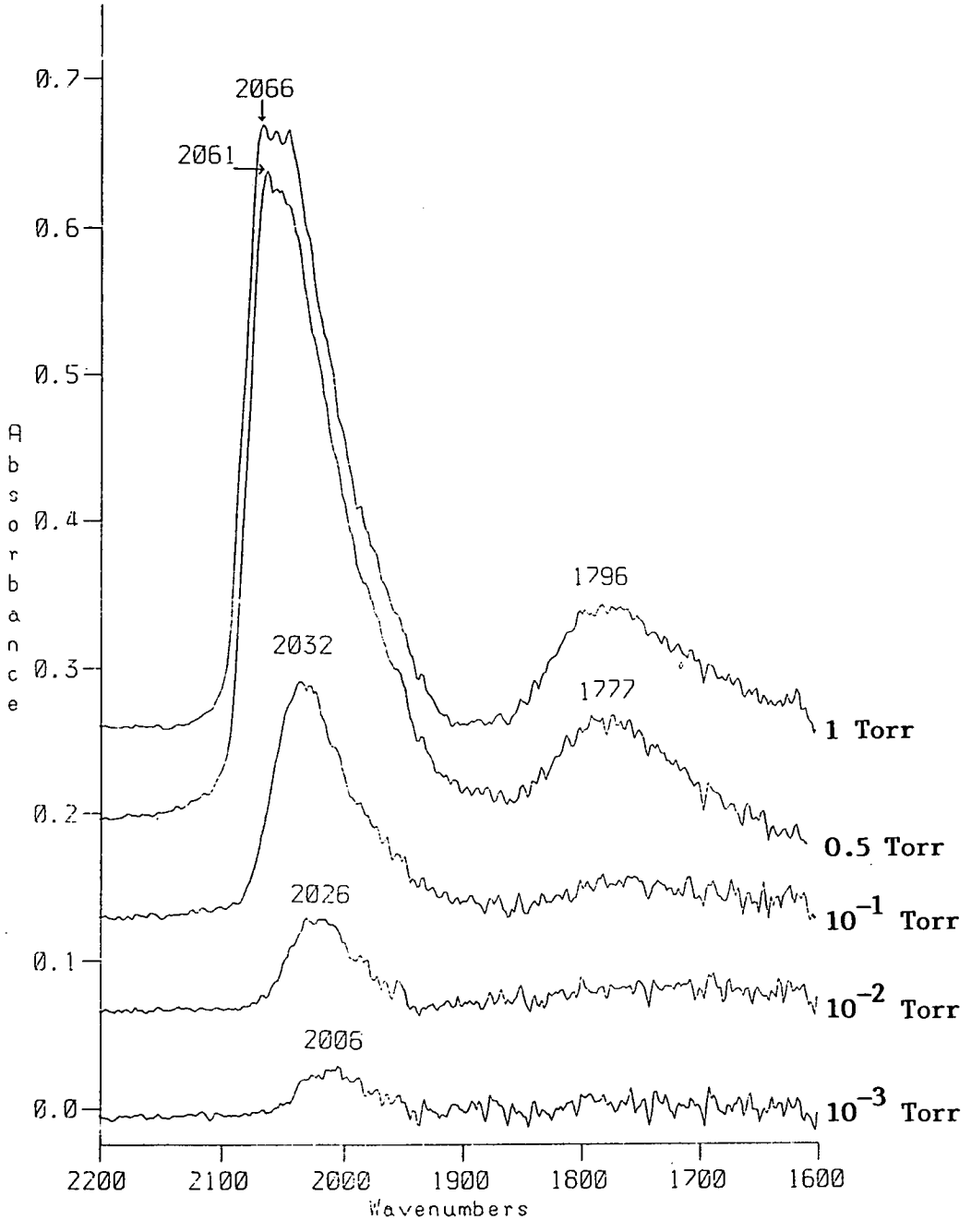

Fig. 5.13 Spectra of 0.50% KOH (wt)/EUROPT-1 Exposed to Increasing Pressure of Carbon Monoxide (see Table 5.3).

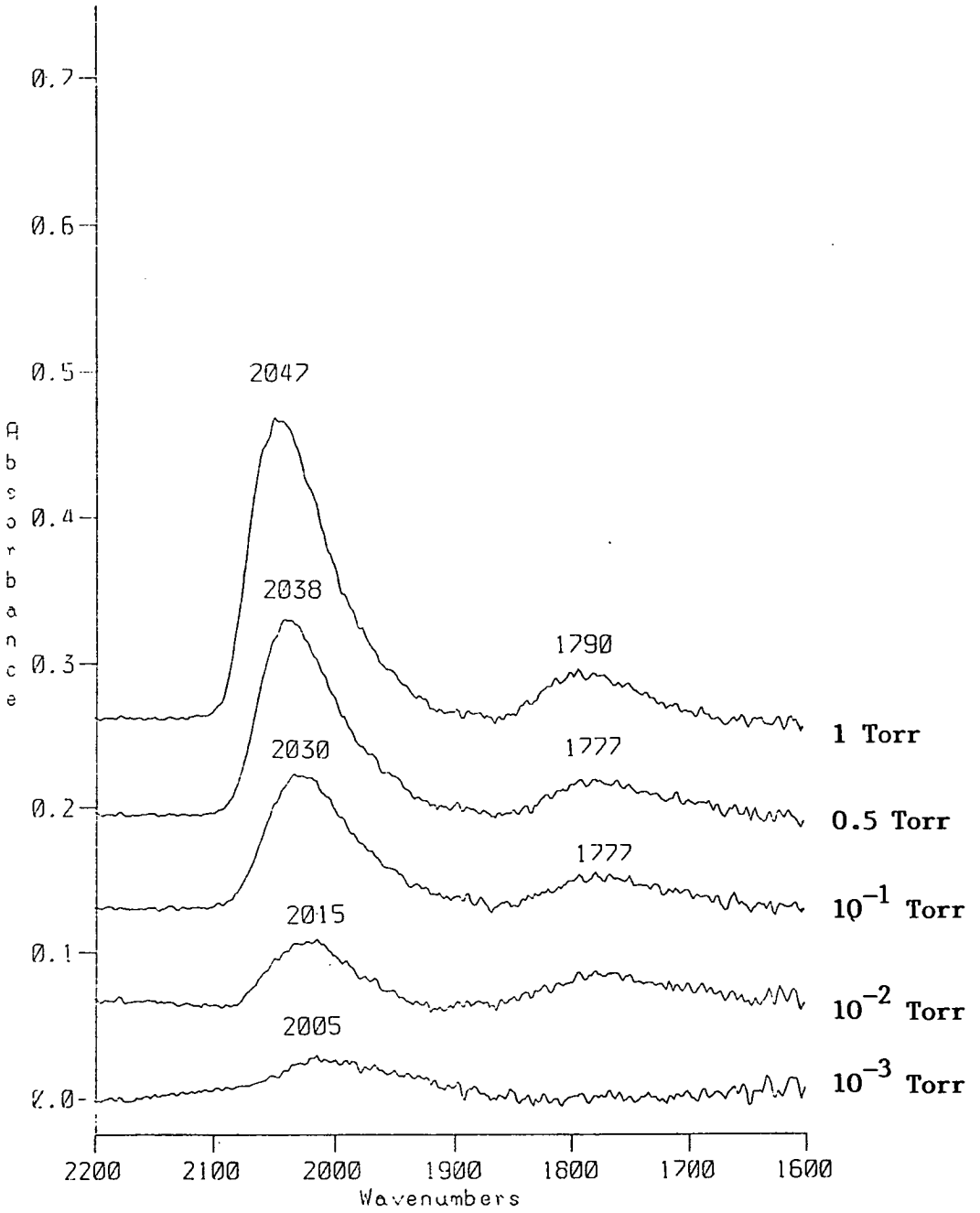

Fig. 5.14 Spectra of 1.0% KOH (wt)/EUROPT-1 Exposed to Increasing Pressure of Carbon Monoxide (see Table 5.3).

that with increasing alkali concentration the bands due to linear and bridge bonded CO broadens, and high asymmetry developed in the low frequency region of the absorption peak. It is interesting to note that the absolute intensity of the linear band decreases with increasing alkali concentration for the 0.25 and 1% KOH (wt) doped EUROPT-1. The catalyst 0.5% KOH (wt)/EUROPT-1 does not behave in the same way, i.e. the absolute intensity of the linear as well as bridged species is more than 0.25% KoH (wt)/EUROPT-1 catalyst, which appeared to be odd in the sequence of the alkali doped set. The ratios of the relative intensities of linear to bridged also varied significantly, observed for all the catalysts doped with KOH, as shown in table 5.3.

The integrated areas of the linear and bridged bands are listed in table 5.3. As with the intensities, the integrated area of the peaks (linear and bridged) due to CO adsorbed on 0.5% KOH doped EUROPT-1 are higher than that observed for 0.25 and 1.0% and even for the 'as-received' EUROPT-1 catalyst.

The studies of CO adsorption were carried out in vacuum at reduced pressure. For thermal desorption studies, the CO adsorption was achieved by controlled pulse chemisorption. Pulses of CO were introduced into the flowing helium (@ 20 cm^3 per minute) at positive pressure, i.e. 0.8 p.s.i.g. The details of the pulse chemisorption method have been mentioned in the

experimental section and also in Chapter 3.

It was observed that the first pulse of CO was almost enough to saturate the surfaces of 'as-received' and alkali doped catalysts. The DRIFTS spectra of pulse chemisorbed CO on the four catalysts is shown by a comparative set of spectra in figure 5.15. Figure 5.16a shows a trace of pulses of CO and uptake by the catalysts. The uptake of CO by four individual catalysts was same as as previously observed and listed in table 3.6. The thermal desorption spectra were obtained by heating the sample in a stepwise manner from room temperature to 923 K. A typical TPD trace is shown in figure 5.16b. The amount of CO desorbed was calculated by integrating the profile using an on-line microcomputer from start to finish. The value obtained corresponded well with the actual TPD (conventional) as detailed in Chapter 3.

Thermal desorption 'DRIFTS' spectra of CO from 'as-received', 0.25%, 0.5% and 1.0% KOH (wt)/EUROPT-1 are shown as stacked sets in figures 5.17-5.20 respectively. A DRIFTS spectrum of each sample was recorded from room temperature to 923 K. It was observed that spectra obtained at room temperature to 373 K were essentially the same in all the cases. Therefore in stacked plots sets of spectra over a temperature range of 373-923 K are presented.

It is worth pointing out here that some interference was expected in the appearance of infrared thermal

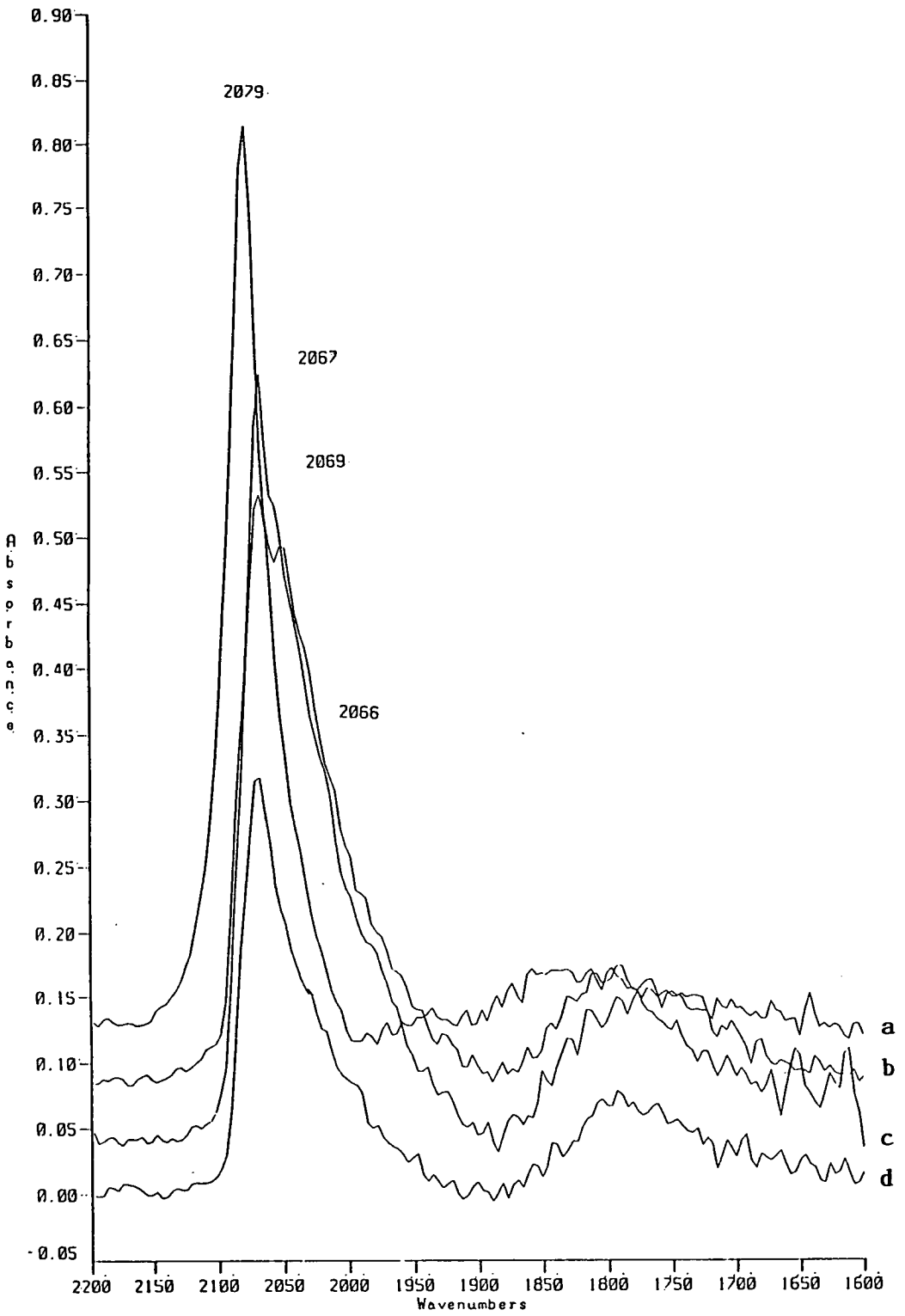

Fig. 5.15 DRIFT Spectra of CO Adsorbed by Pulse Method on
(a) EUROPT-1;
(b) 0.25% KOH (wt)/EUROPT-1;
(c) 0.5% KOH (wt)/EUROPT-1;
(d) 1% KOH (wt)/EUROPT-1.

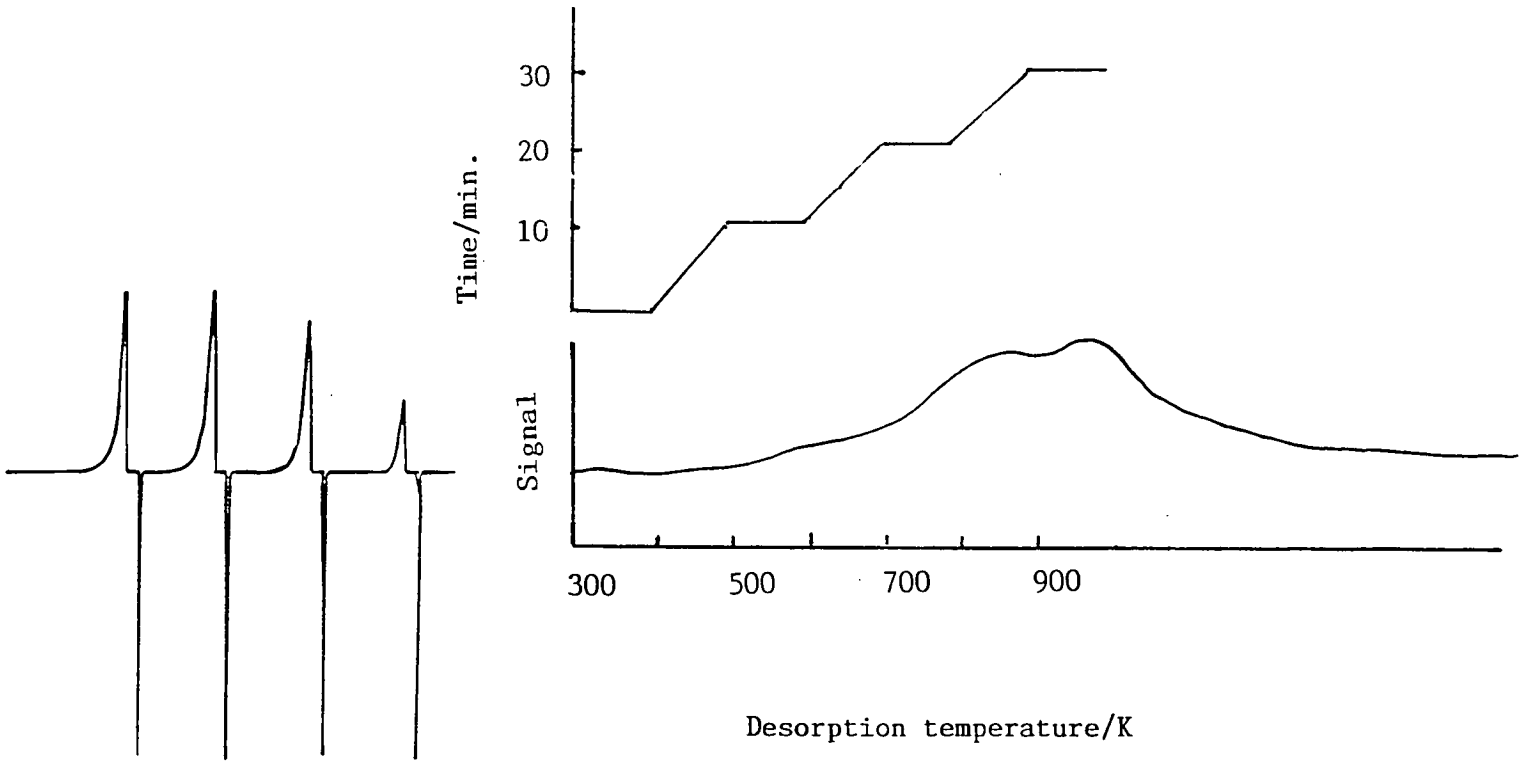

Fig. 5.16 (a) A Recorder Trace of Four CO Pulses Showing Uptake of CO.

(b) CO Desorption Profile Obtained from EUROPT-1 by Increasing DRIFT Cell Temperature.

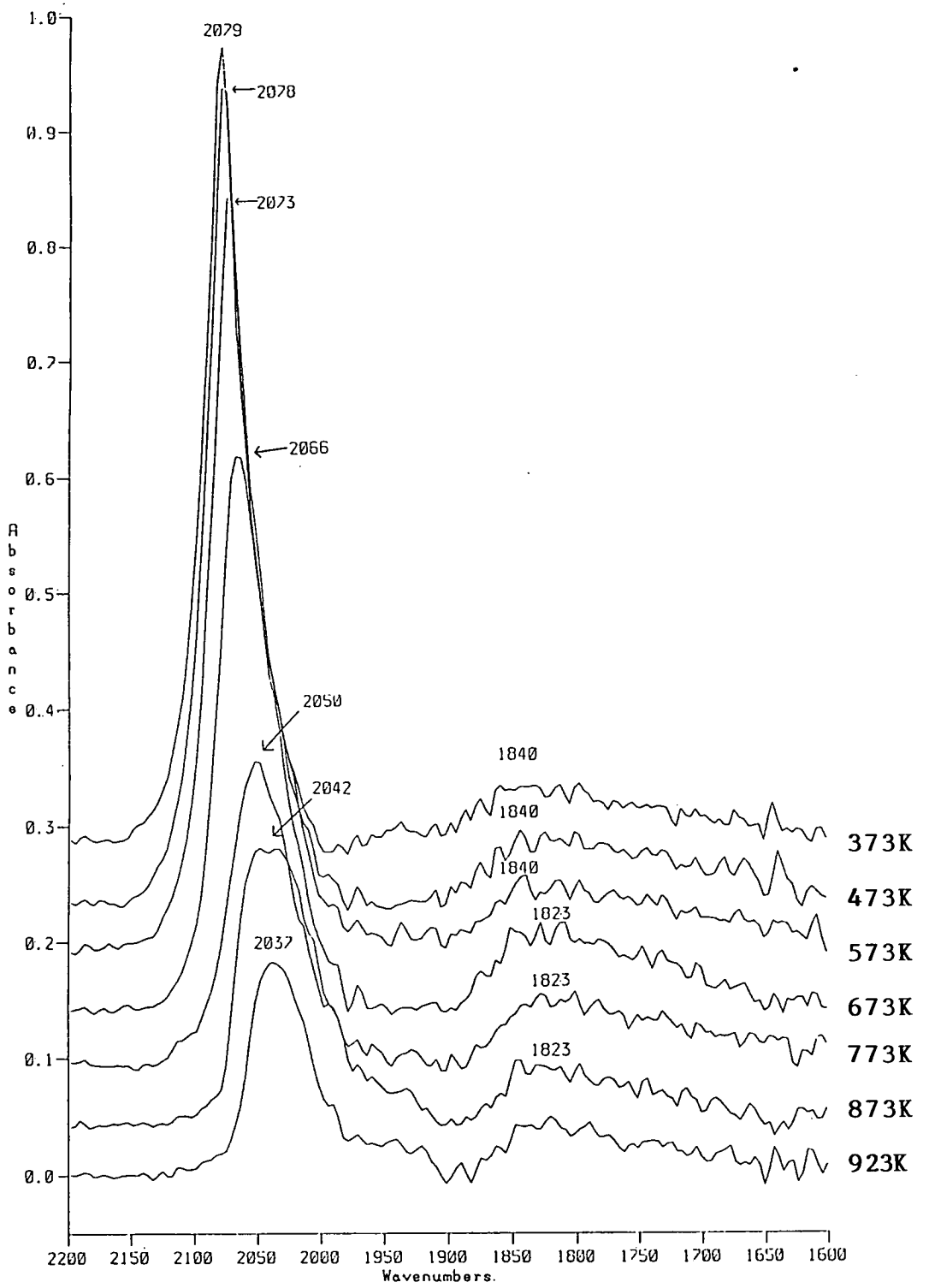

Fig. 5.17 Thermal Desorption Infrared Spectra of Carbon Monoxide Adsorbed on EUROPT-1 (see Table 5.4).

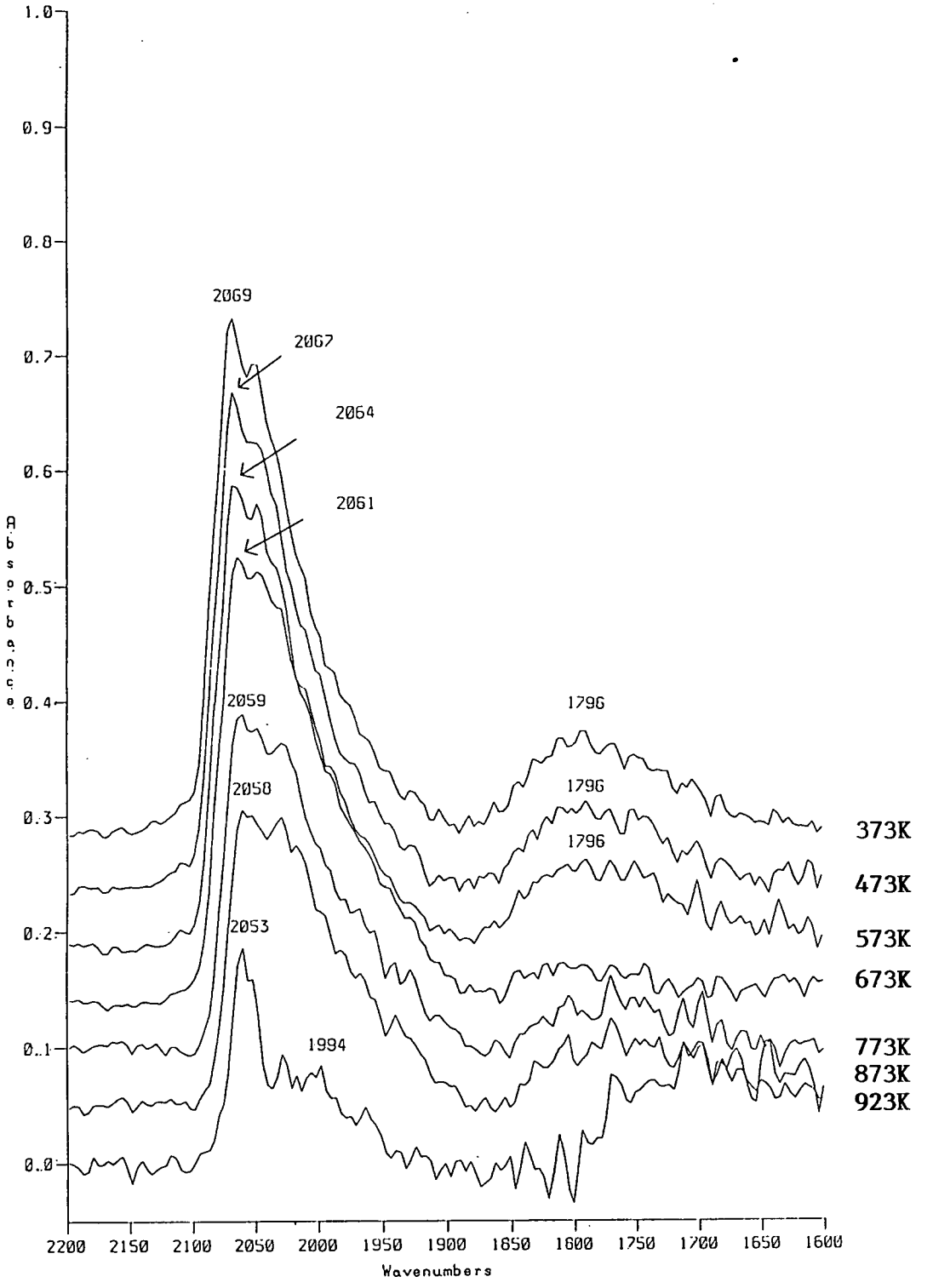

Fig. 5.18 Thermal Desorption Infrared Spectra of Carbon Monoxide Adsorbed on 0.25% KOH (wt)/EUROPT-1 (see Table 5.4).

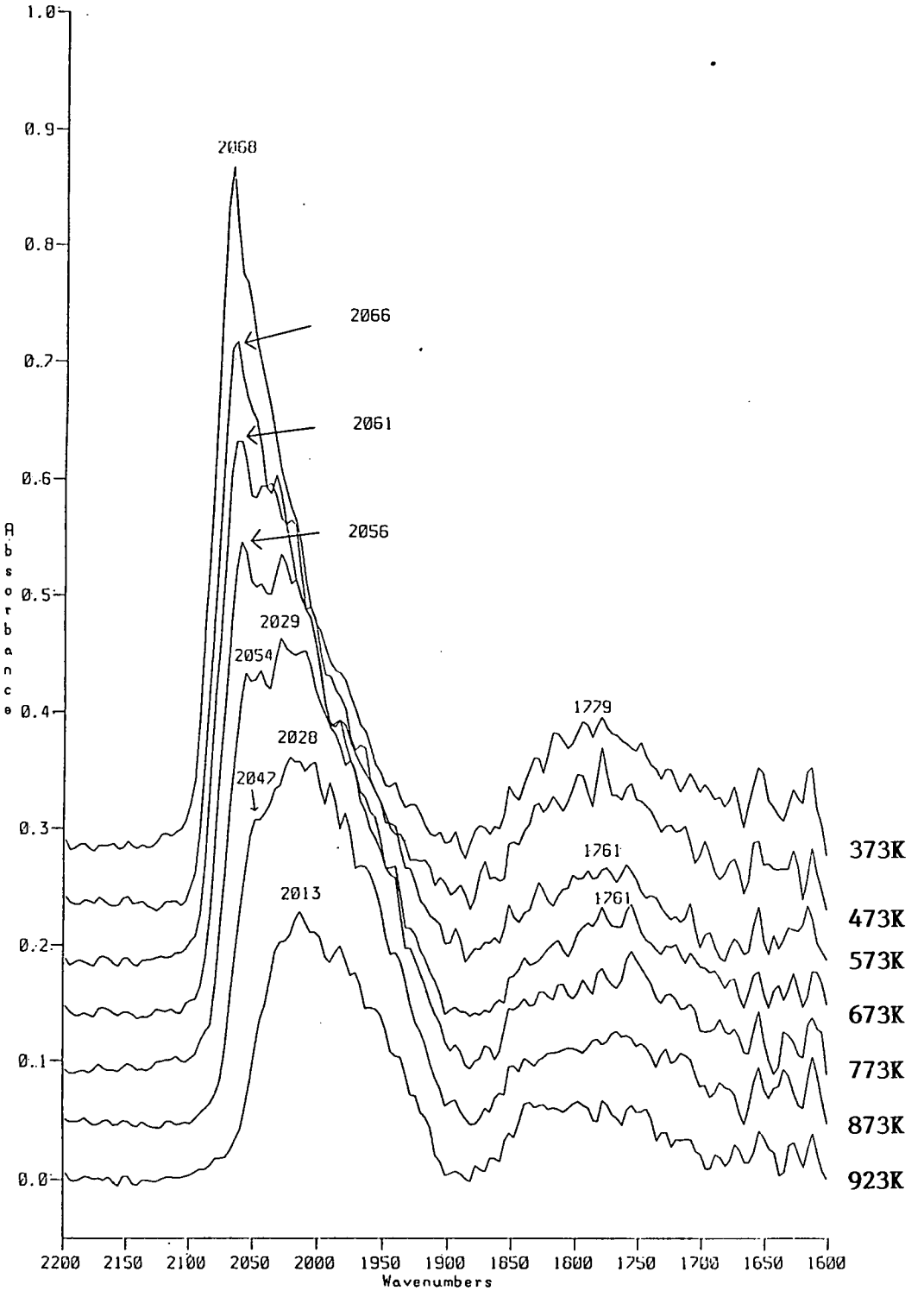

Fig. 5.19 Thermal Desorption Infrared Spectra of Carbon Monoxide Adsorbed on 0.5% KOH (wt)/EUROPT-1 (see Table 5.4).

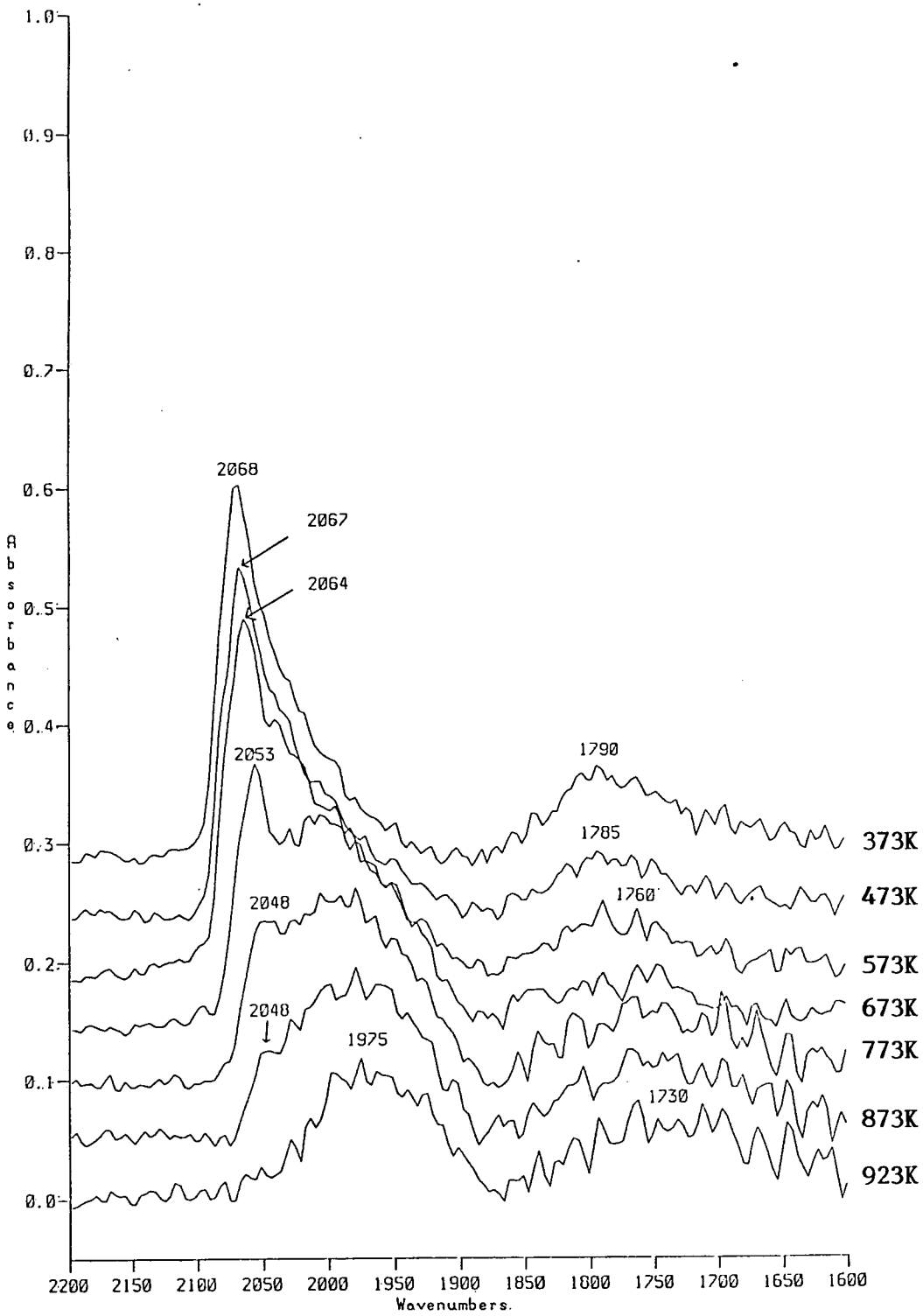

Fig. 5.20 Thermal Desorption Infrared Spectra of Carbon Monoxide Adsor ed on 1.0% KOH (wt)/EUROPT-1

desorption spectra at higher temperature by the silica support. It was therefore decided to carry out a blank thermal desorption spectrum using the silica support only. A set of spectra was obtained under the same experimental conditions (figure 5.21). The spectra thus obtained were subtracted from the thermal desorption spectra of each catalyst for corresponding temperatures.

The desorption spectra of the 'as-received' EUROPT-1, shown in figure 5.17, are considered first. At saturation, two CO bands are seen at 2078 cm^{-1} and 1845 cm^{-1}, corresponding to linear and bridged species respectively (at room temperature). The linear band's position at 2078 cm^{-1} is slightly higher than that observed at saturation during the stepwise CO adsorption as mentioned earlier. This higher shift can be a result of higher CO pulse pressure.

The integrated intensity data and frequency shift as a function of desorption temperature is shown in table 5.4. It is interesting that as the temperature is increased to 473 K, the peak intensity increased, and a slight shift of band position towards lower frequencies was observed. This feature was consistently observed for all the catalysts. For 'as-received' EUROPT-1, as the temperature was raised further to 573 K, the linear band at 2079 cm^{-1} declined in intensity and frequency. The infrared peak remains symmetric throughout the desorption process. Spectra from all other catalysts (alkali doped) initially

Table 5.4

Shift of Frequency (cm^{-1}) and Change of Intensity of Linear Band as Function of Temperature

Desorption Temperature/K	As-Received EUROPT-1 $\nu(cm^{-1})$	Area	0.25% KOH(wt)/EUROPT-1 $\nu(cm^{-1})$	Area	0.5% KOH/EUROPT-1 $\nu(cm^{-1})$	Area	1.0% KOH(wt)/EUROPT-1 $\nu(cm^{-1})$	Area
373	2079	35.95	2069	35.15	2067	42.55	2066	21.63
473	2078	36.87	2067	37.15	2064	42.89	2066	22.16
573	2073	33.83	2067	35.68	2061	45.23	2063	24.76
673	2064	27.52	2064	35.25	2056	43.97	2053	23.00
773	2051	18.94	2060	33.75	2037	42.55	2048	22.873
873	2047	15.17	2058	29.95	2020	36.39	2000	17.31
973	2038	9.31	2058	15.94	2013	22.92	2000	15.47

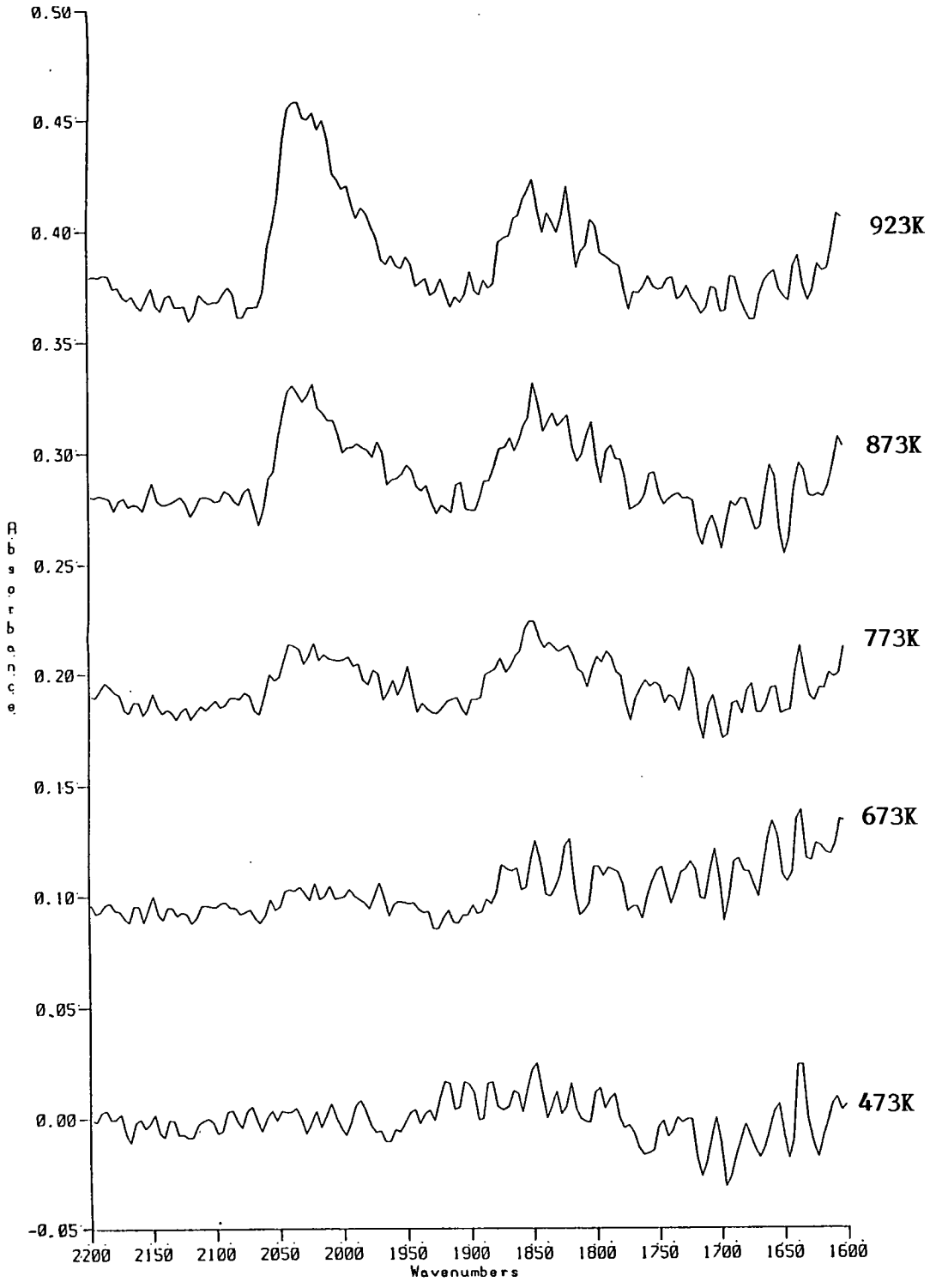

Fig. 5.21 DRIFT Spectrum of Silica Support at Increasing Temperatures.

showing some asymmetry, became highly asymmetric during the desorption process. The linear band for all the catalysts shifted down by approximately 50 cm^{-1} (high frequency feature) and 100 cm^{-1} relative to the band centre. Due to the broad and weak spectra, it was impossible to assign any position exactly to the bridged band. The changes in the integrated intensity for the linear region from 1900-2100 cm^{-1} and bridged band in the region 1800-1900 cm^{-1} are all listed in table 5.4. These changes have been presented graphically in figure 5.22. From this graph we have noted that the area goes through a maximum at 473-573 K and declines thereafter.

Figure 5.23 shows plots of the first derivative of area versus temperature of desorption. This becomes a type of simulated TPD spectrum. The T_{max} of desorption for the 'as-received' EUROPT-1 comes in the range 573-673 K, where for all the alkali doped catalysts, this T_{max} is shifted to higher temperatures *ca.* 773-873 K. These desorption maxima are similar to the T_{max} observed for CO desorption by conventional TPD methods as detailed in Chapter 3.

All the desorption spectra show some CO still present at a desorption temperature of 923 K. The TPD trace obtained, shown in figure 5.16b, shows the total desorption of CO at that temperature. It is possible that the remaining CO, which is undetectable by conventional TPD apparatus, desorbs very slowly at 923 K. It was

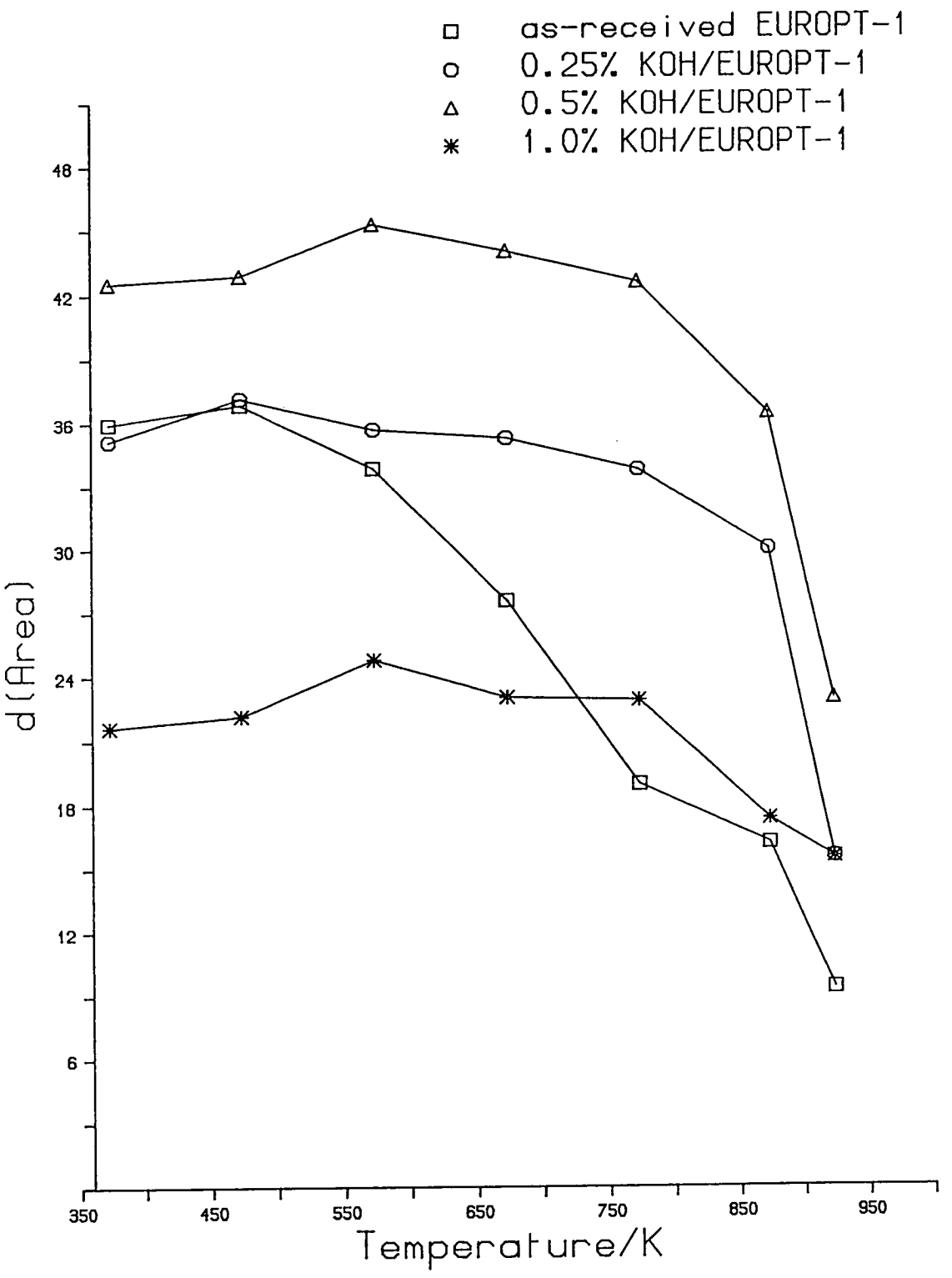

Fig. 5.22 Linear Peaks Versus Temperature

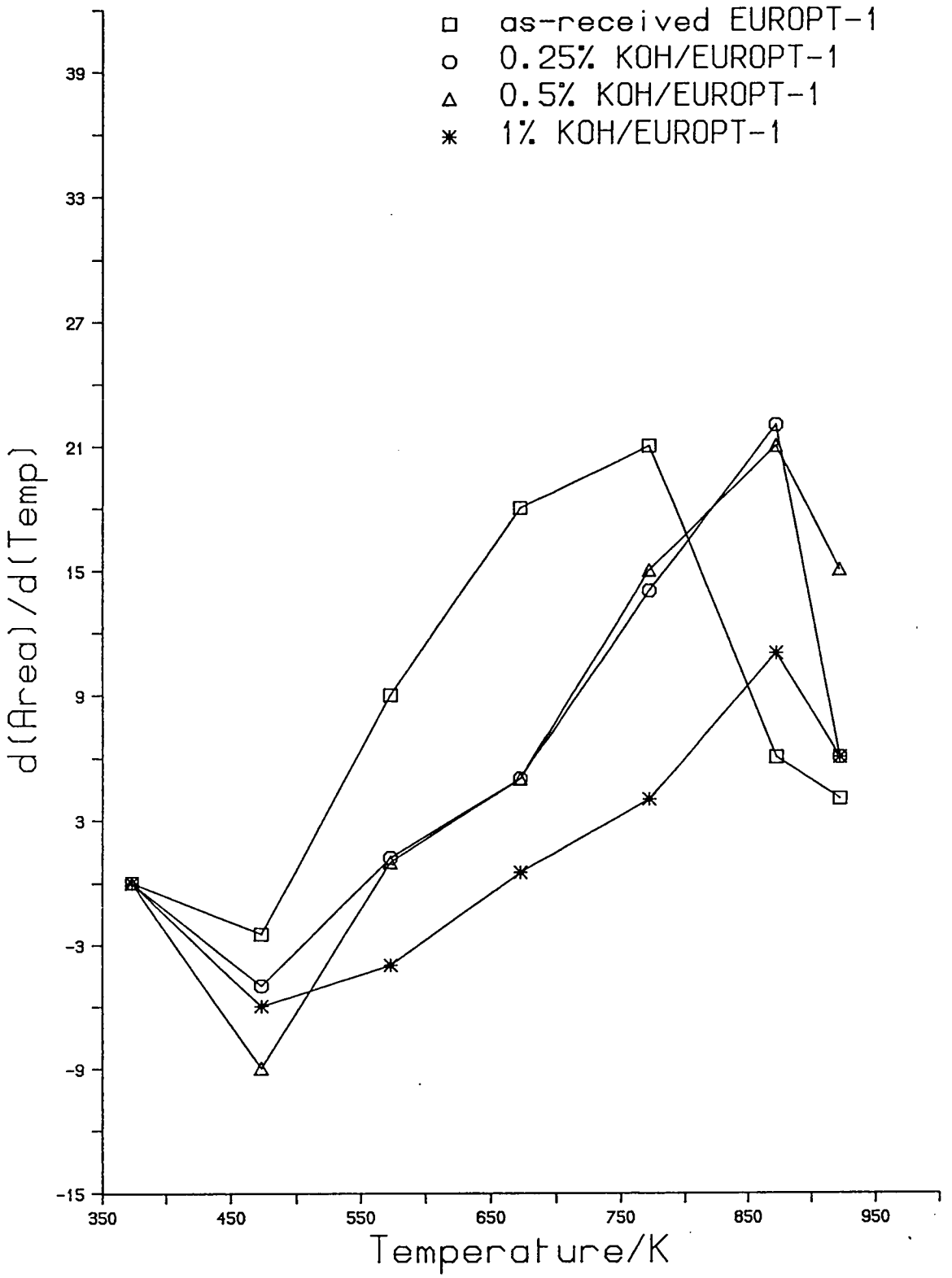

Fig. 5.23 Peak Area Derivatives

further observed that leaving the sample at a desorption temperature of 923 K for 30 minutes (after completion of TPD process) removed all the CO (DRIFTS detectable) from the surface.

5.8 DISCUSSION

CO adsorption on EUROPT-1 at room temperature gave two bands, an intense sharp and symmetric band at 2079 cm^{-1} and a broad band of relatively medium intensity at 1845 cm^{-1}. These bands are attributed to linear and bridged species respectively. Present results are similar to the results of others[1-4] in the appearance and assignments of these bands.

In a recent study of CO adsorption on EUROPT-1 at room temperature, by transmission infrared spectroscopy, McDougall[4] reported an intense and symmetric band at 2079 cm^{-1} and a broad band at 1845 cm^{-1}. The symmetry of the linear band was attributed to the homogeneity of the catalyst. These results are in excellent agreement with the author's results.

Many studies have been made of the infrared spectrum of CO on supported platinum[15,18,39]. Sheppard *et al.*[3] summarised vibrational frequencies for CO chemisorbed on Pt. According to them, at high coverage the linear CO band almost invariably falls in the wavenumber region 2070-2095 cm^{-1}. The authors also reported weaker and broader absorption bands attributable to bridged CO groups

in the wavenumber range 1900-1800 cm^{-1}. These conclusions were supported by the results obtained from CO adsorption on a Pt(111) single crystal[3].

A shift was observed of the ν(CO) band for increasing CO coverage. Figure 5.11 shows stepwise adsorption of CO (function of CO pressure) on EUROPT-1. Such a shift was not unexpected. It was first reported by Eischen[2], and since by other workers. In agreement with the previous workers it was interpreted that the observed shift is a result of dipole-dipole coupling interactions. The linear band observed at low wavenumbers for initially adsorbed CO could be attributed to there being sufficient separation between the adsorbed CO molecules which did not allow dipole-dipole interactions to occur.

The study of dipole-dipole coupling interactions has received considerable attention in the past. Significant shift of the C-O stretch frequency has been reported as a function of coverage. For CO on a Pt(111) single crystal at a substrate temperature of 300 K, a band due to linearly bonded CO was first observed at 2065 cm^{-1}. This band shifts to 2101 cm^{-1} as saturation is achieved. Blyholder[40] suggested that a reduction of $d\pi^*$ back-bonding occurred as the coverage was increased. This was assumed due to competition for metal d-electrons. Hammaker[41] proposed that the shift was due to dipole- dipole coupling between CO molecules aligned parallel to each other on the surface. The author supported his result with the

vibrational spectra of isotopic mixture of ^{13}CO and ^{12}CO. Crossley and King[42], showed that a ^{12}CO molecule couples very weakly into a ^{13}CO environment. Their experiment demonstrated that the entire frequency shift observed for CO on Pt(111) was due to a coupling effect and not to chemical bonding effects. Later on this theory was refined and it suggests that the observed frequency shift is entirely compatible with dipole coupling theory.

There is little available literature on infrared study of alkali effect on CO adsorption on supported platinum catalysts. Analogies can be drawn from EELS study of CO adsorption on a K/Pt(111) single crystal[19]. On clean Pt(111), the authors observed bands at 2120 and 1875 cm^{-1}, corresponding to linear and bridge bonded CO. This was in agreement with the previously reported C-O stretching vibration[43]. Small addition of K changed the CO vibrational frequencies[19]. Both the linear and bridged peaks shifted to lower frequency compared to the potassium-free Pt/CO system. By $\theta K \simeq 0.1$ the bridged CO stretching frequency had decreased by 100 cm^{-1} while the linear vibration had decreased by 65 cm^{-1}. Changes in relative peak height of the linearly bonded CO versus the bridge bonded CO were also reported. This shift of the C-O stretch frequency to lower values, accompanied with a substantial broadening of the peaks increased as K began to cover more than 5% (i.e. $\theta K > 0.15$) of the platinum substrate. At $\theta K \simeq 0.3$ the linear site intensity was much

smaller than that of the bridged site. By $\theta K \simeq 0.6$, only one distinct peak was visible at 1565 cm^{-1}. The authors interpreted this behaviour in terms of three major effects: (1) long range interactions between K and CO; (2) K pushes CO from on top sites into bridge sites; (3) electron charge from strong electropositive K is transferred via Pt-d bands into the antibonding 2π orbital of CO. The authors suggested the latter effect to be responsible for the drastic decrease in the C-O stretch frequency in the presence of K.

Alkali induced effects can be understood by assuming that alkali adatoms on a transition metal surface exist in a partially ionic state. A large fraction of their valence electrons are donated to the metal. This results in a decrease of work function, causing large changes in the adsorption energy, vibrational frequencies and site selectivity of adsorbed CO. Where the back-donation of metal electrons into the CO $2\pi^*$ orbital also leads to the strengthening of the metal-C bond and weakening of the CO bond.

In the present study the effect of coadsorbed potassium could be seen in a shift of the CO stretch frequencies to lower values with a substantial broadening of the peaks. This shift became larger with increasing alkali concentration. On Pt(111) + K this shift has been reported to be continuous with increasing potassium coverage[20]. Furthermore it was observed that the

intensity of the high frequency component, the on-top adsorbed CO ~ 2074 cm^{-1} decreased by ~ 30 cm^{-1} at an alkali concentration of 1% KOH (wt).

The intensity changes and the frequency shifts observed during thermal desorption are shown in figures 5.17-5.20. Consistent symmetry observed for 'as-received' EUROPT-1 during thermal desorption suggests the homogeneity of the catalyst. The area of the peaks in the linear region increased with temperature until 473 K, whereupon they decreased steadily. Even at the highest desorption temperature (923 K), the presence of adsorbed CO was indicated by a significant peak. Figure 5.23 showing a graph of the peak area derivatives indicate the CO desorption had a maximum at 673 K.

Barth *et al.*[18] have reported similar results. The author studies CO desorption (infrared) from alumina supported platinum. The area of the peaks in the linear region increased with temperature until 373 K, whereupon it decreased slowly, reached zero at about 673 K. The authors observed that the rate of disappearance of linearly bonded CO had two maxima, one at 423 K and the other at about 523 K. The authors offered three possible explanations for this behaviour.

1. The absorptivity of some of the linearly adsorbed CO is enhanced.
2. CO, which is not linearly adsorbed, is converted to linearly bonded CO.

3. CO, adsorbed by the support, could migrate to the metal.

The last explanation was thought to be unlikely, as no CO adsorption was observed on support material, although 'spillover' CO cannot be ruled out. The first explanation was thought to become valid if it was assumed that under the influence of temperature, adsorbed molecules migrated to sites where their absorptivity is increased. The author proposed another possibility that purging with helium might create some vacant sites. These could be sites of the most weakly held CO.

Turning to the alkali doped catalysts, all TPD/DRIFTS spectra for these catalysts exhibit broader peaks than EUROPT-1. In each case, as the temperature increases the high frequency component of the band envelope desorbed more rapidly at lower temperatures, in a fashion similar to the desorption of the CO from the undoped sample. Whereas the lower wavenumber tail of the original room temperature spectrum is retained to higher temperature, as a broad maximum. Like the undoped sample, the high frequency component shifts to lower $\bar{\nu}$ as the temperature increased. The behaviour of the lower frequency component is more difficult to discuss as it is originally hidden below the main ($\bar{\nu}$ CO) high frequency component. However, it too may shift downwards in frequency by $\simeq$ 100 cm^{-1} and perhaps gain in relative intensity, presumably due to surface migration of CO in a manner similar to that

suggested to account for the increase in intensity of the linear peak on the EUROPT-1 catalyst in the early TPD/DRIFTS spectra.

The fact that low frequency CO is held more strongly on alkali doped EUROPT-1 is confirmed by the thermal desorption infrared spectra, since this portion of the spectrum is retained at 923 K. This tightly bound CO could be either CO on high miller index sites or sites directly promoted by potassium. The former explanation requires that the alkali causes sintering of the catalyst to provide high miller index sites. CO adsorption on low and high miller index sites has been reported previously. In the conventional CO TPD from EUROPT-1, Kramer reported lower temperature CO adsorbed on flat and low index planes and the higher temperature one to adsorption on more open, high miller index planes. Supporting evidence may also come from the EELS study of CO adsorption on Pt(111) and Pt-6(111) x (100) surfaces[9]. TDS yields only one desorption peak from the 111 surface, while for the stepped surface a second peak with higher temperatures was reported.

The present results are also comparable to the EELS works of CO desorption from a K/Pt(111) single crystal[19]. Figure 5.24 shows plot of $\Delta\bar{\nu}$ of CO on a K/Pt(111) single crystal as a function of θK produced from the data presented by Crowell *et al.*[19]. From this plot are extracted estimates of the range of θK corresponding to

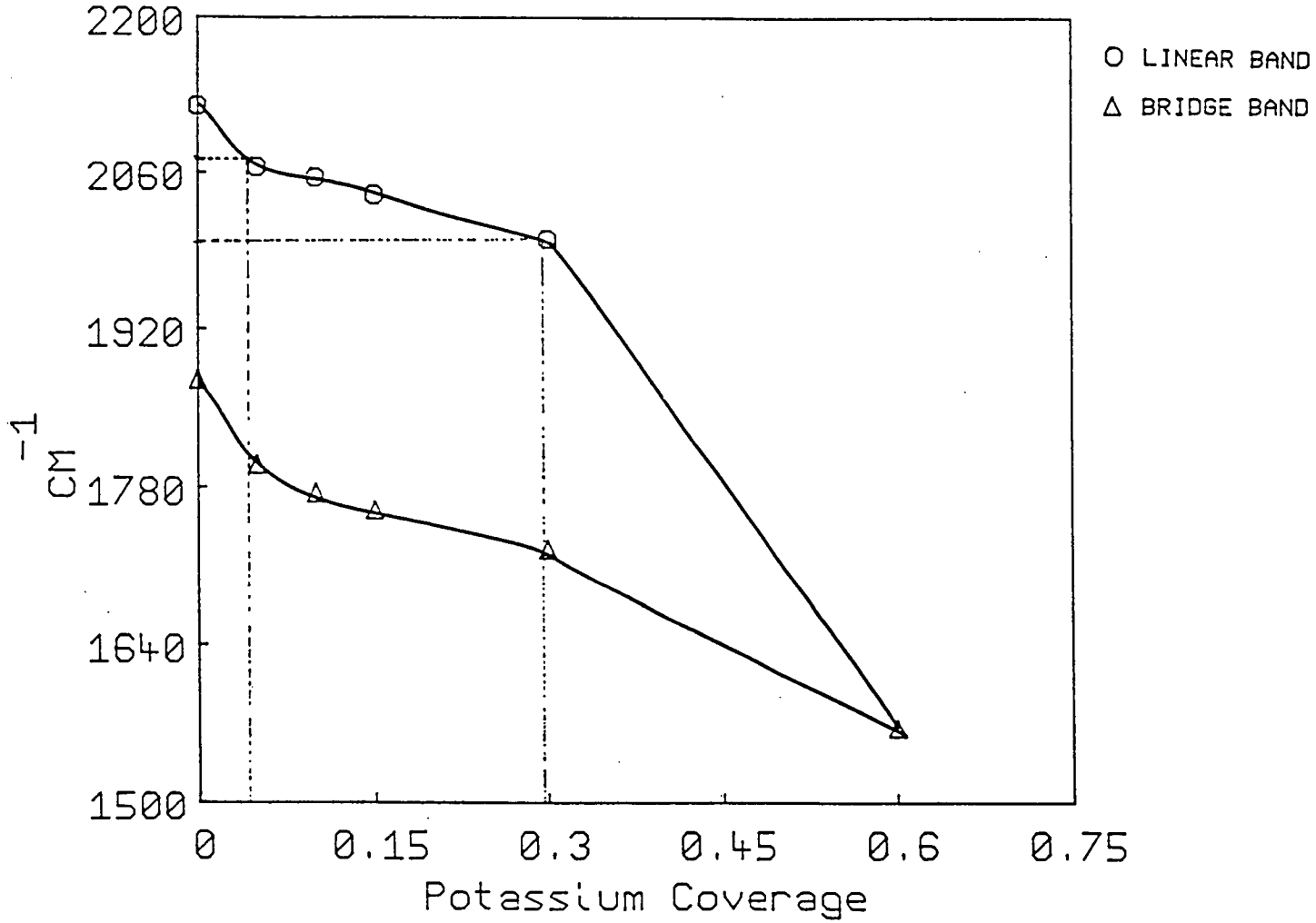

Fig. 5.24 CO Absorption Maxima at Saturation Versus Alkali Coverage (extracted from data presented by Crowell et al, ref.19).

The dotted lines related the frequency shifts observed in this work to potassium coverage

change in frequency observed in the present study. These values of θK fall in the range ~ 0.05 to 0.3, as indicated in the figure 5.24 by the dotted lines. This range is similar to the previously noted value of θK obtained by fitting values of ΔT (table 3.5) to the single crystal data. This gave an approximate alkali coverage of θK = 0.13-0.33. The values of θK of 0.125-0.33 (from figure 3.11) based on % CO uptake and % CO uptake per unit area (table 3.5) are signifiantly higher than these values.

These values can also be compared with the nominal range of alkali concentration presented on the Pt surface calculated earlier. If it is assumed that alkali is spread over the available surface area of the catalyst, 0.25%-1% KOH loadings give an atomic density of 1.5-5.8%, corresponding to approximate alkali coverage of θK, 0.04-0.16.

5.9 CONCLUSION

The present study has shown that the chemisorption properties of CO are significantly altered when adsorbed in the presence of potassium promoted EUROPT-1.

The CO stretching vibrational frequencies decrease with increasing potassium coverage. The vibrational change could be attributed to a substantial charge donation from potassium through the platinum substrate and into the CO $2\pi^*$ orbital. These changes along with the changes in thermal desorption properties of CO in the

presence of potassium are similar to that reported in the EELS study of CO/K/Pt(111) system[19].

Thermal desorption studies proved to be effective in the determination of strength of CO interaction. A plot of the derivative of changes in frequency versus temperature shows similar features as noted previously in CO TPD studies (Chapter 3).

The high frequency component in the spectra of alkali doped samples behave like the 'as-received' sample. This suggests that some of the alkali doped catalyst remains alkali free or unaffected by the alkali.

REFERENCES

1. R.P. Eischen, W.A. Pliskin and S.A. Francis, *J.Chem.Phys.* 22 (1954) 1786.
2. R.P. Eischen, S.A. Frances and W.A. Pliskin, *J.Phys.Chem.* 60 (1956) 194.
3. N. Sheppard and T.T. Nguyen, Advances in Infrared and Raman Spectroscopy, Vol. 5, Eds. R.J.H. Clerk and R.E. Hester (London, 1978).
4. G.S. McDougall, Ph.D. Thesis, U.E.A. (1985).
5. M. Bartok, J. Sarkany and A. Sitkei, *J.Catal.* 72 (1981) 236-245.
6. R.A. Shigeishi and D.A. King, *Surf.Sci.* 58 (1976) 379.
7. A. Crossley and D.A. King, *Surf.Sci.* 68 (1977) 528.
8. B.E. Hayden and A.M. Bradshaw, *Surf.Sci.* 125 (1983) 787.
9. H. Hopster and H. Ibach, *Surf.Sci.* 77 (1978) 787.
10. M.R. McClellan and J.L. Orland and F.R. McFeeley, *Surf.Sci.* 63 (1981) 112.
11. K. Horn and J. Pritchard, *J.Phys.* (Paris) 38 (1977).
12. A. Crossley and D.A. King, *Surf.Sci.* 66 (1977) 101.
13. R. Hardeveld and F. Hartog, *Surf.Sci.* 15 (1969) 189.
14. C.W. Olsen and R.I. Masel, *Surf.Sci.* 201 (1988) 444.
15. H. Miura and R.D. Gonzalez, *J.Phys.* 373 (1982) 15.
16. G.L. Griffin and J.T. Yates, *J.Catal.* 73 (1982) 396.
17. D.M. Haaland, *Surf.Sci.* 185 (1987) 1.
18. R. Barth, R. Pitchai, R.L. Anderson and X.E. Verykios,

J.Catal. 116 (1989) 61.

19. J.E. Crowell, E.L. Garfunkel and G.A. Somorjai, *Surf.Sci.* 121 (1982) 303.
20. H.P. Bonzel, *Surf.Sci.Rept.* 8 (1987) 43.
21. G. Pirug and H.P. Bonzel, *Surf.Sci.* 199 (1988) 371.
22. E.I. Garfunkel and G.A. Somorjai, *J.Phys.Chem.* 86 (1982) 310.
23. Chemical Infrared Fourier Transform Spectroscopy, P.R. Griffiths, Wiley Interscience, London (1975).
24. P. Felgett, Aspen Int. Conf. on Fourier Spect. (1970), (G.A. Vanasse, A.T. Stair, and D.J. Baker, Eds.), AFCRL-71-0019, p. 139.
25. P. Jacquinot, 17^{e} Congres du GAMS, Paris, 1954.
26. R.J. Bell, Introduction to Fourier Transform Spectroscopy (Academic Press, New York, 1972).
27. P.R. Griffith in: Analytical Applications to FT-IR Molecular and Biological System, Eds. J.R. Druig (Ridel, London, 1980).
28. J.W. Cooley and J.W. Tukey, *Maths.Comput.* 19 (1965) 297.
29. M.L. Foreman, *J.Opt.Soc.Am.* 56 (1966) 978.
30. K. Klier, *Am.Chem.Soc.Symp.Ser.1* 137 (1980) 141.
31. G. Kortum and W. Braum, *Ann.Chem.* 104 (1960) 632.
32. K. Klier, *Catal.Rev.1* (1967) 207.
33. R.G. Messerschmidt, *Appl.Spectrosc.* 39 (1985) 737.
34. H.G. Hecht, Proceedings of the Am.Chem. Symposium on Reflectance Spectroscopy held 11-12 Sept. 1987.

35. S. Chandrasckhar, "Radiative Transfer", Dover, New York, 1960.

36. J. Tenter, D.H. Strome, R.G. Herman and K. Klier, *J.Phys.Chem.* 81 (1977).

37. R.G. Herman, K. Klier, *J.Catal.* 56 (1979) 407.

38. K. Klier, R. Herman, P.J. Hulta, *J.Chem.Phys.* 61 (1974).

39. R.P. Eischen and W.A. Pliskin, *Adv.Catal.* 10 (1958).

40. G. Bhyholder, *J.Phys.Chem.* 68 (1964) 2772.

41. R.A. Hammaker, S.A. Francis and R.P. Eischens, Spectrochimica Acta 21 (1965) 1295.

42. A. Crossley and D.A. King, *Surf.Sci.* 95 (1980) 131.

43. C.T. Campbell, G. Ertl, H. Kuipers and J. Segner, *Surf.Sci.* 107 (1981) 207.

CHAPTER 6

ADSORPTION OF HYDROCARBONS ON 'AS-RECEIVED' AND ALKALI DOPED EUROPT-1

The work described in this chapter concerns the adsorption of ethylene, ethane, n-butane and benzene on the 'as-received' and alkali doped EUROPT-1. In the interest of clarity it has been subdivided into four sections: Part I covers ethylene adsorption; Part II benzene adsorption and Part III the saturated hydrocarbons. Part IV is a small section covering a combined study of the reaction of n-butane over the catalyst by gas chromatography and DRIFTS.

6.1 EXPERIMENTAL

The apparatus used in the present study was the same as described earlier in Chapter 5. Source of gases/adsorbates used are listed in table 5.1.

For the adsorption of ethylene, ethane and n-butane, about 12.5 torr of each adsorbate was expanded over the catalysts at room temperature, a pressure of 2.5 torr was used for benzene adsorption. Prior to expansion the hydrocarbons were purified by several freeze and thaw cycles. Each adsorbate was left over the samples for five minutes. The gas phase spectra were recorded at a

resolution of 4 cm^{-1} and 1000 scans. The gas was then evacuated and an infrared spectrum was recorded for adsorbed species.

The treatment of spectra, i.e. base line correction and smoothing, has been described earlier in Chapter 5.

PART I

ADSORPTION OF ETHYLENE

6.2 INTRODUCTION

Earlier infrared spectroscopic studies of ethylene adsorption on supported platinum catalysts were carried out by MOrrow and Sheppard[1]. The purpose of this initial study was to compare the adsorbed species from ethylene on Pt and Ni metals. A well defined spectrum indicating the initially adsorbed species was obtained when ethylene came into contact with a platinum sample at room temperature. The peak at 2880 cm^{-1} was dominant in the spectrum. The other peaks were at 2795 and 2920 cm^{-1}. These peaks were attributed to surface MCH_2-CH_2M groups (M = metal). This suggests σ bonded, associatively adsorbed species.

The spectrum obtained for ethylene adsorption on Ni at 195 K had considerable resemblance to that observed for a Pt catalyst. Adsorption on Ni at higher temperature gave a significantly different spectrum. The spectrum exhibited additional intense peaks at 2960 and 2930 cm^{-1}.

The hydrogenation of ethylene is one of the fundamental reactions in heterogeneous catalysis and has been extensively studied[2-6]. It was generally considered that the hydrogenation proceeds between adsorbed hydrogen and ethylene[7]. On hydrogenation of ethylene adsorbed on silica supported platinum catalyst, the main gas phase product was found to be ethane. This suggested that the

surface species giving the main 2930, 2885 and 2800 cm^{-1} peaks was a C_2 hydrocarbon fragment with the vibrational frequencies expected for MCH_2-group (M - surface metal atom) rather than MCH = or $-CH_3$. The peaks at 2885 and 2930 cm^{-1} were therefore attributable to the symmetric and asymmetric CH_2 stretching vibrations of an associatively adsorbed 1,2 σ-diadsorbed ethylene (MCH_2CH_2M)[1]. The peak at about 2800 cm^{-1} was thought to be an overtone of a deformation mode of the same species brought up in intensity by fermi resonance with the intense fundamental at 2885 cm^{-1}.

In addition to the peaks observed in CH stretch region, there were some additional weaker peaks in the region 3020-2920 cm^{-1}. A peak at 2965 cm^{-1} was observed at temperatures below room temperature. This was thought to be due to physisorbed ethane. At higher temperatures a peak at *ca.* 2960 cm^{-1} was observed. This peak was attributed to the formation of surface n-butyl group. A peak in the range 3010-3020 cm^{-1} was thought to result from surface acetylenic species formed from partial dehydrogenation of the chemisorbed ethylene. Some intensity developed in the region *ca.* 2930 cm^{-1} was also possibly from the same acetylenic species[1].

Infrared studies of ethylene adsorbed on a silica supported Pt catalyst (EUROPT-1) at room temperature were carried out by McDougall[8]. The spectra were found to be identical to those described above. The use of a fourier

transform spectrometer helped extend the useful spectral range down to the silica absorption blackout at 1300 cm^{-1}. The results indicated the presence of π-adsorbed ethylene and ethylidyne surface species from adsorption of ethylene on EUROPT-1. The 3012 cm^{-1} and 1500 cm^{-1} peaks were assigned to the π-adsorbed ethylene and the 2885, 2800 and 1342 cm^{-1} peaks were attributed to a surface ethylidyne species. The remaining peaks between 2970-2920 cm^{-1} were thought to be due to at least one more surface species existing in addition to the ethylidyne and π-adsorbed ethylene. The increase in intensity of the 3012 cm^{-1} and 1500 cm^{-1} as a function of coverage suggested that the 2885, 2800 and 1342 cm^{-1} peaks belong to the same surface species.

The band at 1500 cm^{-1} was first observed by Prentice *et al.*[9]. They found a band of medium intensity at 1500 cm^{-1}. When the adsorbed ethylene was exposed to the controlled amounts of hydrogen, the drop in the intensity of 1500 cm^{-1} band was at a similar rate to the 3012 cm^{-1} band in the CH-stretch region. It indicated that the bands at 3012 and 1500 cm^{-1} belonged to the same surface species.

Recent infrared studies of ethylene adsorbed on a supported platinum catalyst (16% Pt/Si_2O) were carried out by Cruz *et al.*[10]. Spectra were recorded down to 1300 cm^{-1}. The spectra were recorded at 189 K and after warming to 294 K. It was observed that at low temperature

two adjacent bands occurred at 2906 and 2922 cm^{-1}, on warming to room temperature, the second of these absorptions, plus some absorption near 1419 cm^{-1} disappeared and were replaced by 2881 and 1342 cm^{-1} peaks, and were attributable to the ethylidyne species[11-13]. These changes show that the di-σ-adsorbed species is converted to an ethylidyne species as observed on a Pt(111) single crystal[14]. Hence this study provided strong evidence for the existence of the three main adsorbed species from ethylene on Pt/Si_2O[9].

The infrared study of the ethylene adsorption on alumina supported Pt catalysts were carried out by Soma[7,15-16]. Strong infrared absorption by alumina below 1100 cm^{-1} allowed spectra to be recorded down to 1200 cm^{-1}. At 187 K, C=C stretching bands were observed at 1498 cm^{-1}, which was the same π-adsorbed species as found on silica supported platinum catalysts. A total of four bands assigned to π-adsorbed species were observed, these four bands occurred at 3025, 1498, 1199 and 1420 cm^{-1}. Comparing these frequencies with Zeise's salt, (table 6.1) these additional peaks can be assigned as symmetric CH_2 scissors and CH_2 scissors respectively.

Upon warming the alumina supported platinum sample from 187 K to room temperature the peak at 1338 cm^{-1} grew in intensity along with the peak in the C-H stretching region at 2940 and 2880 cm^{-1}. The peak at 1338 cm^{-1} was initially attributed to the deformation mode of the σ

bonded ethylene species[16].

The previous studies of ethylene adsorption on silica or alumina supported platinum show that a typical spectra of ethylene adsorbed on Pt/SiO_2 and Pt/Al_2O_3 should show well defined peaks at *ca.* ~ 3020, 2885, 2800, 1500 and 1342 cm^{-1}.

The ethylene adsorption on transition metal single crystals has been extensively studied[17-20]. The associatively adsorbed ethylene can take two forms. A π bonded state, where the ethylene largely retains its sp^2 hybridization with a carbon-carbon double bond. This has been identified on Cu(100)[17], Pd(100)[18], Ni(100)[19] and Pd(111)[20]. In this state ethylene bonding can be explained by a donor-acceptor interaction. A di-σ bound state can also exist. The ethylene adsorbed in this state forms two covalent bonds to the metal surface. This has been observed on Pt(111)[21], Ni(111)[22], Ni(110)[23] and Fe(110)[24] single crystals at low temperature.

Chemical modification of the metal surface can change the bonding state of ethylene. Oxygen and carbon have been widely studied as modifiers of the surfaces such as Pt(111)[21], Ag(110)[25], Ru(001)[26], Fe(111)[27], Pd(100)[28], and Ni(110)[23].

At present only a few studies have been carried out to determine the effect of potassium on adsorption of hydrocarbons on metal surfaces. Studies of effect of alkali metals on adsorption of ethylene on Pt(111) single

crystal have recently appeared[29-30]. Garfunkel *et al.*[31], studied adsorption of benzene on a potassium doped Pt(111) single crystal.

Recently the coadsorption of ethylene and potassium on a Pt(111) single crystal was studied by Windham *et al.*[29], and Zhou *et al.*[30]. Windham *et al.* used HREELS, UPS and TPD techniques. They observed that small amounts of potassium altered the ethylene dehydrogenation rate and changed the mode of ethylene bonding from di-σ to π. This new π-bound state of ethylene increased concomitantly with increasing potassium coverage. Similar findings were reported by Zhou *et al*[30]. They observed that potassium inhibits the adsorption of di-σ bonded ethylene at low temperatures.

The ethylene coadsorption with potassium on a Pt(111) single crystal is in contrast to the adsorption of CO and NO on a potassium doped Pt(111) single crystal, where bond strength is increased due to potassium. This is because both CO and NO are better π-acceptors than C_2H_4.

The effect of potassium doping (on EUROPT-1) on ethylene adsorption was studied. These infrared studies were carried out at room temperature, using 'DRIFTS' technique.

6.3 RESULTS

A complete spectrum of ethylene adsorbed on EUROPT-1 at room temperature is shown in figure 6.1. The spectrum

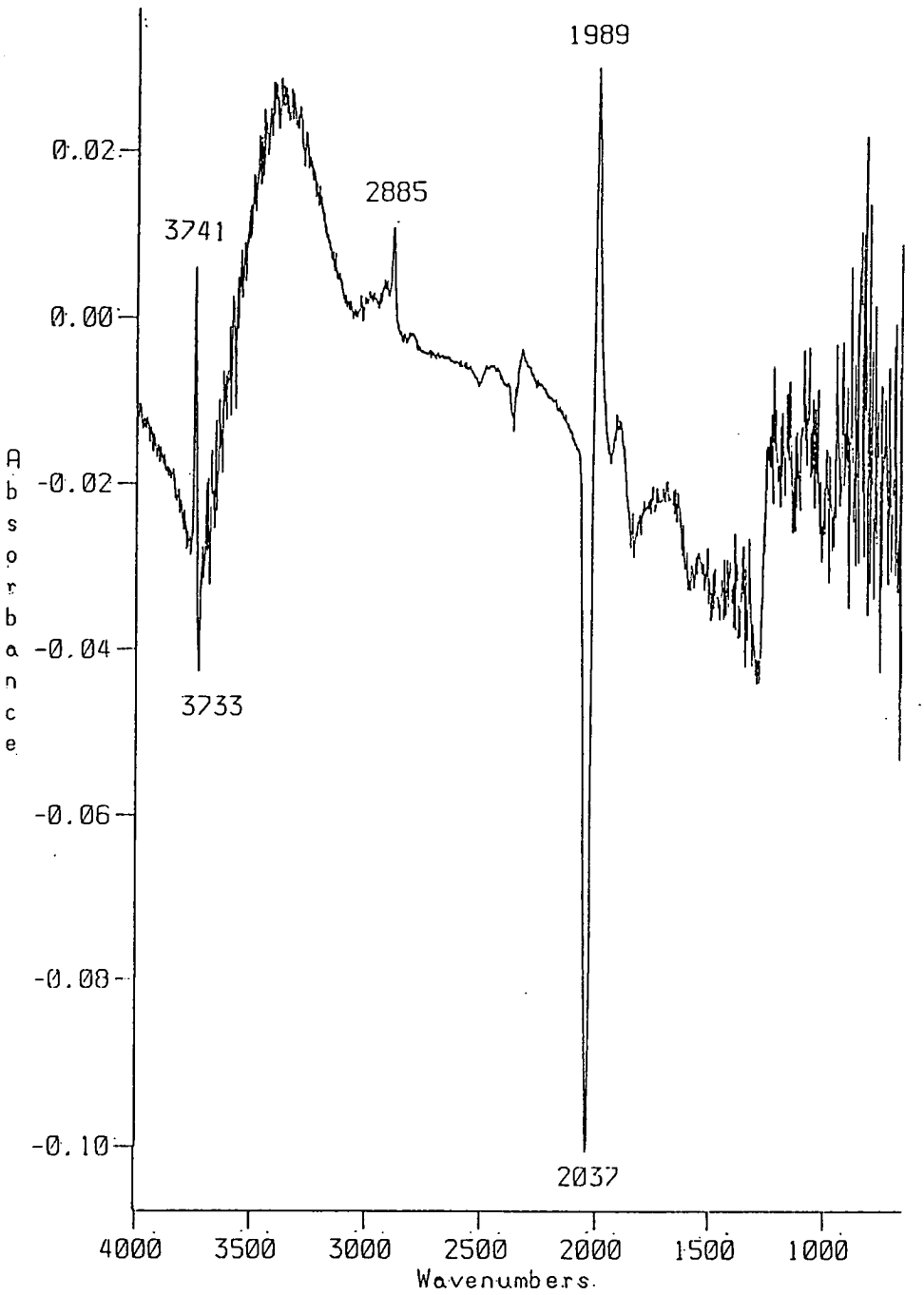

Fig. 6.1 **A DRIFT Spectrum of Ethylene Adsorbed to Saturation on EUROPT-1**

extends from 4000-650 cm^{-1} and was recorded at a resolution of 4 cm^{-1}. The spectrum is the ratio of single beam spectra recorded before and after treatment of the EUROPT-1 catalyst by exposure to 12.5 torr of ethylene for fifteen minutes followed by evacuation.

The spectrum in figure 6.1 shows a number of features in addition to adsorbed hydrocarbons. An intense sharp peak in the spectrum at 3741 cm^{-1} is seen. Normally the free hydroxyl groups of the silica support give a peak around 3750 cm^{-1}[132]. Some features due to hydrogen bonded hydroxyl groups appear in the range 3500-3550 cm^{-1}.

A huge band extending from 3100-3600 cm^{-1} is dominant. This peak is attributed to the ice present in the liquid nitrogen cooled MCT detector. This has been observed previously by others[8]. It has been reported that prolonged evacuation of the detector helps in the reduction of the band's intensity.

When the samples are exposed to 12.5 torr of ethylene, the introduction of moisture or water vapour becomes difficult to avoid. Hence water vapour or moisture is adsorbed on the silica support. This causes a decrease in the number of hydrogen bonded hydroxyl groups, which is indicated by a negative peak in the ratio spectrum. The slope of the spectrum is a common instrumental problem, and has been noted previously by others[8]. Slight variation in the interferometer's mirror velocity can cause such slope. In the present study the spectrum

slopes by 0.06 absorbance units across the spectral range.

Another intense sharp peak centred at 2030 cm^{-1} is due to carbon monoxide as an impurity at the sample surface before adsorption of ethylene. When ethylene is adsorbed the CO stretching frequencies shift to lower wavenumber, i.e. down to 2000 cm^{-1}. This results in a derivative shape peak. The spectrum also shows a negative CO peak indicating the physical displacement of CO upon ethylene adsorption.

Some other non hydrocarbon features in the range 2500-2360 cm^{-1}, and sharp low intensity peaks from 1800-1300 cm^{-1} are caused by the miscancellation of atmospheric carbon dioxide and water vapour respectively.

The higher noise level found in the experiments using 'DRIFTS' compared to the reported transmission spectra[8], did not allow reproducible spectra to be obtained in the C-H deformation region, i.e. 1700-1300 cm^{-1}. It was also noted that the silica blackoution expected at 1300 cm^{-1} appeared at about 1370 cm^{-1}. This is because a DRIFTS spectrum is related to the absorbance of the sample and its reflectivity, (which is related to refractive index). On going through a strong band there is often an associated charge in refractive index. This can give a derivative shape to the band. Thus, unambiguous identification of peaks in this region was not possible.

Figure 6.2 shows the expanded plot of the spectrum (3100-2700 cm^{-1}) for ethylene adsorbed on EUROPT-1 at room

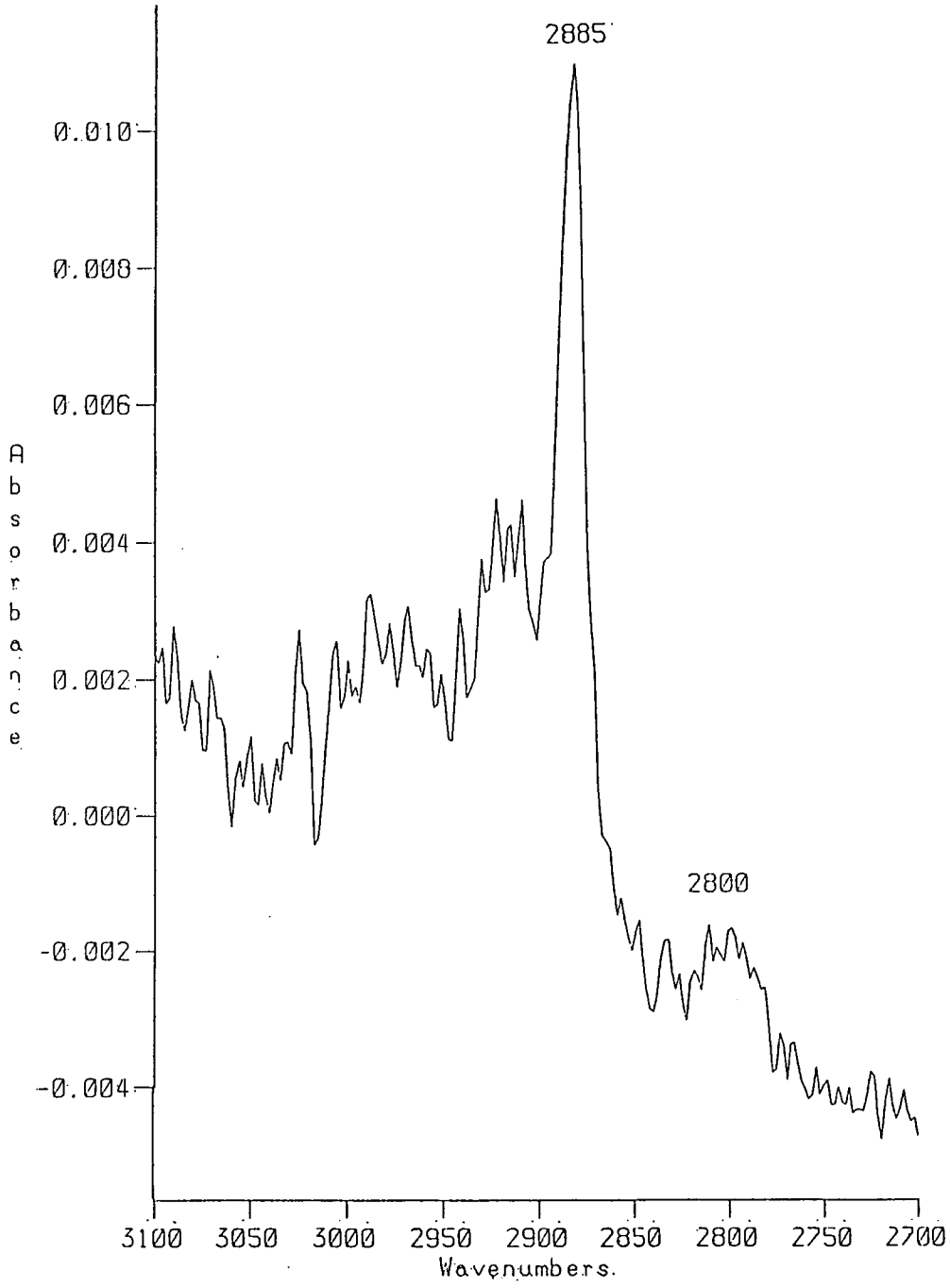

Fig. 6.2 Expanded Plot of the CH Stretch Region of Figure 6.1 , i.e. ethylene adsorbed on EUROPT-1

temperature. The spectrum shows peaks at ~ 2800, 2885, 2920, 2977 and 2990 cm^{-1}. The spectrum also shows some structure in the range 3010-3025 cm^{-1}. The intense peak at 2885 cm^{-1} is the most prominent feature in this part of the spectrum. Figure 6.3 shows the same spectrum after baseline correction. It is observed that peak frequencies and positions remain unchanged. The spectrum was then smoothed to improve the appearance without shifting peak positions or intensities, as shown in figure 6.4.

The expanded plot of the deformation region extending from 1700-1300 cm^{-1} of fig. 6.1 is shown in figure 6.5. Any assignment in this region can be misleading due to the reasons already mentioned. The baseline corrected spectrum is shown in figure 6.6. The same spectrum after smoothing is shown in figure 6.7. It is interesting to note that the saturation peak in the silica blackout region in some spectra takes a shape of a peak or infrared band centred at 1348 cm^{-1}. This is an effect of smoothing and not because of infrared vibrations, as the line width of 60 cm^{-1} is much more than the typical value of 20 cm^{-1} for bands from surface species.

The ethylene adsorption on three alkali doped EUROPT-1 catalysts, 0.25, 0.5 and 1.0% KOH (wt.)/EUROPT-1 were carried out under the same experimental conditions and identical procedure was applied to plot the spectra as used for the 'as-received' EUROPT-1.

The complete spectra of ethylene adsorbed on 0.25 and

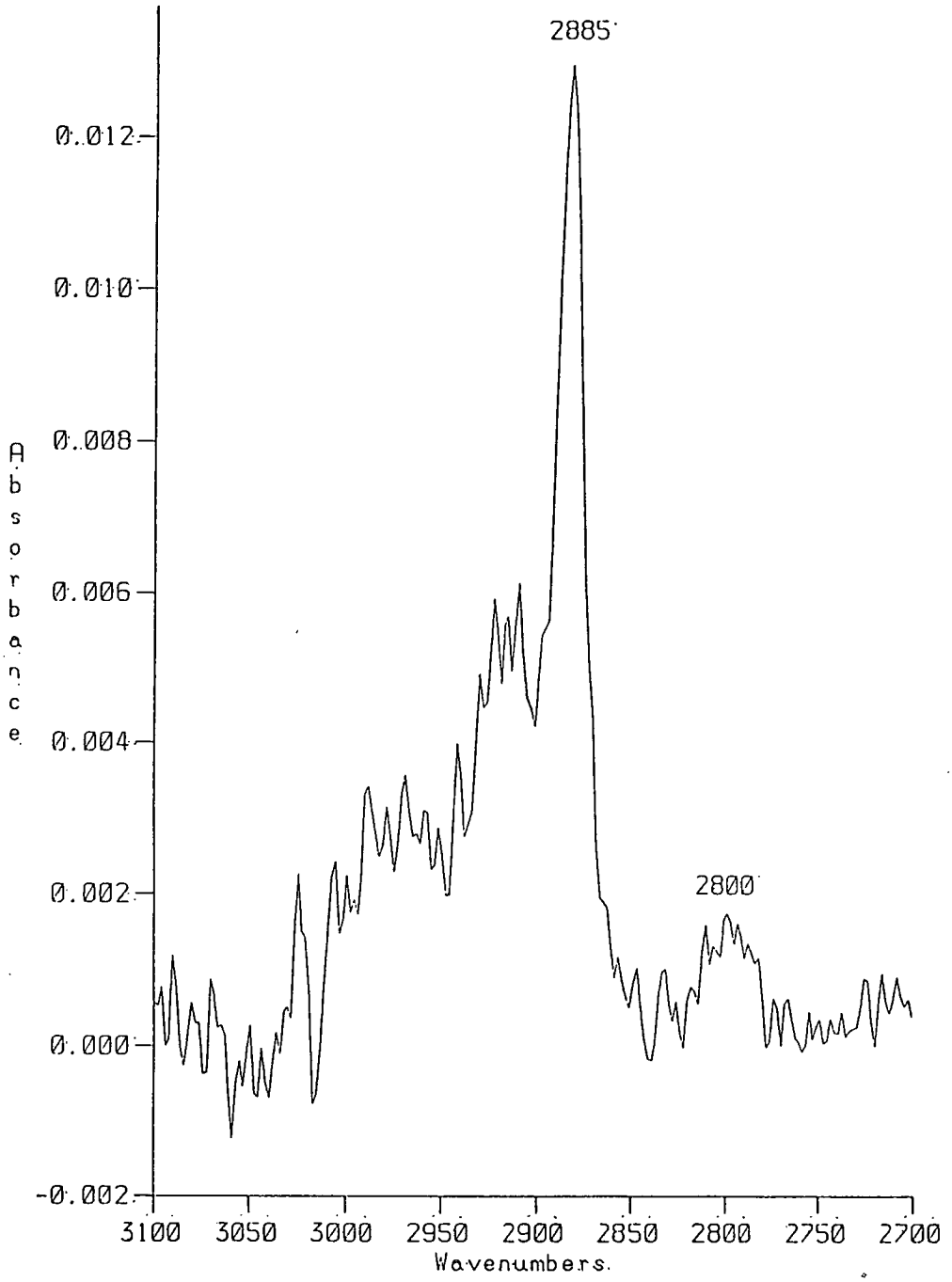

Fig. 6.3 Baseline Corrected Plot of the CH Stretch Region of Figure 6.2 , i.e. ethylene adsorbed on EUROPT-1

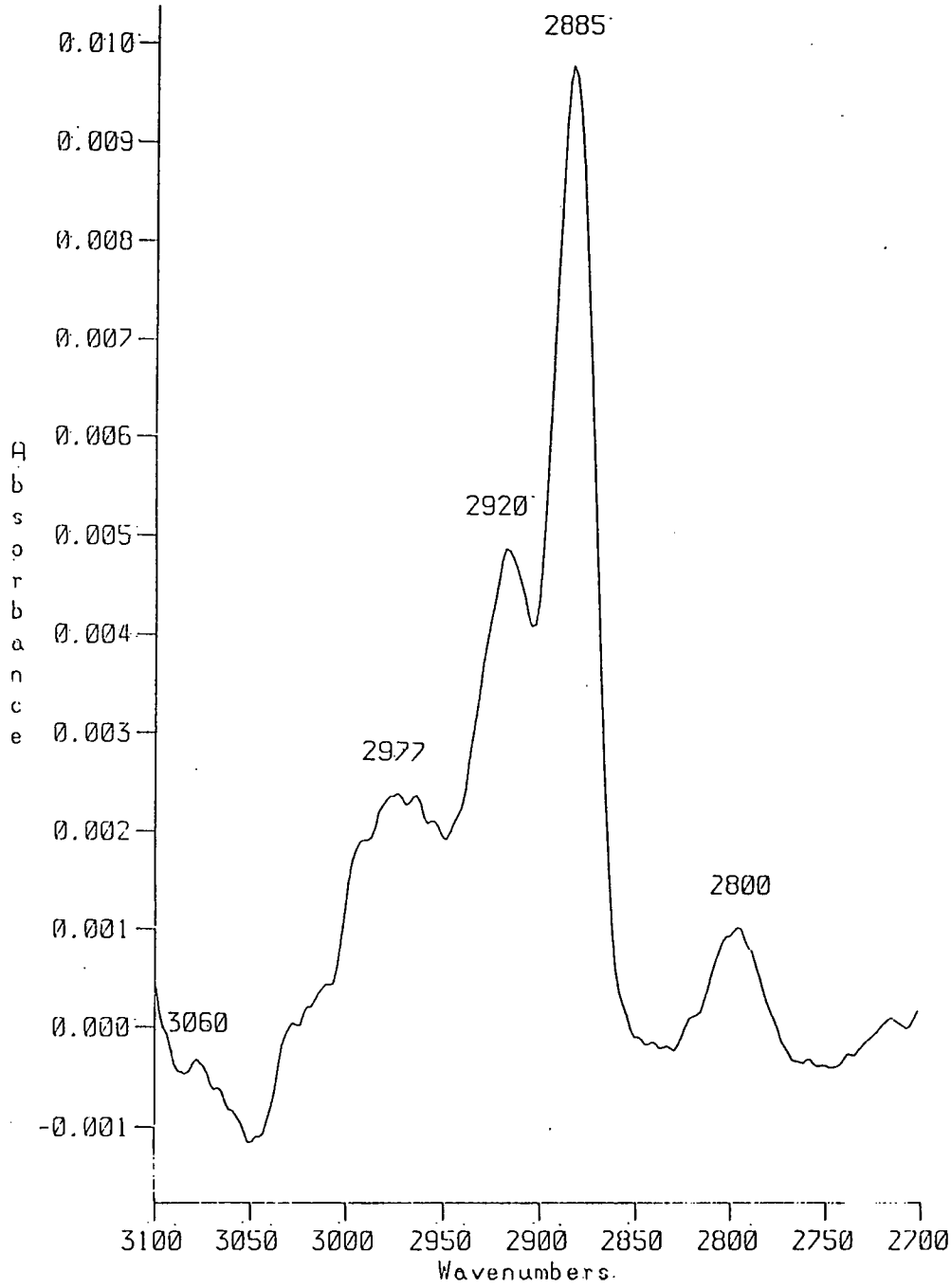

Fig. 6.4 Smoothed Plot of the CH Stretch Region of Figure 6.3 , i.e. ethylene adsorbed on EUROPT-1

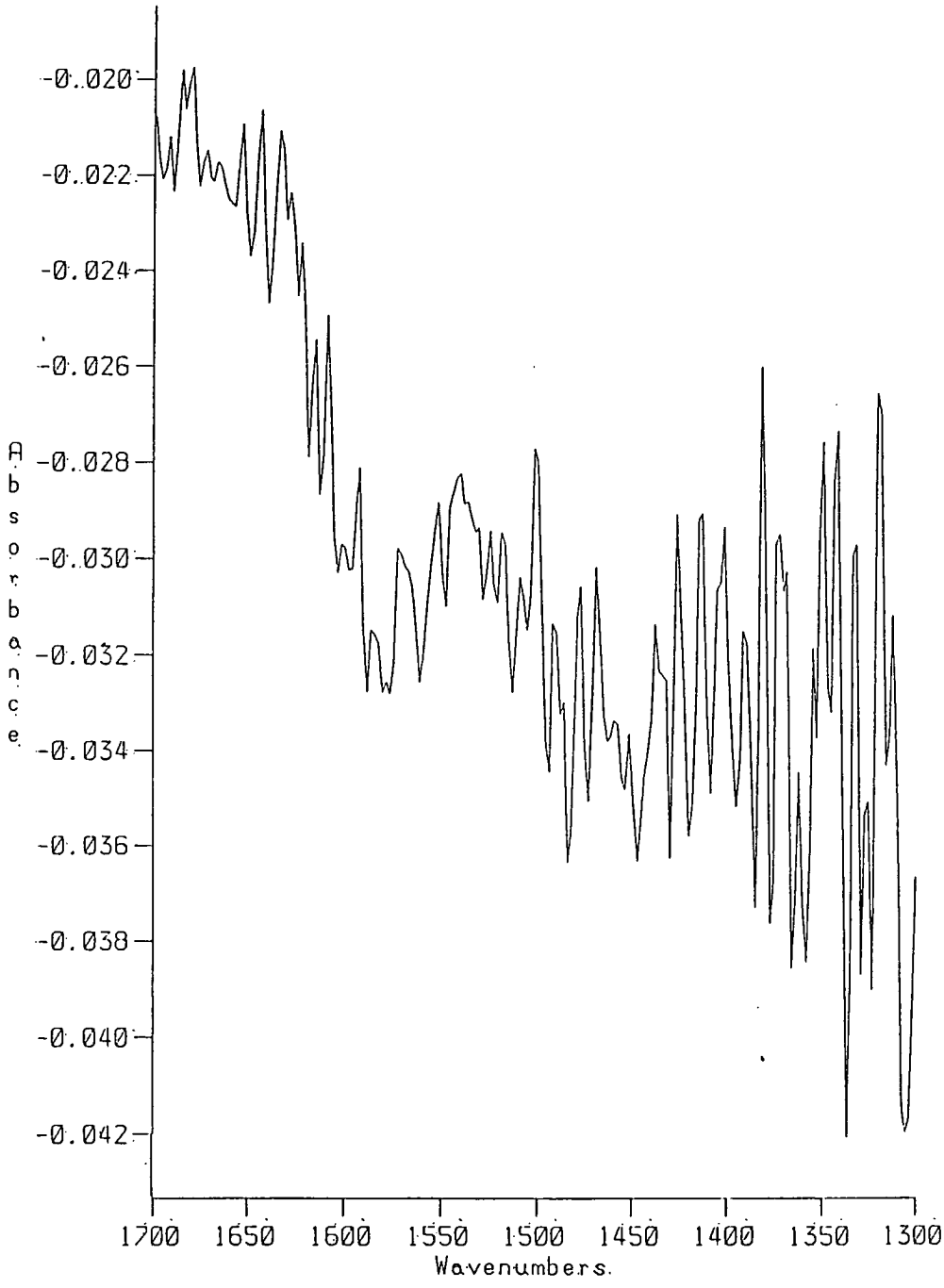

Fig. 6.5 Expanded Plot of the CH Deformation Region of Figure 6.1 , i.e. ethyleneadsorbed on EUROPT-1

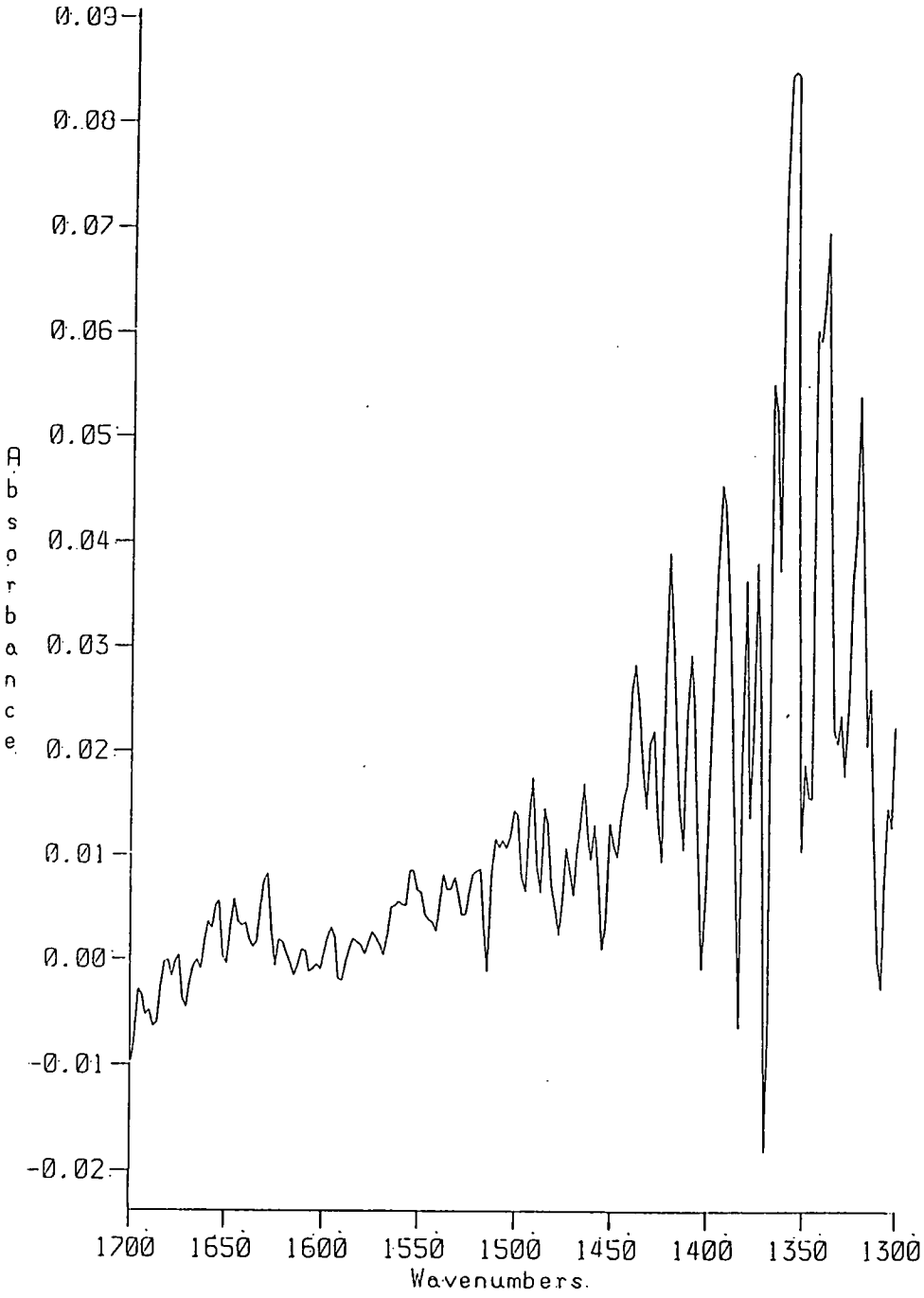

Fig. 6.6 Baseline Corrected Plot of the CH Deformation Region of Figure 6.1, i.e. ethyleneadsorbed on EUROPT-1

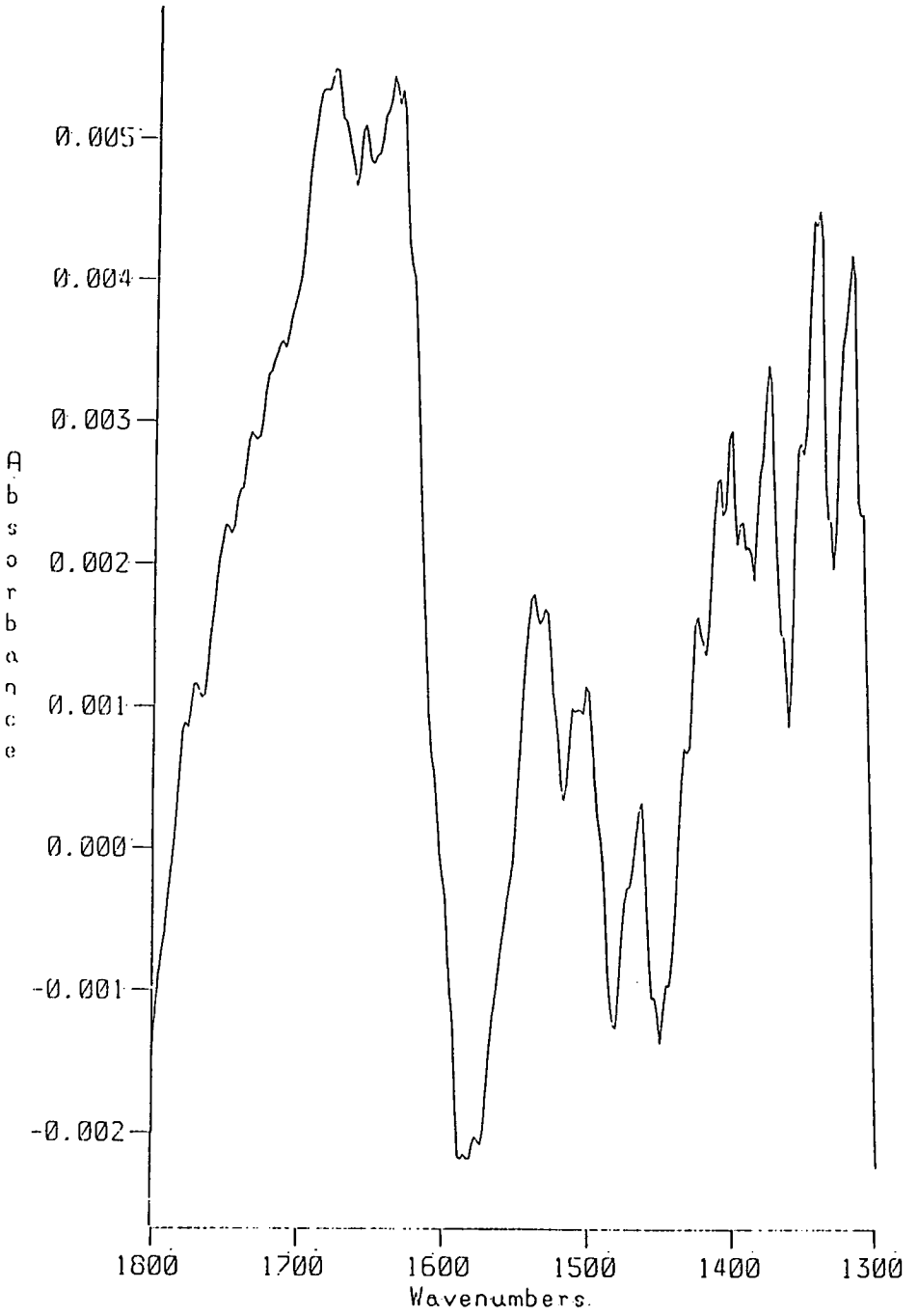

Fig. 6.7 Smoothed Plot of the CH Deformation Region of Figure 6.6, i.e. ethylene adsorbed on EUROPT-1

0.50% KOH (wt.)/EUROPT-1 are shown in figures 6.8 and 6.9 respectively. The spectra are essentially similar in shape, peak positions and intensities to that observed for 'as-received' EUROPT-1. Although all the experimental parameters throughout this study are the same, slight variations in peak intensities are expected because of the variations in the sample position in the 'DRIFTS' cell attributable to evacuation, pumping or degassing procedures.

Figures 6.10 and 6.11 show the expanded and baseline corrected plots of the spectra shown in figures 6.8 and 6.9 respectively. The C-H stretching region, extending from 3100-2700 cm^{-1}, are very similar. These spectra after smoothing are shown in figures 6.12 and 6.13 respectively. The region 2800 cm^{-1} becomes broad giving indications of two peaks at 2800 and 2822 cm^{-1}. The other peaks occur at 2885, 2920 and 2977 cm^{-1}. There are some indications of intensity in the region 3010-3020 cm^{-1}. A low intensity peak at *ca.* 3060 cm^{-1} is observed, which is very close to the noise level but is reproducible.

The expanded plots of the deformation region extending from 1700-1300 cm^{-1} for 0.25 and 0.50% KOH (wt.)/EUROPT-1 are shown in figures 6.14 and 6.15 respectively. The spectra were baseline corrected and smoothed to improve their appearance. These are shown in figures 6.16 and 6.17 respectively. The spectra showed none of the peaks expected in the region, as listed in table 6.1.

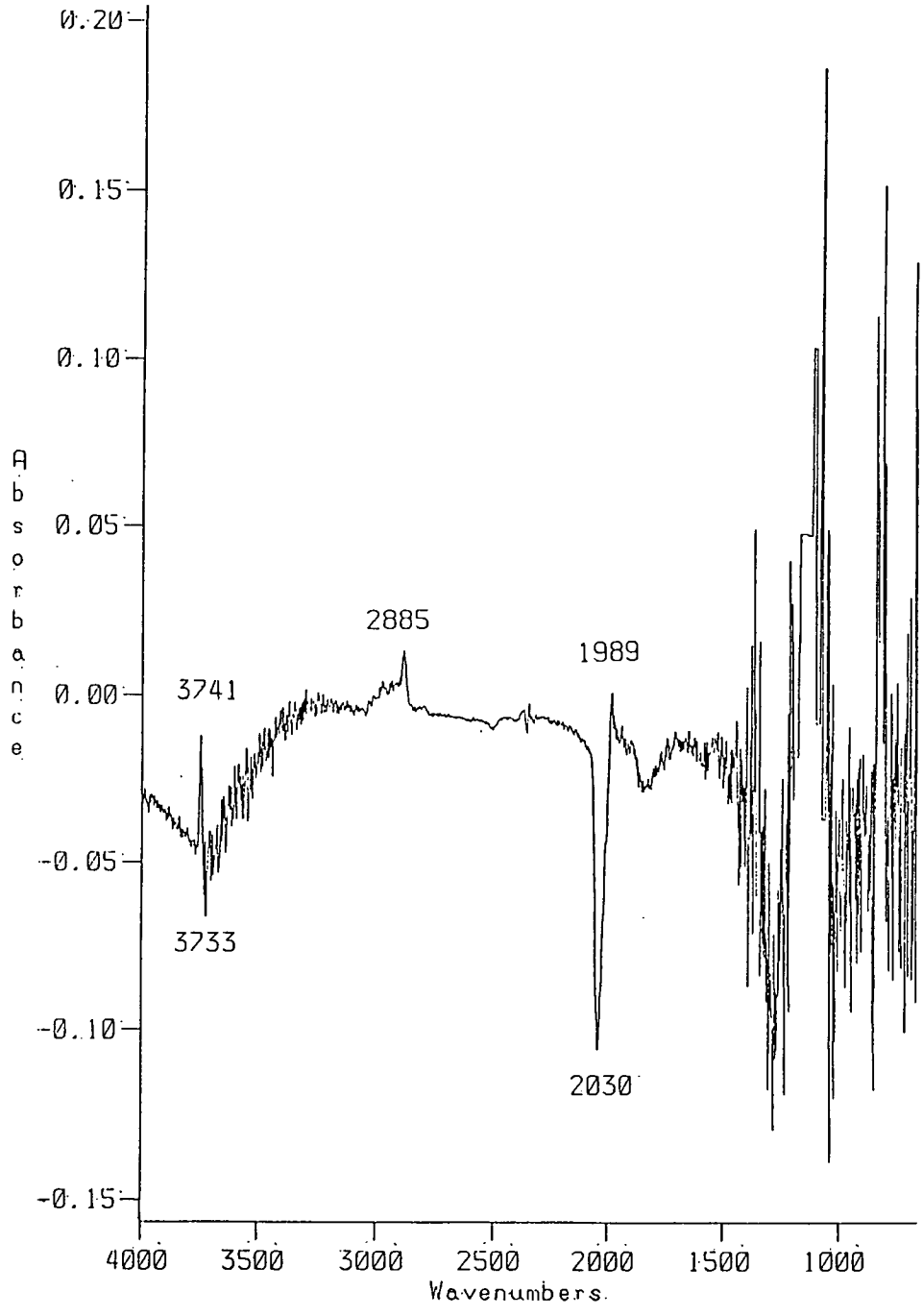

Fig. 6.8 A DRIFT Spectrum of Ethylene Adsorbed to Saturation on 0.25% KOH (wt)/EUROPT-1

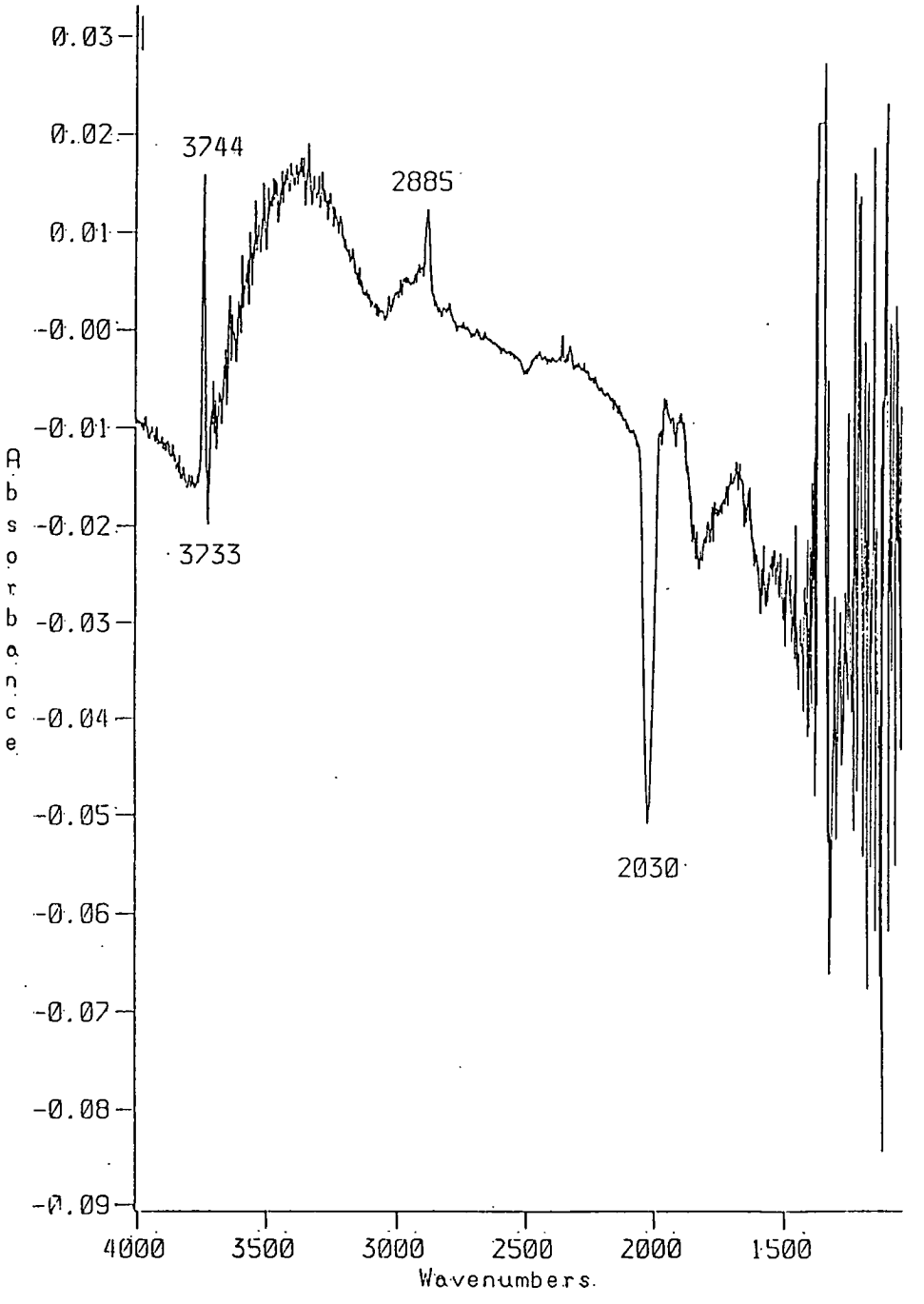

Fig. 6.9 A DRIFT Spectrum of Ethylene Adsorbed to Saturation on 0.5% KOH (wt)/EUROPT-1

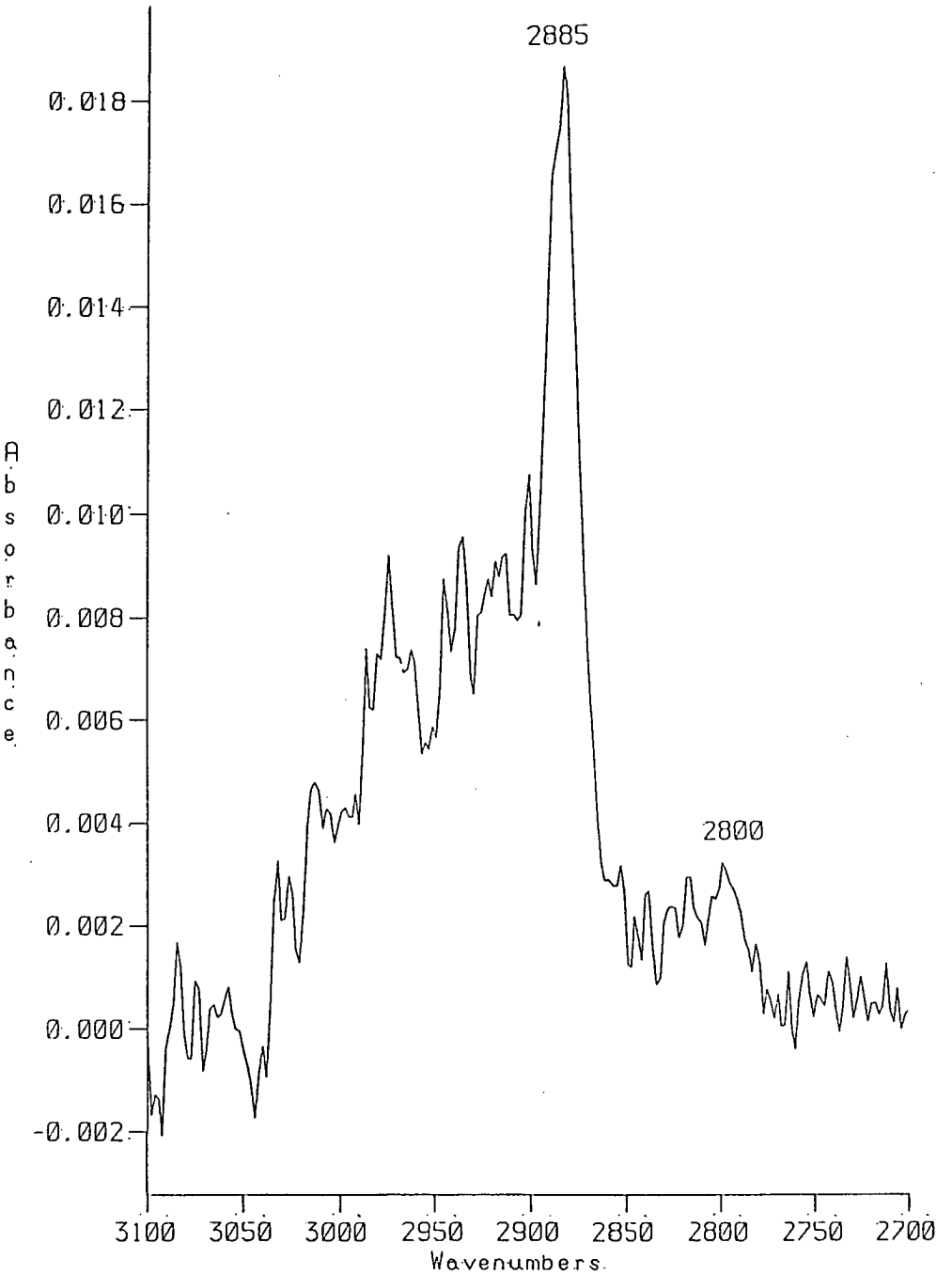

Fig. 6.10 Expanded Plot of the CH Stretch Region of Figure 6.8, i.e. ethylene adsorbed on 0.25 KOH doped catalyst

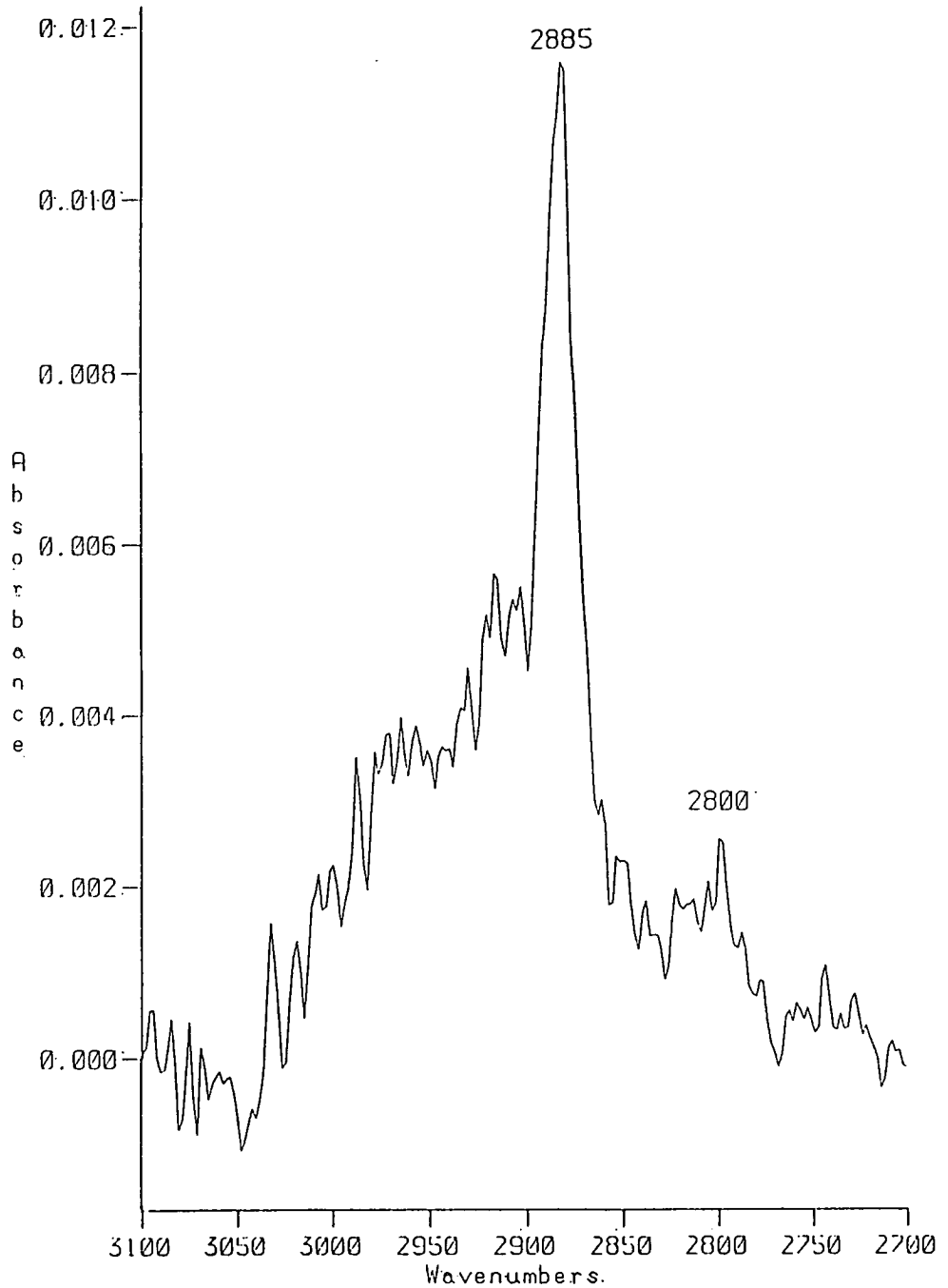

Fig. 6.11 Baseline Corrected Plot of Figure 6.9, i.e. ethylene adsorbed on 0.5% KOH (wt)/EUROPT-1

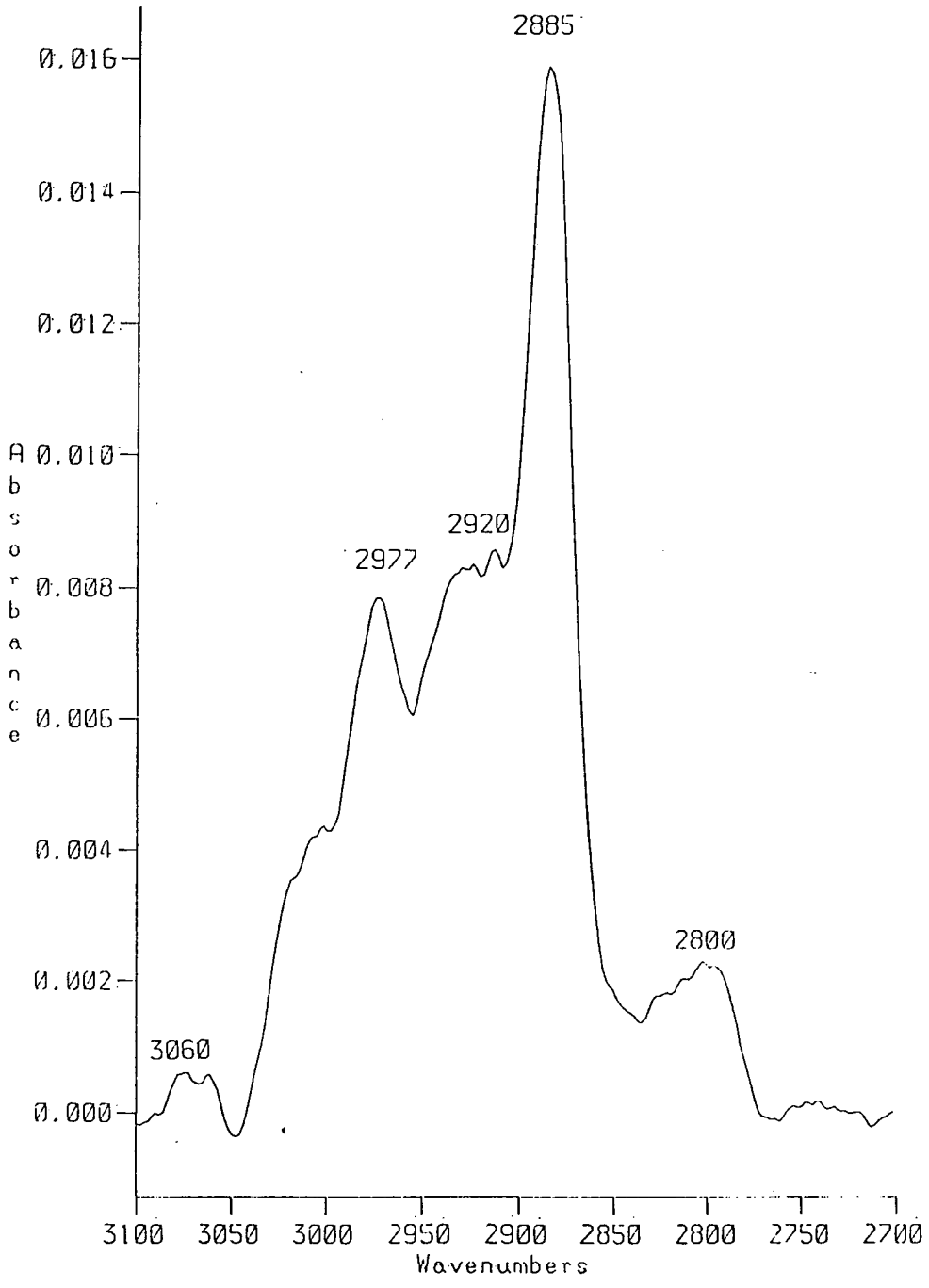

Fig. 6.12 **Baseline Corrected Smoothed Plot of the CH Stretch Region of Figure 6.10. i.e. ethylene adsorbed on 0.25% KOH (wt)/ EUROPT-1**

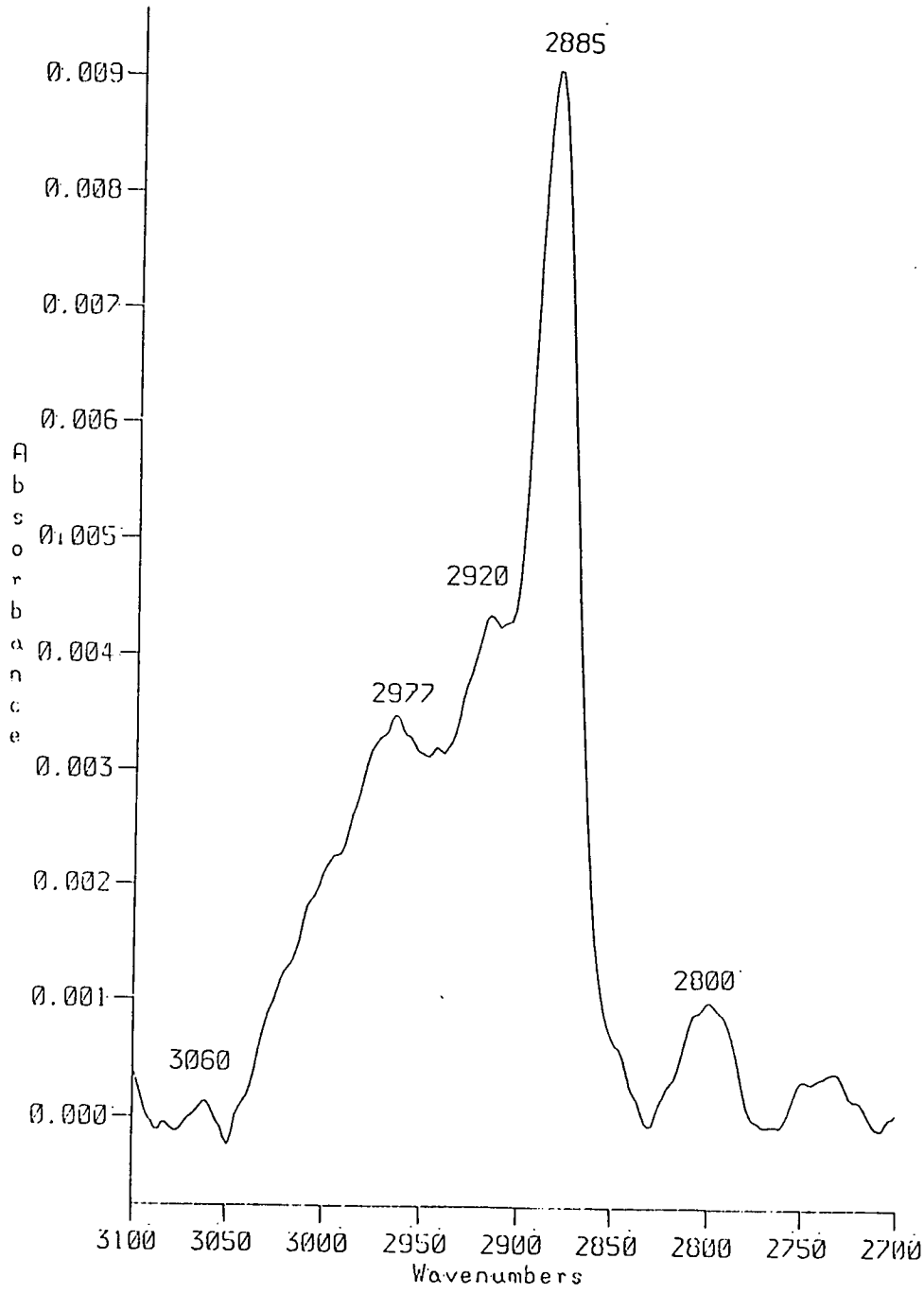

Fig. 6.13 Baseline Corrected Smoothed Plot of the CH Stretch Region of Figure 6.11, i.e. ethylene adsorbed on 0.5% KOH (wt)/EUROPT-1

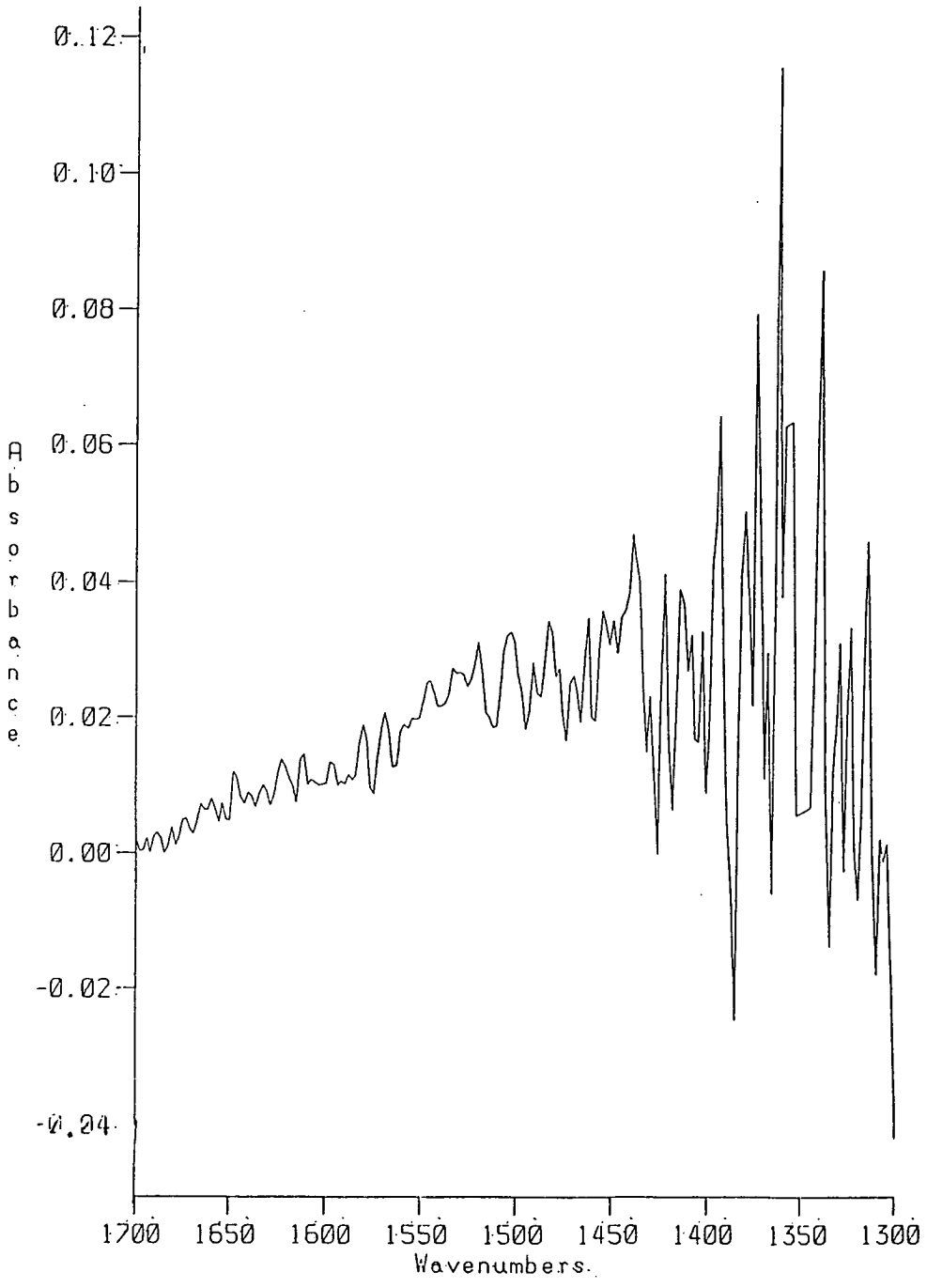

Fig. 6.14 Expanded Plot of the Deformation Region of Figure 6.8 , i.e. ethylene adsorbed on 0.25% KOH (wt)/EUROPT-1

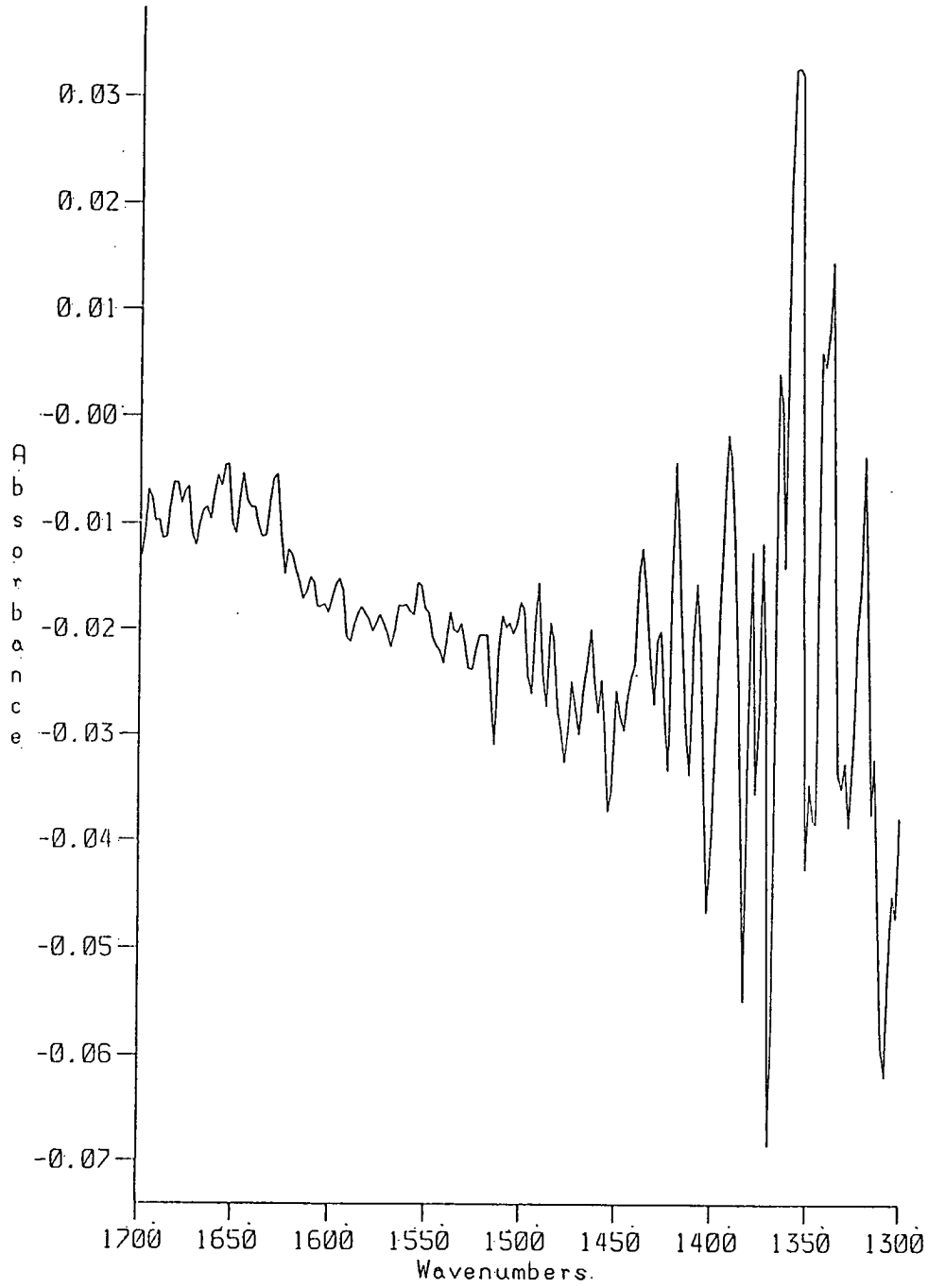

Fig. 6.15 Expanded Plot of the Deformation Region of Figure 6.9, i.e. ethylene adsorbed on 0.5% KOH (wt)/EUROPT-1

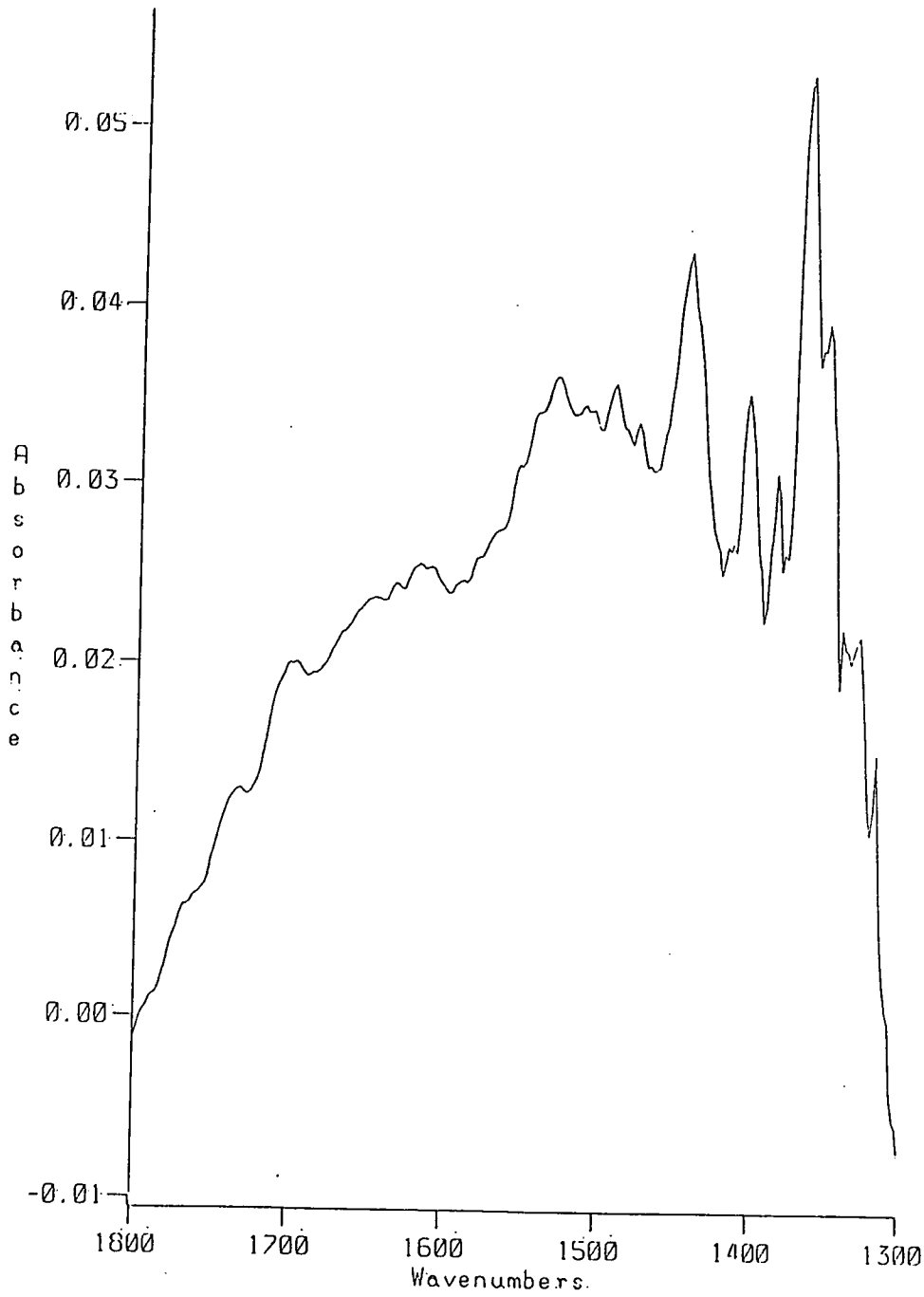

Fig. 6.16 Baseline Corrected Smoothed Plot of Figure 6.14 , i.e. ethylene adsorbed on 0.25% KOH (wt)/EUROPT-1

Table 6.1

$CH_3CCO_3(CO)_9$[a]	assignment	symmetry	$K[PtCl_3(C_2H_4)]$[b]	assignment	symmetry	ethylidyne[c] on Pt(111)	ethylene adsorbed on EUROPT-1	1%KOH/EUROPT-1
			3094 (VW)	$V_{as}CH_3$	A_2			
			3079 (VW)	$V_{as}CH_2$	B_2			
			3013 (VW)	V_sCH_2	A_1		3016	3016
			2983 (VW)	V_sCH_2	B_1			
							2970	
2930 (m)	$V_{as}CH_3$	E				2950 (W)	2920(W)	2920(W)
2888 (m)	V_sCH_3	A_1				2890 (m)	2885 (m)	2885 (m)
2840 (W)	$2\delta_{as}CH_3$	E					2800 (W)	2800 (W)
2822 (W)	$2\delta_{as}CH_3$	A_1						
			1500 (VW)	V_{CC}/δ_sCH_2	A_1			
1420 (m)	$\delta_{as}CH_3$	E	1426-1416(VS)	δ_sCH_2	B_1			
1356 (m)	δ_sCH_3	A_1				1350 (s)	1342[c]	

Table 6.1 A comparison of the Vibrational Frequencies of the Ethylidyne Ligand, Surface Ethylidyne and π-Complexed Ethylene with Typical Frequencies from Ethylene Adsorbed on 'as-received' and Alkali Doped EUROPT-1

a-[34], b-J. Hiraishi, *Spectrochim.Acta* 25 (1969) 749.,
c-observed in ref [8] but not in this study, see text.

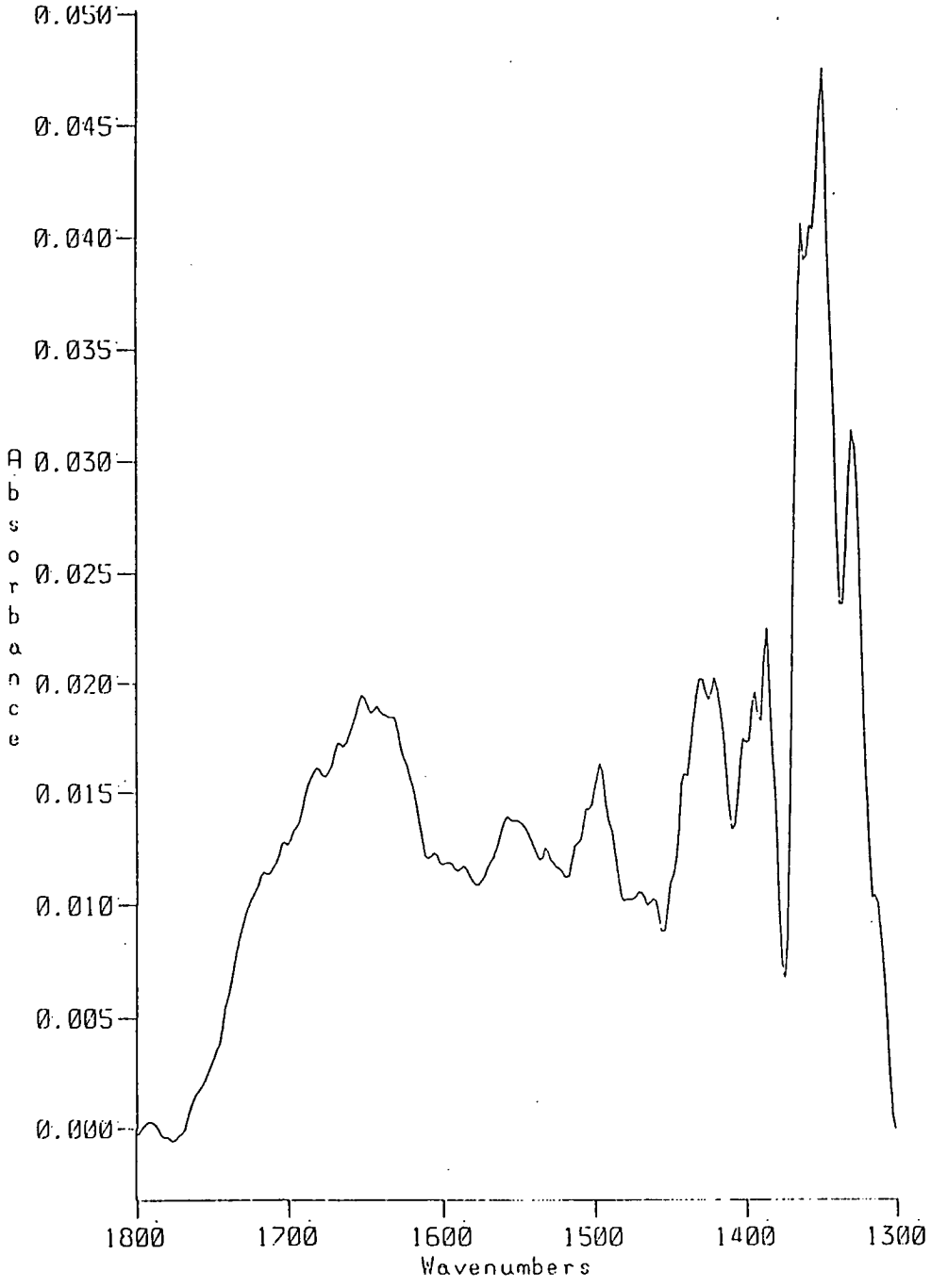

Fig. 6.17 Baseline Corrected Smoothed Plot of Figure 6.15, i.e. ethylene adsorbed on 0.5% KOH (wt)/EUROPT-1

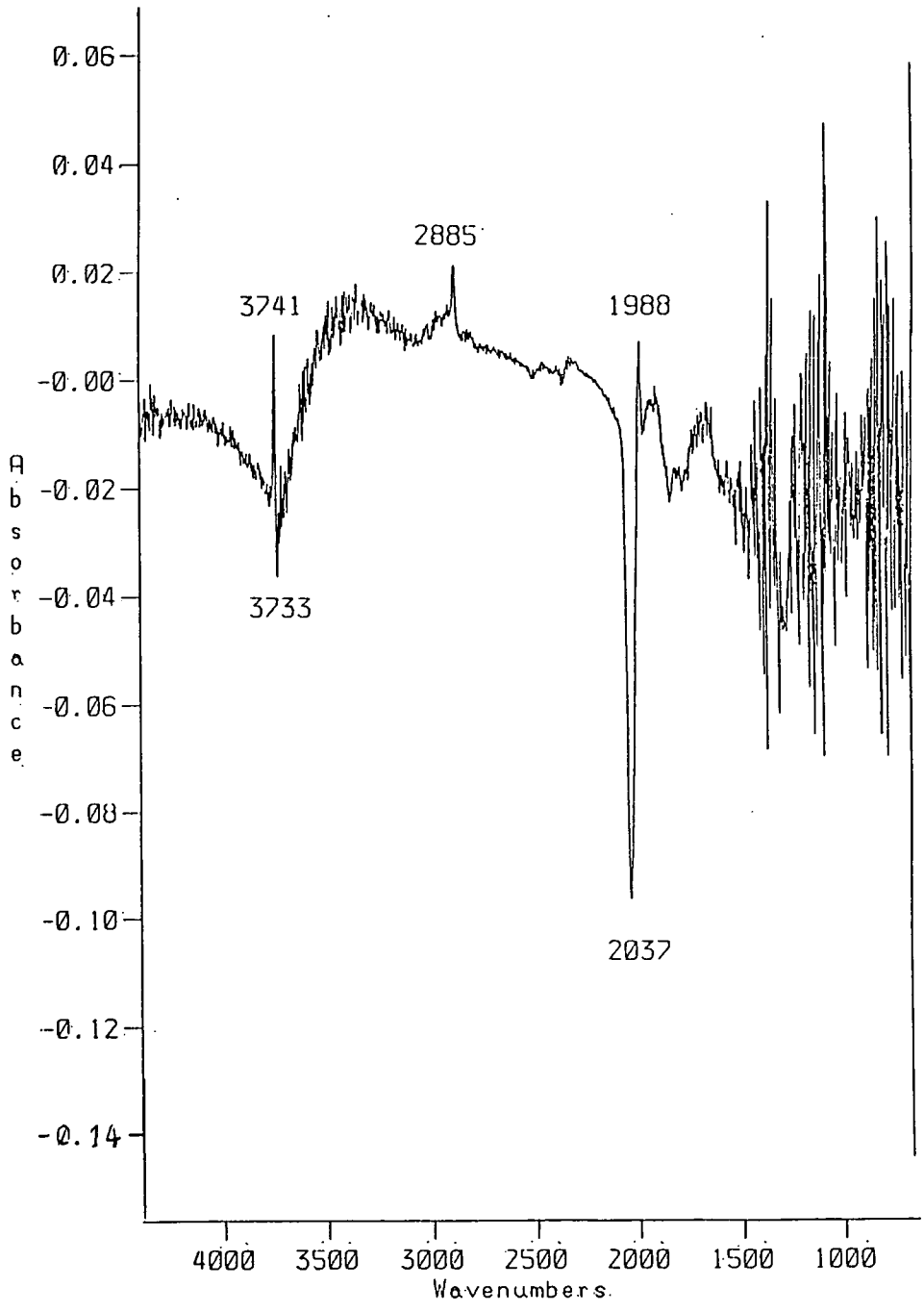

Fig. 6.18 A DRIFT Spectrum of Ethylene Adsorbed to Saturation on 1% KOH (wt)/EUROPT-1

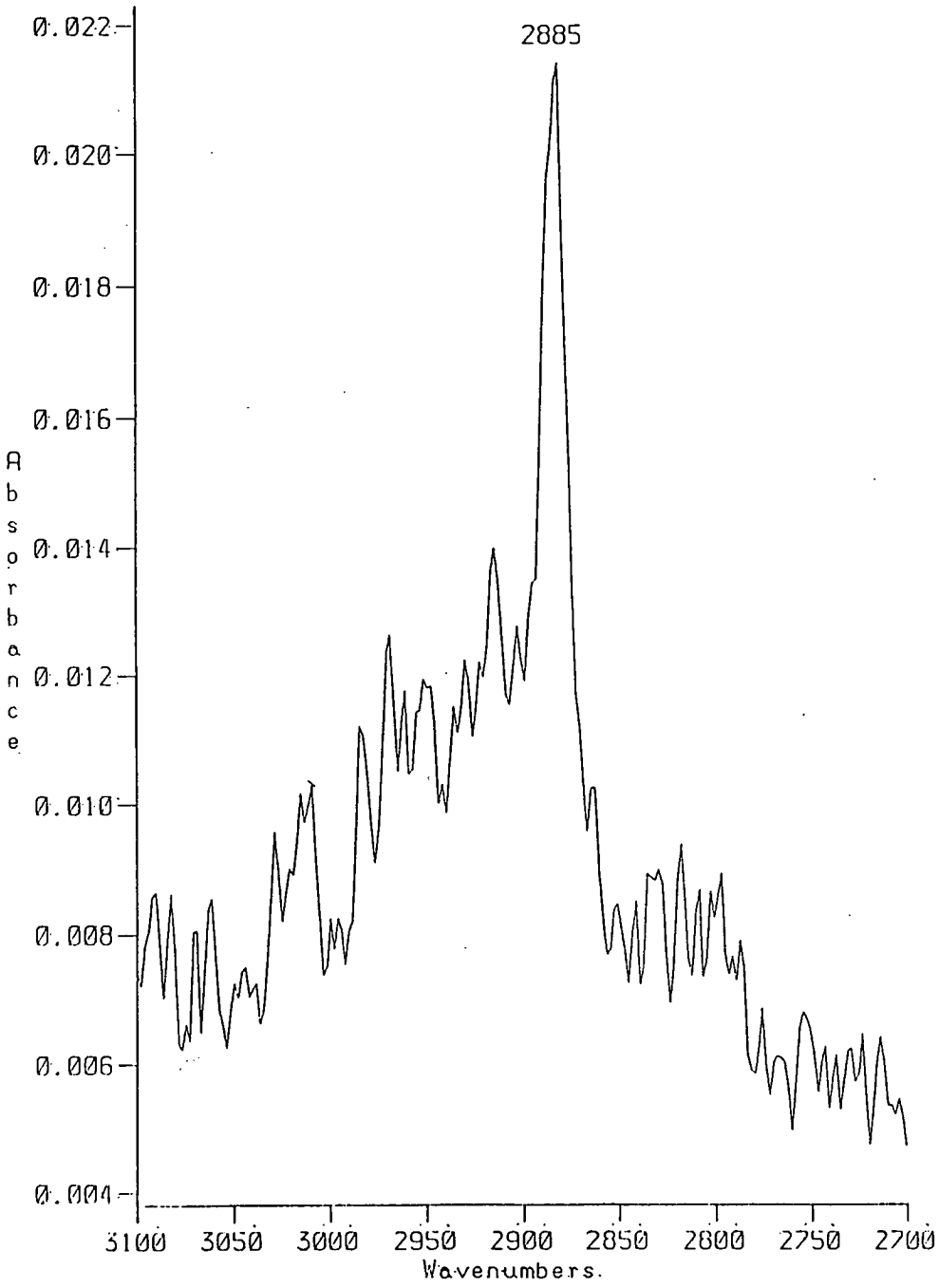

Fig. 6.19 Expanded Plot of the CH Stretch Region of Figure 6.18, i.e. ethylene adsorbed on 1% KOH (wt)/EUROPT-1

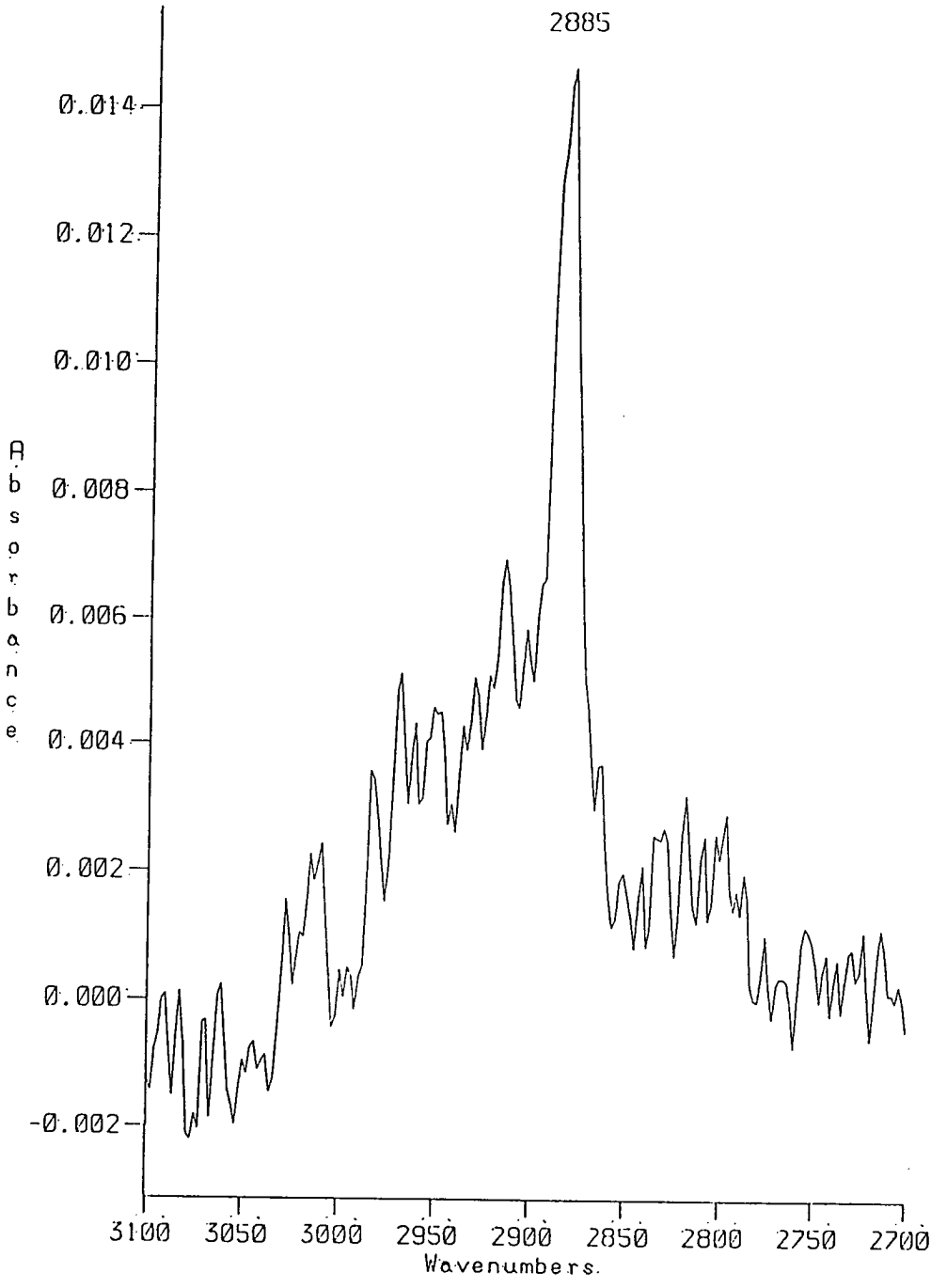

Fig. 6.20 Expanded Plot of the CH Stretch Region of Figure 6.18, i.e. ethylene adsorbed on 1% KOH (wt)/EUROPT-1

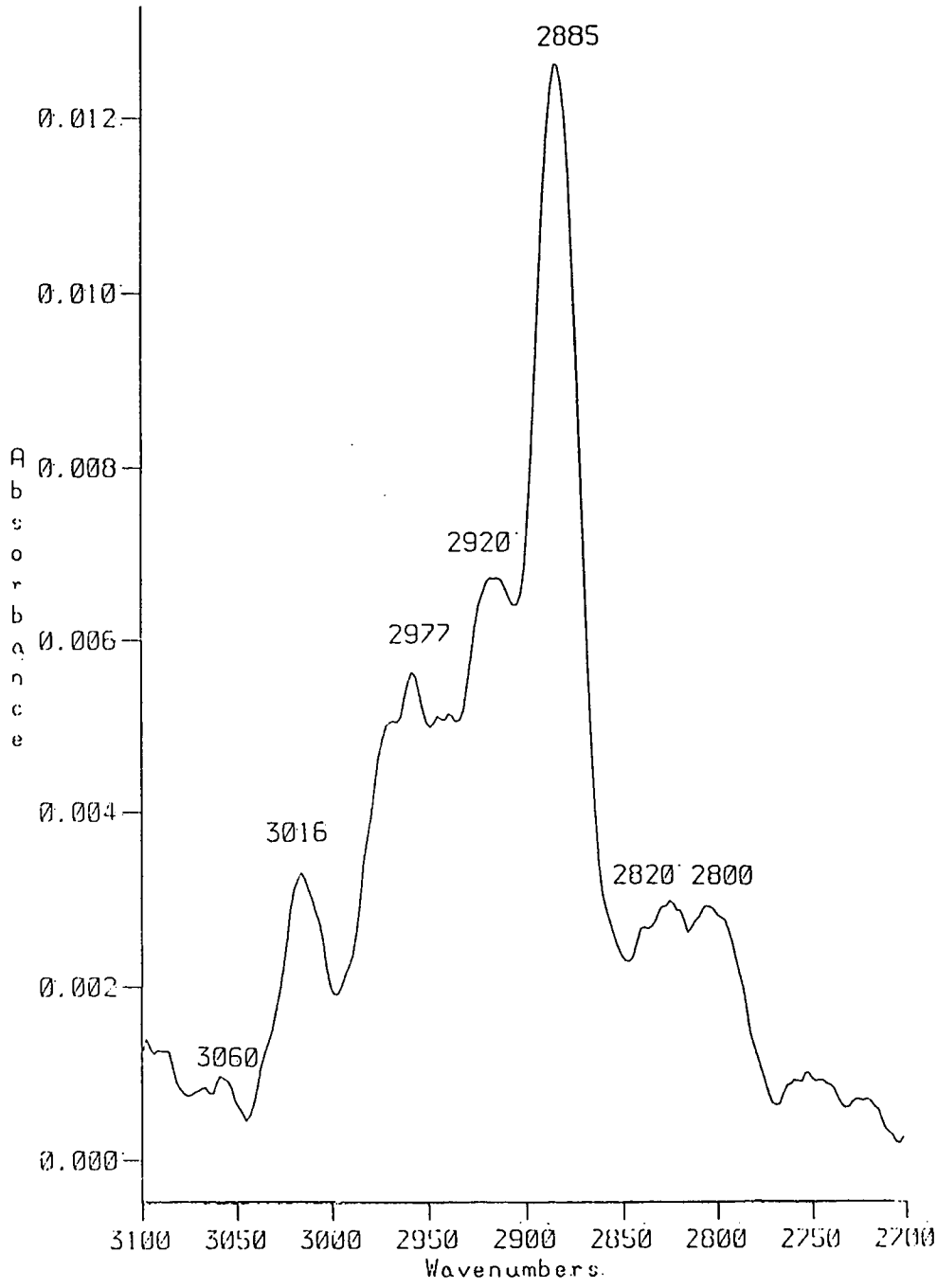

Fig. 6.21 Smoothed Plot of CH Stretch Region of Figure 6.20 i.e. ethylene adsorbed on 1% KOH (wt)/EUROPT-1

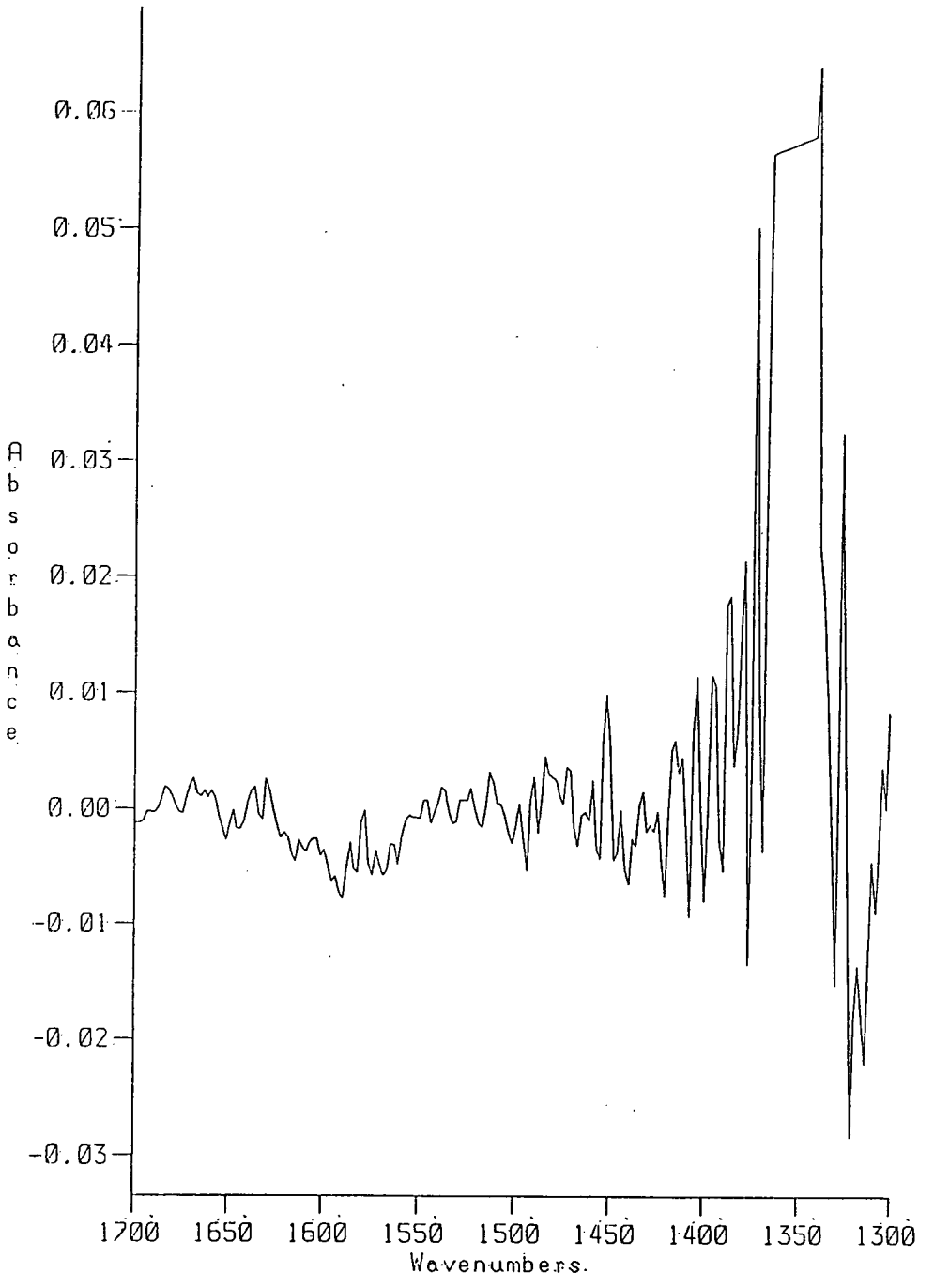

Fig. 6.22 Expanded Plot of the CH Deformation Region of Figure 6.18 , i.e. ethylene adsorbed on 1% KOH (wt)/EUROPT-1

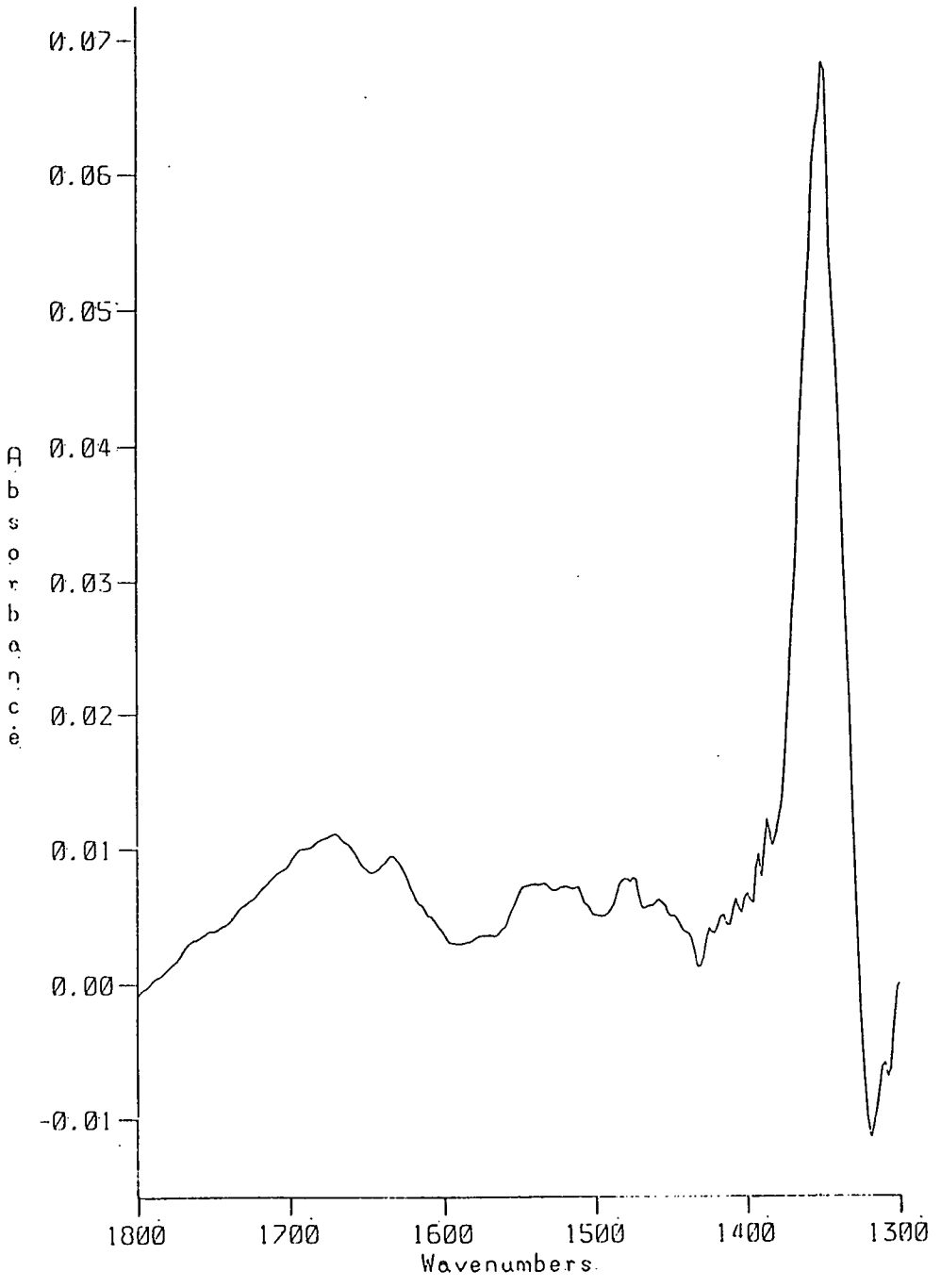

Fig. 6.23 Baseline Corrected Smoothed Plot of Figure 6.22 i.e. ethylene adsorbed on 1% KOH (wt)/EUROPT-1

The complete spectrum of ethylene adsorbed on 1% KOH (wt.)/EUROPT-1 is shown in figure 6.18. The overall spectrum is generally very similar to the spectra previously observed for the other catalysts.

Figure 6.19 shows the expanded spectrum of figure 6.18 extending from 3100-2700 cm^{-1}. The most prominent peak is at 2885 cm^{-1}. The other peaks as listed in table 6.1 are at 2800, 2822, 2825, 2922 cm^{-1}, a broad peak centred at 2977, a clear peak at 3016 cm^{-1} (and a small peak of low intensity at 3064 cm^{-1}). The baseline correction improved the appearance of the spectrum shown in figure 6.20. This was then smoothed and is shown in figure 6.21. The smoothed spectrum shows a broad profile in the region 2970-2900 cm^{-1}. This broad peak may suggest the superposition of a number of peaks giving a maxima at 2970 cm^{-1}.

The deformation region of the spectrum of C_2H_4/1% KOH (wt.)/EUROPT-1 is shown in figure 6.22 for the region extending from 1700-1300 cm^{-1}. After baseline correction and smoothing, the spectrum is shown in figure 6.23. Again the silica blackout region obscures any peak, because of the low S/N ratio of the spectrum.

6.4 DISCUSSION

The 'DRIFTS' results of ethylene adsorption on EUROPT-1 were compared with the transmission infrared work carried out by McDougall[8]. The comparative spectra are

shown in figure 6.24. It is observed that the quality of spectra obtained by transmission spectroscopy is better than those obtained by 'DRIFTS'. This is attributed to the high S/N ratio in transmission spectroscopy. In 'DRIFTS' the effect of the silica absorption goes beyond 1300 cm^{-1}, thus swamping the CH_3 δ(sym) vibration at 1346 cm^{-1}.

The C-H stretch region of the spectrum for C_2H_4 adsorbed on 'as-received' EUROPT-1 at room temperature shows a total of four peaks (fig. 6.4). In the deformation region, as already stated in the results section, the assignment of any peak was impossible because of the low S/N ratio. The frequencies in the C-H stretch region are however consistent with those expected for ethylene adsorbed on Pt/SiO_2 catalysts reported in the literature and listed in table 6.1. This suggests that EUROPT-1, for adsorption of ethylene behaves in a similar way to the previously studied supported Pt catalysts[1,8-10].

Although there are only four clear maxima as shown in figure 6.4 (smoothed spectrum), the number of vibrations may be higher. The same spectrum before smoothing and baseline correction indicates some features in the region 2900-2970 cm^{-1}, suggesting superposition of peaks giving two maxima at 2917 and 2970 cm^{-1}.

The bands at 2800 and 2885 cm^{-1} may be attributable to a surface ethylidyne species. These assignments are

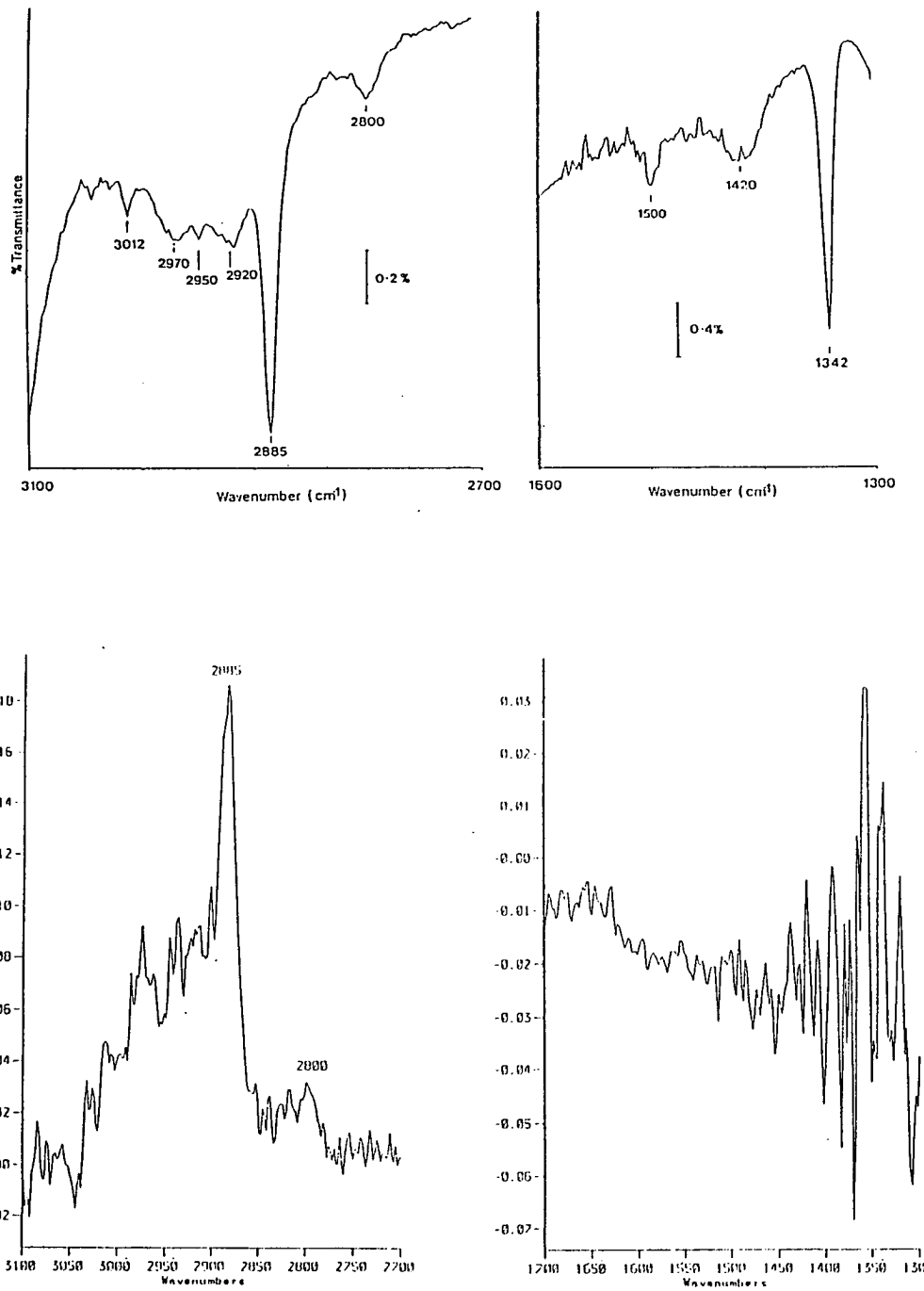

Fig. 6.24 A Comparison of Two Spectral Regions in

(a) a Transmission Infra-red Spectrum (Reference 8), and

(b) a Diffuse Reflectance Infra-red Spectrum (from the present study)

supported by a great deal of evidence available in the literature. Ibach and Lehwald[14] suggested the presence of a methyl-containing species CH_3CH at room temperature, based on their EELS study on a Pt(111) single crystal. Demuth[33] carried out TPD of ethylene from a Pt(111) single crystal and suggested the formation of C_2H_3 species. Recently a review by Skinner *et al.*[34], showed a comparison of the EELS and IR spectra of the model compound $(CH_3C)Co_3(CO)_9$. An excellent agreement between frequencies, intensities and the assignment of modes of the separately obtained EELS and IR data suggested that ethylidyne is the most likely surface species.

The peak at 2885 cm^{-1} can be assigned to the symmetric νCH_3 vibration and 2800 cm^{-1} is assigned to 2 x δCH_3, an overtone from the deformation at about 1400 cm^{-1}. This is supported by the evidence available from the recent reflection/absorption infrared spectra (RAIRS) on Pt(111) single crystals[35]. Similar assignments have been reported by McDougall[8], for ethylene adsorption on EUROPT-1 at room temperature.

The modes in the region 2970-2900 cm^{-1}, i.e. peaks at 2917 and 2970 cm^{-1} may contain contributions from the asymmetric C-H stretching vibrations of ethylidyne[8]. Peaks at 2917 cm^{-1} can be assigned to di-σ adsorbed species on the surface. The earlier study of ethylene adsorption on a Pt(111) single crystal by Ibach and Lehwald[14] showed that at low temperature (< 250 K) the

spectrum indicated the presence of di-σ bonded species. The EELS study confirmed that the low temperature species was converted at room temperature identified, as ethylidyne[21,34]. The assignment suggested in the present study can be strongly supported by the observations of Sheppard *et al.*[36], who studied adsorption of ethylene on Pt/SiO_2, both at low and room temperature. At low temperature two adjacent peaks were observed at 2906 and 2922 cm^{-1}. Upon warming to room temperature these peaks were replaced by peaks at 2887 and 2795 cm^{-1} which are attributable to ethylidyne species. The ethylene adsorption at room temperature showed peaks at 2922 and 1428 cm^{-1} in the deformation region. These were assigned to $\nu(CH_2$ sym.) and δCH_2 sym. modes of the di-σ species, as reported earlier by Prentice *et al.*[9]. In the present study peaks in the deformation region (at 1428 cm^{-1}) are not observed because of the reasons already explained. However there is an excellent agreement of the assignments and peaks with the reported literature for Pt/SiO_2 and EUROPT-1 (ethylene adsorption at room temperature)[8,36], listed in table 6.1.

In the present study the broad peak centred at 2977 cm^{-1} remains unassigned. In this region of the spectrum (2900-3000 cm^{-1}), superposition of a number of peaks showing more than one maximum has been reported earlier for ethylene adsorption on EUROPT-1 at room temperature[8]. A peak at 2958 cm^{-1} has also been reported by Sheppard *et*

al.[36].

In figures 6.10-6.11 very weak bands in the region 3010- 3020 cm^{-1} are observed. Weak features in this region can be assigned to the presence of π adsorbed species. Sheppard[38] observed a peak at 3016 and the related peak in the deformation region at 1496 cm^{-1}, when ethylene was adsorbed on the Pt/SiO_2 at room temperature. A peak at 3015 cm^{-1} attributed to π adsorbed ethylene has also been reported by McDougall[8] on EUROPT-1 at room temperature. A great deal of evidence in the literature shows a fairly generally agreement that absorption bands at 3016 and 1496 cm^{-1} arise from the presence of π-adsorbed species[9,16]. Present results are in good agreement with the vibrational frequencies of the surface species shown by the pattern of analogous, fully symmetrical infrared absorptions for the authentic π-complexed ethylene ligand in 'Zeise's' salt (table 6.1).

Although low alkali coverages (0.25 and 0.5% KOH) there is little observable intensity in the region 3010-3020 cm^{-1}. At higher alkali loading (1% KOH) the peak at 3016 cm^{-1} becomes a prominent feature in the spectrum, which we attribute to π adsorbed ethylene. The prominence of this peak which could be due to potassium induced effect, will be discussed later.

Another very weak peak at 3060 cm^{-1} is observed in all the catalysts. This was not previously observed on EUROPT-1[8]. This peak may be assigned to weakly held π

species.

Although there is little evidence available in the literature regarding the effect of coadsorbed potassium on the vibrational spectra of adsorbed ethylene on Pt/SiO_2 or other Pt catalysts, some analogies can be obtained from high resolution electron energy loss spectroscopy (HREELS) of coadsorption of ethylene and potassium on Pt(111)[29]. HREELS, temperature programmed desorption (TPD), and ultraviolet photoelectron spectroscopy (UPS) were combined to study the effect of preadsorbed potassium on adsorption of ethylene on a Pt(111) single crystal. Addition of potassium increased the relative amount of reversible ethylene adsorption at 100 K. The authors observed a new low temperature ethylene desorption state at 150 K. The authors attributed this new state to the formation of a weakly interacting ethylene species. The EELS results showed new loss peaks at 870, 1360, 1620 and 3060 cm^{-1}. The intensities of these peaks were reported to increase concomitantly with potassium coverage while the losses due to the di-σ bonded ethylene decreased. In the present study peak scan at 3060 cm^{-1} is always very weak and present in all the catalysts including 'as-received' EUROPT-1 catalyst. This may in fact represent a weakly held π-species, but its presence does not appear to vary with alkali in similar fashion to the K/Pt(111) system[29].

The more normal π-species at 3015 cm^{-1} does however appear to show changes in relative intensities that

correlate with alkali content.

A knowledge of ethylene adsorption on transition metals can help to understand the effect of coadsorption of alkali on ethylene adsorption. It is accepted that associative bonding of ethylene to a metal surface can take two forms, a π- or a di-σ complex[21-23]. The π state of ethylene adsorption can be explained in the terms of the Dewar, Chatt and Duncan model (DCD)[37-38]. This model depicts an interrelated co-existence of both, a σ donor interaction and a π acceptor interaction. The σ donor interaction involves a donation of charge from the filled ethylene π-orbital to a metal d-σ orbital. The π acceptor interaction involves a back donation of charge from the filled metal d π-orbital into the empty π^* orbital of ethylene. In this way adsorbed ethylene acts like a two electron σ donor but the π^* orbital also allows it to be a π acceptor[39]. The metal electronic structure plays an important role in explaining the importance of σ donor and π acceptor interactions. Substantial positive charge on the transition metal will favour the σ donor interaction. On the other hand the enhanced electron density on the transition metal surface favours a π acceptor interaction resulting in greater back bonding. Back bonding involves a transfer of charge from the metal d-orbital to the π^* orbital of ethylene. This results in a decrease in the C-C bond order and increases the rehybridisation of the carbon atoms leading to sp^3. In a π-complex, back bonding

has a relatively less important role and the sp^2 hybridization of ethylene is retained.

The π bond in ethylene breaks when the back bonding becomes extensive and the p-orbitals in each carbon atom forms σ bond to the metal atoms leading to the completion of sp^3 hybridization. This type of bonding has been referred to as a di σ bonding, and ethylene adsorption on Pt(111) single crystal at low temperature is a typical example of such a configuration[35].

The potassium induced changes on the adsorption of ethylene on a Pt(111) single crystal were carried out by Zhou *et al.*[30] using TPD, SIMS and $\Delta\Phi$ (work function changes). The authors observed work function changes similar to those previously observed by Windham *et al.*[29]. Insignificant work function changes were observed when ethylene was adsorbed on a K/Pt(111) single crystal. This indicated little or no charge transfer from C_2H_4 to the platinum surface. Thus decrease in work function (increased electron density due to potassium) inhibited the strong ethylene π-donation to the metal d-orbitals reducing the ethylene-Pt interaction and the formation of di-σ bonded ethylene. The work function data also explains the weak interactions of some other molecules such as benzene and ammonia on transition metals. The effect of alkali metal coadsorption on the adsorption properties of a σ-donor NH_3[40], and π-donor benzene[31] have been reported. In both cases a decrease in the activation

energy for desorption indicated weaker interactions.

The effect of potassium coadsorption on ethylene bonding is in contrast to the increased bonding strength of CO. The increased back donation due to enhanced electron density in the presence of potassium increases the bonding strength of Pt-C, discussed in detail in Chapter 3.

Further evidence supporting this explanation comes from the observation that coadsorption of electronegative atoms such as carbon and oxygen on single crystal surfaces decreases the ethylene chemisorption bond strength[29]. The effect of carbon and oxygen on ethylene bonding with transition metal surfaces is to withdraw electrons from the metal and hence reduce the availability of d-electrons for back donation to the adsorbed ethylene. Sheppard[41], proposed another possibility of the reduction in the number of adjacent two metal atom sites needed for the di-σ adsorption leading to a π bonding.

From the above mentioned explanations this can be concluded that, when ethylene is di σ-bonded there are no longer π or π^* molecular orbitals, and potassium coadsorption may not increase the back bonding. As described by Windham *et al.*[29], potassium actually decreases the bond strength of ethylene to potassium, and potassium acts as an inhibitor to the formation of a strong covalent bond between the carbon p-orbital and the metal d-orbital. The π bonded state of ethylene is

favoured by this inhibition.

6.5 CONCLUSION

In the spectrum of ethylene adsorbed on 1% KOH (wt)/EUROPT-1 catalyst π is a most prominent species. Even in 0.25% and 0.5%, relative intensity in this region is more pronounced than in EUROPT-1 catalyst. Thus it would appear that by alkali doping, EUROPT-1 catalysts may show similar trends in chemisorption behaviour to the single crystal system[29].

PART II

BENZENE ADSORPTION

6.6 INTRODUCTION

Benzene adsorption has been extensively studied by vibrational spectroscopy on metals, oxides and supported metals. Being an unsaturated hydrocarbon, benzene may undergo associative chemisorption, similar to olefins and diolefins. Spectroscopic studies have concluded that benzene chemisorbs molecularly on transition metal surfaces with its ring parallel to the surface plane, bonding to the surface through π-orbitals[42]. Vibrational spectroscopic studies of benzene chemisorbed on both single crystal[43-45] and supported metal surfaces[46] show that benzene is oriented with its ring plane parallel to the surface plane and is only weakly distorted from its gas phase molecular structure upon adsorption, indicating π-bonding.

The early studies of benzene adsorption on silica (Degussa Aerosil) were carried out by Galkin and associates[46]. In this work, changes in the infrared spectrum of benzene physisorbed on the silica support have been observed. These changes were interpreted in terms of the interaction of the π-electron system of the benzene molecule and the surface hydroxyl groups. Recently it has also been observed for benzene physisorbed on alumina and Pt/Al_2O_3 by Haaland[47]. Fourier transform infrared

spectroscopy was used. The authors observed that there was a loss in intensity of stretching vibrations of free hydroxyl groups at 3790, 3771 and 3731 cm^{-1}, with a corresponding large increase in the intensity of the perturbed or hydrogen bonded hydroxyl groups centred at 3620 cm^{-1}. This perturbation has also been reported by others for silica and alumina[46-51]. These changes in the spectra suggest that both on silica and alumina benzene interacts initially through the hydroxyl groups of the support materials.

The early studies of benzene chemisorption on metal surfaces were not very successful. Erkelens *et al.*[50] carried out infrared spectroscopic studies of benzene adsorption on silica supported metals. A broad band extending from 3060-2760 cm^{-1} with no clear features was observed for nickel and copper, while on iron and platinum this band was not observed at all. When adsorbed benzene was reacted with hydrogen for 16 hours, two bands at 2849 and 2928 cm^{-1} were observed, attributable to symmetric and asymmetric CH_2 vibrations respectively. A small band due to CH_3 vibrations was also observed. After evacuation the CH_2 bands disappeared, leaving the broad band extending from 3060-2760 cm^{-1} with decreased intensity. The formation of hexane, detected by the GLC, indicated a C-C bond cleavage. It was further reported that chemisorption on a clean palladium surface resulted in C-C bond cleavage. Chemisorption on platinum in the absence or

presence of hydrogen gave CH_2 bands, whose intensity increased with time.

Chemisorption of benzene on silica supported platinum was studied by Sheppard[51]. The authors reported a weak broad band around 3040 cm^{-1}. This band was attributed to aromatic C-H bonds.

The recent work of benzene absorption on Pt/Al_2O_3 at 300 K was performed by Haaland[47]. In the early part of the introduction, the physisorption phenomenon has been discussed in detail. It was demonstrated that benzene chemisorbs on Pt metal and physisorbs on the Al_2O_3 support. The sharp features due to benzene on Pt occurred at 3050, 1398, 1274, 1147 and 1042 cm^{-1}. Corresponding to vibrations of E_{1u} and B_{2u}, indicating that benzene after chemisorption is distorted to C_{3v} symmetry. Sheppard[41] has reported an undissociated benzene lying flat on the metal surface and proposed that if it is π-bonded to a smooth metal surface, then its gas phase symmetry of D_{6h} would be reduced to C_{6v}.

Chemisorption of benzene on various single crystal faces of platinum and nickel has been studied by high resolution electron energy loss spectroscopy[43-45], which shows a general agreement that benzene is π-bonded to the metal, with the plane of the molecule parallel to the metal surface.

Erkelens *et al.*[50] in their earlier work had concluded that benzene was chemisorbed due to loss of its aromatic

character and not due to π-bonding with the surface. Palazove[52] concluded that benzene did form a π complex. Primet *et al.*[53] also reported undissociated π bonding of benzene with the platinum metal. This conclusion was based on the observed decrease in vibrational frequencies of coadsorbed carbon monoxide.

Although benzene adsorption has been studied by a variety of methods such as flow reactor[54], radiotracer[55] and exchange reactions[56], these give mixed conclusions as reported by Wells *et al.*[57]. At present, the vibrational spectroscopic studies strongly suggest an associative π-bonded benzene on Pt and Ni metals and supported catalysts[47,58].

The promotional effect of alkali doping has long been known in heterogenous catalysis. In the previous chapters the alkali effect upon adsorption of carbon monoxide and hydrogen has been discussed in detail. In agreement with the literature, potassium was found to increase the CO bonding strength with platinum, and also a decrease in the CO stretching frequencies were observed. The weakening of the carbon-oxygen bond can be explained in terms of potassium induced enhancement of electron back donation from Pt to the 2π orbital of CO with simultaneous strengthening of the Pt-C bond.

Recently, benzene interaction with coadsorbed potassium on a Pt(111) single crystal has been studied by Garfunkel *et al.*[31]. The main technique used was thermal

desorption spectroscopy. It was observed that coadsorbed potassium significantly weakened the platinum-benzene bond. Most of the benzene was desorbed upon heating, indicating the low activity of a Pt(111) single crystal for C-C or C-H bond fission. The authors observed that more of the benzene desorbed upon heating when the Pt surface was predosed with potassium, as well as lower temperature desorption. Both effects indicate weakening of the benzene- Pt bond in the presence of potassium. Benzene is an electron donor in transition metal complexes, with the π-orbital involved in a symmetric coordination with the metal atom or ion[59]. If platinum metal is already electron rich due to electropositive potassium (which donates its charge to the Pt surface), the benzene may not be able to donate its charge and will be weakly bonded. The details of the potassium induced effect in terms of the lowering of work function and changes in backbonding have been explained in the previous section of ethylene adsorption studies.

In summary the previous infrared studies of benzene adsorbed on Pt/SiO_2 related work on Pt/Al_2O_3, and Pt(111) single crystal, suggest that a typical spectrum of adsorbed benzene would show well defined peaks (table 6.2) at *ca.* 3100-3000 cm^{-1}. There are also a number of unrelated peaks (other than hydrocarbons). This has been reported in the previous literature[47].

'DRIFTS' studies were carried out in an attempt to

understand the interaction of benzene with 'as-received' and alkali doped EUROPT-1.

6.7 RESULTS

A complete spectrum of benzene vapour at room temperature is shown in figure 6.25. The spectrum extended from 4000-650 cm^{-1} and was recorded at 4 cm^{-1} resolution. The spectrum is the ratio of single beam spectra of KBr powder in the DRIFTS cell with and without 2.5 torr of benzene.

The spectrum in figure 6.26 extending from 4000-650 cm^{-1} shows benzene adsorbed on the silica support (sorbosil) at room temperature. The spectrum is the ratio of single beam spectra recorded before and after treatment of the silica support by exposure to 2.5 torr of benzene followed by evacuation. The spectrum shows a number of features in addition to adsorbed hydrocarbons. An intense sharp peak in the spectrum at 3740 cm^{-1} is prominent. This peak is due to the free hydroxyl groups of silica support. In the literature this peak is reported to appear around 3750 cm^{-1}[32]. A huge broad band extending from 3550-3100 cm^{-1} is due to ice on the MCT detector. This detector is cooled by liquid nitrogen. During the expansion of benzene vapours over the samples some water vapours or moisture is also introduced which is adsorbed on the silica. This causes a decrease in the number of hydrogen bonded hydroxyl groups, which is shown by a sharp

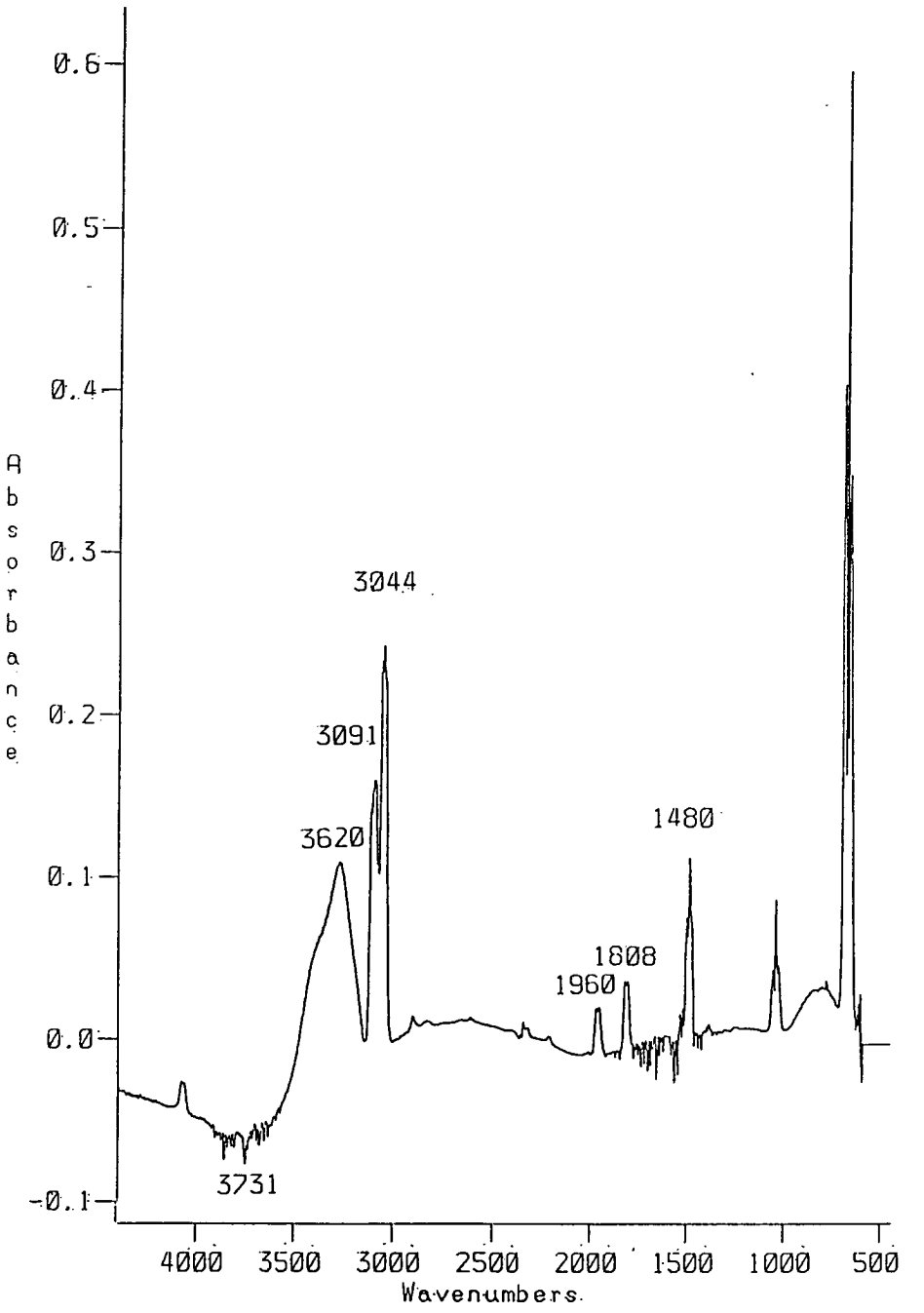

Fig. 6.25 DRIFT Spectrum of Benzene Vapours

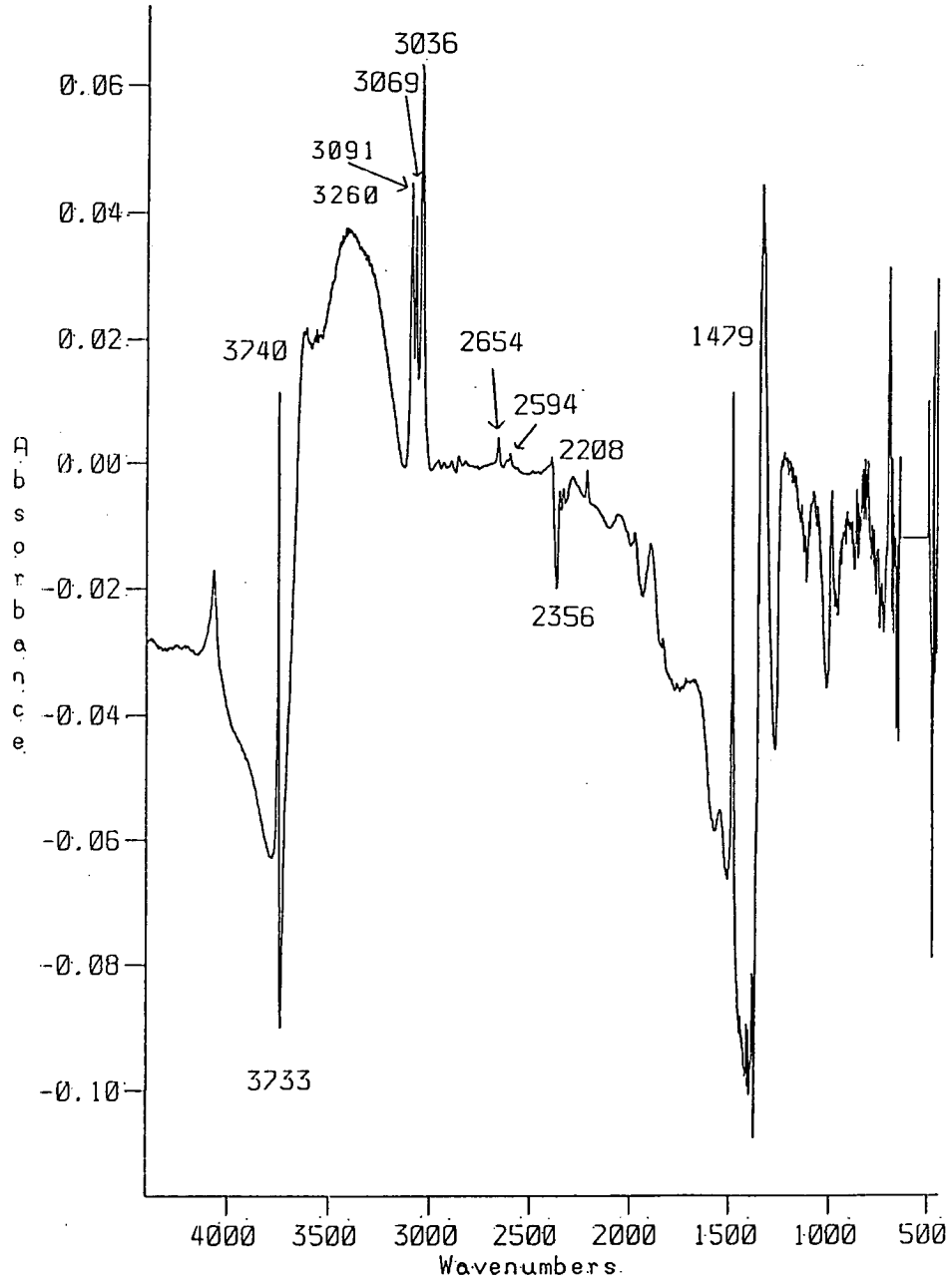

Fig. 6.26 DRIFT Spectrum of Benzene Adsorbed on Silica Support

negative peak centred at 3733 cm^{-1}, and also contribute to the 3500-3100 band. The slope of the spectrum is a common instrumental artefact and has also been observed earlier by others[8]. Some other non-hydrocarbon features in the region 2500-2350 cm^{-1} are caused by the miscancellation of atmospheric carbon dioxide.

Figure 6.27 shows a complete spectrum of benzene adsorbed on 'as-received' EUROPT-1. The appearance of the spectrum is similar to that observed for benzene adsorbed on the silica support. A similar spectrum is obtained when benzene is adsorbed on 1% KOH (wt.)/EUROPT-1 as shown in figure 6.28.

The expanded plot of the spectrum of benzene vapour, for the region 3200-2700 cm^{-1} is shown in figure 6.29. The spectrum is baseline corrected. The peaks due to vapour phase benzene are at 3014, 3044, 3053, 3073, 3091 and a shoulder at 3107 cm^{-1}. Detailed assignments are given in the table 6.2.

The expanded spectrum of benzene adsorbed on silica is shown in figure 6.30. A total of three peaks in the C-H stretch region are observed at 3037, 3069 and 3091 cm^{-1}. Three small peaks can be seen at 2853, 2895 and 2923 cm^{-1} and may be attributable to impurities present in the sample, as these do not coincide with any of expected overtones or combinations bands.

The spectrum for benzene adsorbed on EUROPT-1 is shown in figure 6.31 (in the region 3200-2700 cm^{-1}). In this

TABLE 6.2

Raman[a] cm^{-1}	Infrared[b] cm^{-1}	D_{6h} Symmetry	C_{3v}	Mode	Intensity	Physisorbed on Silica	C_{6v} Symmetry	Chemisorbed on Pt/SiO_2	Chemisorbed on 1%KOH(wt) $/Pt/SiO_2$	Chemisorbed[c] on Pt/Al_2O_3
3187		$A_1g.E_2g$	A_1							
3164		$A_1g.E_2g$	A_1							
	3092	E_1U	E	ν_{12}	S	3090	E_1	3108	3108	3050
	3072	E_1U	E	ν_{12}	W	3069	E_1			
3061		A_1g	A_1	ν_1			A_1	3053	3043	
3046		e_2g	E	ν_{15}			E_2			
	3045	E_1U	E	$\nu_{13}+\nu_{18}$	S	3036	E_1			
2948		$A_1g.E_2g$	A_1	$2\nu_{18}$			A_1E_2			
2925		E_2g	E	$\nu_8+\nu_{114}$			E_2			
	2886	E_1U	E	$\nu_8+\nu_{17}$	V.W		E_1			
						2950				
						2923				
						2887				
						2855				
						2820				
2618		E_2g	E			2594	E_2			
2543		$A_1g.E_2g$	A_1				A_1E_2			
2456		A_1g	A_1				A_1			
2293		A_1g	A_1				A_1			
	2288	E_1U	E	$\nu_{10}+\nu_{17}$		2282	E_1			
	1964	E_1U	E	$\nu_{11}+\nu_{19}$		1975	E_1			
	1906	A_2U	A_1	$\nu_{11}+\nu_{14}$		1895	A_1			
	1807	A_2U	A_1	$\nu_{18}+\nu_{19}$		1830	A_1			
1693		$A_1g.E_2g$	A_1				$A_1.E_2$			
	1669	A_2U	A_1	$\nu_2+\nu_4$	V.W		A_1			
	1617	A_2U	A_1	$\nu_{14}+\nu_{16}$	V.W		E_1			
1606										
						1546				
1584										
	1481	e_1U	E	ν_{13}	S	1479	E_1			
1478		e_1U	E				E_1			
1404		E_1g	E				E_1			
	1377	E_1U	E		W	1380	E_2			
1178	-	e_2g	E				E_2			
	1143	e_1U	E	ν_{7-20}	W		E_1			
	1037	e_1U	E	ν_{14}	S		E_1			
1030	-	e_1U	E				E_1			
999	?	?								
992		A_1g	A_1	ν_2			A_1			
	962									
984		-	-				-			
849		e_1g	E				E_1			
	793	A_2U	A_1	$\nu_{17}-\nu_{20}$	V.W		A_1			
	671	a_2U	A_1	ν_4	S		A_1			
848		e_1g	E							
685	-	-					E_1			
605	-	e_2g	E				E_2			

Table 6.3 Correlation Table for the Symmetries of the Point Group D_{6h} with those of the Sub-groups C_{6v} and C_{3v}

a - [61], b - C.E. Leberknight, *Phys.Rev.* 43 (1933) 967,
c - [47]

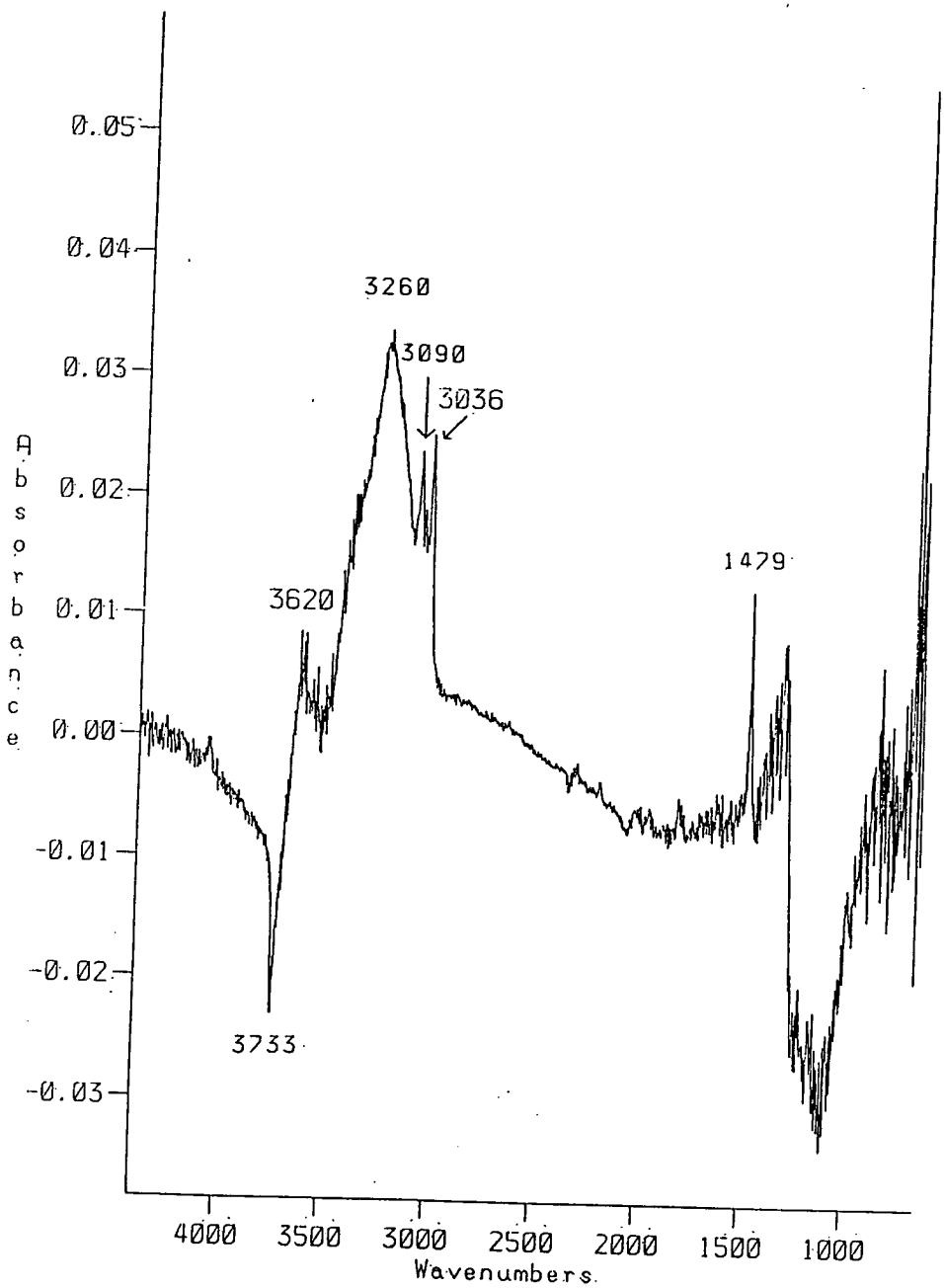

Fig. 6.27 DRIFT Spectrum of Benzene Adsorbed on EUROPT-1

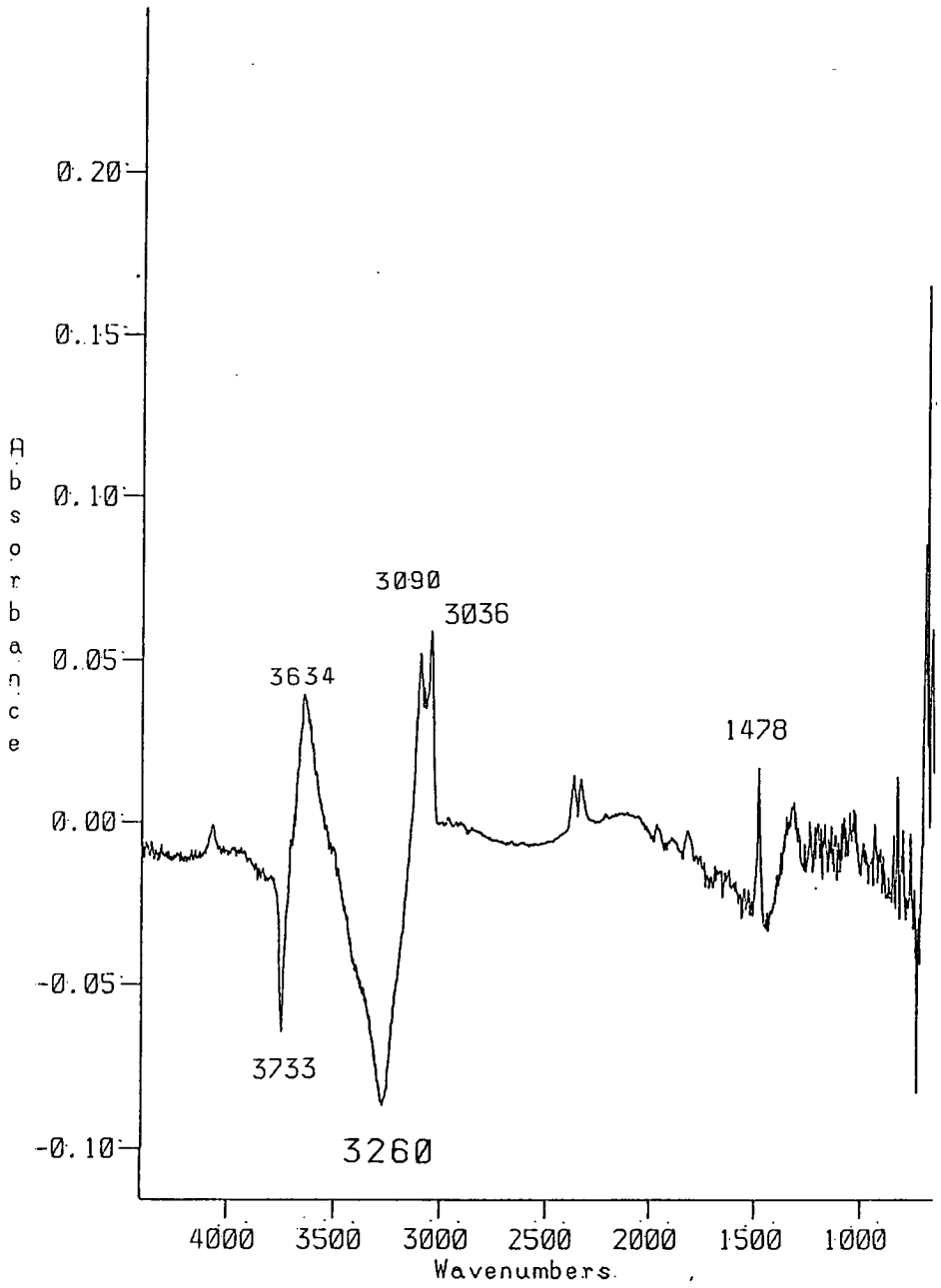

Fig. 6.28 DRIFT Spectrum of Benene Adsorbed on 1% KOH (wt)/EUROPT-1

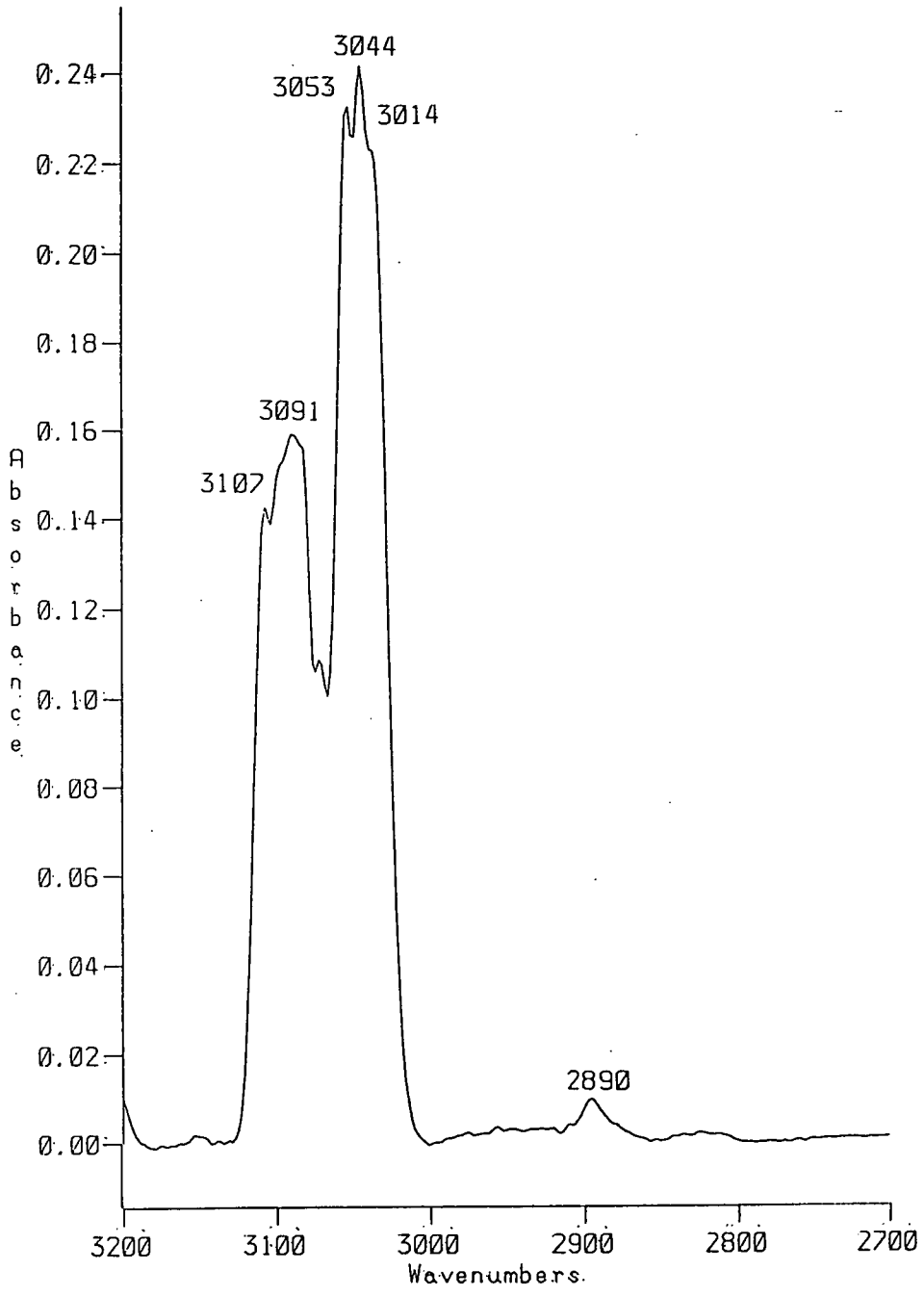

Fig. 6.29 Expanded Plot of the CH Stretch Region of Figure 6.25

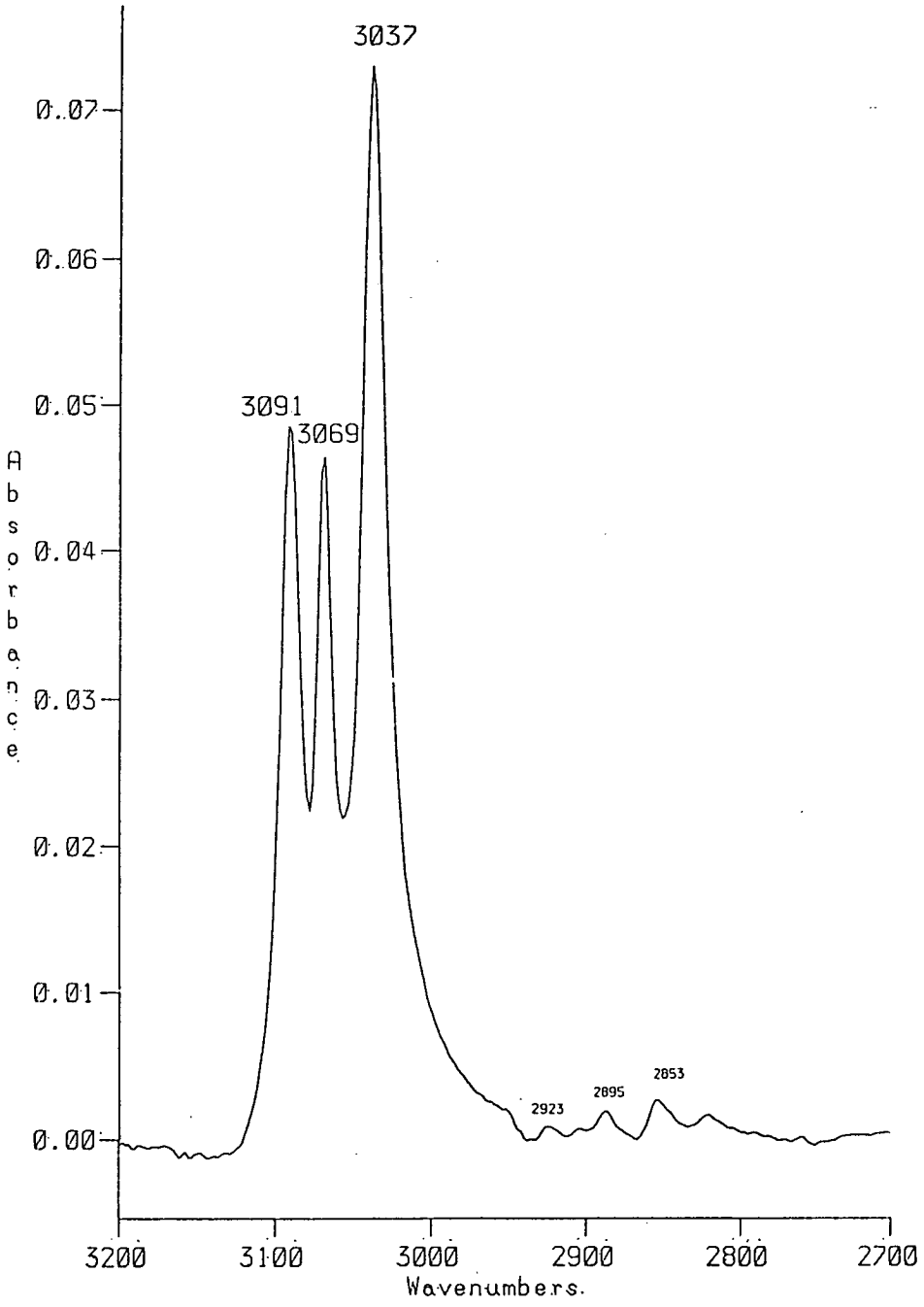

Fig. 6.30 Expanded Plot of the CH Stretch Region of Figure 6.26

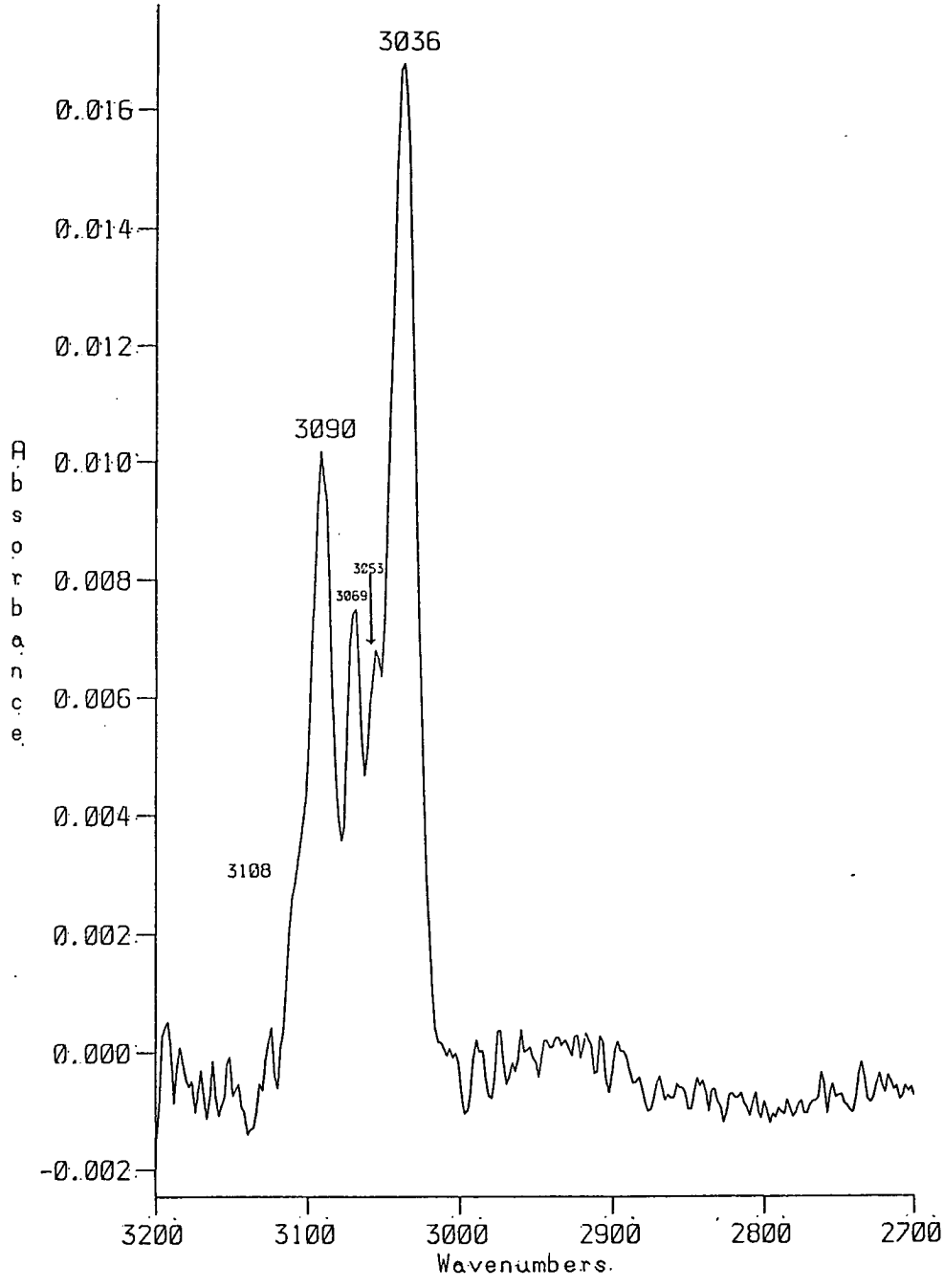

Fig. 6.31 **Expanded Plot of the CH Stretch Region of Figure 6.27, i.e. Benzene Adsorbed on 'as-received' EUROPT-1**

spectrum four distinct peaks are observed. These peaks occur at 3036, 3069 and 3090 cm^{-1} and a small peak or shoulder at 3053 cm^{-1} may be significant and attributable to benzene chemisorbed on EUROPT-1. A similar spectrum in figure 6.32 shows benzene adsorption on 1% KOH (wt.)/ EUROPT-1. The overall peak positions are unchanged but the absolute intensity is quite different compared to the 'as-received' EUROPT-1. Figure 6.33 a and b shows a comparison of the two spectra. Both spectra are very similar. Peak positions are essentially identical. Both spectra show some intensity near *ca.* 3108 cm^{-1}. The absolute and relative intensity in this region observed for 1% KOH (wt)/EUROPT-1 catalyst is significantly higher than those observed for 'as-received' EUROPT-1. Sharp blips in the region 2960-2800 cm^{-1} indicating the surface impurities are also observed.

Figure 6.34 shows an expansion of the plots of the spectrum for benzene vapours, in the region 2600-1400 cm^{-1}. This shows a number of sharp features corresponding very well to the spectrum of gas phase benzene. The most prominent peak in this region is at 1480 cm^{-1}. The expanded spectrum covering the region 1400-700 cm^{-1} is shown in figure 6.35. This shows a small peak at 772 cm^{-1} and a PQR type of peak centred at 1035 cm^{-1}.

Figure 6.36 shows an expanded plot of the spectrum of benzene adsorbed on the silica support in the region 2600-

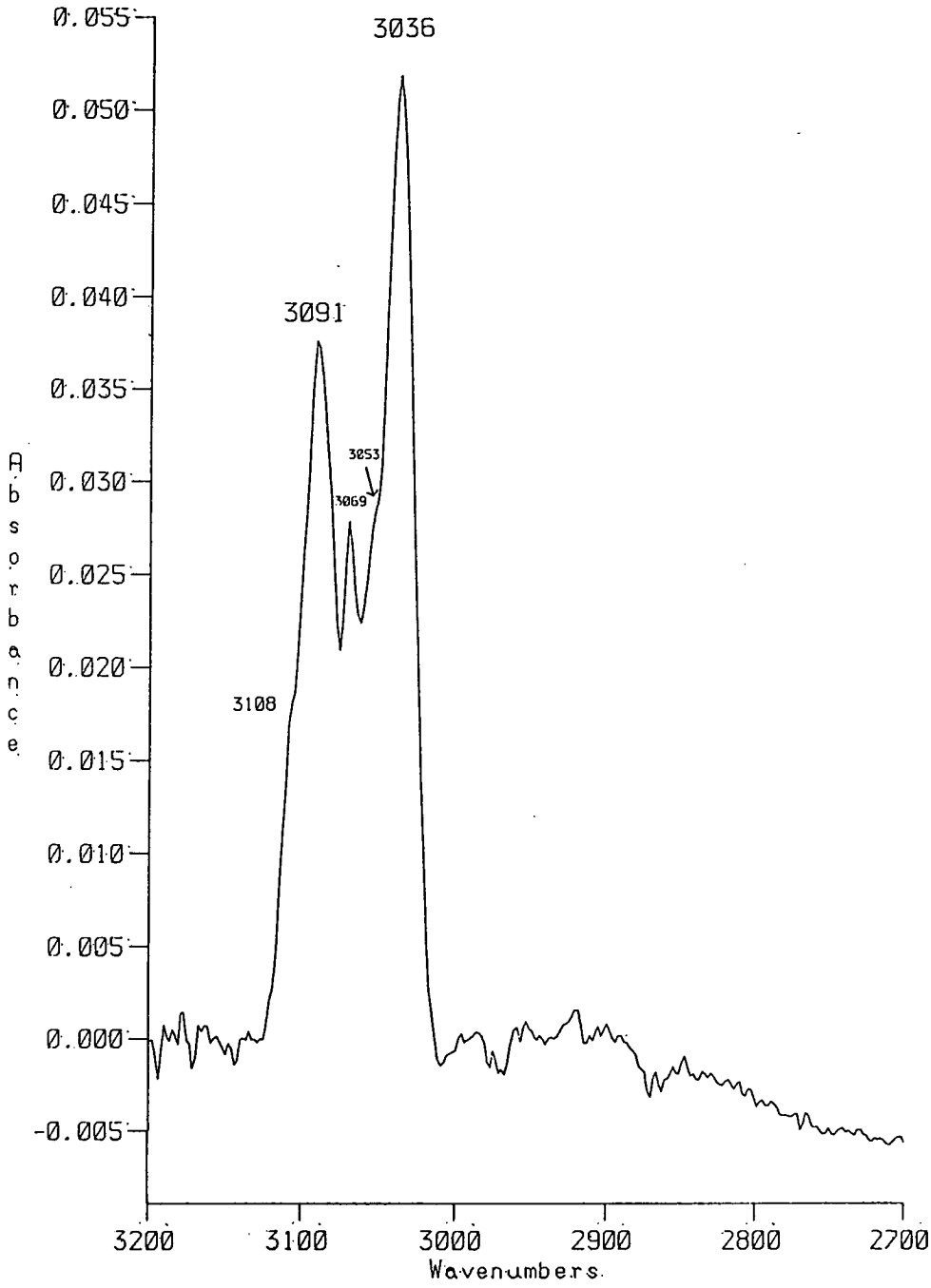

Fig. 6.32 **Expanded Plot of the CH Stretch Region of Figure 6.28 , i.e. Benzene Adsorbed on 1% KOH (wt)/ EUROPT-1**

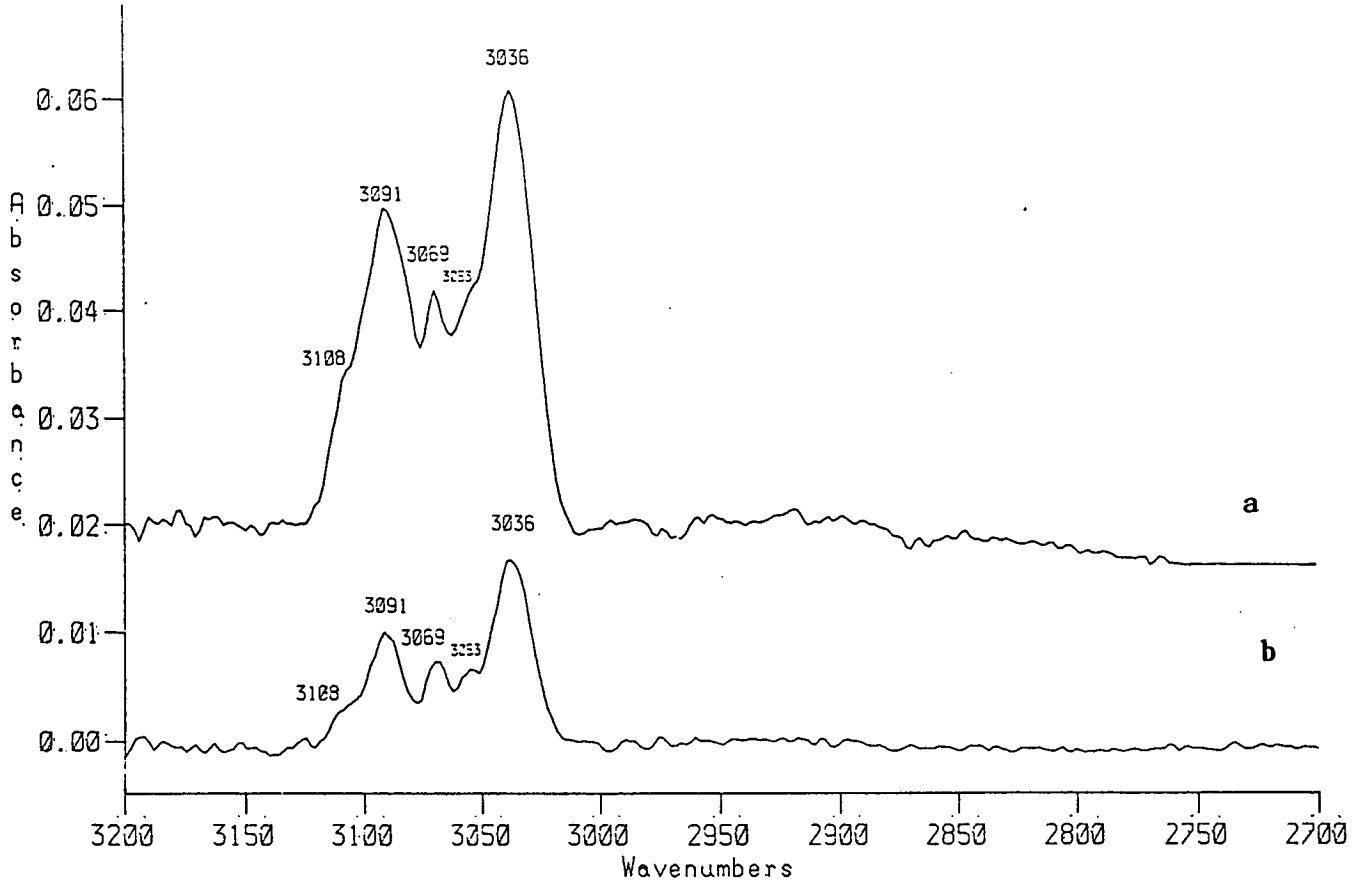

Fig. 6.33 Spectrum of Benzene Adsorbed on (a) 1% KOH (wt)/EUROPT-1; (b) on EUROPT-1

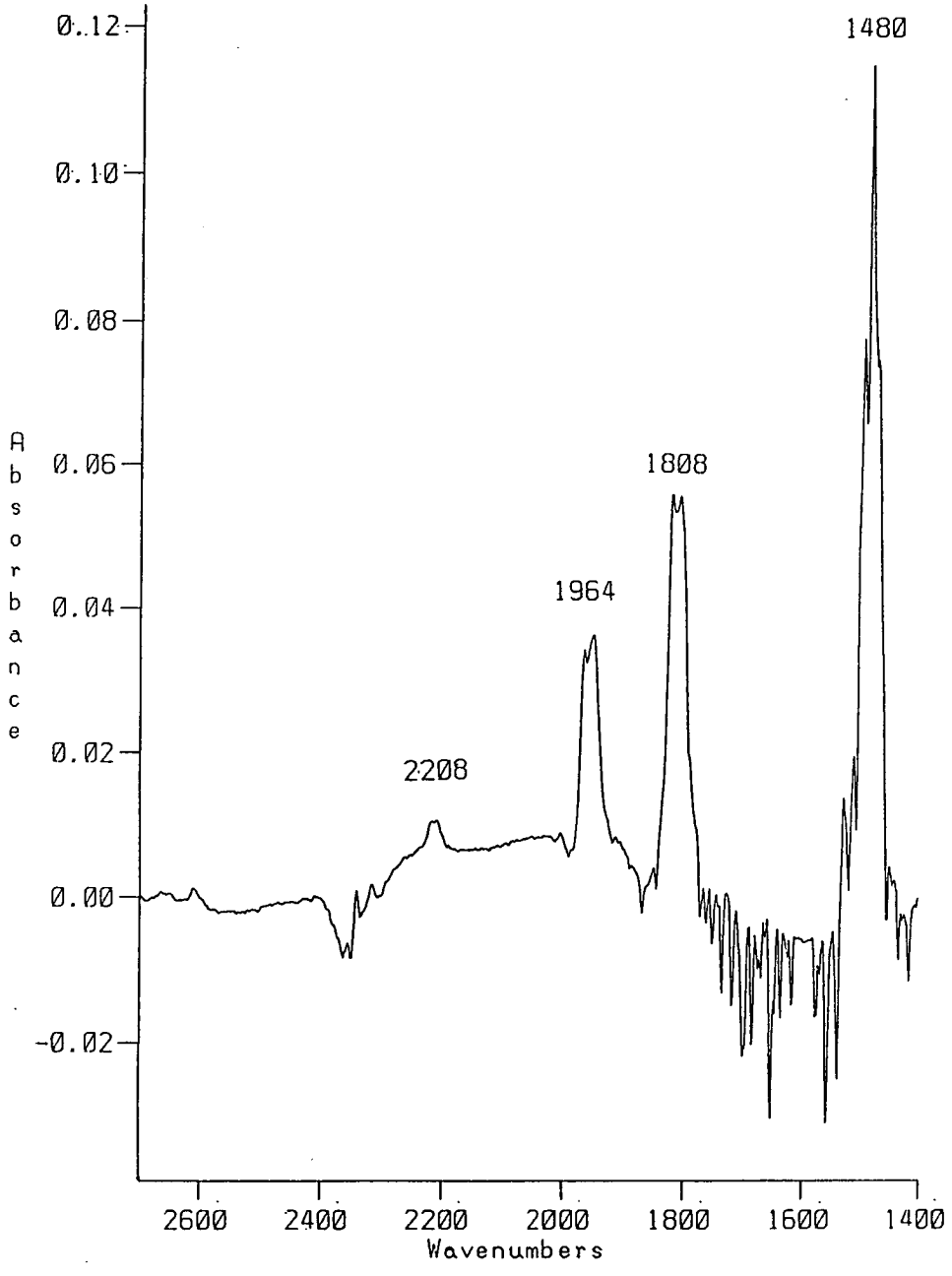

Fig. 6.34 **Expanded Plot of the Region 2700–1400 cm^{-1} of Figure 6.25**

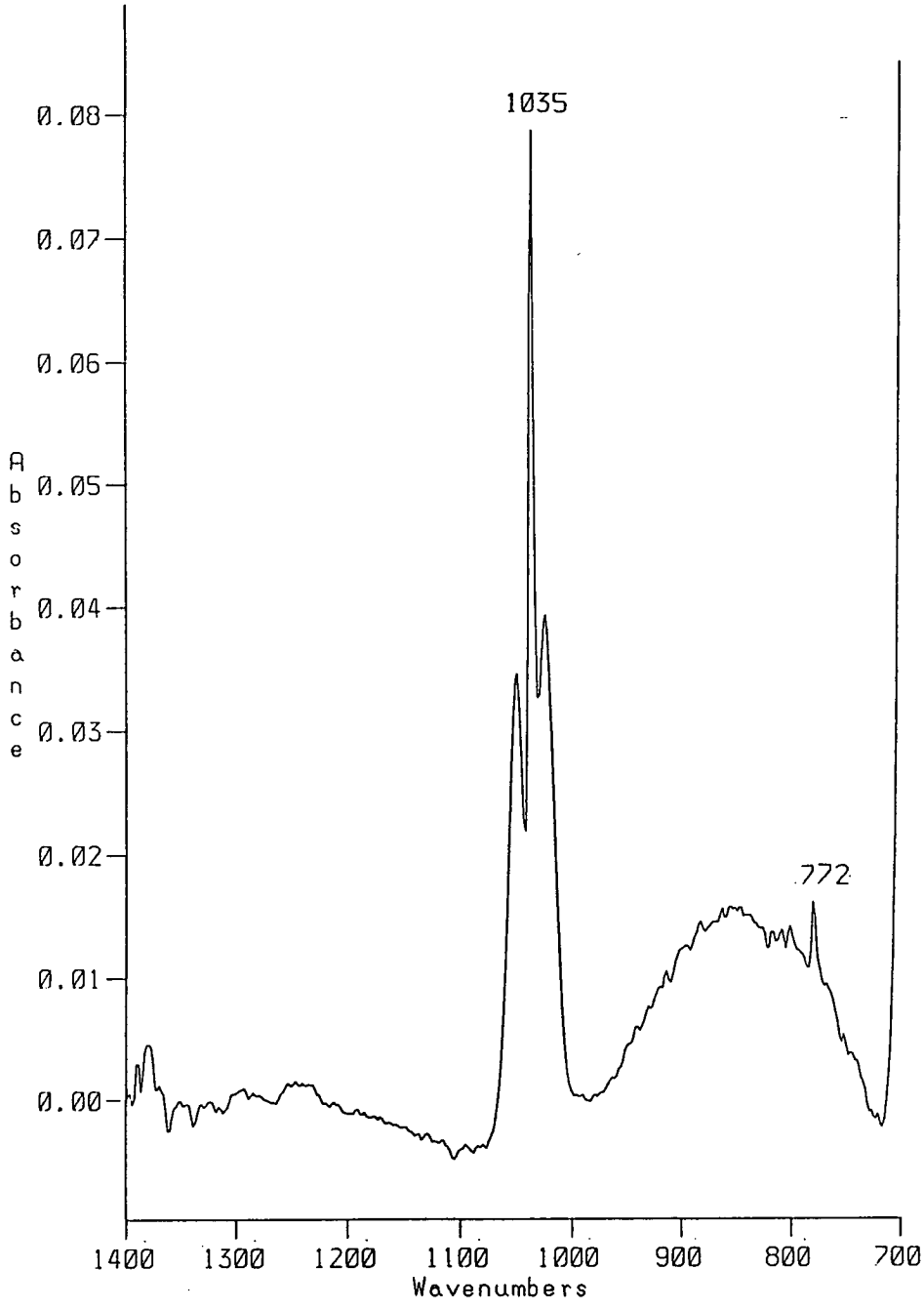

Fig. 6.35 Expanded Plot of the Region 2700–1400 cm^{-1} of Figure 6.25

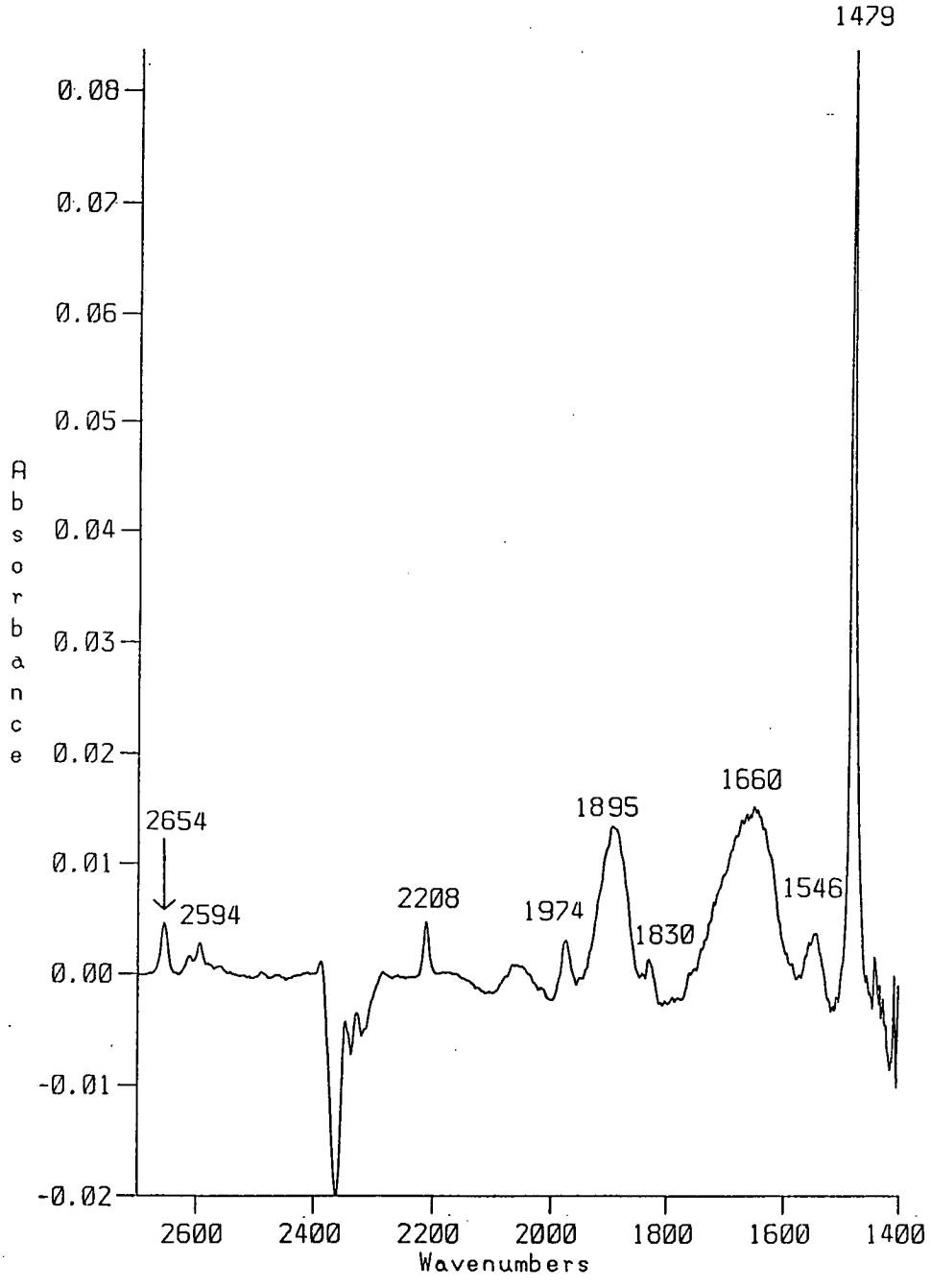

Fig. 6.36 **Expanded Plot of the Region 2700–1400 cm^{-1} of Figure 6.26, i.e. Benzene Adsorbed on Silica Support**

1400 cm^{-1}. A sharp feature at 1479 cm^{-1} is dominant, which may be assigned to the ν_{13} fundamental under e_1u symmetry. The region 1400-700 cm^{-1} of the same spectrum is shown in figure 6.37. A huge absorption band due to silica is centred at 1320 cm^{-1}. In these two regions of the spectra there are a number of other features. A broad profile centred at 1660 cm^{-1} may not be due to adsorbed hydrocarbons. This may be attributable to the presence of ice on the detector. This band may be related to the other huge band centred at 3754 cm^{-1}, which has been mentioned earlier. Three combination bands at 1546, 1830 and 1974 are indicated, along with the CO_2 miscancellation peak and overtones at 2594 and 2654 cm^{-1}.

Figures 6.38 and 6.39 show the expanded spectra of benzene adsorbed on EUROPT-1. The two regions are 2600-1400 and 1400-700 cm^{-1} respectively. These regions of the spectra are similar to that of benzene adsorbed on the silica support.

Benzene adsorbed on 1% KOH (wt.) doped EUROPT-1 is shown in spectra 6.40 and 6.41 extending from 2600-1400 and 1400-700 cm^{-1} respectively. A sharp peak at 1480 cm^{-1} is prominent. Features due to miscancellation of atmospheric CO_2 near 2350 cm^{-1} are the most dominant. Other features are similar to those already stated for benzene adsorption on a silica support. Below 1300 cm^{-1} where silica absorbs completely, it is very difficult to assign any peak confidently.

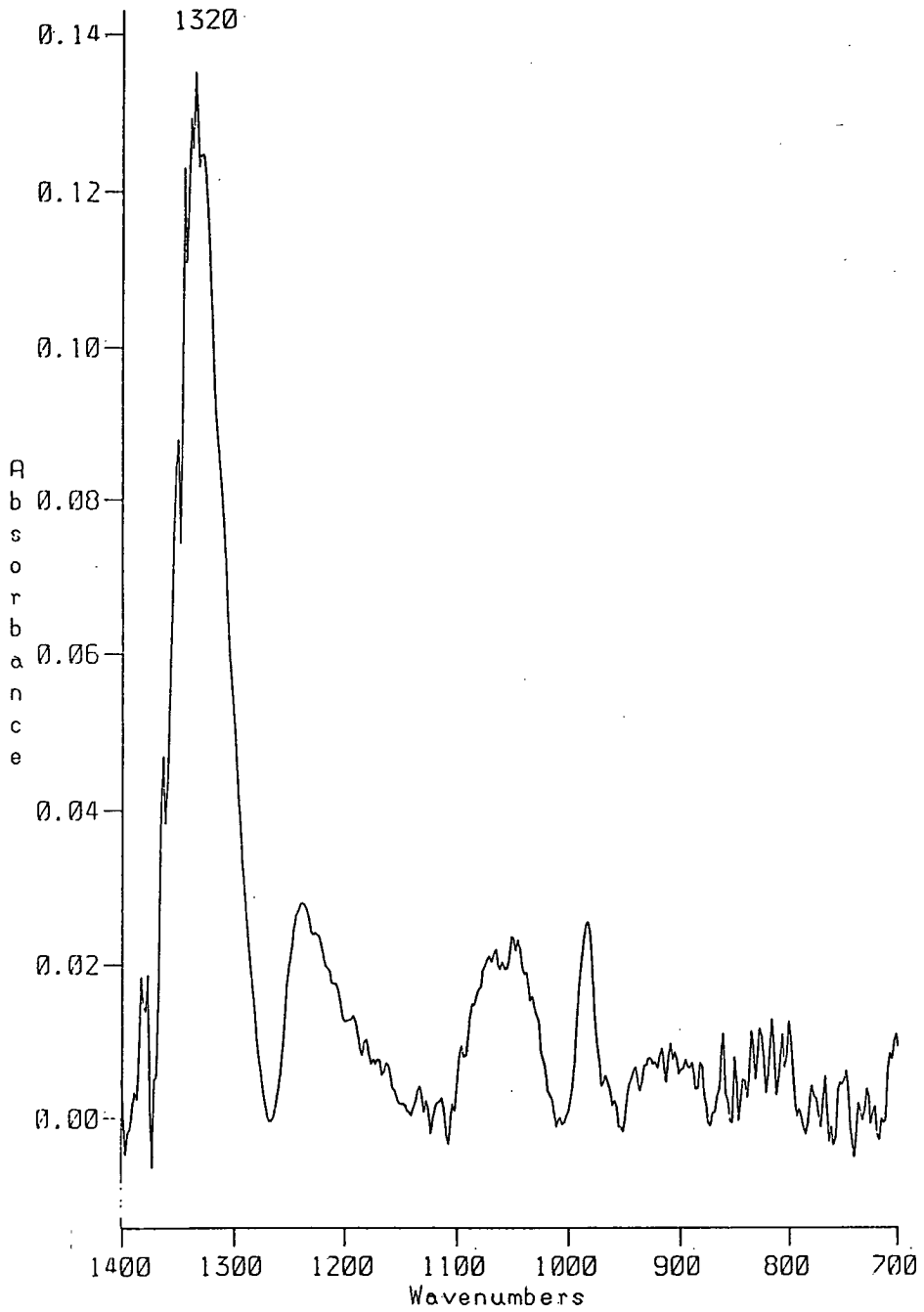

Fig. 6.37 Expanded Plot of the Region 1400–700 cm^{-1} of Figure 6.26 , i.e. Benzene Adsorbed on Silica Support

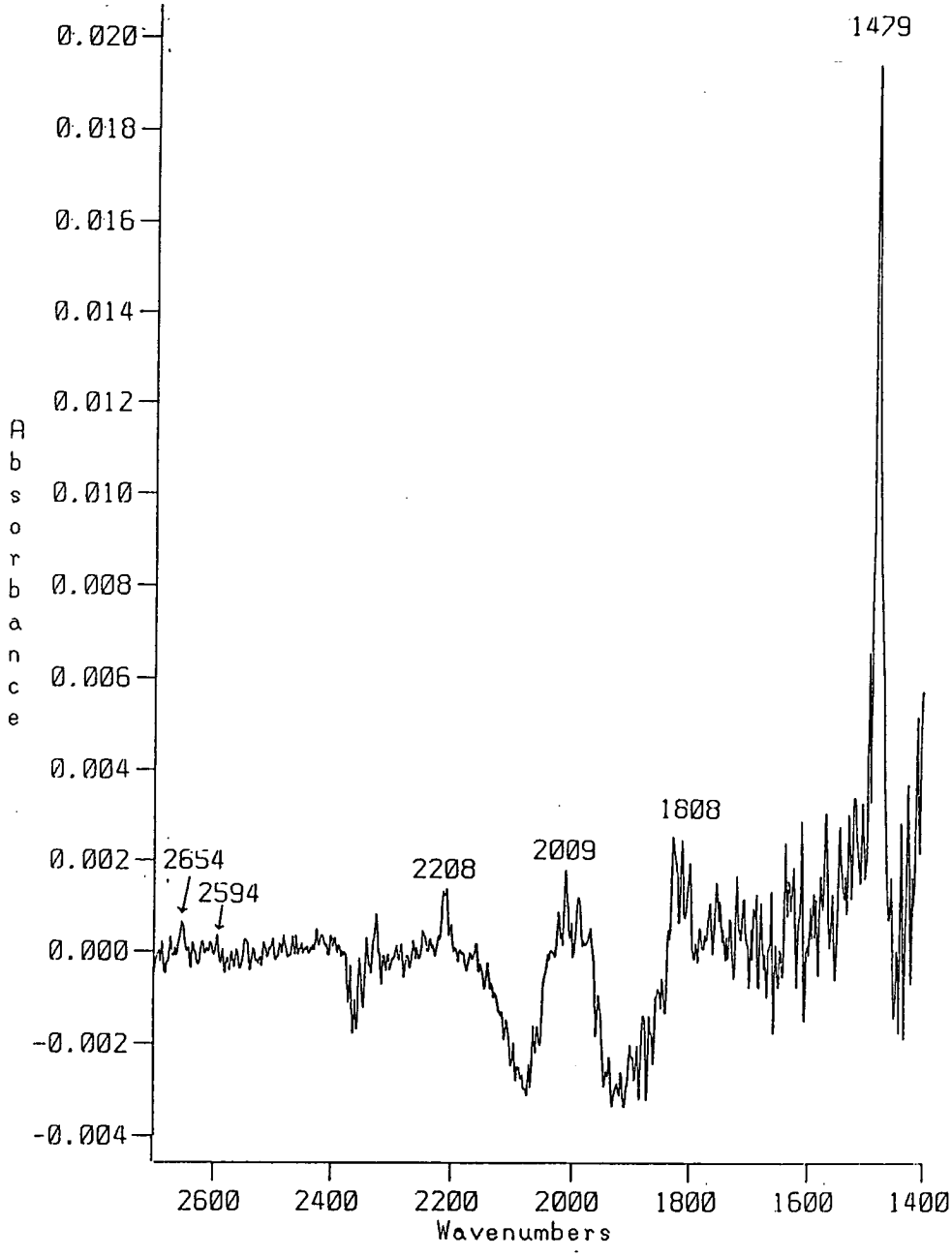

Fig. 6.38 **Expanded Plot of the Region 2700–1400 cm^{-1} of Figure 6.27, i.e. Benzene Adsorbed on 'as-received' EUROPT-1**

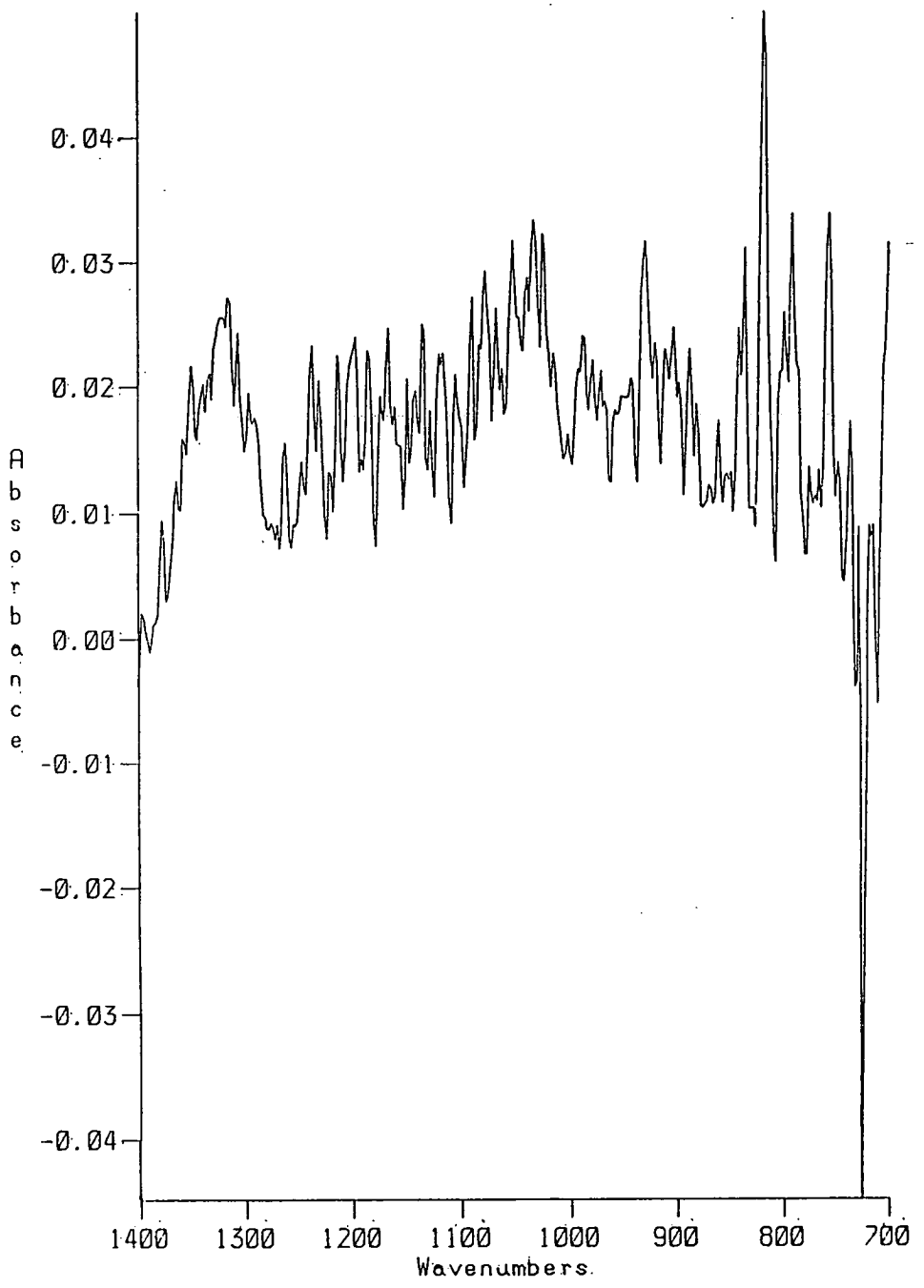

Fig. 6.39 Expanded Plot of the Region 1400–700 cm^{-1} of Figure 6.27 , i.e. Benzene Adsorbed on 'as-received' EUROPT-1

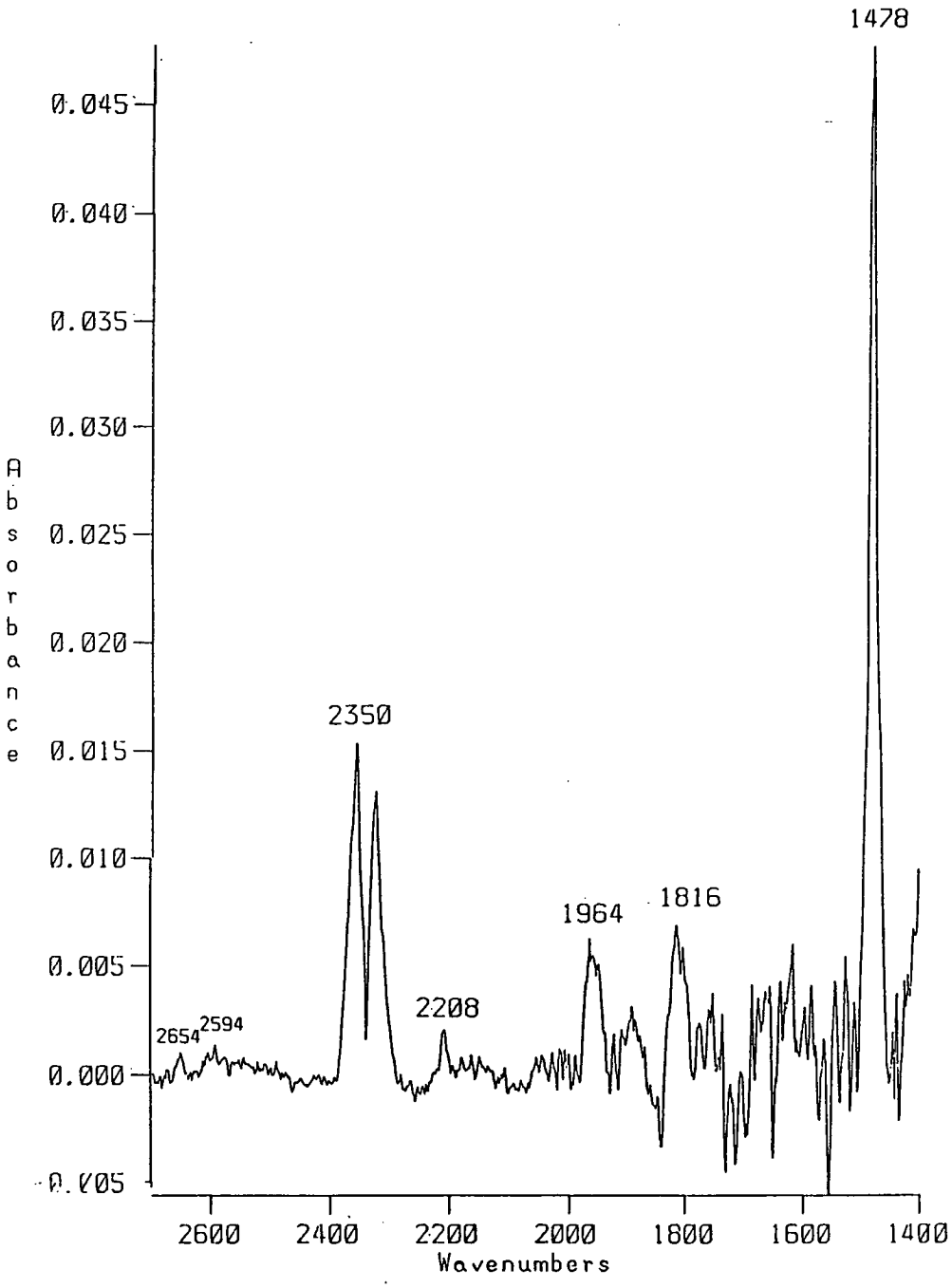

Fig. 6.40 Expanded Plot of the Region 1400–700 cm^{-1} of Figure 6.28 , i.e. Benzene Adsorbed on 1% KOH (wt)/ EUROPT-1

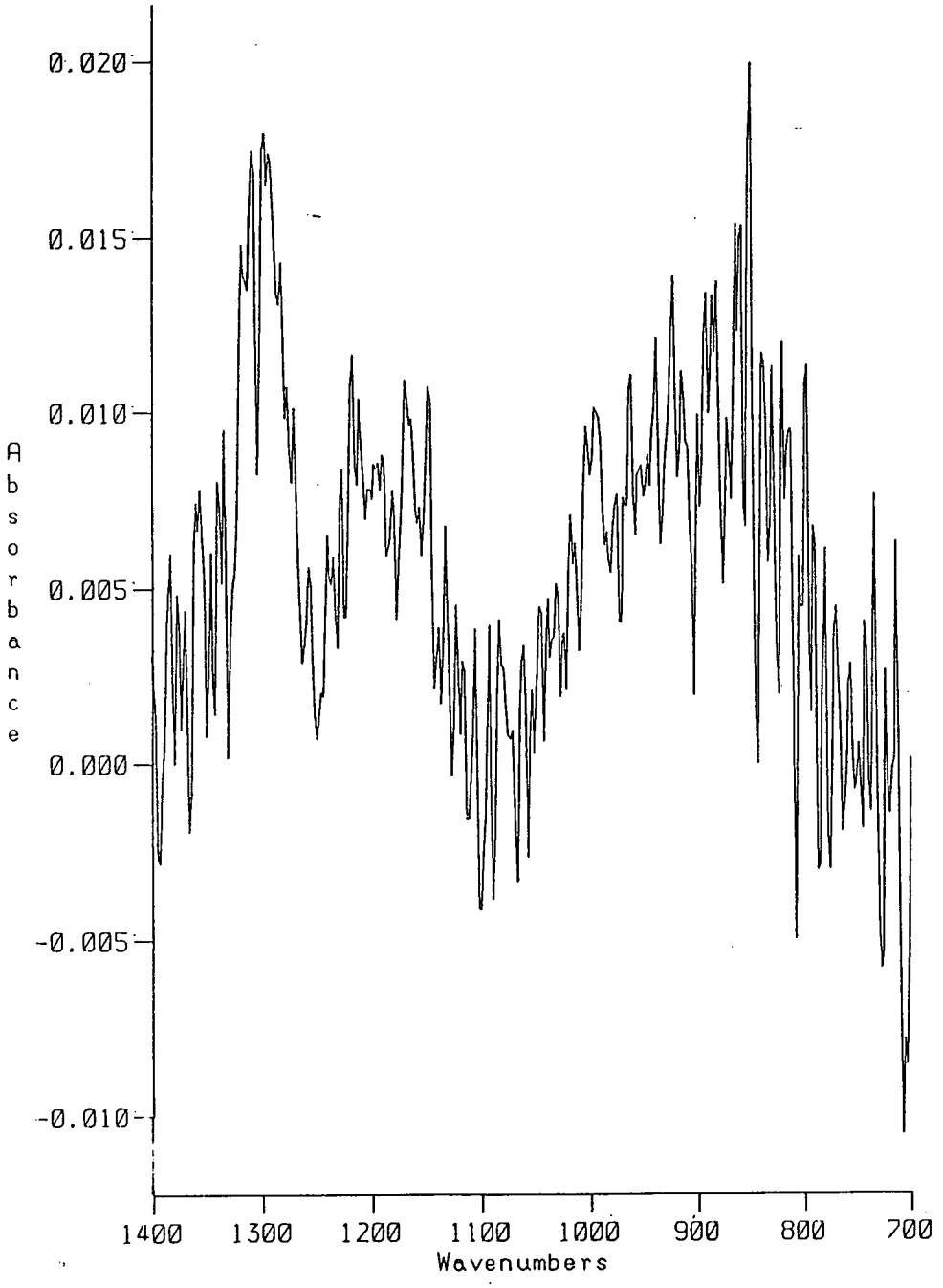

Fig. 6.41 Expanded Plot of the Region 1400–700 cm^{-1} of Figure 6.28, i.e. Benzene Adsorbed on 1% KOH (wt)/ EUROPT-1

6.8 DISCUSSION

The spectra due to adsorbed benzene on silica support is shown in figure 6.26.

The spectra of benzene adsorbed on silica is very similar to those of corresponding vapour and liquid benzene. Differences in the frequencies between adsorbed and liquid phase are ~ 2 cm^{-1} for fundamental vibrations. This difference is similar to that observed on alumina[47], and silica as previously observed by Galkin *et al.*[46]. The strong absorption by silica below 1300 cm^{-1} does not allow the direct observation of the infrared active ν_4 out of plane hydrogen bond mode (670 cm^{-1}). This vibration was observed to change in frequency to 685 cm^{-1}, previously reported by Galkin *et al.*[46]. Galkin has attributed this higher shift to the interaction of the π-electrons of benzene with OH groups on the silica surface. According to Galkin *et al.*[46], with increasing surface coverage the location of this absorption band approaches its position for liquid benzene (675 cm^{-1}), and as the hydroxyl groups are removed by thermal treatment in vacuum or by methylation it shifts towards its position for gas phase benzene (671 cm^{-1}).

The majority of the combination bands experience a shift of frequency from the gas phase value when benzene is adsorbed on silica. These bands occur at 1975, 1895 and 1830 cm^{-1}, assigned as E_1u and A_2u under gas phase

symmetry, $D_{6}h$ point group of benzene molecule, as given in table 6.2. This compares with the work by Haaland[47] for benzene absorption on Pt/Al_2O_3, where a series of five combination bands are reported to shift by 8 cm^{-1} to higher wavenumbers, as in table 6.2. In the present study only two of the five bands reported by Haaland are observed and are noted to have similar shifts. Other combination modes noted at 2282 and 1895 cm^{-1} shift downward in frequency with respect to gas phase value by 6-10 cm^{-1}.

In Haaland's work all the combination bands exhibiting an upward shift in frequency involve one or more out of plane H bending modes. The greatest upward shift in frequency is ~ 20 cm^{-1} and attributable to a combination of two out of plane H-bending modes. Thus all perpendicular H bending fundamentals show an increase in frequencies of ~ 10 cm^{-1} (listed in table 6.2) suggest a π electron interaction with an electrophilic group on silica.

Figure 6.26 shows the perturbation of the π electron system due to an interaction with the free hydroxyl groups on silica. Thus there is a loss in intensity of the stretching vibrations of free OH groups at 3790, 3771 and 3731 cm^{-1} with a corresponding increase in the intensity of the hydrogen bonded (perturbed OH groups) hydroxyl groups centred at 3620 cm^{-1}. Such a perturbation of OH groups has been reported with benzene adsorption on silica

and alumina[46-47,58]. This suggests that hydrogen atoms of hydroxyl groups on silica may interact with the π-electrons of the adsorbed benzene. Hence the benzene interaction with the silica support may be mainly through the hydroxyl groups bound to the silica support.

Although the π-electron system of benzene interacts with the OH groups of silica as observed in the present study and in alumina[47], according to Haaland the interaction is weak as evidenced by the desorption of benzene on evacuation. Evacuation at 300 K removes all adsorbed benzene, indicating that benzene is only physisorbed on alumina. This was also confirmed by the observation that no new vibrations were observed upon adsorption, which showed the weakly bound nature of the physisorbed benzene and the interaction did not significantly alter the high $D_{6}h$ symmetry of the free benzene molecule. Relative intensity changes in absorption bands are a more sensitive probe of molecular interactions and geometry changes[42]. As described earlier, upon adsorption the out of plane H-vibrations are shifted to higher energy relative to that observed in the liquid. However, the relative intensities of the combination bands involving these perpendicular H vibrations are slightly reduced compared to the 3092 cm^{-1} C-H stretching region. A decrease in intensity of these bands is expected when the π-electrons interact with an electrophilic substrate[60]. Haaland has observed a 30%

increase in the relative integrated intensity of the ν_{13} fundamental and its strong combination with ν_{16} (i.e. 1480 and 3069 cm^{-1} respectively). The ν_{13} stretching mode which will cause a distortion in the π-electron cloud which may account for its slightly increased intensity in the adsorbed state.

The spectrum of benzene physisorbed on EUROPT-1 is similar to that of benzene adsorbed on silica support. This indicates that platinum does not appear to influence the physisorption of benzene on the support and the spectrum is therefore still dominated by physisorbed benzene, similar to that for the support alone. It has been previously noted for benzene absorption on Pt/SiO_2 and Pt/Al_2O_3 at room temperature[42,47].

The spectrum for benzene chemisorption on Pt was achieved by subtracting the ratioed spectrum of benzene adsorbed on silica from the ratioed spectrum of benzene adsorbed on EUROPT-1. The resultant spectrum in the expanded region 3200-2700 cm^{-1} is shown by a comparative set of spectra in figure 6.42. The figure shows that upon adsorption on EUROPT-1 two additional features, a small peak at 3053 cm^{-1} and a shoulder at 3108 cm^{-1}. These may be attributable to the weak interaction of benzene with the platinum[60]. The subtracted spectra which corresponds to the chemisorbed benzene on Pt metal surface shows well resolved features at 3053 and 3108 cm^{-1}.

Figure 6.43 shows a set of spectra indicating

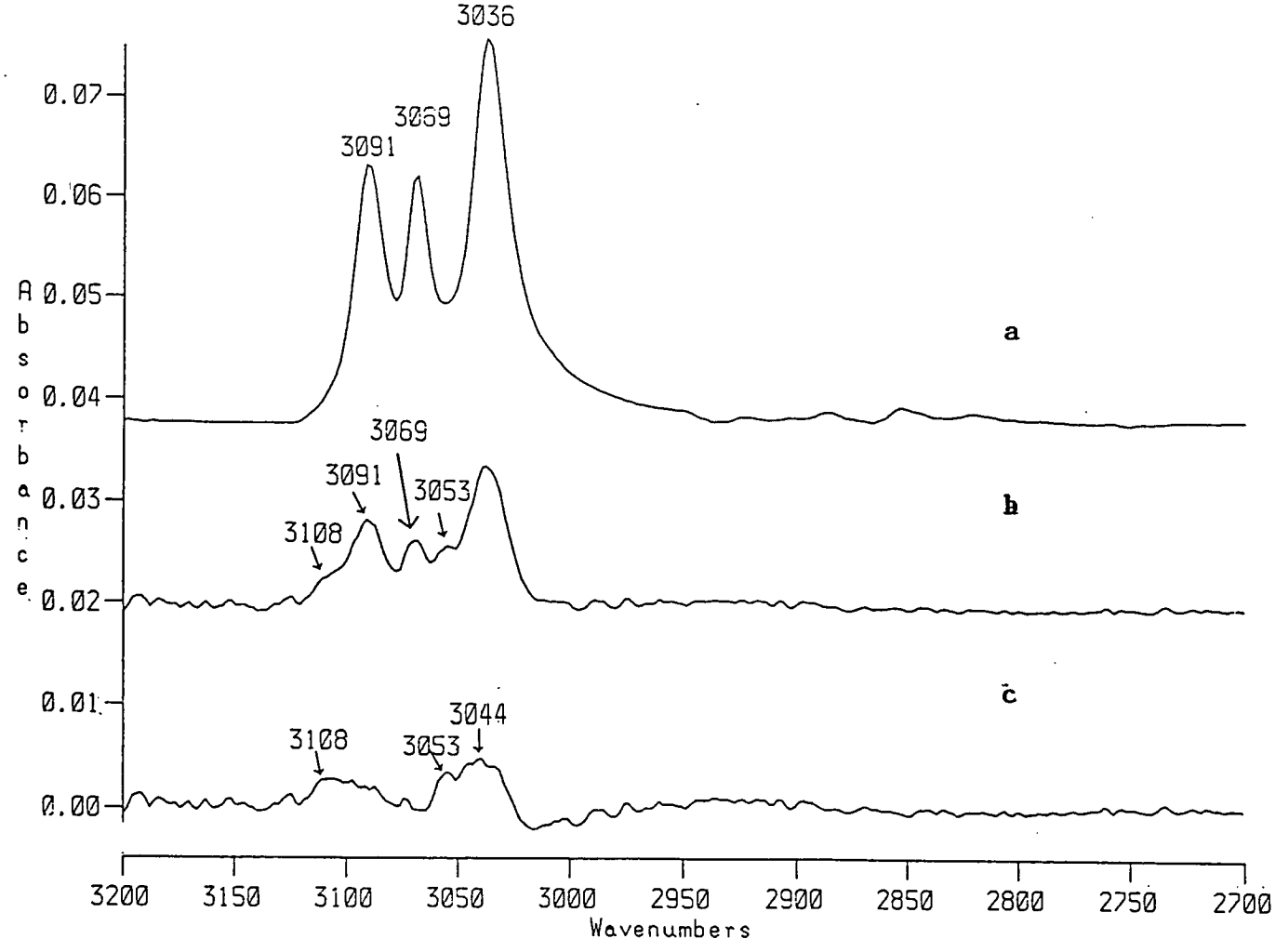

Fig. 6.42 A Comparative Set of Spectra Showing Benzene Adsorbed on (a) Silica Support;
(b) on EUROPT-1;
(c) Chemisorbed on EUROPT-1
i.e. spectra b-a

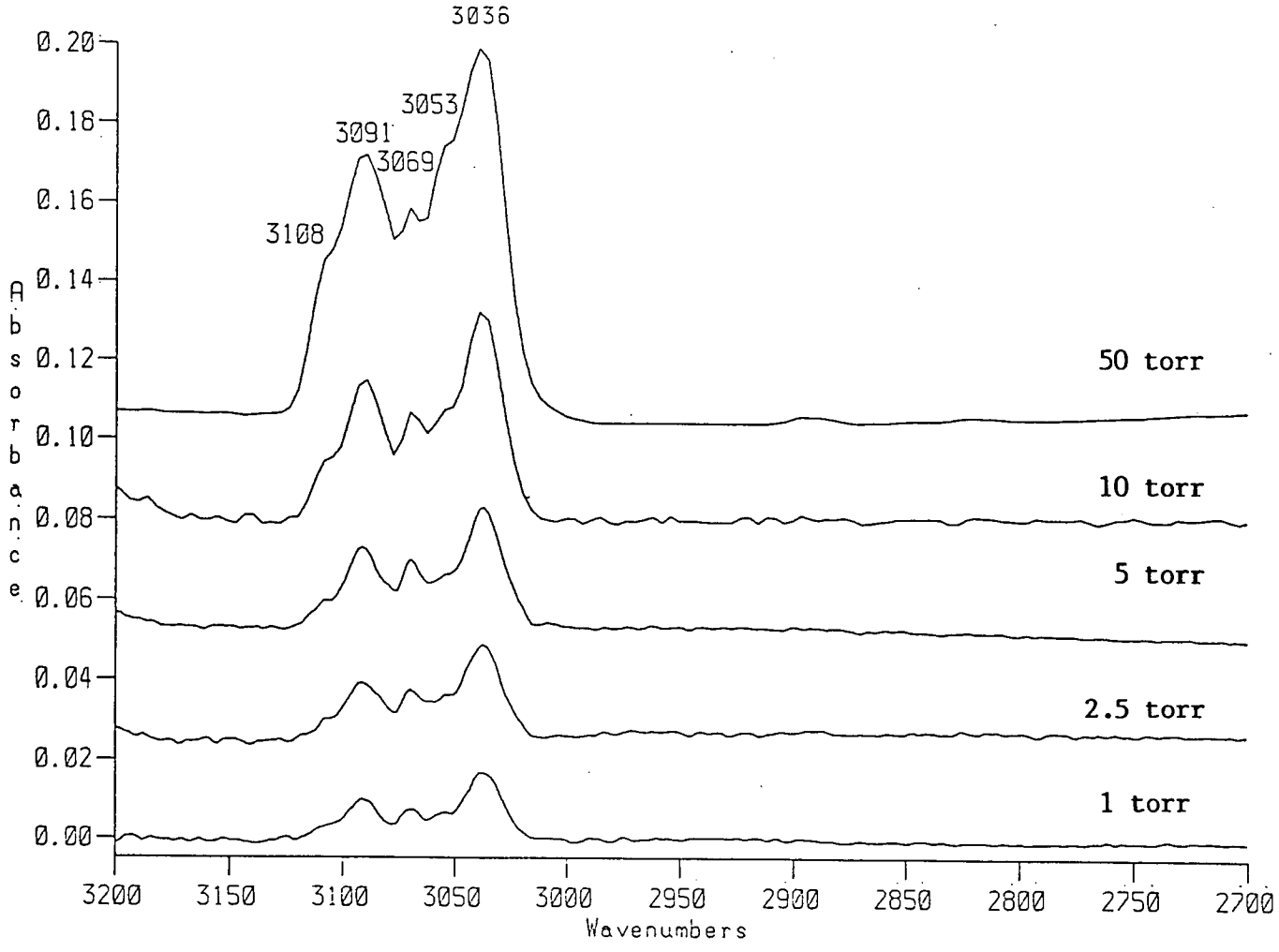

Fig. 6.43 Spectra of EUROPT-1 Exposed to Increasing Pressures of Benzene

adsorption of benzene as a function of benzene pressure. All the spectra are essentially identical in as much as the peaks grow in a parallel fashion with increasing pressure. A set of subtracted spectra, produced by subtraction of benzene physisorption in the support from the spectra shown in figure 6.44 above are similar to that shown previously in figure 6.42. These only vary in intensity as a function of benzene pressure. Relative intensities remain unaffected. A small peak at 3053 cm^{-1} becomes clear and a well resolved peak in the region 3108 cm^{-1} can be seen. These new peaks are almost certainly genuine characteristics of benzene chemisorption on Pt. Lehwald *et al.*[44] presented EELS data on the vibrations of adsorbed benzene. On Pt(111) single crystal, the spectrum has been assigned in terms of benzene occupying a three-fold hollow site. Some of the molecules also occupy on-top sites referred to as pseudo $C_{6\nu}$ sites, by the authors. For the former site weak modes both infrared and Raman inactive in the gas phase but are surface allowed under $C_{3\nu}$ symmetry. For both adsorbed species whether $C_{6\nu}$ on-top site or three fold site, only a single CH stretch is observed near 3000 cm^{-1}.

According to Sheppard[41], if benzene molecules were π-bonded, their gas phase symmetry of $D_{6}h$ would be reduced to C_{6v}. The form of dipole active mode would be assigned as ν_{CH} ($A_1g \longrightarrow A_1$), ν_{CC} ($A_1g - A_1$) and ν_{CH} ($A_{2u} \longrightarrow A_1$). Following the Herzberg[61] numbering system, these modes

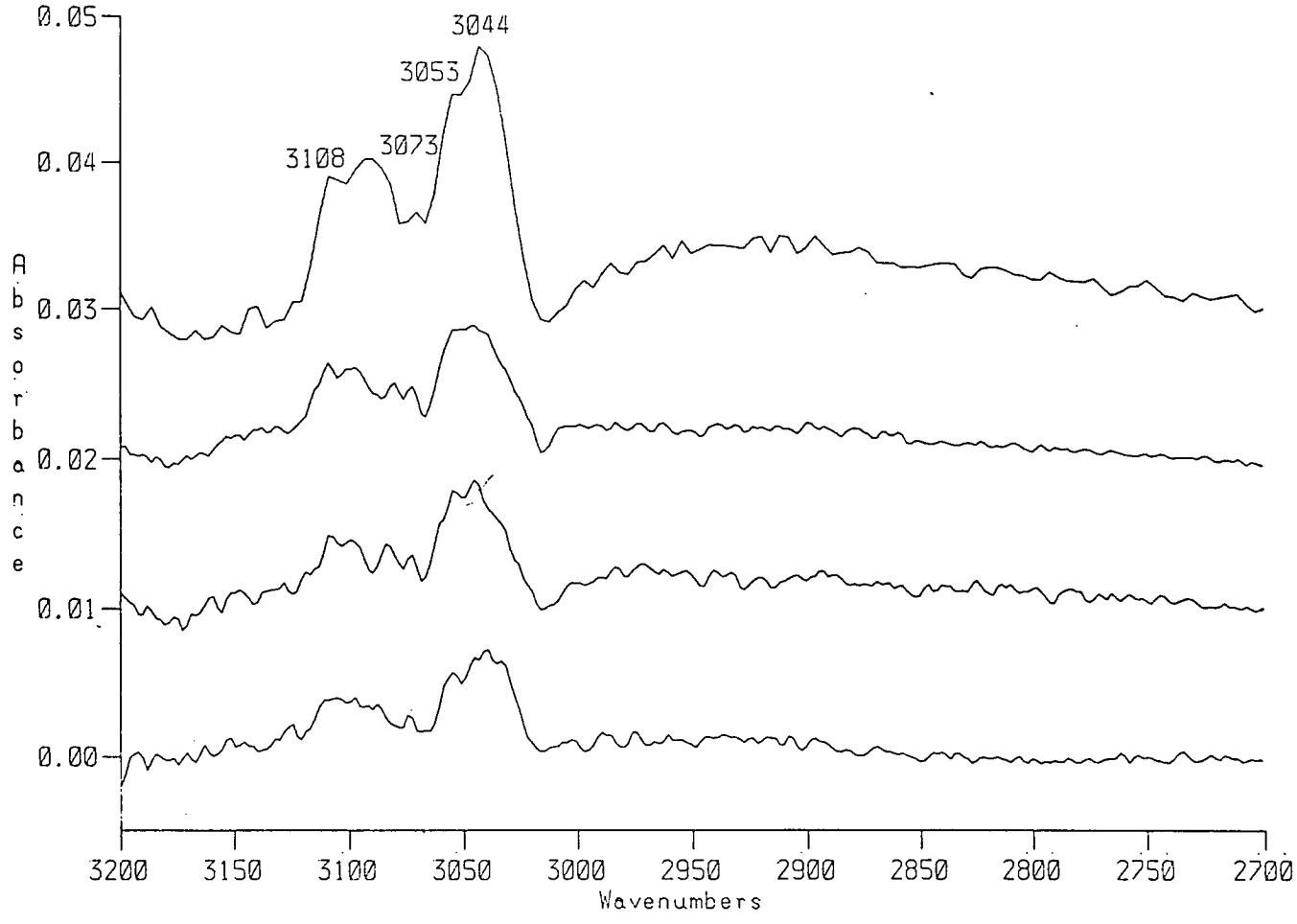

Fig. 6.44 A Set of Spectra of Benene Chemisorbed on EUROPT-1 After Subtraction of Physisorbed (Benzene)

would be ν_1, ν_2 and ν_4 respectively.

As presented in table 6.2 benzene chemisorbed on Pt/SiO_2 shows two peaks at 3108 and 3053 cm^{-1}. The peak at 3053 cm^{-1} is similar to that previously observed by Haaland[47] on Pt/Al_2O_3 and the single ν_{CH} band observed on Pt(111) single crystal[44]. This would be assigned to ν_{12} A_1g mode under gas phase D_6h symmetry and totally symmetric and therefore surface infrared active under any reduced symmetries.

The remaining mode 3108 cm^{-1} is more difficult to assign as there is no further ν_{CH} fundamentals. Surface allowed unless under still lower symmetries than C_{6v} or C_{3v}, i.e. C_s or C_1.

On Pt(111) Lehwald *et al.*[44] observed two separate absorptions attributed to the single ν_4, A_{2u} out of plane H-bending vibrations. These were assigned to benzene adsorbed on different crystallite sites.

On Pt/Al_2O_3 Haaland[47] argued that peaks at 3050 cm^{-1} corresponds to E_{1u} vibration indicating that chemisorbed benzene is distorted to C_{3v} symmetry. On deconvolution this broad peak revealed four peaks. Following Lehwald interpretation, Haaland attributed these multiple peaks to benzene chemisorbed on different crystallite sites. Neither of these symmetries would explain the 3108 cm^{-1} band. Other possible explanations may be:

(1) Observation on non-totally symmetric modes, namely 3090 cm^{-1}, E_1 in gas phase shifted to 3108 cm^{-1}.

Evidence for this comes from ethylene adsorption on EUROPT-1 studied by McDougall[8]. In that work non-totally symmetric modes were observed although nominally forbidden in the infrared by the 'metal selection rule'. This was explained by either symmetries lower than C_{3v} for ethylidyne where these 'forbidden' modes become allowed or alternatively low symmetry adsorption sites provided by the supported metal particles. The observation of weak 'totally non-symmetric' modes therefore do not seem unreasonable.

(2) The 3108 cm^{-1} band may infact be totally symmetric combinations in gas phase (3187 cm^{-1}, $2\nu_2 + 2\nu_{18}$, and 3164 cm^{-1}, $2\nu_{16}$ modes) rather than ν_{CH} fundamentals shifted down accompanied with increase in relative intensity due to fermi resonance.

A spectrum of benzene on 1% KOH doped EUROPT-1 is shown in figure 6.45a. This result is based on the single experiment performed. Figure 6.45b shows the subtracted spectrum of chemisorbed benzene. As before two broad peaks at 3053 and 3108 cm^{-1} are observed. However, the high frequency region (3108 cm^{-1}) is more intense for this particular catalyst than that noted in the undoped sample. Further, the absolute intensity of the chemisorbed benzene is greater than the range shown in figure 6.42. This is in spite of similar experimental conditions and range of pressures (i.e. 2.5 torr). This suggests more extensive

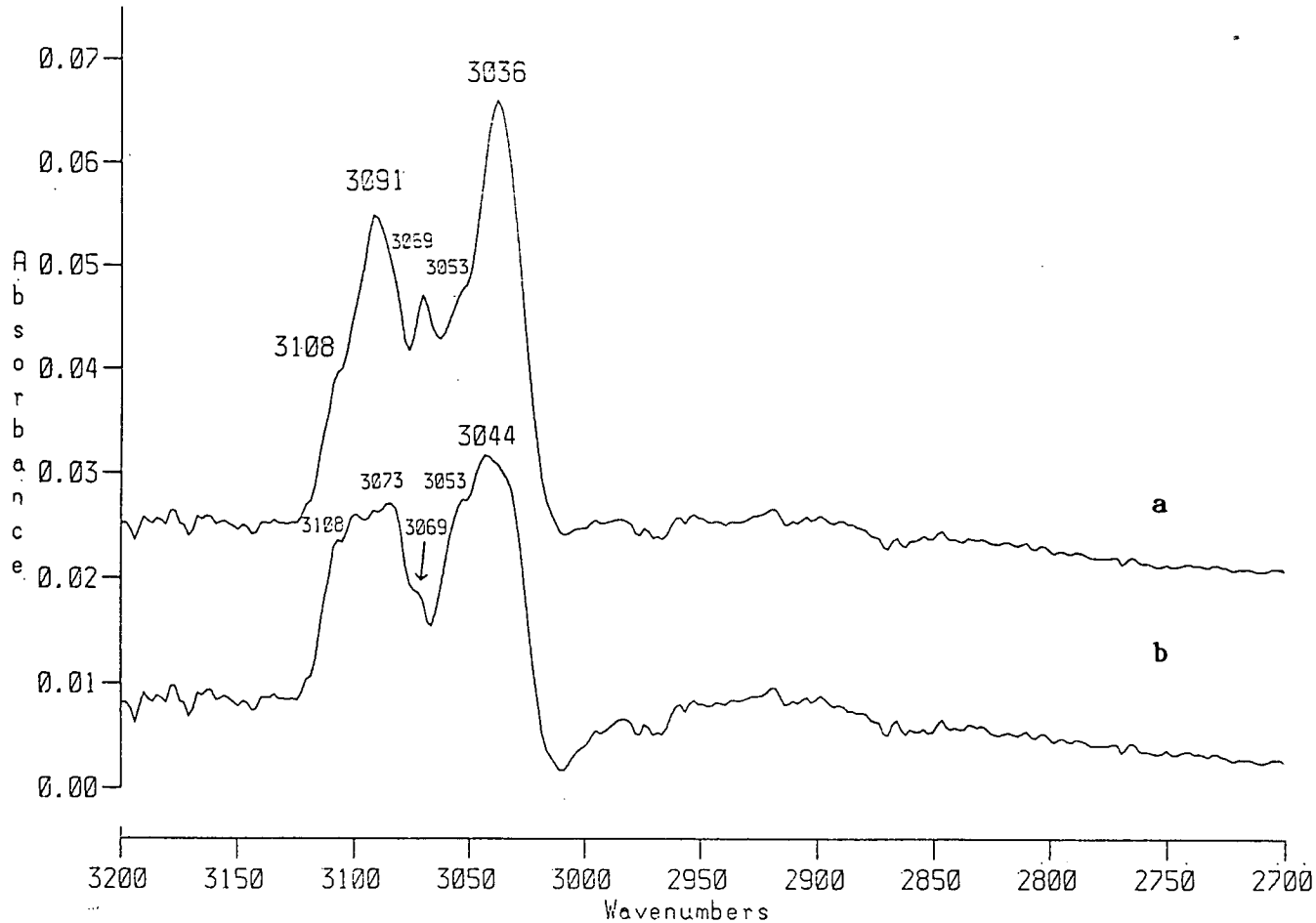

Fig. 6.45 Spectrum of Benzene (a) Adsorbed on 1% KOH (wt)/EUROPT-1;
(b) Same Spectrum after Subtraction of Physisorbed Benzene on Silica Support

chemisorption on the alkali doped catalyst.

Although we do not find any literature evidence directly relevant to benzene adsorption on alkali doped supported catalysts, analogies can be drawn from the work of benzene desorption (TDS) studies from potassium doped Pt(111) single crystals. Garfunkel *et al.*[31] noted that much more of the benzene desorbed intact upon heating when the Pt surface was doped with potassium. A smaller fraction of carbon was found to remain on the surface (as detected by AES) after heating. Lower temperature for the benzene maximum desorption rate was also observed. The authors attributed these results to the weakened benzene-platinum bond strength. This can be explained in terms of charge transfer. It is assumed that benzene donates electrons when π orbitals are involved in a symmetric coordination with the metal atoms or ions[59]. In the presence of potassium, the platinum surface becomes electron rich due to charge transfer from electropositive potassium to the metal. When the platinum surface is enriched with electron density, benzene may not be able to donate. Hence the benzene-platinum interaction would be expected to be weaker. The alkali effect is explained in detail on the basis of the Duncan, Chatt and Dewar[37-38] model. This has been discussed in the previous section on ethylene adsorption. It would be worth mentioning that the benzene interaction with a potassium doped Pt(111) single crystal is in contrast to the carbon monoxide

adsorption on a K/Pt(111) single crystal[31]. The increased CO bonding strength in the presence of potassium is attributable to a substantial charge donation from potassium through the platinum substrate and into the $2\pi^*$ orbital of carbon monoxide.

6.9 CONCLUSIONS

Present results and observations could lead to the following conclusions:

(i) If it is assumed that benzene adsorption on supported metal catalysts is partially dissociative at room temperature, then the observed increase in overall intensity of the spectrum on alkali doping in the present results would agree with the observations from the single crystal studies that dissociation of benzene occurs at steps or other defect sites because of the geometric (steric) and/or electronic variation at these sites. In supported metal catalysts, these types of sites will be more prevalent.

(ii) The changes in relative intensity are slightly more difficult to rationalise. Simply having more benzene on surface might lead to changes in relative intensity, but it did not appear to be the case. Also if these changes are due to formation of multilayers there should be a shift

in appearance of the spectrum towards the liquid phase. In fact, change in relative intensities is opposite to that expected for liquid benzene. In single crystal experiments, the alkali changes the strength of bonding, certainly producing change in relative intensities. Since alkali is thought to weaken the interaction, a shift towards solution-like spectra, might again be expected, but this is not the case.

Finally, like Haaland[47] it would always be possible to interpret spectra in terms of different chemisorbed species on different sites, i.e. those in the range *ca.* 3100 cm^{-1} become more important on alkali doped catalysts. But this is a rather unsatisfactory conclusion.

PART III

6.10 ADSORPTION OF SATURATED HYDROCARBONS ON 'AS-RECEIVED' AND ALKALI DOPED EUROPT-1

The study of the interaction of n-alkanes with metal surfaces is of great importance in the context of heterogenous catalysis, particularly for hydrogenation, dehydrogenation and hydrogenolysis reactions of n-alkanes over metal catalysts.

6.10.1 Adsorption of Ethane on EUROPT-1

A few spectroscopic studies on the interaction of saturated hydrocarbons with with single crystal metal surfaces are reported. In earlier studies of ethane adsorption on metal single crystal systems, such as Cu(110) at 77 K and Pt(111) at 80 K were carried out by Horn and Pritchard[62]. A weak interaction was observed and extensive physisorption of ethane was found to occur.

Cyclohexane adsorption on metal surfaces has been studied previously to investigate the process of bond weakening on metal surfaces[63]. Demuth *et al.*[63] and Ibach *et al.*[64] studied cyclohexane adsorption on Ni(111) and Pt(111) at 140 K, and observed a shift of 200-300 cm^{-1} to lower energy in the C-H stretch region. They observed two bands in the region of 2900 cm^{-1}, i.e. in the normally expected ν_{CH} stretch for saturated hydrocarbons.

Adsorption of ethane on EUROPT-1 at room temperature was studied by McDougall[8]. The author reported a spectrum due to adsorbed ethane, very similar in terms of the frequencies of the peaks to those from adsorbed ethylene. The similarity of the two spectra indicated a partial dehydrogenation of ethane upon adsorption. The differences in the relative intensities of the peaks at 2885 and 1342 cm^{-1} of the two spectra indicated that, the surface species formed from adsorbed ethane was not necessarily ethylidyne but some methyl containing surface hydrocarbon fragments such as ethylidene ($M=CH.CH_3$) or ethyl (MCH_2CH_3).

More recently Chesters *et al.*[65] carried out RAIRS study of n-alkanes on a Pt(111) single crystal at low temperature. They observed a band at 2958 and 2853 cm^{-1} due to monolayer coverage of ethane, that at 2958 was found to diminish after subsequent multilayer adsorption while the band at 2853 cm^{-1} which was assigned to the totally symmetric methyl stretch, ν, mode disappeared. At multilayer adsorption a new band appeared at 2884 cm^{-1}, and this was assigned to the symmetric methyl stretch of A_2u symmetry. This indicated the disruption of the monolayer during multilayer growth. No evidence of C-H metal hydrogen bonding was reported, as found for cyclohexane on Cu(110)[66].

In the case of ethane adsorption in this work, the position of the main peak at 2886 cm^{-1} is very similar to

that observed for ethylene adsorbed on EUROPT-1 at room temperature. This has been previously reported by McDougall[8]. The spectrum shown in Figure 6.46 was recorded after the evacuation of gas phase ethane, so the peaks due to ethane are obviously not because of the physisorbed ethane. Hence it is concluded that the peak at 2886 cm^{-1} may be due to methyl containing species, ethylidene $MCH.CH_3$ or ethyl MCH_2CH_3 group.

6.10.2 Adsorption of n-Butane on EUROPT-1

Figure 6.47 shows a spectrum of n-butane adsorbed on EUROPT-1 at room temperature. The spectrum is the ratio of single beam spectra recorded before and after treatment of EUROPT-1 by exposure to 12.5 torr of n-butane. The spectrum was recorded after evacuation of gas phase butane, so the peaks due to butane are not because of the physisorbed n-butane, as previously reported for ethane adsorption. The spectrum was dominated by a peak at 2958 cm^{-1}. According to the assignments proposed by Chester and associates[65] the peak at 2958 cm^{-1} may be due to asymmetric methyl stretching.

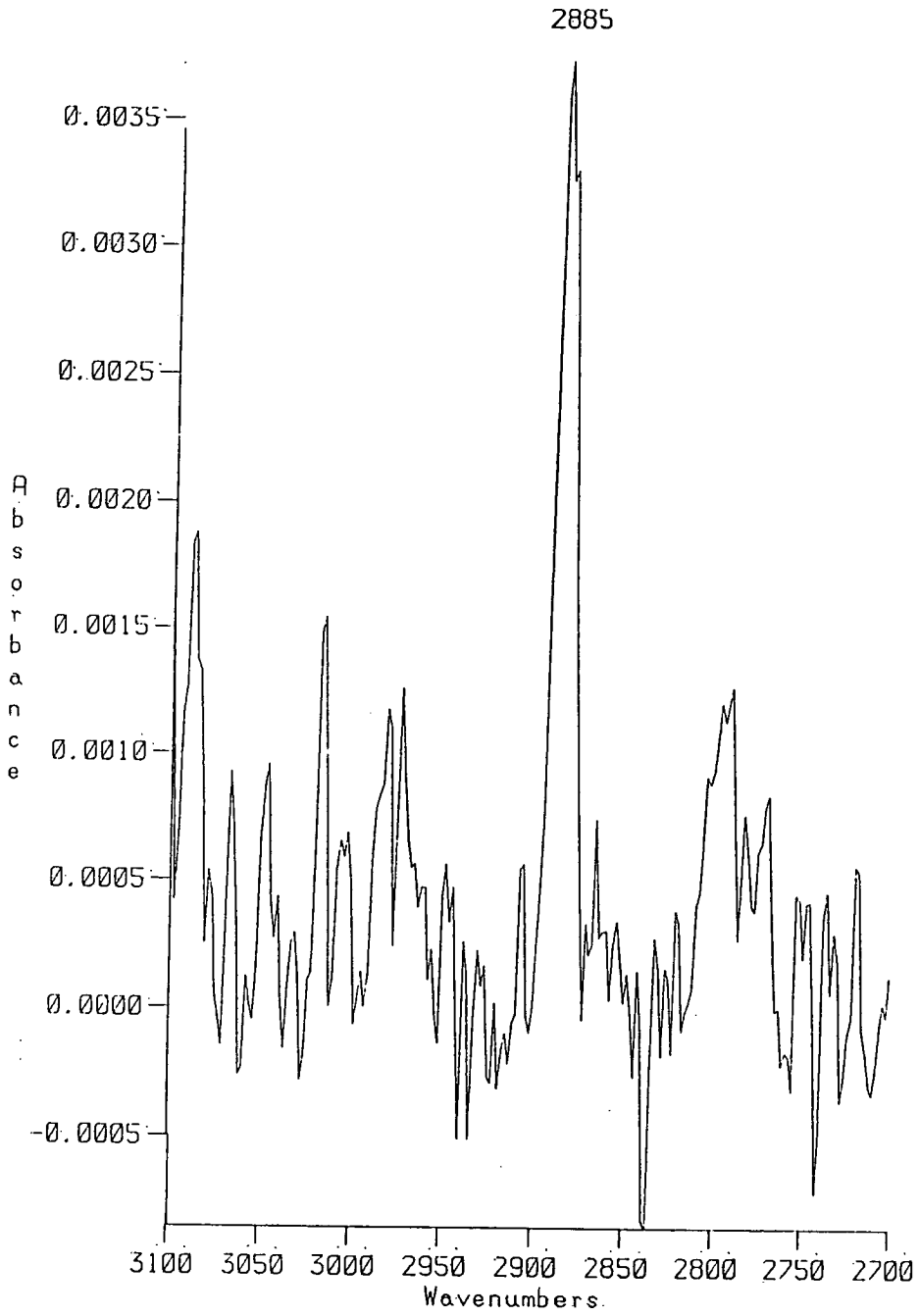

Fig. 6.46 Spectrum of Ethane Adsorbed on EUROPT-1 at Room Temperature

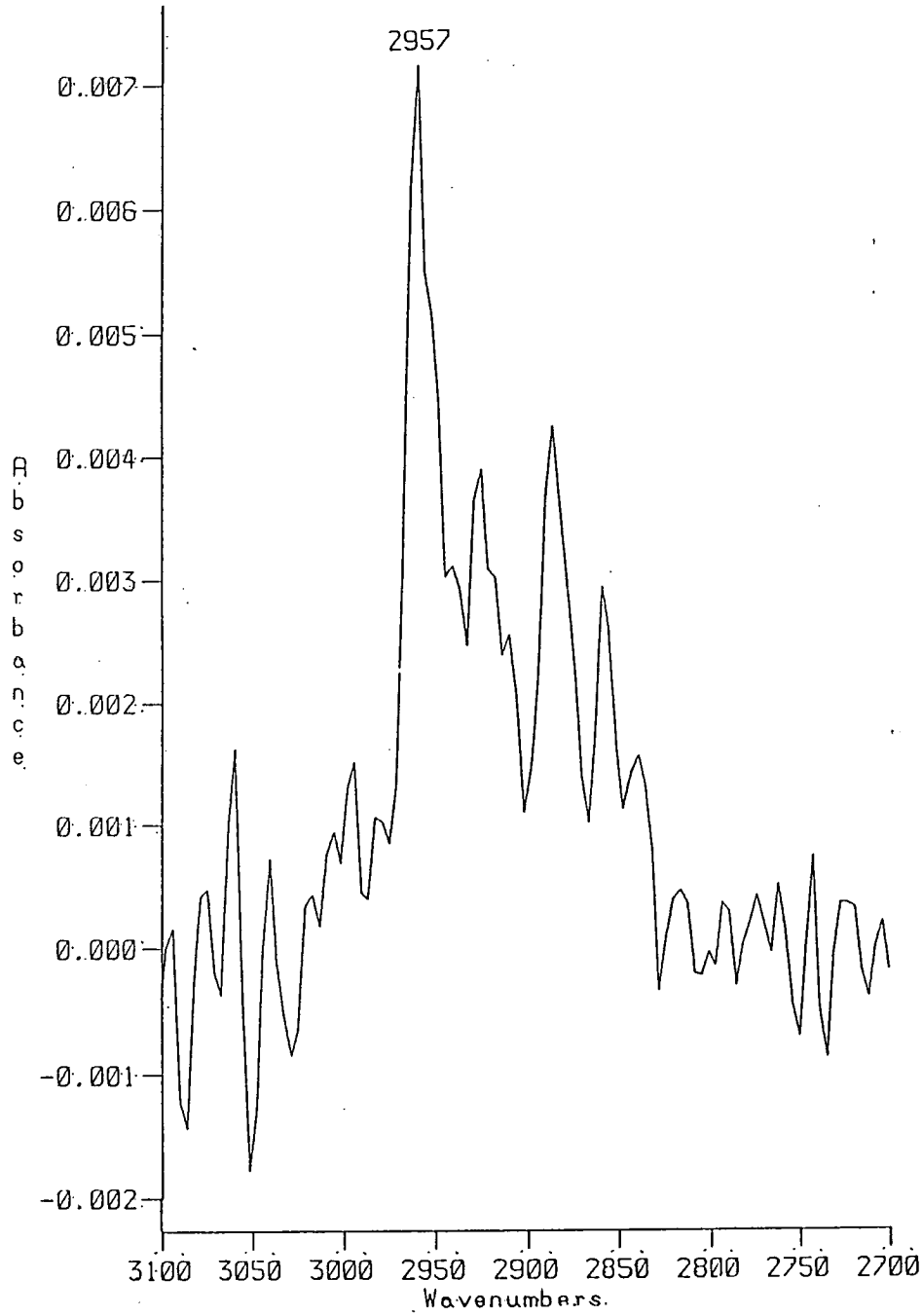

Fig. 6.47 Spectrum of n-butane Adsorbed on EUROPT-1 at Room Temperature

PART IV

6.11 STUDY OF n-BUTANE HYDROGENOLYSIS USING DRIFTS/GC TECHNIQUE

DRIFTS studies of n-butane hydrogenolysis were carried out in an attempt to investigate the adsorbed surface species on the catalyst surface during reaction. The details of the experiments are given in Chapter 5.

The small volume of the DRIFTS cell allowed only one GC sample to be taken. This sample was taken at the end of the experiment, taken in all cases after 40 minutes. The amount of butane reacted and products produced were assumed to be linear from time=0 to the sample time. The rates and the products thus obtained are shown in table 6.3. The results obtained were not unexpected when compared with the conventional hydrogenolysis experiments in Chapter 4.

Investigations of activity of the silica support towards hydrogenolysis were carried out. Gas chromatography indicated that no hydrogenolysis took place on the silica support alone. The DRIFT spectrum (Figure 6.48) confirmed this result showing no obvious signs of gaseous products. The spectrum is the ratio of single beam spectra recorded before and after treatment of silica support by exposure to reactants mixture (as described in Chapter 4) at 713 K (calibrated temperature) for 40 minutes. The spectrum was dominated mainly by a huge band

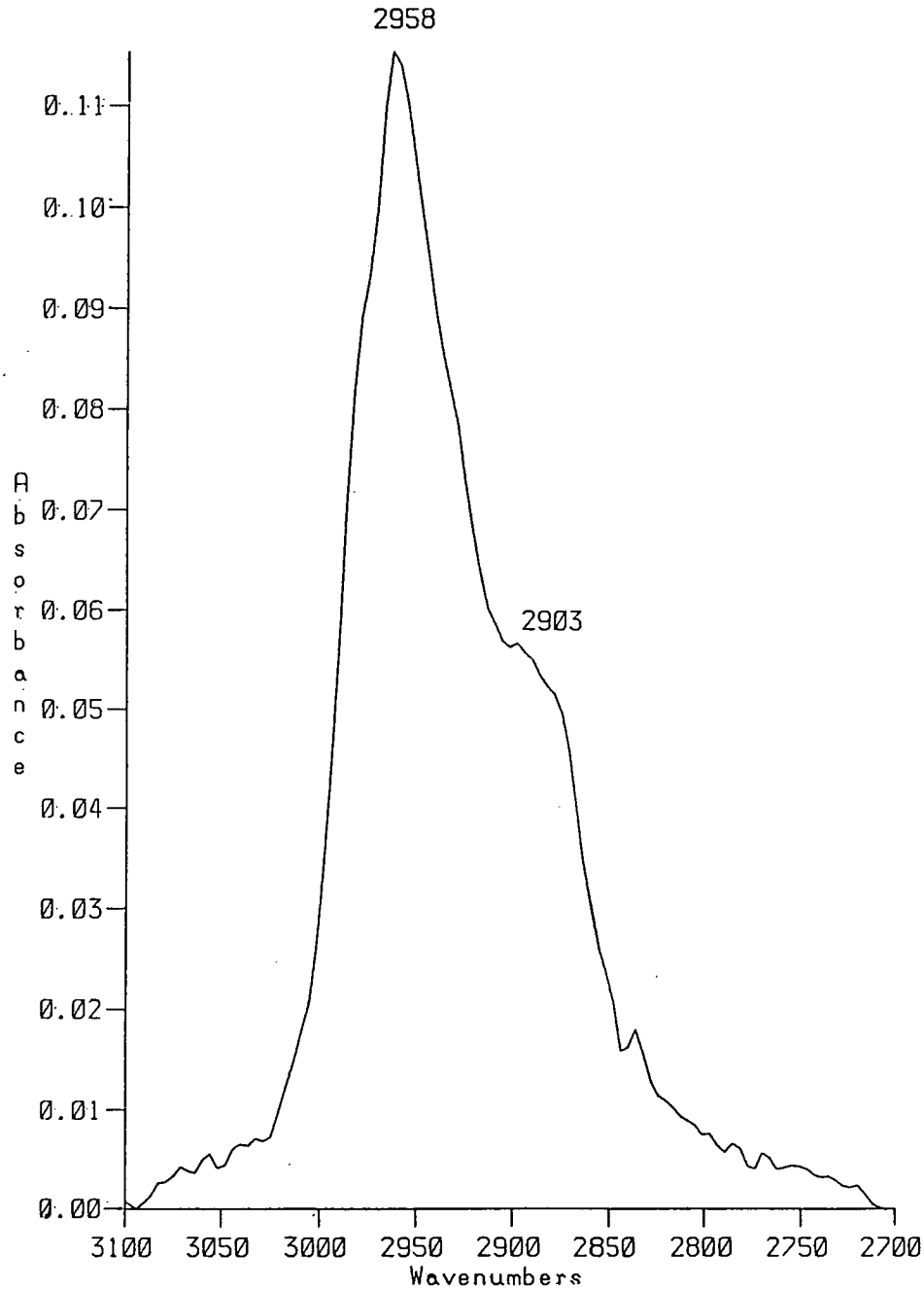

Fig. 6.48 DRIFT Spectrum of Gas Phase Reactants over Silica Support after 40 Minutes of Reaction at 523 K (sample temperature).

at 2958 cm^{-1} due to physisorbed butane. This band disappeared after 30 minutes evacuation at reaction temperature.

The results of n-butane hydrogenolysis over 'as-received', 0.25, 0.50 and 1% KOH doped EUROPT-1 samples are given in Table 6.3. The table shows the rate of disappearance of n-butane and the product distributions. The deactivation of the catalysts due to potassium doping, and increased isomerisation follows the trend observed in the conventional hydrogenolysis reaction (Chapter 4).

Figures 6.49-6.52 show spectra recorded after treatment of 'as-received' 0.25%, 0.50% and 1.0% KOH doped EUROPT-1, with 110 torr of n-butane-hydrogen (1:10) mixture at reaction temperature 713 K (heater temperature, 523 K actual sample temperature). The spectra are very similar to a typical spectrum of n-butane adsorbed on EUROPT-1 (Figure 6.47).

All the spectra shown in Figures 6.49-6.53 are essentially the same. The main peak is centred at 2958 cm^{-1}. There are negligible differences in the appearance of these gas phase spectra.

Figures 53-56 show spectra after evacuation of the gas phase reactants at reaction temperature. All the spectra are very weak. There are very weak bands in the region 2950 and 2880 cm^{-1}, in the case of 'as-received' and 0.25% KOH catalysts. There are no obvious peaks in the 0.5 and

Table 6.3

Results of n-butane Hydrogenolysis Studied by DRIFTS/G.C. at 523 K After 40 Minutes Reaction

Catalyst	Rate of Reaction* S^{-1} g^{-1}	% n-Butane Conversion	Initial Product Distribution %			
			CH_4	C_2H_6	C_3H_8	iso-C_4H_{10}
EUROPT-1	1.32×10^{19}	40	14.9	13.7	5.14	8.2
0.25% KOH (wt)/EUROPT-1	1.62×10^{18}	30	12.5	3.27	1.7	1.59
0.5% KOH (wt)/EUROPT-1	1.17×10^{17}	20	9.12	9.55	3.74	7.1
1.0% KOH (wt)/EUROPT-1	1.7×10^{16}	4.3	1.38	1.12	1.60	0.25

* Assumed linear with time from t = 0 to t = 40

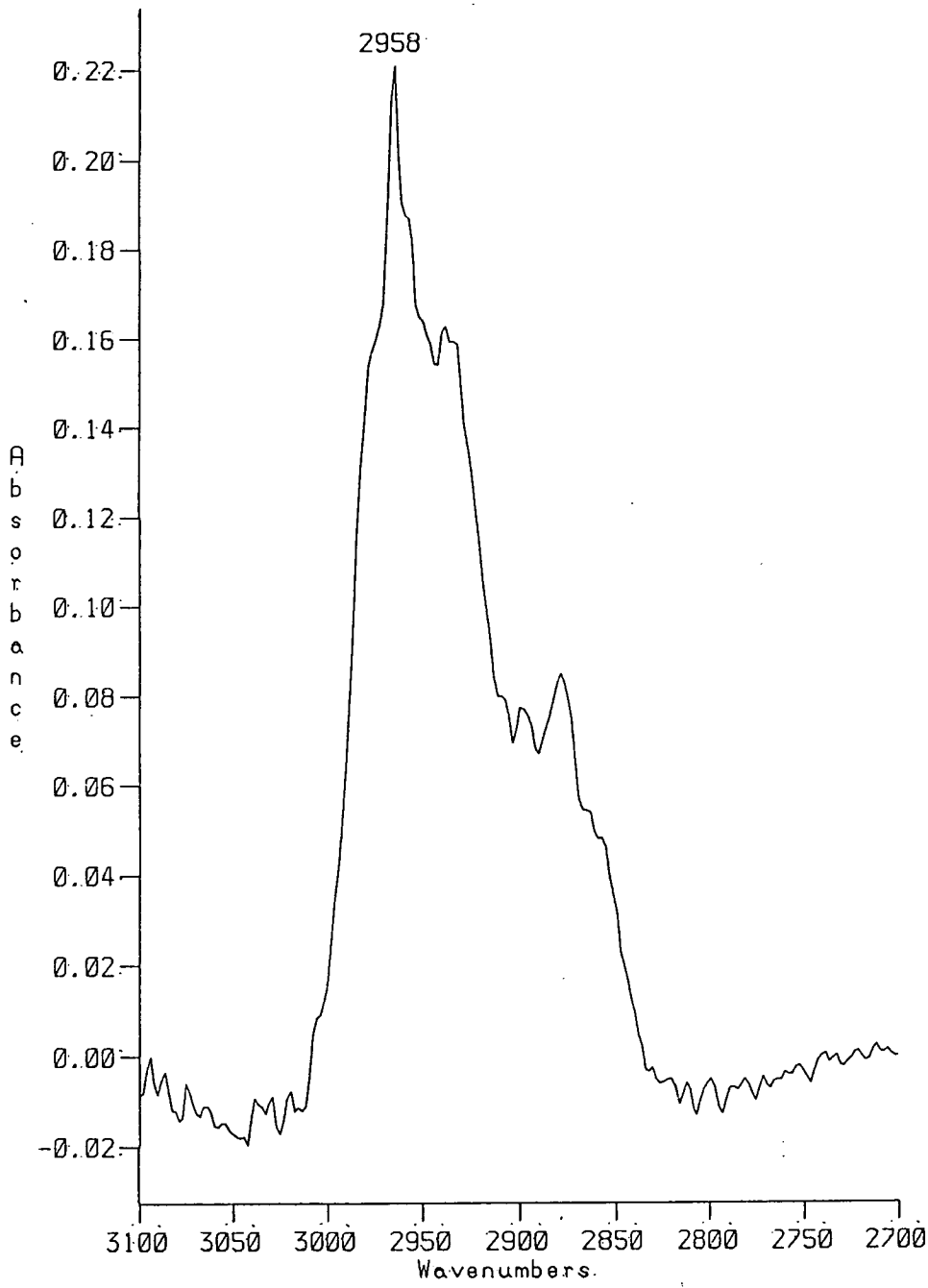

Fig. 6.49 Spectrum of Gas Phase Reactants over 'as-received' EUROPT-1 at 523 K (sample temperature).

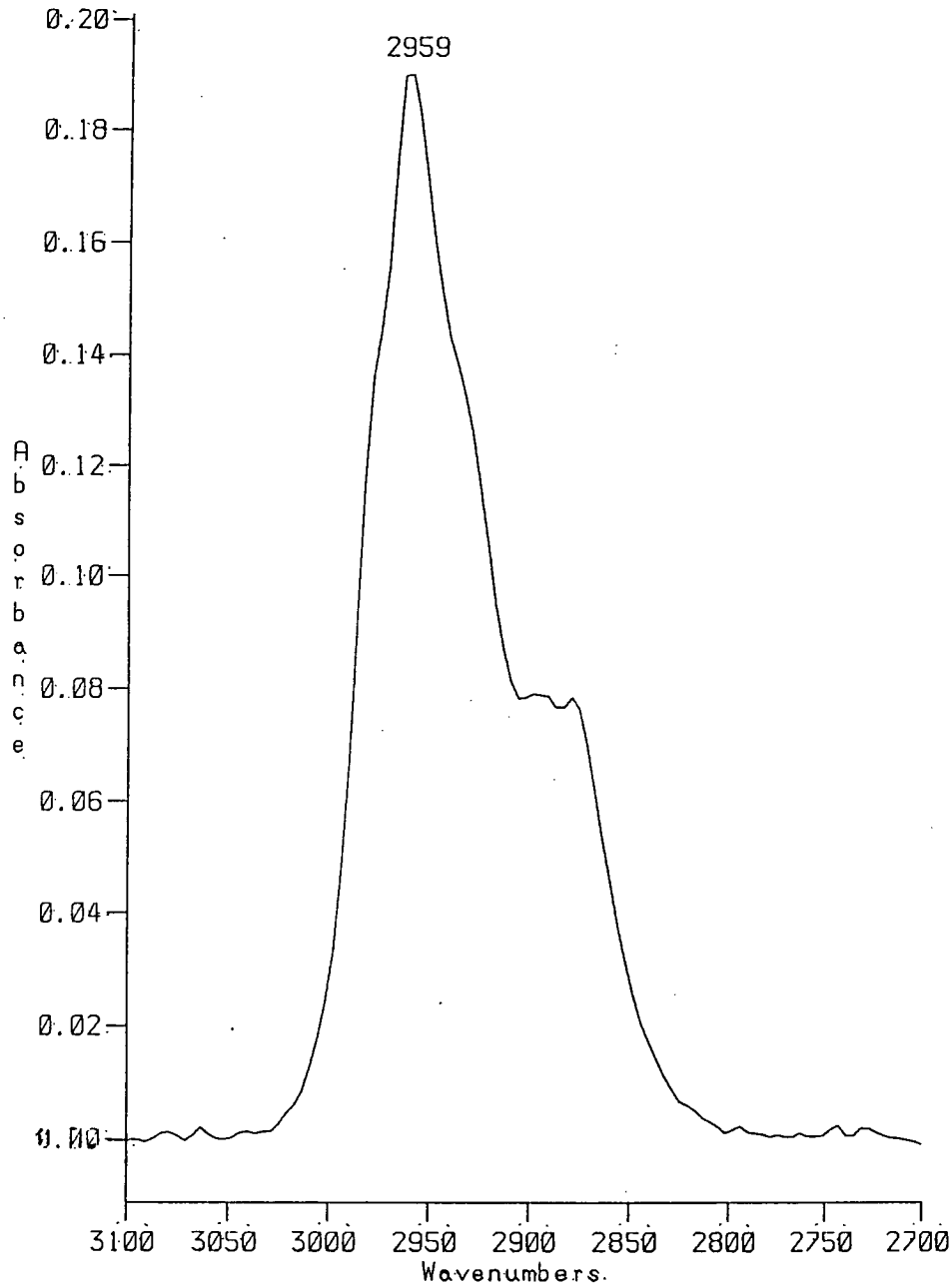

Fig. 6.50 Spectrum of Gas Phase Reactants over 0.25% KOH (wt)/ EUROPT-1 at 523 K (sample temperature).

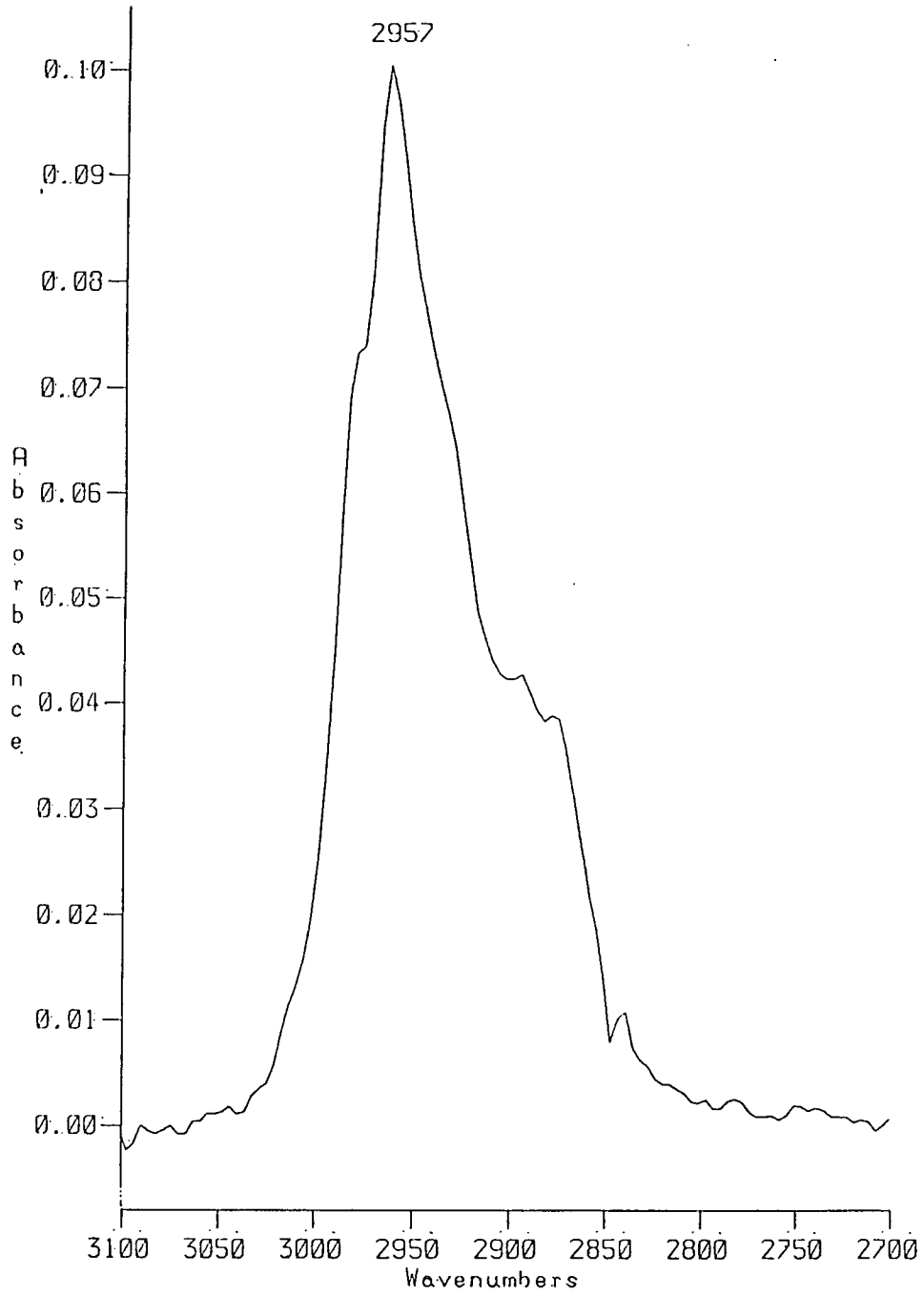

Fig. 6.51 Spectrum of Gas Phase Reactants over 0.50% KOH (wt)/ EUROPT-1 at 523 K (sample temperature).

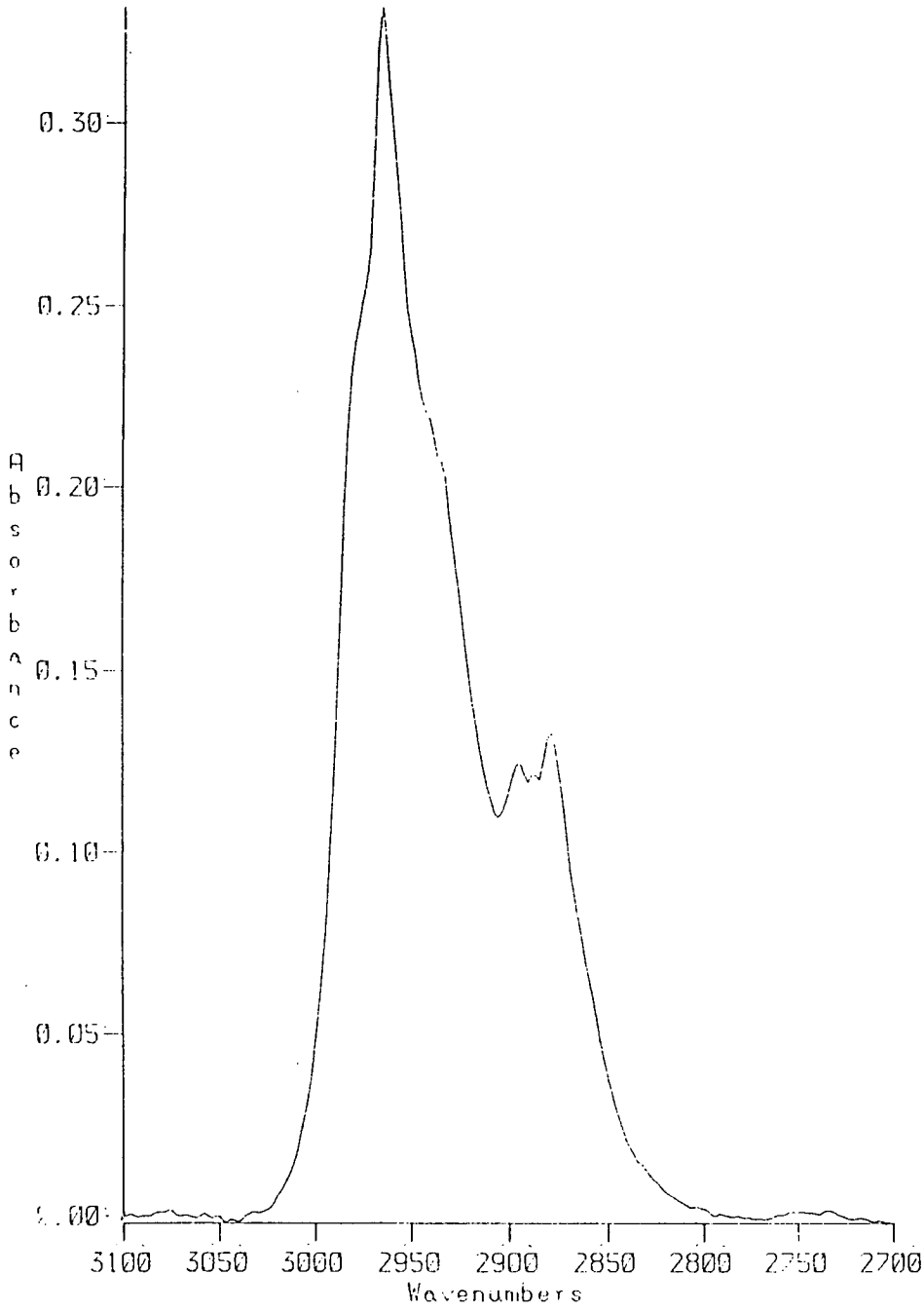

Fig. 6.52 Spectrum of Gas Phase Reactants over 1.0% KOH (wt)/ EUROPT-1 at 523K (sample temperature).

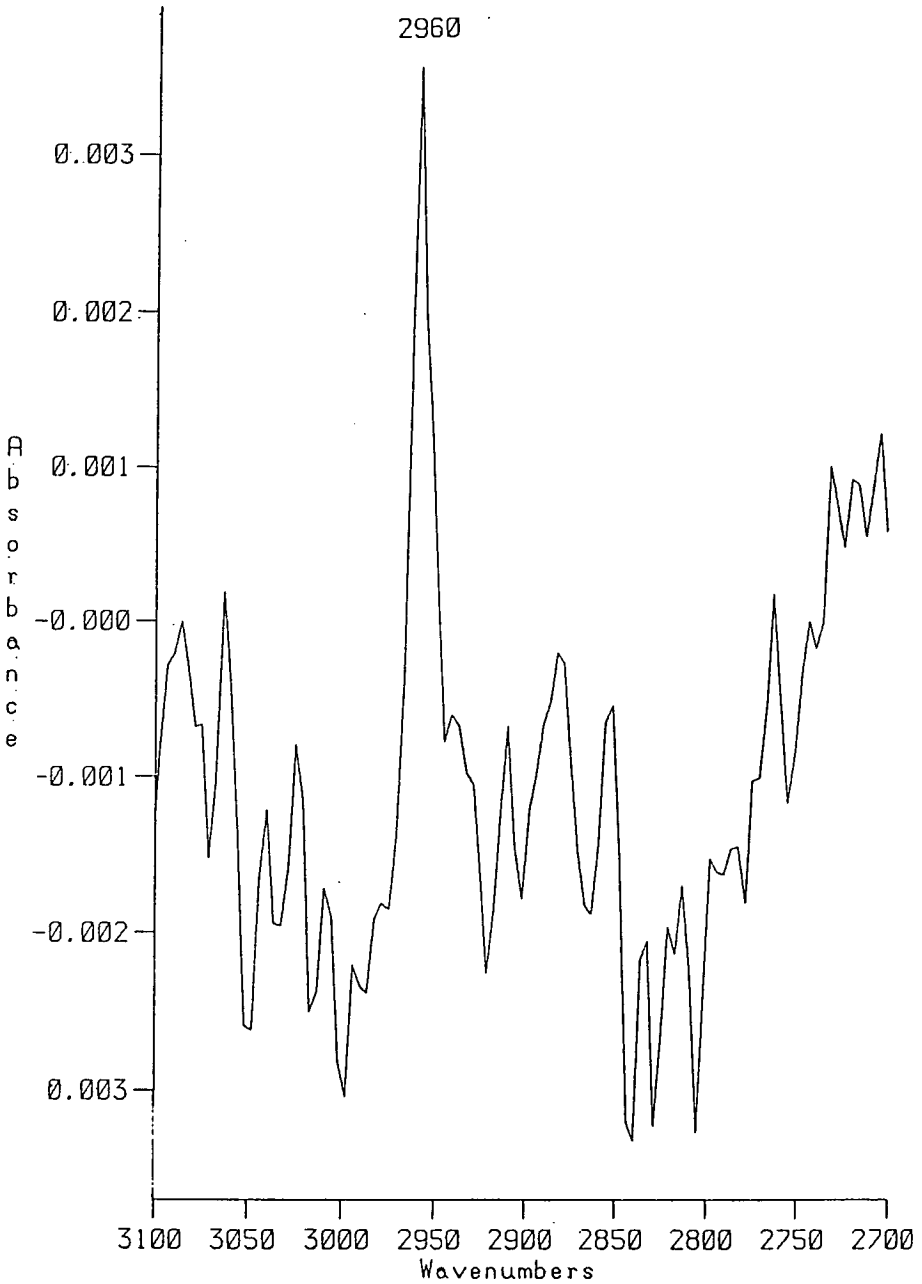

Fig. 6.53 **Spectrum of Residues After Evacuation of Reactants from 'as-received' EUROPT-1 at 523 K (sample temperature).**

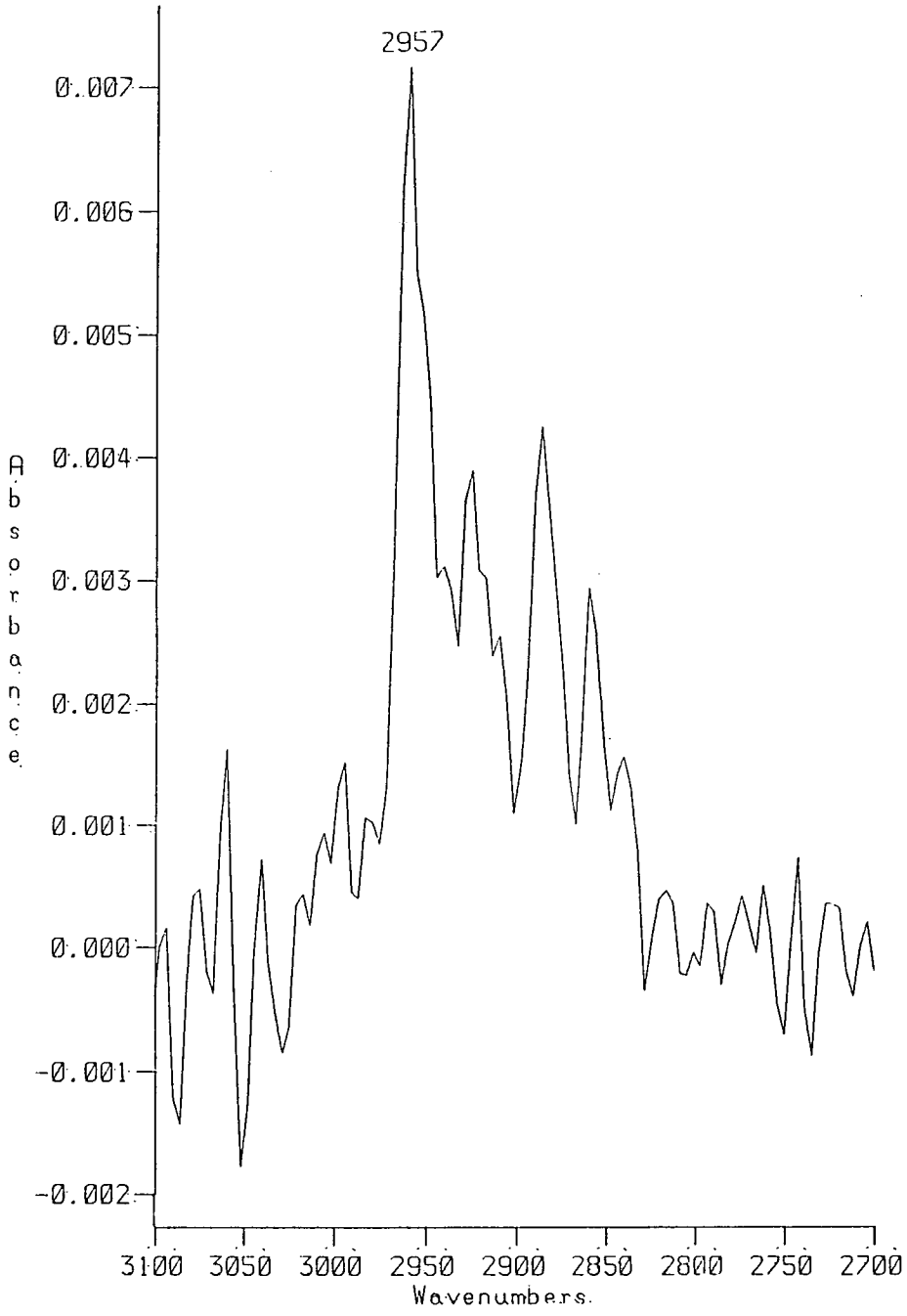

Fig. 6.54 Spectrum of Residues after Evacuation of Reactants from 0.25% KOH (wt)/EUROPT-1 at 523 K (sample temperature).

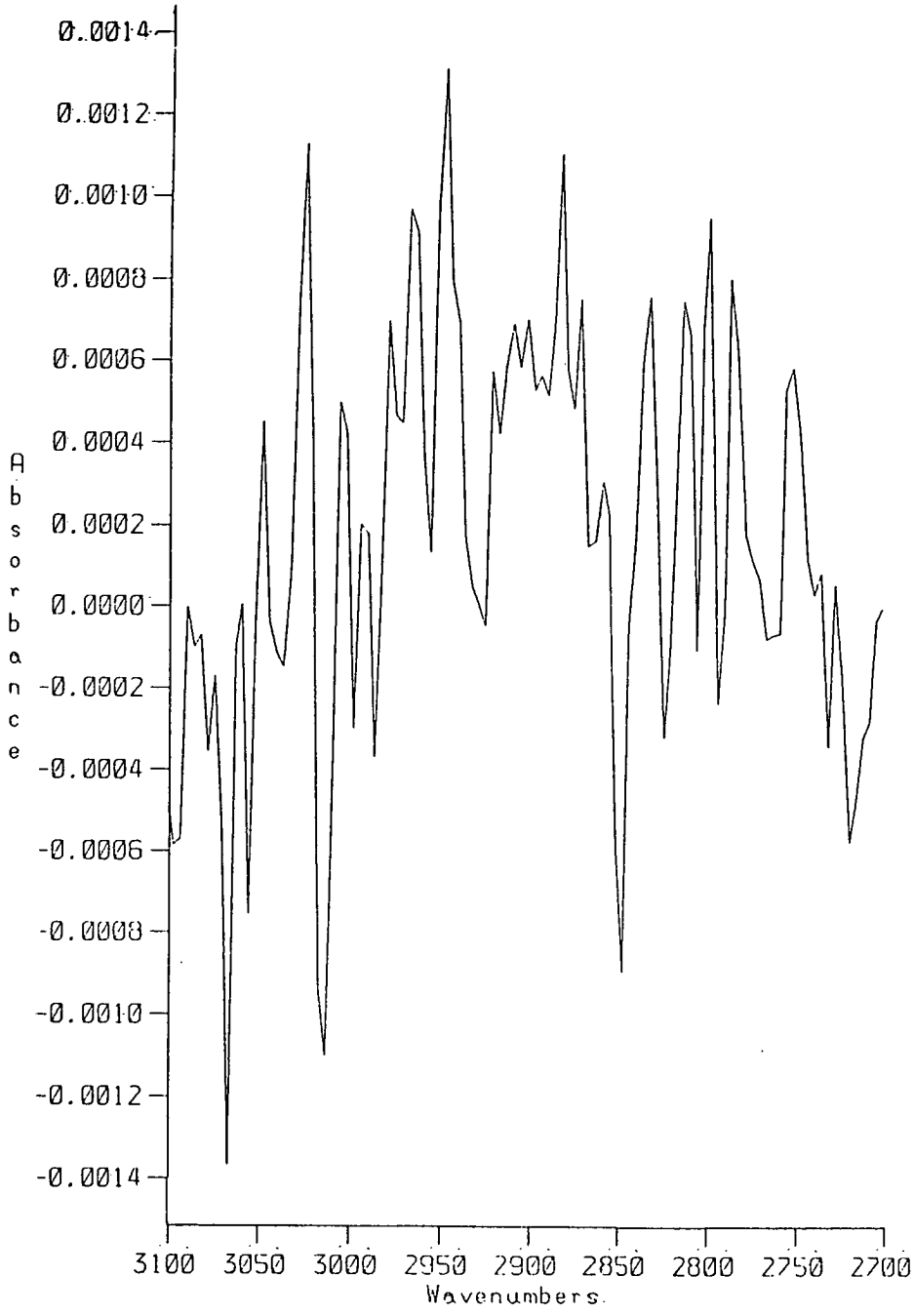

Fig. 6.55 Spectrum of Residues after Evacuation of Reactants from 0.5% KOH (wt)/EUROPT-1 at 523 K (sample temperature).

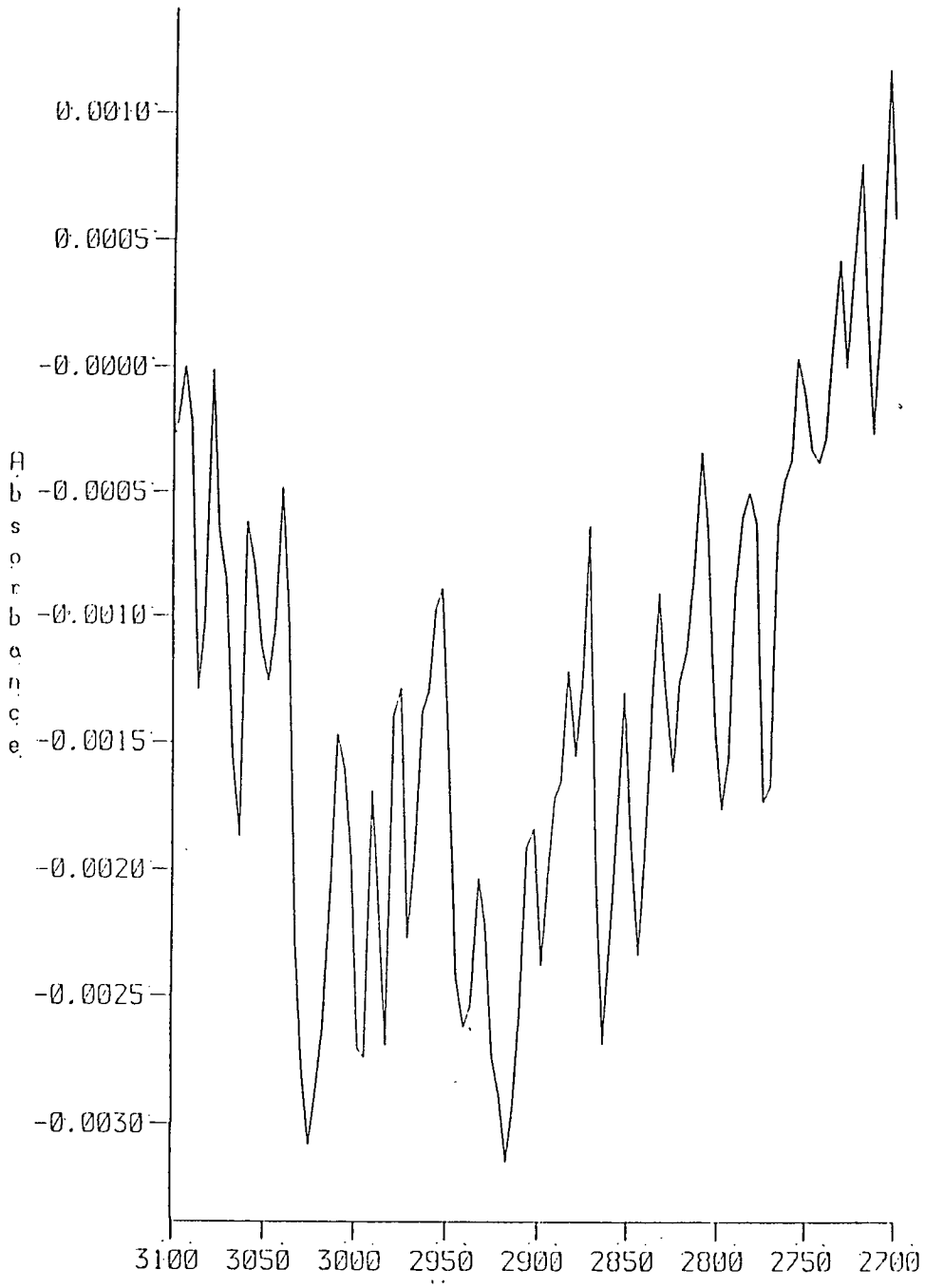

Fig. 6.56 Spectrum of Residues after Evacuation of Reactants from 1.0% KOH (wt)/EUROPT-1 at 713 K (sample temperature).

1.0% KOH doped catalysts.

The hydrogenolysis reactions were also carried out at low temperature, i.e. 523 K (heater temperature) as a part of setting up the apparatus. Figures 6.57-6.58 show spectra after evacuation of the gas phase at reaction temperature. Both spectra are very weak and similar, showing the same structure in the regions ~ 2800 and 2900-2950 cm^{-1}.

Finally, it is concluded that, there might be some suitable conditions to study the n-butane hydrogenolysis involving FTIR techniques.

The spectra obtained are very similar regardless of alkali doping.

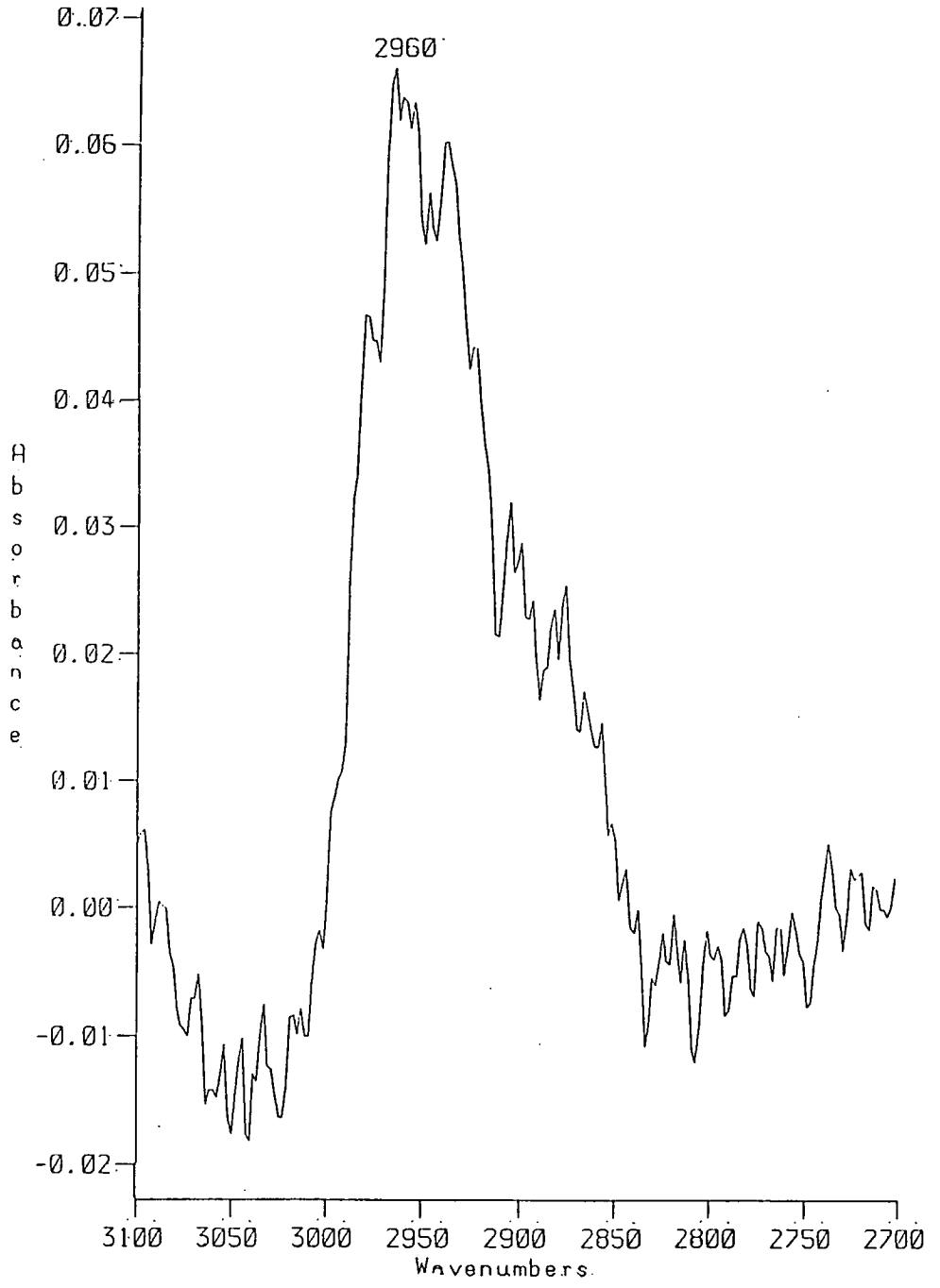

Fig. 6.57 Spectrum of Residue after Evacuation of Reactants from EUROPT-1 at 400 K (sample temperature).

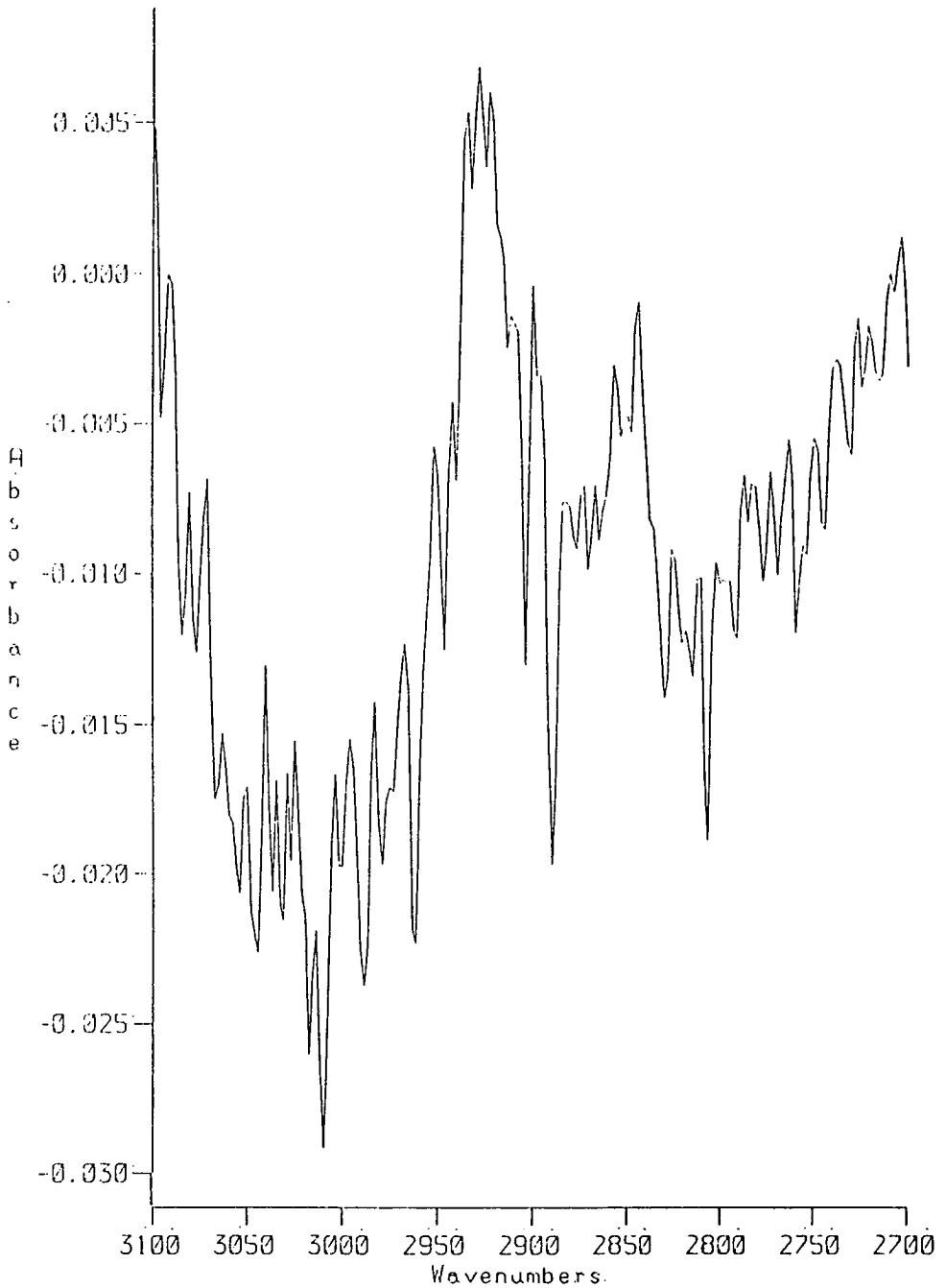

Fig. 6.58 Spectrum of Residue after Evacuation of Reactants from EUROPT-1 at 400 K (sample temperature).

REFERENCES

1. B.A. Marrow and N. Sheppard, *Proc.Roy.Soc.A* 311 (1969) 391.
2. O. Beeck, *Discuss.Faraday Soc.* 8 (1950) 118.
3. G.C. Bond, J.J. Phillipson, P.B. Wells and J.M. Winterbottom, *Trans.Faraday Soc.* 60 (1964) 1847.
4. C. Kemball, *J.Chem.Soc.* (1956) 735.
5. S. Sato, *J.Res.Inst.*, Hokkaido Univ. 24 (1976) 127.
6. G.C. Bond and P.B. Wells, *Adv.Catal.* 15 (1964) 91.
7. Y. Soma, *J.Catal.* 75 (1982) 267.
8. G.S. McDougall, Ph.D. Thesis, University of East Anglia, 1985.
9. J.D. Prentice, A. Lesiunas and N. Sheppard, *J.Chem.Soc., Chem.Commun.* (1976) 76.
10. C. de la Cruz, Ph.D. Thesis, University of East Anglia, 1987.
11. B.J. Bandy, M.A. Chesters, D.I. James, G.S. McDougall, M.E. Pemble and N. Sheppard, *Phil.Trans.Roy.Soc.A* 318 (1986) 141.
12. T.P. Beebe, Jr., M.R. Albert and J.T. Yates, Jr., *J.Catal.* 96 (1985) 1.
13. N. Sheppard, D.I. James, A. Lesianas and J.D. Prentice, Commun. Dept. Chemistry, Bulgarian Acad. Sci. 17 (1984) 95.
14. H. Ibach and S. Lehwald, *J.Vacuum Sci.Technol.* 15 (1978) 407.

15. Y. Soma, *J.Catal.* 59 (1979) 239.

16. Y. Soma, *J.Chem.Soc., Chem.Soc.Commun.* (1976) 1004.

17. C. Nyberg, C.G. Tengstal and S. Anderson, *Chem.Phys. Letters* 87 (1982) 87.

18. M.A. Chesters, G.S. McDougall, M.E. Pemble and N. Sheppard, *Appl.Surf.Sci.* 22/23 (1985) 369.

19. F. Zaera, R.B. Hall, *Surf.Sci.* 1 (1987) 180.

20. J.A. Gates and L.I. Kemodel, *Surf.Sci.* 120 (1982) L461.

21. H. Steininger, H. Ibach and S. Lehwald, *Surf.Sci.* 117 (1982) 685.

22. S. Lehwald and H. Ibach, *Surf.Sci.* 89 (1979) 425.

23. C.E. Anson, B.J. Bandy, M.A. Chesters, B. Keiller, I.A. Oxton and N. Sheppard, *J.Electron Spectrosc.Relat. Phenom.* 29 (1983) 315.

24. W. Erley, M.A. Barrow and H. Ibach, *Surf.Sci.* 120 (1982) 273.

25. C. Backx, C.P.M. de Groot and P. Biloem, *Appl.Surf. Sci.* 6 (1980) 256.

26. M.A. Barteau, J.Q. Broughton and D. Menzel, *Appl.Surf. Sci.* 19 (1984) 92.

27. U. Seip, M.C. Tsai, I. Kuppers and G. Ertl, *Surf.Sci.* 147 (1985) 65.

28. E.M. Stuve, R.J. Madix and C.R. Brundle, *Surf.Sci.* 152/153 (1985) 532.

29. R.G. Windham, M.E. Bartram and B.E. Koel, *J.Phys. Chem.* 92 (1988) 2860.

30. X.L. Zhou, X.Y. Zhu, and J.M. White, *Surf.Sci.* 193 (1988) 387.

31. E.L. Garfunkel, J.J. Maj, C.J. Frost, M.H. Farlas and G.A. Somorjai, *J.Phys.Chem.* 87 (1983) 3629.

32. J.B. Peri, in: Catalysis - Source and Technology, vol. 5, Page 171, 1984.

33. J.E. Demuth, *Surf.Sci.* 80 (1979) 367.

34. P. Skinner, M.W. Howard, T.A. Oxton, S.F.A. Kettle, D.B. Powell and N. Sheppard, *J.Chem.Soc., Faraday Trans.II* (1981) 1203.

35. M.A. Chester, and E.M. McCash, *Surf.Sci.* 187 (1987) L639.

36. C. de la Cruz and N. Sheppard, *J.Chem.Soc., Chem.Commun.* 1987.

37. M.J.S. Dewar, *Bull.Soc.Chim.Fr.* 18 (1951) C79.

38. J. Chatt, L.A. Duncan, *J.Chem.Soc.* (1953) 2939.

39. P.J. Coleman, S.L. Hegedus, J.R. Norton and R.G. Finke, in: Principles and Applications of Organo-transition Metal Chemistry, University Science Books : Mill Valley, Ca., 1987.

40. T.E. Madey and C. Benndorf, *Surf.Sci.* 152/153 (1985) 587.

41. N. Sheppard, *Ann.Rev.Phys.Chem.* 39 (1988) 589.

42. G.C. Bond, in: Catalysis by Metals,(Academic Press, London and New York, 1963).

43. J.C. Bertoline, G. Dalmai-Imelik and J. Rosseau, *Surf.Sci.* 67 (1977) 478.

44. S. Lehwald, H. Ibach and J.E. Demuth, *Surf.Sci.* 78 (1978) 577.

45. J.C. Bertoline and J. Rosseau, *Surf.Sci.* 89 (1979) 467.

46. G.A. Galkin, A.V. Kiselev and V.I. Lygin, *Trans. Faraday Soc.* 60 (1964) 431.

47. D.M. Haaland, *Surf.Sci.* 102 (1981) 405.

48. R.E. Semples and P.G. Rouxhet, *J.Colloid Interface Sci.* 55 (1976) 263.

49. E. Baumgarten and F. Weinstrauch, *Spectro Chim. Acta* 34A (1978) 1155.

50. J. Erkelens and S.H. Eggink - Du Burck, *J.Catal.* 15 (1969) 62.

51. N. Sheppard, N.R. Avery, M. Clerk, B.A. Marrow, R. Smart, C. Tanaka and J.W. Ward, *Proced.Conf.Mol. Spectroscop.* 4 (1968) 97.

52. A. Palazov, *J.Catal.* 30 (1973) 13.

53. M. Primet, J.M. Basset, M.V. Mathieu and M. Prettre, *J.Catal.* 29 (1979) 213.

54. R.C. Pitkeathly and A.G. Goble, *Proced. Int.Congr. Catal.* Paris, 1960.

55. L. Babernics and P. Teteny; *J.Catal.*, 17 (1970), 35.

56. J.L. Garnett and W.A. Solich-Baumgartner, *J.Phys. Chem.* 68 (1964) 3177.

57. R.B. Moyes and P.B. Wells, *Adv.Catal.* 23 (1973) 121.

58. A.V. Kiselev and V.I. Lygin, in: Infrared Spectra of Surface Compounds (Willey, New York, 1975).

59. M.P. Kiskinova, *Surf.Sci.* 11 (1981) 584.

60. R.D. Kross, V.A. Fassel and M. Margoshes, *J.Am.Chem. Soc.* 78 (1956) 1332.

61. G. Herzberg, Infrared and Raman Spectra, Van Nostrand Company, New York, 1945.

62. K. Horn and J. Pritchard, *Surf.Sci.* 52 (1975) 437.

63. J.E. Demuth, H. Ibach, S. Lehwald, *Phys.Rev.Lett.* 40 (1978) 1044.

64. H. Ibach, H. Hopster and B. Sexton, *Appl.Surf.Sci.* 1 (1977) 1.

65. M.A. Chesters, P. Gardener, and E.M. McCash, *Surf.Sci.* 209 (1989) 89.

66. M.A. Chesters, S.F. Parker and R. Raval, J.Electron Spectrosc. Related Phenomena 9 (1986) 155.